95

PROBABILISTIC ANALYSIS AND DESIGN OF DIMENSIONALLY STABLE COMPOSITE STRUCTURES

by

Erik Abernathy

B. S., Massachusetts Institute of Technology
(1993)

Submitted to the Department of Aeronautics and Astronautics
in partial fulfillment of
the requirements for the degree of

Master of Science
in Aeronautics and Astronautics

at the
Massachusetts Institute of Technology

December 1995

Signature of Author _____
Department of Aeronautics and Astronautics
December 8, 1995

Certified by _____
Professor Hugh L. McManus
Thesis Supervisor

Accepted by _____
Professor Harold Y. Wachman
Chairman, Departmental Graduate Committee

PROBABILISTIC ANALYSIS AND DESIGN OF DIMENSIONALLY STABLE COMPOSITE STRUCTURES

by

Erik Abernathy

Submitted to the Department of Aeronautics and Astronautics on December 8, 1995 in partial fulfillment of the requirements for the Degree of Master of Science in Aeronautics and Astronautics

ABSTRACT

Objects in orbit are exposed to extreme temperatures. These can lead to deformations which complicate the design of dimensionally critical space structures. Composites offer the major advantage of tailorable properties. Theoretically, dimensionally stable composite laminates can be made with coefficients of thermal expansion (CTE's) of zero. In practice, the laminate properties deviate from predicted properties due to variations in material properties and manufacturing parameters. The goal of the present investigation is to develop an analytical methodology to predict means and standard deviations of laminate engineering properties from given means and standard deviations of ply material properties, fiber volume fractions, and manufacturing parameters. This objective is successfully met through a combination of analytical modeling and experimental investigation. In the analysis, the means and standard deviations of the laminate properties are found using Classical Laminated Plate Theory (CLPT) and simple statistical methods. A new laminate property, the thermal bending coefficient, is defined. The thermal bending coefficient is the out-of-plane analog to the in-plane CTE. Many unsymmetric laminates exhibit large-deformation effects which depart from CLPT predictions. These effects are accounted for in a separate analysis using an energy method. The analyses are implemented in a set of computer codes which can analyze any user-defined laminate. Extensive experimental results provide verification of the analyses. Ninety specimens, from eighteen AS4/3501-6 graphite/epoxy panels with sixteen different layups, are tested to investigate the effects of ply angle, ply grouping, thickness, zero degree plies, and asymmetry on the thermal bending coefficients. Specimens are mounted in a thermal environment chamber, and deflections at chamber temperatures of 25°C and 100°C are measured by two laser displacement sensors. The data is reduced to find the thermal bending coefficients of the specimens. Correlations between experimental results and the analyses are generally very good. The analytical predictions bracket the data in most cases. Most predicted trends are seen in the experimental data. Parametric studies are also conducted. The variations of the laminate properties, and their sensitivities to the input parameters, are found to be very dependent on the laminate considered. The computer code which implements the analytical model is a useful design tool. It can be used to conduct trade studies, and to find which parameters are most important to control in order to maintain low standard deviations of critical laminate properties.

Thesis Supervisor: Hugh L. McManus
Title: Class of 1943 Assistant Professor,
Department of Aeronautics and Astronautics,
Massachusetts Institute of Technology

ACKNOWLEDGMENTS

This project would never have been completed without the help of many people. To anyone left out of the following list- No offense.

I am grateful to Prof. McManus for allowing me the opportunity to work on this project. His guidance throughout my time as a grad student has added a lot to my education that won't necessarily be found in this document. Hugh has a vast amount of knowledge, both theoretical and practical, and can communicate complicated ideas well (a much more difficult feat, I think).

My family has supported me in innumerable ways throughout the years with money and sage advice. I only hope I can live up to the examples they set for years.

I would also like to thank Prof. Hagood for letting me use his environmental chamber (I only broke it once), and Paul, Mark, Ed, and Prof. Dugundji for many helpful criticisms and suggestions during my time in the lab. Also, a huge thank you to Ping, Al, Deb, and Sharon, without whom nothing would ever get done around the lab. Kudos to Yannick, Sanith, and Chris for helping get the experiments off the ground, Aaron and John for help around the SERC lab, Kamyar for athena help, Wes and Chris for emergency equipment procurement, and everybody that came in and out of the mezz for distracting me for a few minutes. Good luck to everyone in the labs, and I'll try to send out a replacement goon for IM sports. I've had a good time and learned a lot, especially from Brian "email rules" Wardle, Jason "better double-bag it" Maddocks, Mark "Florida rules" Tudela, and Ronan "I'll bring in a hurl tomorrow" Cunningham.

In six years at MIT, I learned the importance of taking time out for fun. My interaction with all my fellow Betas has shown the possibility of a balance between fun and productivity. I'd like to especially single out Wes "If it bleeds, we can kill it" Williams, Kevin "The Animal" Frye, Ethan "mellow intensity" Close, Andrew "Quentin" Heitner, Kevin "Rogaine" Walsh, and the members of my pledge class- Frank "start by making a bunch of folders" Leibly, Godard "pleasure is the presence of pain" Abel, Randy "Brewmeister" West, Chris "Tastes like chicken" Shutts, and Mike "Career of the week" McDermott.

Very special thanks are also due to Frank, Randy, and Kevin, who agreed on September 1, 1995 to let me crash on the dining room floor for "two weeks." (Note the turn-in date). Finally, thanks to the guys in Michigan- Mike "Sack" Duffy, William Baines Johanssen Mason Scruggs LIX, and Pooky "Mike" Bowers for helping me find a job and a place to live.

Push off, and sitting well in order smite
The sounding furrows, for my purpose holds
To sail beyond the sunset, and the baths
Of all the western stars, until I die.

-Alfred, Lord Tennyson, *Ulysses*

It's better to burn out than to fade away.

-Neil Young

FOREWORD

This work was performed in the Technology Laboratory for Advanced Composites (TELAC) and the Space Engineering Research Center (SERC) in the Department of Aeronautics and Astronautics at the Massachusetts Institute of Technology. This work was sponsored by the National Science Foundation under NSF Grant 9257612-CMS, NASA under NASA Research Grant NAGW-1335 and NASA Training Grant NGT-10032, and the NASA Langley Research Center under NASA Grant NAG1-1717.

TABLE OF CONTENTS

LIST OF FIGURES

LIST OF TABLES

NOMENCLATURE

$\mathbf{a}^*$	Part of inverse laminate stiffness matrix
$\mathbf{A}$	Laminate extensional stiffness matrix
$\mathbf{b}^*$	Part of inverse laminate stiffness matrix
$\mathbf{B}$	Laminate coupling stiffness matrix
B	Distance along specimen between laser spots
c_{jk}	Coupling coefficient between input variables
C	Center of Mohr's circle of curvature
$\mathbf{d}^*$	Part of inverse laminate stiffness matrix
d_{ij}	Sensitivity metric which is the derivative of laminate property i with respect to input variable j
d_{ij}^{σ}	Sensitivity metric which is the contribution of the variation of input variable j to the variation of laminate property i
$\overline{d}_{ij}$	Sensitivity metric which is the proportional change in laminate property for a given proportional change in input variable
$\mathbf{D}$	Laminate bending stiffness matrix
E_{11}	Laminate axial stiffness
E_{22}	Laminate transverse stiffness
E_{f11}	Longitudinal fiber stiffness
E_{f22}	Transverse fiber stiffness
E_{lk}	Longitudinal stiffness of ply k
E_m	Matrix stiffness
E_{tk}	Transverse stiffness of ply k
G	Laminate shear stiffness
G_{f12}	Fiber shear stiffness

G_{ltk}	Shear stiffness of ply k
G_m	Matrix shear stiffness
h	Laminate thickness
k_{fk}	Fiber volume fraction of ply k
$\bar{k}_f$	Laminate fiber volume fraction
L	Distance along specimen from clamp to laser spots
L_x	Laminate length in the x direction
L_y	Laminate width in the y direction
$\mathbf{M}$	Laminate moment vector
$\mathbf{M}^{\mathbf{H}}$	Laminate hygral moment vector
$\mathbf{M}^{\mathbf{T}}$	Laminate thermal moment vector
nply	Number of plies in laminate
nmatl	Number of materials in laminate
$\mathbf{N}$	Laminate load vector
$\mathbf{N}^{\mathbf{H}}$	Laminate hygral load vector
$\mathbf{N}^{\mathbf{T}}$	Laminate thermal load vector
$\mathbf{Q}$	Reduced ply stiffness matrix in ply coordinates
$\overline{\mathbf{Q}}$	Reduced ply stiffness matrix in laminate coordinates
R	Radius of Mohr's circle of curvature
$\mathbf{S}$	Stability matrix
t_k	Ply thickness of ply k
$\mathbf{T}$	Transformation matrix
T	Temperature
u°	Midplane displacement in the x direction
U	Potential energy
v°	Midplane displacement in the y direction
w	Out-of-plane displacement of the midplane in the z direction

$\mathbf{W}^{\mathbf{H}}$	Hygral bending coefficients vector
$\mathbf{W}^{\mathbf{T}}$	Thermal bending coefficients vector
x	Global coordinate system axis
x'	Principal curvature coordinate system axis
X_j	Input parameter j
$\overline{X}_j$	Mean value of input parameter j
y	Global coordinate system axis
y'	Principal curvature coordinate system axis
Y_i	Laminate property i
z	Global coordinate system axis

$\boldsymbol{\alpha}$	Laminate in-plane coefficients of thermal expansion vector in ply coordinates
$\overline{\boldsymbol{\alpha}}$	Laminate in-plane coefficients of thermal expansion vector in laminate coordinates
α_{f11}	Fiber longitudinal coefficient of thermal expansion
α_{f22}	Fiber transverse coefficient of thermal expansion
α_{lk}	Longitudinal in-plane coefficient of thermal expansion of ply k in ply coordinates
α_m	Matrix coefficient of thermal expansion
α_{tk}	Transverse in-plane coefficient of thermal expansion of ply k in ply coordinates
$\boldsymbol{\beta}$	Laminate in-plane coefficients of hygral expansion vector in ply coordinates
$\overline{\boldsymbol{\beta}}$	Laminate in-plane coefficients of hygral expansion vector in laminate coordinates
β_{lk}	Longitudinal coefficient of hygral expansion of ply k in ply coordinates
β_m	Matrix coefficient of hygral expansion
β_{tk}	Transverse coefficient of hygral expansion of ply k in ply coordinates

ΔH	Moisture content
ΔT	Change in temperature relative to stress free temperature
$\boldsymbol{\varepsilon}$	Laminate strain vector in ply coordinates
$\bar{\boldsymbol{\varepsilon}}$	Laminate strain vector in laminate coordinates
$\boldsymbol{\varepsilon}^{\circ}$	Laminate midplane strain vector
ϕ	Rotation angle from laminate to principal curvature axes
$\boldsymbol{\kappa}$	Laminate curvature
$\boldsymbol{\kappa}^{\mathbf{H}}$	Moisture-induced curvature
$\boldsymbol{\kappa}^{\mathbf{T}}$	Thermally induced curvature
λ	Ratio of principal curvatures
ν_{12}	Laminate major Poisson's ratio
ν_{f12}	Fiber Poisson's ratio
ν_{ltk}	Ply Poisson's ratio
ν_m	Matrix Poisson's ratio
θ_k	Ply angle of ply k
$\boldsymbol{\sigma}$	Laminate in-plane stress vector in ply coordinates
$\bar{\boldsymbol{\sigma}}$	Laminate in-plane stress vector in laminate coordinates
$\hat{\sigma}$	Standard deviation
ψ	Strain energy density

CHAPTER 1

INTRODUCTION

Advanced composite materials have become more common in structural applications in recent years. Their advantages over traditional metallic structures include high specific stiffness and strength, tailorable mechanical and hygrothermal properties, and excellent fatigue characteristics. The low coefficients of thermal expansion (CTE's) of certain composite laminates have also made them extremely attractive for dimensionally critical aerospace structures such as antennae and their supports, optical platforms, solar reflectors, truss tubes, and instrument support panels.

Objects in orbit are exposed to a wide range of temperatures. Without active temperature control, an exposed object experiences temperature swings of approximately ±150°F in low Earth orbit, and ±250°F in geosynchronous orbit. In a large structure, these temperature changes can lead to undesirable large deflections which can, in the extreme, lead to failure to meet mission objectives. Thus there is a large demand for dimensionally stable materials, i.e. those which do not deform with temperature changes. For instance, truss tubes for an early Space Station Freedom design have a CTE requirement of $0 \pm 0.9 \times 10^{-6}$/°C [1]. Composite materials are well-suited to meet these dimensional stability requirements. On the ply level, the slightly negative fiber CTE can be offset exactly by the larger positive CTE of

the matrix, creating a theoretically zero-CTE ply. Similarly, plies with different CTE's can be combined to obtain a zero-CTE laminate.

Methods exist to predict laminate properties based on the stiffness and hygrothermal properties of individual plies, their thicknesses, and their layup angles. While these methods perform well in predicting mean properties, there is always some scatter of actual laminate properties about the predicted mean. This scatter is due to variations in the material properties of individual plies and manufacturing variations. Manufacturing variations include distributions of ply thicknesses and ply layup angles. In particular, the ply angle distribution can be thought of as the scatter caused by slight misalignment of the plies with respect to the desired angles during layup. Property distributions are especially important in dimensionally stable materials, where deformations are critical. In theoretically-zero CTE composites, the performance metric becomes the standard deviation of the CTE around the zero point. A large standard deviation in CTE could lead to a large number of manufactured parts failing to meet design criteria, even if the mean value were exactly zero.

The observed variation of laminate properties establishes a need to predict laminate property variations based on variations in ply properties and manufacturing processes. Such a methodology could be useful to both the designer and analyst of composite structures. A laminate could be designed to meet given laminate property tolerance requirements. The predicted distribution information could be used as a factor in selecting from proposed laminates for a particular application. Sensitivity information could show which are the most important parameters to control during manufacturing.

The goal of the present work is to establish an analytical methodology to predict the statistical distributions of the laminate properties. The

analysis uses Classical Laminated Plate Theory (CLPT) and simple statistical methods to predict the means and standard deviations of laminate properties. Stiffnesses and hygrothermal properties are predicted, along with a new laminate property. The thermal bending coefficients $\mathbf{W}^T$ are introduced as the out-of-plane analogs to the in-plane CTE's, and thus predict laminate curvatures as functions of temperature. In addition to variation in ply material properties and manufacturing variables, the influence of volume fraction variations is included in the analysis. Volume fraction is an important parameter because of its tendency to vary both within and between batches of materials and its large influence on laminate properties. The possibility that the ply angle variations are not independent is also included. Ply angle variations may become correlated due to certain manufacturing practices. The analysis is integrated into a simple, easy to use computer code which provides thorough statistical information about any user-defined general laminate.

Extensive parametric studies were performed to examine trends predicted by the model. The standard deviations of the thermal bending coefficients were studied as functions of layup. The analysis was also used to determine the relative importance of variations in the different ply material properties and manufacturing parameters to the variations in laminate properties.

In addition, experimental studies were completed to verify the analysis. Multiple specimens of different layups were exposed to varying temperatures, and out-of-plane deformations were measured. Both unsymmetric (with non-zero mean thermally induced out-of-plane deformation) and symmetric (which in theory do not deform out of plane, but in practice do, due to manufacturing and material variations) were tested.

Using this data, comparisons between the actual and predicted distributions of the thermal bending coefficients were made.

Previous work relevant to the problem is reviewed in Chapter 2. This includes both analytical and experimental studies of near-zero CTE composites, and background on the analytical tools used in the current work. A problem statement summarizing the present work is presented in Chapter 3. Chapter 4 establishes the analytical methodology. The experimental procedures used are described in Chapter 5. Results from experiments, as well as correlations of experimental data with model predictions and parametric studies are presented and discussed in Chapter 6. Finally, conclusions and recommendations for future work are presented in Chapter 7.

CHAPTER 2

BACKGROUND

Their potential for use in dimensionally stable applications has long been recognized as an important advantage of composite materials. Most recent studies conclude that composite materials should be used for applications where thermal deformations are critical, both for in-orbit structures [2-7], and ground-based structures such as optical benches [8]. Early works studied the possibility of dimensionally stable laminates and the implications of the concept for the design of stable structures. Many of these early studies concentrated on the prediction of CTE's on the ply and laminate level. On the experimental front, many studies have focused on dimensionally stable composite materials for specific applications. Other studies examined complicating factors such as deviations in curvature from shapes predicted by Classical Laminated Plate Theory (CLPT) for many unsymmetric laminates. More recent analytical work has examined statistical distributions of properties on ply, laminate, and complete structural levels. Bending deformations have been examined, but this phenomenon has not been integrated into a methodology for predicting statistical distributions of laminate properties.

2.1 EARLY ANALYTICAL WORK

There has been considerable work devoted to the prediction of ply and laminate properties based on properties of the fiber and matrix materials [9-15]. When attempting to design dimensionally stable structures, the requirement for accurate predictions becomes more demanding, as small errors can lead to a failure to meet functional requirements. Bowles and Tompkins [16] compared the unidirectional laminate longitudinal and transverse CTE predictions of several different analyses with each other and experimental data. The analyses included several different micromechanics methods, and two finite element methods developed by Bowles, which used different meshes and element geometries, for determining the thermal and mechanical response of unidirectional composites. They found that while all analyses predicted the longitudinal CTE well, there was considerable difficulty in predicting transverse CTE. Analytical sensitivity studies concluded that longitudinal CTE was most sensitive to longitudinal ply properties and transverse CTE was most sensitive to matrix properties. Sensitivity to volume fraction decreased as volume fraction increased. The volume fraction effects were not a major focus of the study, however, and the effects of manufacturing variations were not considered at all.

2.2 EARLY EXPERIMENTAL WORK

Several studies in dimensionally stable structures have examined the effect of different factors on CTE. Rogers *et al.* [17, 18] measured the CTE's of several different laminates as functions of temperature. While they mention that some of the specimens of the same layup had different CTE's, there is no attempt to explain the source of the differences. Jones *et al.* [3]

examined the effects of thermal cycling on two composite struts designed for the Space Station. They found that CLPT predicted the actual axial CTE of the specimens within 13 percent. Once again, this study showed differences between supposedly identical layups without any explanation.

One of the major difficulties in experimental work with near-zero CTE composites is the measurement of the CTE. The small magnitude of the CTE leads to extremely small deformations for reasonably sized test specimens, which places difficult requirements on the resolution of measurement equipment. Most experimenters use lasers to measure the deflections [3, 19, 20]. The advantages of laser measurements include increased resolution, reduction of creep and thermal lag effects, and elimination of contact fastening induced stresses. There are difficulties in using lasers, however, such as possible sensitivity of the lasers to temperature changes in the laser itself and the air between laser and specimen, and the fact that the surface finish of composite materials is often not well-suited to laser measurement [21]. Nevertheless, the advantages usually outweigh the drawbacks, so most researchers today use lasers to measure thermal deformations of composite materials, usually through extremely sensitive interferometer techniques. When the resolution required for longitudinal expansion measurement is not necessary, less accurate techniques are used. For instance, Doxsee and Springer [22] quantified thermally induced curvatures in composite shells by measuring the change in position of a laser spot along a wall as a specimen with a mirror attached to it deformed with temperature.

2.3 THERMAL BENDING

Thermally induced bending in composite materials has one of two origins. The first is a temperature gradient, which can also cause bending in isotropic materials. In an isothermal environment, bending can be caused by material asymmetry about the centerline. A classic example of this situation is the bimetallic strip problem, originally solved by Timoshenko [23]. Consisting of metals with different CTE's and stiffnesses bonded perfectly together, the bimetallic strip curves as the temperature changes from the bonding temperature. The amount of curvature increases as the temperature difference from the bonding temperature increases.

Composite laminates can also have curvatures as functions of temperature because of asymmetry about the centerline. This can be intentional, as in the case of an unsymmetric laminate, or unintentional, as in the case of slight layup errors causing asymmetry in the laminate. Laminates have zero curvature at the stress-free temperature, which is usually assumed to be the cure temperature (350°F (177 °C) for the AS4/3501-6 graphite/epoxy material system). Unsymmetric laminates are curved at room temperature, at which the difference from a manufacturing temperature of 350°F (177 °C) is -280°F (155 °C) . For laminates with a large degree of asymmetry, such as $[0/90]_T$, the large curvature at room temperature is unmistakable. In practice, many laminates, including nominally symmetric ones, are observed to have curvature at room temperature after manufacture.

CLPT predicts that certain types of unsymmetric laminates will have a saddle-shaped curvature at temperatures other than the stress-free temperature. In the case of many thin unsymmetric laminates, however, many experimenters observed that the shape at room temperature was a

right circular cylinder. In addition, some laminates exhibited two stable room-temperature cylindrical configurations. It was possible to switch from one stable configuration to the other by means of a snap-through behavior. Hyer first attempted to explain this oft-noted discrepancy between CLPT predictions and reality [24]. Each stable shape in the thinner laminates he produced had curvature in one direction close to that predicted by CLPT, while the other curvatures were zero. After noting that thicker laminates tended to conform to CLPT predictions in all directions, he proceeded to develop a Rayleigh-Ritz minimization of potential energy approach to predict the curvature behavior of square cross-ply laminates with different layups and side lengths [25, 26]. The difference between Hyer's approach and CLPT is the inclusion of large deflection behavior in the former. Out-of-plane deformations which are large in comparison to the laminate thickness are not accounted for in CLPT. While Hyer's analysis seems to explain the observed phenomenon well, it was not extended to general laminates, nor was any statistical information provided. The work played a key role, however, in explaining an often-seen behavior of unsymmetric laminates.

At approximately the same time as Hyer was completing his analysis of curvature shapes, Wong was attempting to explain the same phenomenon in unsymmetric laminates of the $[0_n/\theta_n]_T$ family [27]. The material system and cure cycle he used were the same as those used in the current work. Enough data was collected to establish some distribution information. Laminates studied by Hyer and Wong are used in the current study in order to allow direct comparisons with previous work.

The works of both Hyer and Wong examined laminates with a large degree of asymmetry, and the room-temperature curvatures of the specimens were visible to the unaided eye. Smaller, unintentional curvatures can exist

in laminates designed to be symmetric, but which in fact are somewhat asymmetric due to slight layup errors. For instance, a laminate designed as $[30/-30/0/-30/30]_T$ might actually be laid up as $[33/-27/0/-26/32]_T$. The actual laminate's curvature at room temperature in this case would not be as large as any of Hyer's specimens at room temperature, but could cause problems in a dimensionally critical application. If such a layup mistake occurred in the manufacture of a component for a satellite, there would be changes in component shape in the space environment relative to the room temperature assembly.

2.4 RECENT WORK

Substantial amounts of recent effort has focused on the statistical aspect of composite material properties. Tompkins and Funk [28] examined the sensitivity of laminate CTE to ply properties. In their study, the effect on laminate longitudinal CTE of changing thermoelastic properties by 10% from mean values was examined for several material systems and layups using CLPT. They found that the largest sensitivities of CTE were to ply CTE's and ply longitudinal stiffnesses. The effects of volume fraction were not considered. Hinckley [29] found that variations in CTE due to angle misalignment could be reduced by using a "rotate and fold" technique. In this method, ply angle variations are symmetric about the centerline and their effects thus cancel each other out. This technique has been verified through experimental testing.

McManus [30] developed a predictive methodology for laminate property means and standard deviations given distributions of ply material properties and manufacturing variables. The result was a computer model

based on CLPT and basic statistics. It was assumed that standard deviations were small so derivatives could be estimated by a numerical linearization around mean points, that mean laminate properties depended only on mean ply properties, and that all properties were independent normally distributed random variables. Volume fraction variations were not included because of fundamental difficulties with the formulation. The coupling between ply material properties introduced by volume fractions invalidates the independent properties assumption. The computer model developed by McManus was modified for the current work.

Hedgepeth [31] examined the influence of fabrication methods on antenna structures. His statistical analysis is proposed as a useful design tool in determining surface errors of different types of antenna structures. The surface error of the entire structure is found from a combination of the manufacturing tolerances of individual detailed parts. Material variations are ignored, and the only variables are the dimensions of truss members.

Sable [32] used the statistics methods and computer program developed by McManus, the fabrication influence on antenna accuracy of Hedgepeth, and a finite-element-based Monte Carlo methodology to determine sensitivities to many levels of detail in larger space structures. Specifically, he used the output of McManus' computer program as inputs to a finite element model of a parabolic reflector dish. The final outputs were variations in antenna performance parameters such as defocus, tilt, focal length, and surface roughness.

2.5 ANALYTICAL TOOLS

Several different analytical methods were used to obtain solutions in the present work, all of which are outlined in Chapter 4. The first group of tools were used in the analysis of the composite materials and the laminates built from them. Micromechanical relations were used to predict ply properties from fiber and matrix properties, and to form the material correlation coefficient matrix. After a survey of several different micromechanical formulations, that of Chamis [13] was chosen for the present work. The rationale behind this choice included tractability of the relations and consistency with available data for the AS4/3501-6 material system. The next step was to obtain laminate properties from ply properties and layup. The Classical Laminated Plate Theory used in this work is developed in Jones [33] and Tsai [34]. CLPT is also used to derive the thermal bending coefficients.

Micromechanics and CLPT were sufficient to calculate mean values for ply and laminate properties, but probability and statistics were needed to find the distributions. Hoel [35] gave an introduction to basic statistical and probabilistic methods. Hines and Montgomery [36] developed the relations for finding distributions of variables which are combinations of other variables. In the present work, these relations are used to find laminate property distributions from distributions of the material and manufacturing parametric.

The introduction of volume fraction as an input variable coupled ply material properties, so additional statistical methods were needed. Brownlee [37] rigorously derived the correlation coefficients between normally distributed random variables, although he did not give examples of practical use. Brownlee also developed the multivariate distribution, giving key

examples and visualization aids such as the three-dimensional hill representation of probability for the bivariate normal distribution, where the x and y axes are variables, and the z axis is probability. He also showed the statistical methods for calculating the correlation coefficients from data. Mendenhall [38] gave several practical examples of the use and interpretation of the correlation coefficients. More importantly, he developed equations with which the correlation coefficients could be calculated.

CHAPTER 3

APPROACH

3.1 PROBLEM STATEMENT

The objective of the present research is to develop an analytical methodology to predict means and standard deviations of laminate engineering properties from given means and standard deviations of ply material properties, fiber volume fractions, and manufacturing parameters. The ply material properties are the ply longitudinal and transverse stiffness E_l and E_t, major Poisson's ratio ν_{lt}, shear stiffness G_{lt}, longitudinal and transverse CTE's α_l and α_t, longitudinal and transverse coefficients of moisture expansion β_l and β_t, and fiber volume fraction k_f. The manufacturing parameters are the thicknesses t and layup angles θ of the plies, and the correlation coefficients between the ply angles. The laminate engineering properties of interest are laminate longitudinal stiffness E_{11}, transverse stiffness E_{22}, major Poisson's ratio ν, shear stiffness G_{12}, coefficients of thermal expansion $\boldsymbol{\alpha}$, coefficients of moisture expansion $\boldsymbol{\beta}$, thermal bending coefficients $\mathbf{W}^{\mathbf{T}}$, hygral bending coefficients $\mathbf{W}^{\mathbf{H}}$, and laminate volume fraction $\bar{k}_f$. Analytical modeling and experimental verification are used to achieve this research objective.

The aims of the analysis are to provide a capability for prediction of laminate property distributions given distributions of material properties and manufacturing variables, and to aid in identifying key factors to control in the production of dimensionally stable structures through sensitivity studies.

The current work differs from earlier work in several ways. A new laminate property, the thermal bending coefficient, is defined and calculated. The method incorporates several input parameters not previously considered. Volume fraction variations are included, which couple ply material properties. Inclusion of correlations between ply layup angles is also an option. Manufacturing techniques may result in ply angle correlations, either accidentally (e.g. consistent cutting errors) or by design (e.g. use of the rotate and fold technique).

The purpose of the experimental investigation is to provide a quantitative verification of the analysis, and to gain qualitative insights into the problem. There are several important features to the experimental investigation. The experimental test program is analysis-driven, in that the analytical methodology was used to design a test matrix which would show interesting trends. This allowed a systematic approach to the collection and analysis of experimental data. Trends due to changes in variables such as ply angle, laminate thickness, ply grouping, the addition of 0° and 90° plies, and stacking sequence were all studied. Finally, a greater amount of data is presented herein than in previous studies.

3.2 ANALYTICAL APPROACH

The analysis primarily uses a Classical Laminated Plate Theory (CLPT) approach coupled with simple statistical methods. All ply material properties and manufacturing parameters are assumed to be normally distributed random variables. Inputs to the analysis are means and standard deviations of ply material properties and manufacturing parameters. The mean laminate properties are found from the mean inputs using CLPT.

Sensitivity metrics are found by using a finite difference formulation to obtain derivatives of laminate properties with respect to input variables in a small region around the means. Simple statistical methods are used to calculate laminate standard deviations. The correlation coefficients between material properties, which are necessary when there are variations in volume fraction, are calculated from fiber and matrix properties using micromechanics and a Monte Carlo method to generate and correlate simulated data. Correlation coefficients between ply layup angles due to manufacturing techniques are included as an input option. Finally, a model is developed to analyze the behavior of specimens which undergo large deformations. This analysis uses a minimization of strain energy approach and principal curvatures to find the shapes of unsymmetric laminates as functions of temperature, material properties, and layup.

The analytical methodology is implemented in a set of computer codes. A parametric study is then used to determine the importance of the various input variables to laminate properties.

3.3 EXPERIMENTAL APPROACH

All laminates are manufactured at the MIT Technology Laboratory for Advanced Composites. The material system chosen is AS4/3501-6, because of the experience with this material in the laboratory. Sixteen different layups are used to identify the effects of layup angles, laminate thickness, ply placement, and ply grouping.

Five specimens 2.54 cm by 15.24 cm (1" by 6") are machined from each panel. Prior to testing, the specimens have thermocouples attached, and are desiccated in a postcure oven. Specimens are progressively heated from room

temperature to 100°C (212°F) in a thermal environment chamber. End displacements of the specimens, which are supported as cantilevered (clamped-free) beams, are measured with laser displacement sensors. The change of end displacements with temperature provides values of the thermal bending coefficients. Means and standard deviations of the thermal bending coefficients for each panel are calculated. The experimental data is correlated with the analytical predictions to verify the analytical methodology.

CHAPTER 4

ANALYTICAL METHODS

In this chapter the derivation and implementation of analyses to predict distributions of laminate engineering properties are presented. The primary analysis uses Classical Laminated Plate Theory (CLPT) and statistics to find laminate property means and standard deviations from material and manufacturing parameter means and standard deviations. Section 4.1 contains a review of CLPT relevant to the current problem. A new laminate property, the thermal bending coefficient, is defined in Section 4.2. Probabilistic methods used in the current work are introduced in Section 4.3. Micromechanics and methods for calculating material correlation coefficients are presented in Section 4.4, as are examples of angle correlation coefficient matrices. Section 4.5 contains a summary of the sensitivity metrics and a description of the implementation scheme. Finally, Section 4.6 presents an analysis of the large-deformation response of unsymmetric laminates. Previous work in the area of large deformations has been extended to general laminates by allowing non-zero midplane shear strain and shear CTE, and by considering twisting as well as bending curvatures.

4.1 CLASSICAL LAMINATED PLATE THEORY

Classical Laminated Plate Theory (CLPT) allows prediction of laminate elastic, thermoelastic, and hygroelastic properties from

manufacturing parameters and the material properties of individual plies. This section presents a review of the portions of CLPT relevant to the current work.

Several key assumptions are made in the development of CLPT: the thickness of the laminate is small compared to the other dimensions, strain varies linearly through the laminate thickness, and plane sections of the laminate remain plane and perpendicular to the midplane.

We consider a laminate aligned with a global coordinate system *xyz*. The laminate is made up of *nply* unidirectional plies. Ply properties are designated here by the subscript k, where k=1,2,...,*nply*. The plies have thickness t_k. The material axes of the plies, *ltz*, are rotated an angle θ_k relative to the laminate axes. Each ply has the following known material properties: longitudinal and transverse stiffness E_{lk} and E_{tk}, major Poisson's ratio ν_{ltk}, shear stiffness G_{ltk}, longitudinal and transverse CTE's α_{lk} and α_{tk}, longitudinal and transverse coefficients of moisture expansion β_{lk} and β_{tk}, and fiber volume fraction k_{fk}, where a subscript l designates a longitudinal property, and a subscript t designates a transverse property.

4.1.1 Constitutive Relations

For each ply, in ply coordinates, the constitutive equations are

$$\boldsymbol{\sigma} = \mathbf{Q}(\boldsymbol{\varepsilon} - \boldsymbol{\alpha}\Delta T - \boldsymbol{\beta}\Delta H) \tag{4.1}$$

where $\boldsymbol{\sigma}$ is the in-plane stress vector, $\mathbf{Q}$ is the reduced ply stiffness matrix, $\boldsymbol{\varepsilon}$ is the in-plane engineering strain vector, $\boldsymbol{\alpha}$ is the in-plane coefficient of thermal expansion vector, $\boldsymbol{\beta}$ is the in-plane coefficient of hygral expansion vector, ΔT is the difference in temperature from the stress-free temperature, and ΔH is the moisture content. The Kirchoff-Love hypothesis on plate strain

is that total strain $\boldsymbol{\varepsilon}$ includes contributions from the laminate midplane strain $\boldsymbol{\varepsilon}^{\circ}$ and the laminate curvature $\boldsymbol{\kappa}$:

$$\boldsymbol{\varepsilon} = \boldsymbol{\varepsilon}^{\circ} + \boldsymbol{\kappa} z \tag{4.2}$$

The reduced ply stiffness matrix for ply k is a symmetric 3x3 matrix. Using the usual notation [33], the indices of the rows and columns take the values of 1, 2, and 6, and

$$\begin{aligned} Q_{11(k)} &= \frac{E_{lk}}{D_k} \qquad Q_{12(k)} = \frac{\nu_{ltk} E_{tk}}{D_k} \\ Q_{22(k)} &= \frac{E_{tk}}{D_k} \qquad Q_{66(k)} = G_{ltk} \\ Q_{16(k)} &= Q_{26(k)} = 0 \\ D_k &= 1 - \nu_{ltk}^2 \frac{E_{tk}}{E_{lk}} \end{aligned} \tag{4.3}$$

The vectors of CTE's and coefficients of moisture expansion (CME's) for each ply in ply coordinates are

$$\boldsymbol{\alpha}_k = \begin{Bmatrix} \alpha_{lk} \\ \alpha_{tk} \\ 0 \end{Bmatrix} \qquad \boldsymbol{\beta}_k = \begin{Bmatrix} \beta_{lk} \\ \beta_{tk} \\ 0 \end{Bmatrix} \tag{4.4 a, b}$$

In finding laminate properties, the ply material properties must first be transformed from individual ply coordinates to laminate coordinates. Vectors and matrices in laminate coordinates are denoted by a bar over the symbol. Material properties for each ply are transformed with the transformation matrix $\mathbf{T}_k$:

$$\mathbf{T}_k = \begin{bmatrix} \cos^2\theta_k & \sin^2\theta_k & 2\sin\theta_k\cos\theta_k \\ \sin^2\theta_k & \cos^2\theta_k & -2\sin\theta_k\cos\theta_k \\ -\sin\theta_k\cos\theta_k & \sin\theta_k\cos\theta_k & \cos^2\theta_k - \sin^2\theta_k \end{bmatrix} \tag{4.5}$$

where θ_k is the layup angle of ply k. The ply reduced stiffness in laminate coordinates is found from $\mathbf{Q}_k$ by transformation of coordinates [33].

$$\overline{\mathbf{Q}}_k = \mathbf{T}_k^{-1}\mathbf{Q}_k\mathbf{T}_k^{-\mathrm{T}} \tag{4.6}$$

where a superscript T denotes a matrix transpose. The transformations for the vectors of stress, strain, CTE's and CME's are given in Eqs. 4.7–4.10.

$$\overline{\boldsymbol{\sigma}} = \mathbf{T}_k^{-1}\boldsymbol{\sigma} \tag{4.7}$$

$$\overline{\boldsymbol{\varepsilon}} = \mathbf{T}_k^{\mathrm{T}}\boldsymbol{\varepsilon} \tag{4.8}$$

$$\overline{\boldsymbol{\alpha}}_k = \mathbf{T}_k^{\mathrm{T}}\boldsymbol{\alpha}_k \tag{4.9}$$

$$\overline{\boldsymbol{\beta}}_k = \mathbf{T}_k^{\mathrm{T}}\boldsymbol{\beta}_k \tag{4.10}$$

Transforming the ply constitutive equations of Eqs. 4.1 to the laminate coordinate system gives

$$\overline{\boldsymbol{\sigma}} = \overline{\mathbf{Q}}(\overline{\boldsymbol{\varepsilon}} - \overline{\boldsymbol{\alpha}}\Delta T - \overline{\boldsymbol{\beta}}\Delta H) \tag{4.11}$$

We then integrate through the thickness of the laminate. The total thickness of the laminate is h, and the origin of the z axis is located at the laminate midplane.

$$\int_{-h/2}^{h/2}\overline{\boldsymbol{\sigma}}dz = \int_{-h/2}^{h/2}\overline{\mathbf{Q}}\boldsymbol{\varepsilon}^{\circ}dz + \int_{-h/2}^{h/2}\overline{\mathbf{Q}}\boldsymbol{\kappa}zdz - \int_{-h/2}^{h/2}\overline{\mathbf{Q}}\overline{\boldsymbol{\alpha}}\Delta Tdz - \int_{-h/2}^{h/2}\overline{\mathbf{Q}}\overline{\boldsymbol{\beta}}\Delta Hdz \tag{4.12}$$

We make the following definitions for the resultant forces **N**, extensional stiffness matrix **A**, coupling stiffnesses **B**, bending stiffnesses **D**, thermal forces $\mathbf{N}^{\mathbf{T}}$, and hygral forces $\mathbf{N}^{\mathbf{H}}$:

$$\mathbf{N} = \int_{-h/2}^{h/2}\overline{\boldsymbol{\sigma}}dz \tag{4.13}$$

$$\mathbf{A} = \int_{-h/2}^{h/2}\overline{\mathbf{Q}}dz \tag{4.14}$$

$$\mathbf{B} = \int_{-h/2}^{h/2}\overline{\mathbf{Q}}zdz \tag{4.15}$$

$$\mathbf{D} = \int_{-h/2}^{h/2} \overline{\mathbf{Q}} z^2 dz \tag{4.16}$$

$$\mathbf{N}^{\mathrm{T}} = \int_{-h/2}^{h/2} \overline{\mathbf{Q}}\,\overline{\boldsymbol{\alpha}} \Delta T dz \tag{4.17}$$

$$\mathbf{N}^{\mathrm{H}} = \int_{-h/2}^{h/2} \overline{\mathbf{Q}}\,\overline{\boldsymbol{\beta}} \Delta H dz \tag{4.18}$$

Using Eqs. 4.13–4.18, Eq. 4.12 can be rewritten as

$$\mathbf{N} = \mathbf{A}\boldsymbol{\varepsilon}^{\mathrm{o}} + \mathbf{B}\boldsymbol{\kappa} - \mathbf{N}^{\mathrm{T}} - \mathbf{N}^{\mathrm{H}} \tag{4.19}$$

Rearranging gives

$$\mathbf{N} + \mathbf{N}^{\mathrm{T}} + \mathbf{N}^{\mathrm{H}} = \mathbf{A}\boldsymbol{\varepsilon}^{\mathrm{o}} + \mathbf{B}\boldsymbol{\kappa} \tag{4.20}$$

Similarly, moments are calculated by multiplying Eq. 4.11 by the out-of-plane coordinate z and integrating through the thickness.

$$\int_{-h/2}^{h/2} \overline{\boldsymbol{\sigma}} z dz = \int_{-h/2}^{h/2} \overline{\mathbf{Q}} \boldsymbol{\varepsilon}^{\mathrm{o}} z dz + \int_{-h/2}^{h/2} \overline{\mathbf{Q}} \boldsymbol{\kappa} z^2 dz - \int_{-h/2}^{h/2} \overline{\mathbf{Q}}\,\overline{\boldsymbol{\alpha}} \Delta T z dz - \int_{-h/2}^{h/2} \overline{\mathbf{Q}}\,\overline{\boldsymbol{\beta}} \Delta H z dz \tag{4.21}$$

The resultant moments **M**, thermal moments $\mathbf{M}^{\mathrm{T}}$, and hygral moments $\mathbf{M}^{\mathrm{H}}$ are defined as

$$\mathbf{M} = \int_{-h/2}^{h/2} \overline{\boldsymbol{\sigma}} z dz \tag{4.22}$$

$$\mathbf{M}^{\mathrm{T}} = \int_{-h/2}^{h/2} \overline{\mathbf{Q}}\,\overline{\boldsymbol{\alpha}} \Delta T z dz \tag{4.23}$$

$$\mathbf{M}^{\mathrm{H}} = \int_{-h/2}^{h/2} \overline{\mathbf{Q}}\,\overline{\boldsymbol{\beta}} \Delta H z dz \tag{4.24}$$

Using Eqs. 4.15, 4.16, 4.22, 4.23, and 4.24 in Eq. 4.21 gives

$$\mathbf{M} = \mathbf{B}\boldsymbol{\varepsilon}^{\mathrm{o}} + \mathbf{D}\boldsymbol{\kappa} - \mathbf{M}^{\mathrm{T}} - \mathbf{M}^{\mathrm{H}} \tag{4.25}$$

or

$$\mathbf{M}+\mathbf{M}^{T}+\mathbf{M}^{H}=\mathbf{B}\boldsymbol{\varepsilon}^{o}+\mathbf{D}\boldsymbol{\kappa} \tag{4.26}$$

Combining Eqs. 4.20 and 4.26 in matrix form yields

$$\begin{Bmatrix}\mathbf{N}+\mathbf{N}^{T}+\mathbf{N}^{H}\\ \mathbf{M}+\mathbf{M}^{T}+\mathbf{M}^{H}\end{Bmatrix}=\begin{bmatrix}\mathbf{A} & \mathbf{B}\\ \mathbf{B} & \mathbf{D}\end{bmatrix}\begin{Bmatrix}\boldsymbol{\varepsilon}^{o}\\ \boldsymbol{\kappa}\end{Bmatrix} \tag{4.27}$$

Inverting Eq. 4.27 gives

$$\begin{Bmatrix}\boldsymbol{\varepsilon}^{o}\\ \boldsymbol{\kappa}\end{Bmatrix}=\begin{bmatrix}\mathbf{A} & \mathbf{B}\\ \mathbf{B} & \mathbf{D}\end{bmatrix}^{-1}\begin{Bmatrix}\mathbf{N}+\mathbf{N}^{T}+\mathbf{N}^{H}\\ \mathbf{M}+\mathbf{M}^{T}+\mathbf{M}^{H}\end{Bmatrix} \tag{4.28}$$

For convenience in the current work, we introduce another notation for the inverse laminate stiffness matrix in Eq. 4.28.

$$\begin{bmatrix}\mathbf{a}^{*} & \mathbf{b}^{*}\\ \mathbf{b}^{*T} & \mathbf{d}^{*}\end{bmatrix}=\begin{bmatrix}\mathbf{A} & \mathbf{B}\\ \mathbf{B} & \mathbf{D}\end{bmatrix}^{-1} \tag{4.29}$$

With this notation, Eq. 4.28 becomes

$$\begin{Bmatrix}\boldsymbol{\varepsilon}^{o}\\ \boldsymbol{\kappa}\end{Bmatrix}=\begin{bmatrix}\mathbf{a}^{*} & \mathbf{b}^{*}\\ \mathbf{b}^{*T} & \mathbf{d}^{*}\end{bmatrix}\begin{Bmatrix}\mathbf{N}+\mathbf{N}^{T}+\mathbf{N}^{H}\\ \mathbf{M}+\mathbf{M}^{T}+\mathbf{M}^{H}\end{Bmatrix} \tag{4.30}$$

where $\mathbf{a}^{*}$, $\mathbf{b}^{*}$, and $\mathbf{d}^{*}$ are 3x3 matrices whose indices follow the previously mentioned convention, taking the values 1, 2, and 6.

4.1.2 Laminate Engineering Constants

The mean laminate engineering constants and their standard deviations are the outputs of the analytical methodology of the current work. The total laminate thickness h is the sum of the individual ply thicknesses t_k.

$$h=\sum_{k=1}^{nply}t_k \tag{4.31}$$

The laminate stiffnesses are calculated using elements of the inverted reduced laminate stiffness matrix and the total thickness of the laminate. E_{11} is longitudinal laminate modulus, E_{22} is transverse laminate modulus, ν_{12} is

laminate major Poisson's ratio, and G_{12} is laminate longitudinal shear modulus.

$$E_{11} = \frac{1}{a_{11}^* h} \tag{4.32}$$

$$E_{22} = \frac{1}{a_{22}^* h} \tag{4.33}$$

$$\nu_{12} = \frac{a_{12}^*}{a_{11}^*} \tag{4.34}$$

$$G_{12} = \frac{1}{a_{66}^* h} \tag{4.35}$$

The laminate volume fraction $\bar{k}_f$ is the average of the ply volume fractions, as in Eq. 4.36

$$\bar{k}_f = \frac{\sum_{k=1}^{nply} k_{fk} t_k}{h} \tag{4.36}$$

Laminate CTE's and CME's are found as follows. For a temperature change not dependent on position in the laminate, setting **N**, **M**, $\mathbf{N}^{\mathbf{H}}$ and $\mathbf{M}^{\mathbf{H}}$ to zero, substituting the definition of $\mathbf{N}^{\mathbf{T}}$ and $\mathbf{M}^{\mathbf{T}}$ from Eqs. 4.17 and 4.23 into Eq. 4.30 and replacing the integral through the thickness with an equivalent summation on the plies shows the thermally induced deformation to be ΔT multiplied by the laminate CTE's, which are given by

$$\bar{\boldsymbol{\alpha}} = \mathbf{a}^* \sum_{k=1}^{nply} \bar{\mathbf{Q}}_k \bar{\boldsymbol{\alpha}}_k t_k + \mathbf{b}^* \sum_{k=1}^{nply} \bar{\mathbf{Q}}_k \bar{\boldsymbol{\alpha}}_k t_k \bar{z}_k \tag{4.37}$$

Similarly,

$$\bar{\boldsymbol{\beta}} = \mathbf{a}^* \sum_{k=1}^{nply} \bar{\mathbf{Q}}_k \bar{\boldsymbol{\beta}}_k t_k + \mathbf{b}^* \sum_{k=1}^{nply} \bar{\mathbf{Q}}_k \bar{\boldsymbol{\beta}}_k t_k \bar{z}_k \tag{4.38}$$

where $\bar{z}_k$ is the z coordinate of the midplane of the kth ply. The second terms of these definitions are zero for symmetric laminates and are often omitted.

The methods of CLPT provide a methodology for calculating laminate properties. CLPT is extended in Section 4.2 to define new laminate properties, the thermal and hygral bending coefficients.

4.2 DERIVATION OF THERMAL BENDING COEFFICIENT

This section presents a derivation of the thermal and hygral bending coefficients $\mathbf{W}^T$ and $\mathbf{W}^H$. The derivation begins with Eq. 4.30 in Section 4.1. For the case of no mechanical or moisture loading, **N**, **M** (mechanical forces and moments), $\mathbf{N}^H$ and $\mathbf{M}^H$ (hygral forces and moments), are all zero. Deformation is then caused only by temperature. For a temperature change not dependent on position in the laminate, substituting the definition of $\mathbf{N}^T$ and $\mathbf{M}^T$ from Eqs. 4.17 and 4.23 into Eq. 4.30 and replacing the integral through the thickness with an equivalent summation on the plies shows the thermally induced curvature to be

$$\boldsymbol{\kappa}^T = \left[\mathbf{b}^{*T}\sum \overline{\mathbf{Q}}_k \overline{\boldsymbol{\alpha}}_k t_k + \mathbf{d}^*\sum \overline{\mathbf{Q}}_k \overline{\boldsymbol{\alpha}}_k t_k \bar{z}_k\right]\Delta T \tag{4.39}$$

The terms inside the brackets are only dependent on material properties and geometry, so one can define a laminate property

$$\mathbf{W}^T \equiv \mathbf{b}^{*T}\sum \overline{\mathbf{Q}}_k \overline{\boldsymbol{\alpha}}_k t_k + \mathbf{d}^*\sum \overline{\mathbf{Q}}_k \overline{\boldsymbol{\alpha}}_k t_k \bar{z}_k \tag{4.40}$$

where $\mathbf{W}^T$ is the thermal bending coefficient vector. In a case where there is no mechanical or temperature loading and the moisture distribution through the laminate is constant, the hygrally induced curvature is

$$\boldsymbol{\kappa}^H = \left[\mathbf{b}^{*T}\sum \overline{\mathbf{Q}}_k \overline{\boldsymbol{\beta}}_k t_k + \mathbf{d}^*\sum \overline{\mathbf{Q}}_k \overline{\boldsymbol{\beta}}_k t_k \bar{z}_k\right]\Delta H \tag{4.41}$$

hence

$$\mathbf{W}^H \equiv \mathbf{b}^{*T}\sum \overline{\mathbf{Q}}_k \overline{\boldsymbol{\beta}}_k t_k + \mathbf{d}^*\sum \overline{\mathbf{Q}}_k \overline{\boldsymbol{\beta}}_k t_k \bar{z}_k \tag{4.42}$$

where $\mathbf{W}^H$ is the hygral bending coefficient vector. $\mathbf{W}^T$ and $\mathbf{W}^H$ are new laminate properties, which are the out-of-plane analogs to the in-plane vectors of coefficients of thermal and hygral expansion α and β, respectively.

The laminate engineering constants, as defined in Subsection 4.1.2, are usually defined only for symmetric laminates. In contrast, in a perfectly symmetric laminate, $\mathbf{W}^T$ and $\mathbf{W}^H$ are both zero.

4.3 PROBABILISTIC METHODS

The objective of this analysis is to calculate distributions of laminate properties based on distributions of ply material and manufacturing parameters. The methods used to achieve this objective are described in the next three sections. The simple statistical methods used are presented in Section 4.3. The calculations are all straightforward, except for the need to calculate correlation coefficients between some ply material and manufacturing parameters under some circumstances. Fortunately, these correlation coefficients can be calculated separately, as described in Section 4.4. The implementation of the analytical method in the VARBEND computer program is discussed in Section 4.5.

The mean laminate properties are calculated with CLPT using the mean input parameters, as outlined in Sections 4.1 and 4.2. The laminate properties, collectively referred to herein as Y_i where i=1,2,...,17, are defined in Table 4.1. The input parameters, collectively designated herein as X_j, are shown in Table 4.2.

Table 4.1 Laminate Properties

	Symbol	Property
Y_1	E_{11}	Longitudinal Modulus
Y_2	E_{22}	Transverse Modulus
Y_3	ν_{12}	Major Poisson's Ratio
Y_4	G_{12}	Shear Modulus
Y_5	α_{11}	Longitudinal Coef. of Thermal Expansion
Y_6	α_{22}	Transverse CTE
Y_7	α_{12}	Shear CTE
Y_8	β_{11}	Longitudinal Coef. of Moisture Expansion
Y_9	β_{22}	Transverse CME
Y_{10}	β_{12}	Shear CME
Y_{11}	$\bar{k}_f$	Fiber Volume Fraction
Y_{12}	W_1^T	Longitudinal Coef. of Thermal Bending
Y_{13}	W_2^T	Transverse CTB
Y_{14}	W_6^T	Shear CTB
Y_{15}	W_1^H	Longitudinal Coef. of Hygral Bending
Y_{16}	W_2^H	Transverse CHB
Y_{17}	W_6^H	Shear CHB

Table 4.2 Input Parameters

	Symbol	Name
X_1	t_1	Thickness of ply 1
. . .		
X_{nply}	t_{npl}	Thickness of ply *nply*
X_{nply+1}	θ_1	Angle of ply 1
. . .		
X_{2nply}	θ_{nply}	Angle of ply *nply*
$X_{2nply+1}$	E_l	Ply Longitudinal Modulus
$X_{2nply+2}$	E_t	Ply Transverse Modulus
$X_{2nply+3}$	ν_{lt}	Ply Major Poisson's Ratio
$X_{2nply+4}$	G_{lt}	Ply Shear Modulus
$X_{2nply+5}$	α_l	Ply Longitudinal CTE
$X_{2nply+6}$	α_t	Ply Transverse CTE
$X_{2nply+7}$	β_l	Ply Longitudinal CME
$X_{2nply+8}$	β_t	Ply Transverse CME
$X_{2nply+9}$	k_f	Ply Fiber Volume Fraction

This is for a laminate with *nply* plies.
The last 9 entries are repeated (with the index incremented by 9) for each additional material used.

Standard deviations of laminate properties are somewhat more difficult to determine. McManus developed a method for laminate distribution predictions upon which the current analysis is based. In his development, McManus assumed that all ply material properties and manufacturing parameters were independent normally distributed random variables. The laminate properties calculated were also normally distributed random variables. In addition, standard deviations were assumed to be small enough that derivatives could be accurately calculated using numerical methods.

In the current work, the method is extended to include non-independent input parameters. The laminate standard deviations are calculated from ply material properties and manufacturing parameters. The input variables and laminate properties are assumed to be normally distributed random variables, and variations are assumed to be small. The laminate property standard deviations are found from

$$\hat{\sigma}_{Yi}^2 = \sum_{j=1}^{n} \sum_{k=1}^{n} \frac{\partial Y_i}{\partial X_j} \frac{\partial Y_i}{\partial X_k} c_{jk} \hat{\sigma}_{Xj} \hat{\sigma}_{Xk} \tag{4.43}$$

where the derivatives are changes in laminate properties with respect to material and geometric properties, $\hat{\sigma}_{Xj}$ is the standard deviation of input parameter X_j, $\hat{\sigma}_{Yi}$ is the standard deviation of laminate property Y_i, and c_{jk} is the correlation coefficient between input parameters X_j and X_k. The notation for standard deviation in statistical literature is usually σ, but $\hat{\sigma}$ is used in the current work to avoid confusion between standard deviations and stresses. When the input parameters are independent, the correlation coefficients are either zero (for $j \neq k$) or one.

The derivatives in Eq. 4.43 are calculated by assuming the laminate property distributions can be approximated as linear within one standard

deviation of the mean. This assumption requires that the standard deviations of the input parameters be small. Large variations in the input parameters would invalidate this assumption because of the generally nonlinear relations between the laminate properties and the input parameters. For the purposes of this analysis, "small" is defined to be small enough that the linearity assumption on the laminate property distributions remain valid. The derivatives are calculated by a finite difference approximation as in Eq. 4.44

$$\frac{\partial Y_i}{\partial X_j} = \frac{Y_i(X_1, X_2, ..., X_j + \hat{\sigma}_{Xj}, ..., X_n) - Y_i(X_1, X_2, ..., X_j - \hat{\sigma}_{Xj}, ..., X_n)}{2\hat{\sigma}_{Xj}} \tag{4.44}$$

where $Y_i(X_1, X_2, ..., X_n)$ is the value of laminate property Y_i calculated by CLPT for the ply properties and manufacturing parameters X_j.

When variation in volume fraction is considered as an input (such as transverse modulus), or when there are known correlations between the errors in input parameters such as the angles in the layups, the input parameters can no longer be assumed to be independent. The correlation coefficients in Eq. 4.43 then need to be calculated. The approach used in the current work is to assume all correlation coefficients can be found separately for any given material or manufacturing method. Then, for any given laminate, the laminate property distributions can be found from Eqs. 4.43 and 4.44 quickly and easily. The correlation coefficients are discussed further in the next section.

4.4 CORRELATION COEFFICIENTS

The original development of McManus assumed the input parameters were independent, so there was no coupling between them. Volume fraction

variations were not included. As will be seen in Subsection 4.4.1, all ply material properties depend on the volume fraction, so variations in volume fractions will cause variations in all ply material properties. This effect means that all ply properties are coupled to each other. There is a strong motivation to include volume fraction as an input parameter, for it is one of the measurable properties most likely to vary within and between finished composite laminates. As will be seen in Chapter 6, volume fraction variations are a strong contributor to variations in the laminate properties. Correlation coefficients must also be included in the analysis if the ply angle variations are coupled. The couplings in a real laminate can be inadvertent, as in systematic cutting or layup errors. They can also be purposeful, as in the "rotate and fold" technique, wherein plies are cut and laid up such that errors will nominally cancel each other. Methods for the calculation of material and angle correlation coefficients are developed in the following subsections.

4.4.1 Micromechanical Relations

To find the correlation coefficients between material properties, a set of micromechanical relations is necessary. Micromechanical equations relate fiber elastic and hygrothermal properties, matrix elastic and hygrothermal properties, and volume fraction to ply elastic and hygrothermal properties. Several different approaches to deriving micromechanics equations exist in the literature. While there is general agreement on some methods, such as a rule of mixtures approach to longitudinal ply stiffness, methods for finding other properties, especially those in the transverse ply direction, are vigorously debated. Here, the relations of Chamis are used. The rationale behind this choice includes tractability in the formulation of the relations, which eliminates the self-consistent method and finite element methods, and

consistency with known properties of the AS4/3501-6 graphite/epoxy material system used in the experimental investigation of the present work. Chamis' micromechanics relations are listed in Eqs. 4.45 to 4.52, with slight changes in notation to avoid confusion in the current work. In the micromechanics equations, a subscript *f* designates a fiber property, *m* a matrix property, *l* a longitudinal ply property, and *t* a transverse ply property.

$$E_l = k_f E_{f11} + (1 - k_f) E_m \tag{4.45}$$

$$E_t = \frac{E_m}{1 - \sqrt{k_f}\left(1 - \frac{E_m}{E_{f22}}\right)} \tag{4.46}$$

$$\nu_{lt} = k_f \nu_{f12} + (1 - k_f) \nu_m \tag{4.47}$$

$$G_{lt} = \frac{G_m}{1 - \sqrt{k_f}\left(1 - \frac{G_m}{G_{f12}}\right)} \tag{4.48}$$

$$\alpha_l = \frac{k_f \alpha_{f11} E_{f11} + (1 - k_f) \alpha_m E_m}{E_l} \tag{4.49}$$

$$\alpha_t = \alpha_{f22}\sqrt{k_f} + (1 - \sqrt{k_f})\left(1 + \frac{k_f \nu_m E_{f11}}{E_l}\right)\alpha_m \tag{4.50}$$

$$\beta_l = \beta_m (1 - k_f)\frac{E_m}{E_l} \tag{4.51}$$

$$\beta_t = \beta_m (1 - \sqrt{k_f})\left[1 + \frac{\sqrt{k_f}(1 - \sqrt{k_f})E_m}{\sqrt{k_f}E_t + (1 - \sqrt{k_f})E_m}\right] \tag{4.52}$$

4.4.2 Analytical Approach to Material Coupling Coefficients

One way to calculate the coupling coefficients is to assume the input parameters are sets of bivariate normal distributions. Analytical solutions

exist for the coupling coefficients in this case. The coupling coefficients are found to be

$$c_{jk} = \frac{\left[\mathrm{E}(X_k \mid X_j) - \overline{X}_k\right]\hat{\sigma}_{Xj}}{(X_j - \overline{X}_j)\hat{\sigma}_{Xk}} \tag{4.53}$$

where $\mathrm{E}(X_k \mid X_j)$ is the expected value of ply property X_k given a known value for another ply property X_j, and $\overline{X}_j$ is the mean of ply property X_j. The couplings between ply properties in Eq. 4.53 can conceptually be derived from micromechanics relations. In practice, the algebra proves intractable in all but a few cases.

For those cases where the algebra proves tractable (the couplings between volume fraction and the other ply material properties), the following methodology is used. It is assumed that means and standard deviations of ply stiffnesses, ply hygrothermal properties, matrix stiffnesses, matrix hygrothermal properties, and volume fraction are known. Data is much more readily available for these properties than for fiber stiffnesses and fiber hygrothermal properties. In addition, some fiber properties (such as transverse modulus) are extremely difficult to obtain experimentally. Ply material properties for the AS4/3501-6 graphite/epoxy material system used in the current work are given in Table 4.3. Matrix material properties are given in Table 4.4. Each of the micromechanics relations in Eqs. 4.45–4.50 is rearranged algebraically to find fiber stiffnesses and CTE's resulting in Eqs. 4.54–4.59. Fiber CME's are assumed to be zero.

$$E_{f11} = \frac{E_l - E_m}{k_f} + E_m \tag{4.54}$$

$$E_{f22} = \frac{\sqrt{k_f}}{\dfrac{1}{E_t} - \dfrac{(1-\sqrt{k_f})}{E_m}} \tag{4.55}$$

Table 4.3 Mean Ply Properties for AS4/3501-6

Property	Symbol	Value
Ply Longitudinal Modulus	E_l	20.59 Msi
Ply Transverse Modulus	E_t	1.42 Msi
Ply Major Poisson's Ratio	ν_{lt}	0.30
Ply Shear Modulus	G_{lt}	0.87 Msi
Ply Longitudinal CTE	α_l	-0.167 με/°F
Ply Transverse CTE	α_t	15.6 με/°F
Ply Longitudinal CME	β_l	0
Ply Transverse CME	β_t	0.05/%M
Ply Fiber Volume Fraction	k_f	0.62

Table 4.4 Matrix Properties

Property	Symbol	Value
Tensile modulus	E_m	0.50 Msi
Poisson's ratio	ν_m	0.35
Shear modulus	G_m	0.185 Msi
Thermal exp. coef.	α_m	36 με/°F
Moisture exp. coef.	β_m	0.33/%M

$$\nu_{f12} = \frac{\nu_{lt} - \nu_m}{k_f} + \nu_m \tag{4.56}$$

$$G_{f12} = \frac{\sqrt{k_f}}{\frac{1}{G_{lt}} - \frac{(1-\sqrt{k_f})}{G_m}} \tag{4.57}$$

$$\alpha_{f11} = \frac{\alpha_l E_l - (1-k_f)\alpha_m E_m}{k_f E_{f11}} \tag{4.58}$$

$$\alpha_{f22} = \frac{\alpha_t - (1-\sqrt{k_f})\left(1 + \frac{k_f \nu_m E_{f11}}{E_l}\right)\alpha_m}{\sqrt{k_f}} \tag{4.59}$$

Calculated AS4 graphite fiber properties are presented in Table 4.5. Once the fiber properties are calculated, the ply volume fraction is incremented by one standard deviation.

$$k_f' = k_f + \hat{\sigma}_{k_f} \tag{4.60}$$

This incremented ply volume fraction is used to calculate incremented ply material properties, which correspond to $\mathrm{E}(X_k \mid X_j)$ in Eq. 4.53. For instance, the incremented ply longitudinal modulus is

$$E_l' = k_f' E_{f11} + (1-k_f')E_m \tag{4.61}$$

Following Eq. 4.53, the mean ply material property is subtracted from the incremented ply material property, and the result divided by the increment in volume fraction and multiplied by the ratio of standard deviations. In the example of ply longitudinal modulus, the result is Eq. 4.62, where $c_{E_l k_f}$ is the material correlation coefficient between tensile modulus and fiber volume fraction.

$$c_{E_l k_f} = \frac{E_l' - E_l}{k_f' - k_f} \frac{\hat{\sigma}_{k_f}}{\hat{\sigma}_{E_l}} \tag{4.62}$$

Table 4.5 Calculated AS4 Fiber Properties

Property	Symbol	Value
Long. tensile modulus	E_{f11}	34.9 Msi
Transv. tensile modulus	E_{f22}	2.5 Msi
Long. Poisson's ratio	ν_{f12}	0.19
Long. shear modulus	G_{f12}	5.0 Msi
Long. th. exp. coef.	α_{f11}	-0.62 με/°F
Transv. th. exp. coef.	α_{f22}	3.1 με/°F

Just as in the calculation of derivatives of laminate properties with respect to input parameters, this method assumes that the relations between ply material properties can be approximated as linear in the region surrounding the mean values, so standard deviations must be small.

While the analytical method for calculating material correlation coefficients works well for the example of coupling between ply longitudinal modulus and ply volume fraction, the algebra becomes intractable for any correlation coefficients except those involving volume fraction as one of the parameters. Thus another method for calculating material correlation coefficients is needed.

4.4.3 Simulated Data Approach to Material Coupling Coefficients

To calculate all required correlation coefficients, a simulated data method was developed. The approach uses random number generation, micromechanics, and statistics to calculate the correlation coefficients numerically. This method is implemented in a Matlab [39] script.

The simulated data approach begins with fiber and matrix material properties, and fiber volume fraction. All of these variables are assumed to be independent normally distributed random variables. Sets of these variables are randomly selected from their distributions. These sets are then used in the micromechanics relations to yield sets of ply material properties. One hundred thousand sets of ply simulated data are generated in this manner. The simulated ply data is then used to find the correlation coefficients using Eq. 4.63.

$$c_{jk} = \frac{\sum_{i=1}^{100000}(X_{ij} - \overline{X}_j)(X_{ik} - \overline{X}_k)}{\sqrt{\sum_{i=1}^{100000}(X_{ij} - \overline{X}_j)^2 \sum_{i=1}^{100000}(X_{ik} - \overline{X}_k)^2}} \tag{4.63}$$

where X_{ij} is the ith randomly generated value for ply property X_j, $\overline{X}_j$ is the mean of ply property X_j, X_{ik} is the ith randomly generated value for ply property X_k, and $\overline{X}_k$ is the mean of ply property X_k. A copy of the Matlab script used to generate the correlation coefficients is in Appendix A. The mean fiber and matrix properties used are those of AS4 fiber and intermediate modulus high strength epoxy matrix as listed in Tables 4.4 and 4.5. Standard deviations are assumed to be 2% of the mean values in all cases. This assumption yields ply property standard deviations similar to measured values for the AS4/3501-6 material system. These results were checked against those cases where the correlation coefficients could be calculated directly using Eq. 4.53. Results from the analytical and simulated data approaches in these cases correlated very well.

It was found that the correlation coefficients were relatively constant over a range of reasonable fiber and matrix properties and volume fractions for a given material. Large changes in material properties can cause significant changes in the material correlation coefficient matrix, however. For instance, the use of fibers notably different from the AS4 fibers used throughout the current work would result in a notably different material correlation coefficient matrix. Therefore, the simulated data method should be used to recalculate material correlation coefficient matrices for material systems notably different from AS4/3501-6.

There are several notable features of the correlation coefficient matrix, which is presented in Table 4.6 for the AS4/3501-6 material system. The diagonal elements have a value of 1 and the matrix is symmetric. The

Table 4.6 Correlation Coefficient Matrix for AS4/3501-6

$$
\mathbf{c} = \begin{array}{c} \begin{matrix} E_l & E_t & \nu_{lt} & G_{lt} & \alpha_l & \alpha_t & \beta_l & \beta_t & k_f \end{matrix} \\ \begin{bmatrix} 1.00 & 0.55 & -0.37 & 0.64 & -0.66 & -0.54 & -0.81 & -0.66 & 0.70 \\ 0.55 & 1.00 & -0.43 & 0.70 & -0.47 & -0.58 & -0.59 & -0.73 & 0.77 \\ -0.37 & -0.43 & 1.00 & -0.51 & 0.38 & 0.43 & 0.49 & 0.52 & -0.54 \\ 0.64 & 0.70 & -0.51 & 1.00 & -0.65 & -0.66 & -0.81 & -0.85 & 0.90 \\ -0.66 & -0.47 & 0.39 & -0.65 & 1.00 & 0.81 & 0.76 & 0.68 & -0.73 \\ -0.54 & -0.58 & 0.43 & -0.66 & 0.81 & 1.00 & 0.67 & 0.71 & -0.75 \\ -0.81 & -0.59 & 0.49 & -0.81 & 0.76 & 0.67 & 1.00 & 0.93 & -0.89 \\ -0.66 & -0.73 & 0.52 & -0.85 & 0.68 & 0.71 & 0.93 & 1.00 & -0.93 \\ 0.70 & 0.77 & -0.54 & 0.90 & -0.73 & -0.75 & -0.89 & -0.94 & 1.00 \end{bmatrix} \end{array} \begin{matrix} E_l \\ E_t \\ \nu_{lt} \\ G_{lt} \\ \alpha_l \\ \alpha_t \\ \beta_l \\ \beta_t \\ k_f \end{matrix}
$$

correlation coefficient matrix calculated from simulated data is fully populated, since the stiffnesses are related through volume fraction, and hygrothermal properties are related through ply longitudinal stiffness.

4.4.4 Angle Coupling Coefficients

The other type of correlation considered in the current work is coupling between ply angles. Mathematically, this is handled in the same way as the coupling between material properties detailed above. The angle correlation coefficients are user inputs rather than calculated quantities, however.

The size of the angle correlation coefficient matrix depends on the number of plies in the laminate. The angle correlation coefficient matrix is a $nply$ by $nply$ matrix. The correlations between ply angles can change depending on the layup techniques used. These techniques can create no coupling between ply angles, or systematic errors which couple ply angles of all or some plies. In any case, the angle matrix must be symmetric with ones on the diagonals, and all elements are bounded by -1 and 1 inclusive.

Some example angle correlation coefficient matrices follow. All assume a six-ply laminate. The examples would be similar for other numbers of plies, but the matrices would be different sizes. First is the case of no special layup techniques, so there is no coupling between angles. The angle correlation matrix is simply a 6x6 identity matrix.

$$\begin{bmatrix} 1 & 0 & 0 & 0 & 0 & 0 \\ 0 & 1 & 0 & 0 & 0 & 0 \\ 0 & 0 & 1 & 0 & 0 & 0 \\ 0 & 0 & 0 & 1 & 0 & 0 \\ 0 & 0 & 0 & 0 & 1 & 0 \\ 0 & 0 & 0 & 0 & 0 & 1 \end{bmatrix} \tag{4.64}$$

In a laminate where there is a systematic error in the ply angles or, equivalently, an error in cutting test samples out of the laminate, the variations in all of the angles are coupled together. If there are no other sources of ply angle error, the angle correlation matrix is fully populated with ones.

$$\begin{bmatrix} 1 & 1 & 1 & 1 & 1 & 1 \\ 1 & 1 & 1 & 1 & 1 & 1 \\ 1 & 1 & 1 & 1 & 1 & 1 \\ 1 & 1 & 1 & 1 & 1 & 1 \\ 1 & 1 & 1 & 1 & 1 & 1 \\ 1 & 1 & 1 & 1 & 1 & 1 \end{bmatrix} \tag{4.65}$$

The final example is for a laminate with ply angles correlated with neighboring plies. The correlations decrease as the number of intervening plies increases. Physically, this example represents a case where a hand layup worker lays up the laminate with a tendency to reference ply angles to the previous ply angle, or where mechanical ply layup techniques have a correlated error which drifts randomly.

$$\begin{bmatrix} 1 & .5 & .3 & .1 & 0 & 0 \\ .5 & 1 & .5 & .3 & .1 & 0 \\ .3 & .5 & 1 & .5 & .3 & .1 \\ .1 & .3 & .5 & 1 & .5 & .3 \\ 0 & .1 & .3 & .5 & 1 & .5 \\ 0 & 0 & .1 & .3 & .5 & 1 \end{bmatrix} \tag{4.66}$$

The angle correlation coefficient matrices presented in this subsection do not exhaust the set of possible matrices. For any manufacturing technique, an angle correlation coefficient matrix can be developed. By comparing the influence of different angle correlation matrices, different layup techniques can be evaluated for effectiveness in reducing the standard deviation of the laminate properties of interest for a particular application.

4.4.5 Other Coupling Coefficients

The preceding subsections have developed the material and angle correlation coefficient matrices. Mathematically, Eq. 4.43 allows correlation coefficients between any two input parameters. In the current work, the remainder of the correlation coefficients are assumed to be one if between an input parameter and itself, and zero in all other cases. For example, correlation between material property variations and ply angle variations is assumed to be zero. Correlation coefficients between ply thicknesses of different plies are also assumed to be zero.

For each material considered, only one set of input parameters is specified (see Table 4.2). If multiple plies are made from the same material, the properties of the plies are effectively fully correlated with each other. In reality, the material properties of each ply could be anywhere from fully independent from the properties of the other plies, to fully correlated, much in the same fashion as the ply angles. The only provision for this range of possibilities made in the current implementation is that material properties can be made fully independent on a ply-by-ply basis by specifying a new material for each ply.

4.5 IMPLEMENTATION

The analytical methodology developed in this chapter is implemented in VARBEND, an easy-to-use computer program written in FORTRAN. A listing of the program and a user's manual are in Appendix B. The user inputs are the mean values and standard deviations of the ply material properties and manufacturing parameters. Options include specifying the

material correlation coefficient matrix (required if volume fraction variation is included) and including an angle correlation coefficient matrix. Sample inputs and the resultant outputs are also provided in Appendix B. VARBEND provides means and standard deviations of laminate properties, as well as values for three different sensitivity metrics.

The first sensitivity metric used is the individual derivative as calculated in Eq. 4.44.

$$d_{ij} = \frac{\partial Y_i}{\partial X_j} \tag{4.67}$$

The derivatives are useful in calculations, but are difficult to interpret or compare. The units, (unit of laminate property)/(unit of input parameter), are also awkward.

The next sensitivity metric has units of the laminate property. It shows the contribution of the variation of input parameter X_j to the variation of laminate property Y_i:

$$d_{ij}^{\sigma} = \frac{\partial Y_i}{\partial X_j}\hat{\sigma}_{Xj} \tag{4.68}$$

This metric can also be thought of as the standard deviation of Y_i if the only input parameter with a non-zero standard deviation were X_j.

The final metric is dimensionless, and shows the proportional change in laminate property for a given proportional change in the input parameter:

$$\bar{d}_{ij} = \frac{\partial Y_i}{\partial X_j}\frac{\bar{X}_j}{\bar{Y}_i} \tag{4.69}$$

This metric is useful in that it can be used to compare sensitivities with each other, but is meaningless if the mean of the laminate or ply variable is zero.

All three sensitivity metrics can be helpful to the user as an indication of which input parameters are the most important contributors to the

variation of the laminate properties. This information can be used to help decide which input parameters need to be carefully controlled, and conversely, which (if any) can be ignored or given a low priority for quality control.

4.6 LARGE-DEFORMATION CURVATURE

Thin unsymmetric laminates undergoing a temperature change as they cool from the cure temperature often assume a right cylindrical shape rather than the saddle shape predicted by CLPT. Hyer [25] used higher-order plate theory and a minimization of potential energy to show that the cylindrical shape was the lower energy state under many conditions. In this section, Hyer's formulation for cross-ply laminate shape prediction is reviewed, and the method is extended to general laminates. The current solution follows Hyer's published solution. Some notation is changed to maintain consistency within the current work. More importantly, Hyer's solution is generalized in several ways. Hyer assumed that the midplane shear would always be zero. This assumption has been eliminated. Hyer also assumed that laminates had no "shear CTE" (α_{12}). This assumption was reasonable for the cross-ply laminates in Hyer's investigation, but it does not hold for general laminates. Finally, Hyer's analysis concentrated on square laminates, while the current analysis holds for general rectangular geometries.

The approach used in the current work to determine the stable shape for a laminate is to calculate the total potential energy U as a function of the laminate midplane strains and curvatures. Large-displacement strain-displacement relations and assumed displacement shapes are used to find the strains. Three assumed displacement shapes–a saddle and two right circular

cylinders–are considered. For each assumed shape, the first variation of the total potential energy is set to zero to find the magnitudes of the displacements. The total potential energy of the three assumed shapes are then compared, and the shape with the lowest potential energy is assumed to be the stable shape. For unbalanced laminates, twist curvatures exist in the laminate axis system, which complicates the analysis. In these cases, the assumed shapes are calculated in a set of principal curvature axes. Principal curvature axes, discussed in detail below, are axes in which the twist curvature is zero. Shapes in the principal curvature axes are then rotated to the laminate axes.

4.6.1 Problem Formulation

The approach used by Hyer to find the large-deformation behavior of a laminate involves the minimization of potential energy. The total potential energy of the laminate is given by

$$U = \int_V \psi dV \tag{4.70}$$

$$\psi = \frac{1}{2}\boldsymbol{\varepsilon}^{\mathrm{T}}\overline{\mathbf{Q}}\boldsymbol{\varepsilon} - \boldsymbol{\varepsilon}^{\mathrm{T}}\overline{\mathbf{Q}}\overline{\boldsymbol{\alpha}}\Delta T \tag{4.71}$$

where U is the total potential energy, ψ is strain energy density, the other variables are as defined in Section 4.1, and moisture-induced deformations are assumed to be zero. All properties are assumed to be temperature-independent, and the net work done by any external tractions on the laminate as it cools and curves to its final state is assumed to be zero. The curvatures are defined in Eqs. 4.72–4.74.

$$\kappa_x = -\frac{\partial^2 w}{\partial x^2} \tag{4.72}$$

$$\kappa_y = -\frac{\partial^2 w}{\partial y^2} \tag{4.73}$$

$$\kappa_{xy} = -\frac{\partial^2 w}{\partial y \partial x} \tag{4.74}$$

The large-deformation strain-displacement relations are given in Eqs. 4.75–4.77, where u° is the midplane displacement in the x direction, v° is the midplane displacement in the y direction, and w is the out-of-plane displacement of the midplane in the z direction.

$$\varepsilon_x^\circ = \frac{\partial u^\circ}{\partial x} + \frac{1}{2}\left(\frac{\partial w}{\partial x}\right)^2 \tag{4.75}$$

$$\varepsilon_y^\circ = \frac{\partial v^\circ}{\partial y} + \frac{1}{2}\left(\frac{\partial w}{\partial y}\right)^2 \tag{4.76}$$

$$\varepsilon_{xy}^\circ = \frac{1}{2}\left(\frac{\partial u^\circ}{\partial y} + \frac{\partial v^\circ}{\partial x} + \left(\frac{\partial w}{\partial x}\right)\left(\frac{\partial w}{\partial y}\right)\right) \tag{4.77}$$

Expanding Eq. 4.71 in terms of these equations yields

$$\begin{aligned}\psi = {} & \frac{1}{2}\overline{Q}_{11}\varepsilon_{11}^2 + \overline{Q}_{12}\varepsilon_{11}\varepsilon_{22} + 2\overline{Q}_{66}\varepsilon_{12}^2 + \frac{1}{2}\overline{Q}_{22}\varepsilon_{22}^2 + 2\overline{Q}_{16}\varepsilon_{11}\varepsilon_{12} + 2\overline{Q}_{26}\varepsilon_{22}\varepsilon_{12} \\ & -(\overline{Q}_{11}\overline{\alpha}_x + \overline{Q}_{12}\overline{\alpha}_y + \overline{Q}_{16}\overline{\alpha}_{xy})\varepsilon_{11}\Delta T - (\overline{Q}_{12}\overline{\alpha}_x + \overline{Q}_{22}\overline{\alpha}_y + \overline{Q}_{26}\overline{\alpha}_{xy})\varepsilon_{22}\Delta T \\ & -2(\overline{Q}_{16}\overline{\alpha}_x + \overline{Q}_{26}\overline{\alpha}_y + \overline{Q}_{66}\overline{\alpha}_{xy})\varepsilon_{12}\Delta T\end{aligned} \tag{4.78}$$

Equations 4.75–4.77 represent a departure from CLPT. Nonlinear geometric effects are included in the second-order terms in the strain-displacement relations. Equation 4.78 differs from Hyer's analysis by including midplane shear strain and shear CTE terms.

The out-of-plane displacement is assumed to be of the form

$$w(x, y) = \frac{1}{2}(ax^2 + by^2) + cxy \tag{4.79}$$

where a, b, and c are coefficients to be determined. Substituting Eq. 4.79 into Eqs. 4.72–4.74 yields the following results for the laminate curvatures:

$$\kappa_x = -a \tag{4.80}$$

$$\kappa_y = -b \tag{4.81}$$

$$\kappa_{xy} = -c \tag{4.82}$$

The coefficient a represents the x bending curvature, b the y bending curvature, and c the twist curvature for the laminate. In an unsymmetric cross-ply laminate such as those considered by Hyer, a=-b denotes a saddle shape solution, and c=0, since there is no twist due to temperature for a cross-ply laminate. The two different cylindrical shapes observed by Hyer also have c=0. The two shapes are a=0, $b\neq 0$ and b=0, $a\neq 0$. Assumed solutions for u° and v° which include large-deformation effects are given in Eqs. 4.83 and 4.84, where d, e and f are also coefficients to be determined. The coefficients d, e and f represent x, y, and shear midplane strains, respectively. The coefficients a, b, c, d, e and f are collectively referred to as the shape constants.

$$u^\circ(x,y) = dx - \frac{a^2x^3}{6} + fy \tag{4.83}$$

$$v^\circ(x,y) = ey - \frac{b^2y^3}{6} + fx \tag{4.84}$$

Using 4.79, 4.83, and 4.84 in Eqs. 4.75–4.77 and Eq. 4.79 in Eqs. 4.72–4.74, and putting these results into the strain-curvature relations of Eqs. 4.2, yields the following values for laminate strains:

$$\varepsilon_x = d + acxy + \frac{c^2y^2}{2} - az \tag{4.85}$$

$$\varepsilon_y = e + bcxy + \frac{c^2x^2}{2} - bz \tag{4.86}$$

$$\varepsilon_{xy} = \frac{acx^2}{2} + \frac{bcy^2}{2} + \frac{(ab+c^2)xy}{2} + f - cz \tag{4.87}$$

The problem becomes the determination of the constants a, b, c, d, e, and f for a specific laminate at a specific temperature. By substituting Eqs. 4.85–4.87 into Eq. 4.78, and using Eq. 4.70, the total potential energy U of the laminate as a function of a, b, c, d, e, and f can be found.

The problem of finding a minimum of the potential energy U becomes a problem of finding values of a, b, c, d, e, and f such that the first variation of the potential energy is zero, i.e.

$$\delta U = \left(\frac{\partial U}{\partial a}\right)\delta a + \left(\frac{\partial U}{\partial b}\right)\delta b + \left(\frac{\partial U}{\partial c}\right)\delta c + \left(\frac{\partial U}{\partial d}\right)\delta d + \left(\frac{\partial U}{\partial e}\right)\delta e + \left(\frac{\partial U}{\partial f}\right)\delta f = 0 \quad (4.88)$$

For a small-deformation (e.g. CLPT) method, Eq. 4.88 would lead to six linear equations in six unknowns, and could be solved by a variety of methods. In the current work, however, the non-linear strains in Eqs. 4.85–4.87 make the solution much more complicated. The approach used here to make the solution tractable is to assume three possible shapes in the principal curvature axes. Principal curvature axes, which are discussed further in the next subsection, are axes in which the twist curvature is zero. The shapes in the principal curvature axes can be rotated to find shapes in the laminate axes.

4.6.2 Principal Curvatures

Principal curvatures are an analog to the more common principal stresses. A set of axes, rotated with respect to the structural axes, can always be found in which the twist is zero. In the current work, the principal curvature axes are denoted by x' and y', and the principal curvatures in these directions are indicated by κ_1 and κ_2, respectively. The z axis is the same in both sets of coordinate axes. This subsection reviews the concept of principal curvature axes, and shows its application to the current work.

For the cross-ply laminates studied by Hyer, the laminate does not undergo twist, so c in Subsection 4.6.1 is equal to zero. For general laminates, however, twist might be present. Twist in the room-temperature shape results from the fact that the directions of principal curvature are not aligned with the laminate axes. Considering curvatures in the principal axes allows general laminates to be included in the analysis without making the calculations required too lengthy.

The rotation angle from laminate axes to principal curvature axes is designated ϕ. Hyer found that while CLPT did not predict the magnitudes of curvature well in thin unsymmetric laminates, it did predict the rotation angles well. The rotation angle is found from

$$\tan(2\phi) = \frac{2\kappa_{xy}}{\kappa_x - \kappa_y} \tag{4.89}$$

where the curvatures are those predicted by CLPT in laminate axes.

The principal curvatures are found by constructing Mohr's circle of curvature, which is similar to Mohr's circle of stress. On the horizontal axis the quantities κ_x and κ_y are plotted, and κ_{xy} is plotted along the vertical axis. The center of Mohr's circle of curvature, C, is given by

$$C = \frac{\kappa_x + \kappa_y}{2} \tag{4.90}$$

and the radius, R, is given by

$$R = \sqrt{\left(\frac{\kappa_x - \kappa_y}{2}\right)^2 + \kappa_{xy}^2} \tag{4.91}$$

The principal curvatures are given by the points on Mohr's circle of curvature on the horizontal axis, where the twist curvature is zero. Their values are

$$\kappa_1 = C + R \tag{4.92}$$

$$\kappa_2 = C - R \tag{4.93}$$

The center and radius of Mohr's circle of curvature can be expressed in terms of principal curvatures:

$$C = \frac{\kappa_1 + \kappa_2}{2} \tag{4.94}$$

$$R = \sqrt{\left(\frac{\kappa_1 - \kappa_2}{2}\right)^2} \tag{4.95}$$

For a general laminate, using the principal curvatures instead of the laminate axis curvatures make the potential energy simpler to calculate. The out-of-plane displacement of the midplane in Eq. 4.79 can also be expressed as

$$w = \frac{1}{2}(a'x'^2 + b'y'^2) \tag{4.96}$$

where the primes signify principal curvature axes. The principal curvatures for this assumed out-of-plane displacement are given by

$$\kappa_1 = -a' \tag{4.97}$$

$$\kappa_2 = -b' \tag{4.98}$$

The shape constants in laminate axes can be found in terms of the shape constants in principal curvature axes:

$$a = C + R\cos(2\phi) \tag{4.99}$$

$$b = C - R\cos(2\phi) \tag{4.100}$$

$$c = R\sin(2\phi) \tag{4.101}$$

It is assumed that ϕ, the rotation angle between coordinate axes, is a function only of the layup and material used; therefore, ϕ is a constant for a given laminate. This assumption means that the only two independent variables in the total potential energy expression are a' and b', the coefficients of the curvatures in the principal directions. The coefficients of the curvatures in laminate axes, a, b, and c, are found in terms of a' and b' by substituting Eqs. 4.97 and 4.98 into Eqs. 4.94 and 4.95, and then substituting the results into Eqs. 4.99–4.101, yielding

$$a = \frac{a'+b'}{2} + \frac{a'-b'}{2}cos(2\phi) \tag{4.102}$$

$$b = \frac{a'+b'}{2} + \frac{b'-a'}{2}cos(2\phi) \tag{4.103}$$

$$c = \frac{a'-b'}{2}sin(2\phi) \tag{4.104}$$

With these relations, three variables (a, b, and c) can be reduced to two (a' and b') in the potential energy expressions in Subsection 4.6.1, making the solution easier.

4.6.3 Solution Procedure

The Matlab/Maple symbolic toolbox [39] was used to find large-deformation solutions. The intermediate results generated by Matlab/Maple are too involved to be reproduced here. Instead, the solution method is outlined. The routines used by Matlab/Maple are found in Appendix C.

Numerical values for $\overline{\mathbf{Q}}$ and $\overline{\boldsymbol{\alpha}}$ for the laminate are substituted into the strain energy expression in Eq. 4.78. The result is a function that can be expressed as

$$\psi = \psi(a, b, c, d, e, f, \Delta T, x, y, z) \tag{4.105}$$

Equation 4.105 is then substituted into Eq. 4.70 and symbolically integrated over the dimensions of the laminate using the Matlab/Maple symbolic toolbox to find an expression for the total potential energy in terms of a, b, c, d, e, and f.

The total potential energy integration of Eq. 4.70 is performed in the laminate axes to keep the boundary conditions simple. The origin of the laminate axes is assumed to be in the geometric center of the laminate. The laminate is thus defined by the region specified in Eqs. 4.106–4.108.

$$-L_x/2 \le x \le L_x/2 \tag{4.106}$$

$$-L_y/2 \le y \le L_y/2 \tag{4.107}$$

$$-h/2 \le z \le h/2 \tag{4.108}$$

These limits make Eq. 4.70 a function of the material properties and spatial variables of the form

$$U = \int_{x=-L_x/2}^{L_x/2} \int_{y=-L_y/2}^{L_y/2} \int_{z=-h/2}^{z=h/2} \psi(a,b,c,d,e,f,\Delta T,x,y,z)\,dx\,dy\,dz \tag{4.109}$$

The integration in Eq. 4.109 is performed symbolically using the Matlab/Maple symbolic toolbox. In the current work, stable shapes for unsymmetric laminates are found as functions of temperature and of laminate size. For the first case, the laminate dimensions are substituted into the strain energy density expression prior to integration, giving a total energy in terms of the temperature, as in Eq. 4.110.

$$U = U(a,b,c,d,e,f,\Delta T) \tag{4.110}$$

In the other case, the temperature difference is substituted into the strain energy density, and the total energy is found in terms of the laminate dimensions, as in Eq. 4.111.

$$U = U(a, b, c, d, e, f, L_x, L_y, h) \tag{4.111}$$

Equation 4.110 or 4.111 is used to compute laminate shapes for various ΔTэо or various specimen sizes, respectively. Numerical values for ΔT or the specimen dimensions are substituted into Eq. 4.110 or 4.111, yielding

$$U = U(a, b, c, d, e, f) \tag{4.112}$$

Equations 4.102–4.104 are substituted into Eq. 4.112 to express the total potential energy in terms of a', b', d, e, and f.

$$U = U(a', b', d, e, f) \tag{4.113}$$

Taking the first variation of the total potential energy and setting it equal to zero yields

$$\delta U = \left(\frac{\partial U}{\partial a'}\right)\delta a' + \left(\frac{\partial U}{\partial b'}\right)\delta b' + \left(\frac{\partial U}{\partial d}\right)\delta d + \left(\frac{\partial U}{\partial e}\right)\delta e + \left(\frac{\partial U}{\partial f}\right)\delta f = 0 \tag{4.114}$$

Satisfaction of Eq. 4.114 requires that all bracketed terms be identical to zero. This results in five equations (4.115–4.119) in five unknowns (a', b', d, e and f). The derivatives are performed symbolically by Matlab. The notation used in Eqs. 4.115–4.119 is defined such that f_i represents the ith equation derived from the first variation of U, with the terms in parentheses showing the variables present in the equation.

$$\left(\frac{\partial U}{\partial a'}\right) = f_1(a', b', d, e, f) = 0 \tag{4.115}$$

$$\left(\frac{\partial U}{\partial b'}\right) = f_2(a', b', d, e, f) = 0 \tag{4.116}$$

$$\left(\frac{\partial U}{\partial d}\right) = f_3(a', b', d, e, f) = 0 \tag{4.117}$$

$$\left(\frac{\partial U}{\partial e}\right) = f_4(a', b', d, e, f) = 0 \tag{4.118}$$

$$\left(\frac{\partial U}{\partial f}\right) = f_5(a', b', d, e, f) = 0 \tag{4.119}$$

The next step in the solution is to find d, e, and f in terms of a' and b'. For this formulation, f_3, f_4, and f_5, while complicated, are a linear system of equations in d, e and f. Therefore, solving Eqs. 4.117–4.119 for these constants algebraically is straightforward. This is done using the Matlab/Maple symbolic manipulation toolbox. The expressions for d, e and f are substituted into Eqs. 4.115 and 4.116 symbolically to get

$$f'_1(a', b') = 0 \tag{4.120}$$

$$f'_2(a', b') = 0 \tag{4.121}$$

Equations 4.120 and 4.121 are very non-linear. The approach used in the current work to solve these equations is to assume three possible deformation states for the laminate. The first assumed shape contains curvature in both directions, and will reduce to the CLPT solution if the laminate has small in-plane dimensions or a large thickness. This shape is specified by Eq. 4.122.

$$b' = \lambda a' \tag{4.122}$$

where λ is the ratio of principal curvature in the x' direction to that in the y' direction predicted by CLPT. The second assumed shape is a right circular cylinder in the principal axes, with no curvature in the y' direction. This shape is specified by Eq. 4.123.

$$b' = 0 \tag{4.123}$$

The final assumed shape is also a cylinder in principal curvature axes, but with the only non-zero curvature along the other principal axis. This shape is specified by Eq. 4.124.

$$a' = 0 \tag{4.124}$$

Each possible shape allows the first variation of the energy with respect to a' or b' to be expressed in terms of one variable. This is done by substituting Eqs. 4.122–4.124 one at a time into Eq. 4.120 or 4.121, yielding, respectively, Eqs. 4.125–4.127.

$$f''_1(a') = 0 \tag{4.125}$$

$$f''_2(a') = 0 \tag{4.126}$$

$$f''_3(b') = 0 \tag{4.127}$$

Equations 4.125–4.127 are cubic equations, which yield three roots: one real root and a pair of complex conjugate roots. The real root is the minimum energy value of the principal curvature for each assumed shape. In the first case, b' is found from Eq. 4.122. In all cases, a' and b' are substituted into Eqs. 4.117–4.119, which are then used to find values for d, e, and f. All shape constants are then substituted into Eq. 4.113 to find the total potential energy U of the laminate. The shape or shapes with the lowest total potential energy are taken to be the stable shape(s) for the laminate.

As mentioned throughout this section, the extensive algebra required is accomplished using Matlab/Maple. The complete Matlab script can be found in Appendix C.

4.6.4 Large-Deformation Example and Verification

This subsection presents the results of the large-deformation analysis for an example laminate. The layup of the example laminate studied is $[0_2/90_2]_T$. This layup is one which was investigated by Hyer in Reference 25, and is also used in the experimental portion of the current work. Material properties used are those of the T300/5208 graphite/epoxy material system used in Hyer's study. The laminate is assumed to be square, and the temperature is assumed to be room temperature. The laminate is loaded only by cooling from the stress-free temperature, which is assumed to be 350°F. Since the layup is a cross-ply, the principal curvature axes are coincident with the laminate axes, and the twist curvature is zero.

The first difference between Hyer's study and the current work is the solution technique used. The methodology developed above was used in the current work, while Hyer used a numerical technique. To verify the solution technique, the large-deformation formulation of the current work was modified to use Hyer's assumptions, i.e. in-plane shear strains and shear CTE's were eliminated. The results are shown in Figures 4.1 and 4.2. Figure 4.1 shows the calculated x direction curvature κ_x for the three assumed shapes as functions of laminate sidelength. Figure 4.2 shows the calculated total potential energies for each shape. Figure 4.3, replicated from Reference 25, shows Hyer's solution for κ_x of the $[0_2/90_2]_T$ layup, as well as a solution to the layup using the current solution technique.

In Figure 4.1, the solid line represents a saddle shape. At zero sidelength, the minimum energy solution for this shape is identical to the CLPT solution. The change in curvature for this assumed shape with laminate sidelength is identical to that presented by Hyer for this layup. The curvatures are smaller than predicted by CLPT for non-zero sidelength

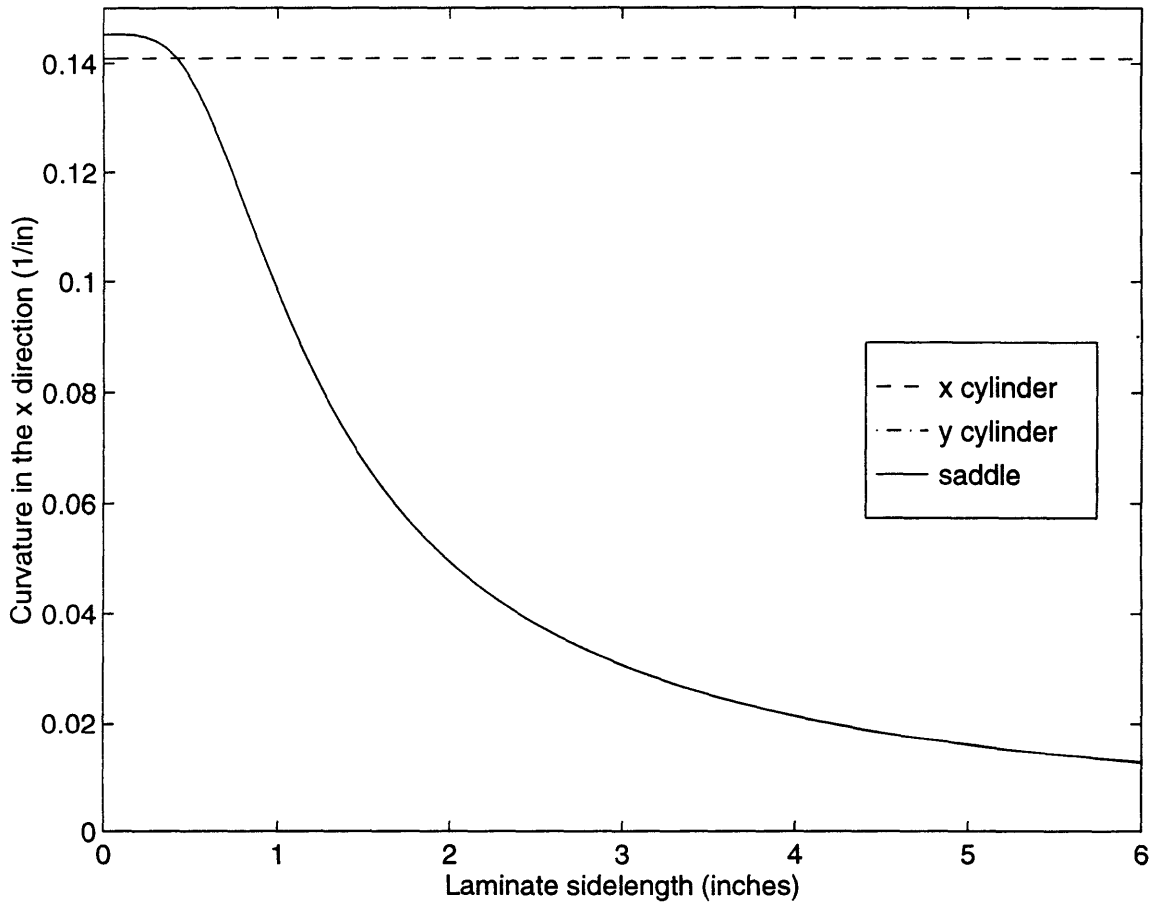

Figure 4.1 Laminate x curvature vs. sidelength for $[0_2/90_2]_T$ layup with zero shear assumption.

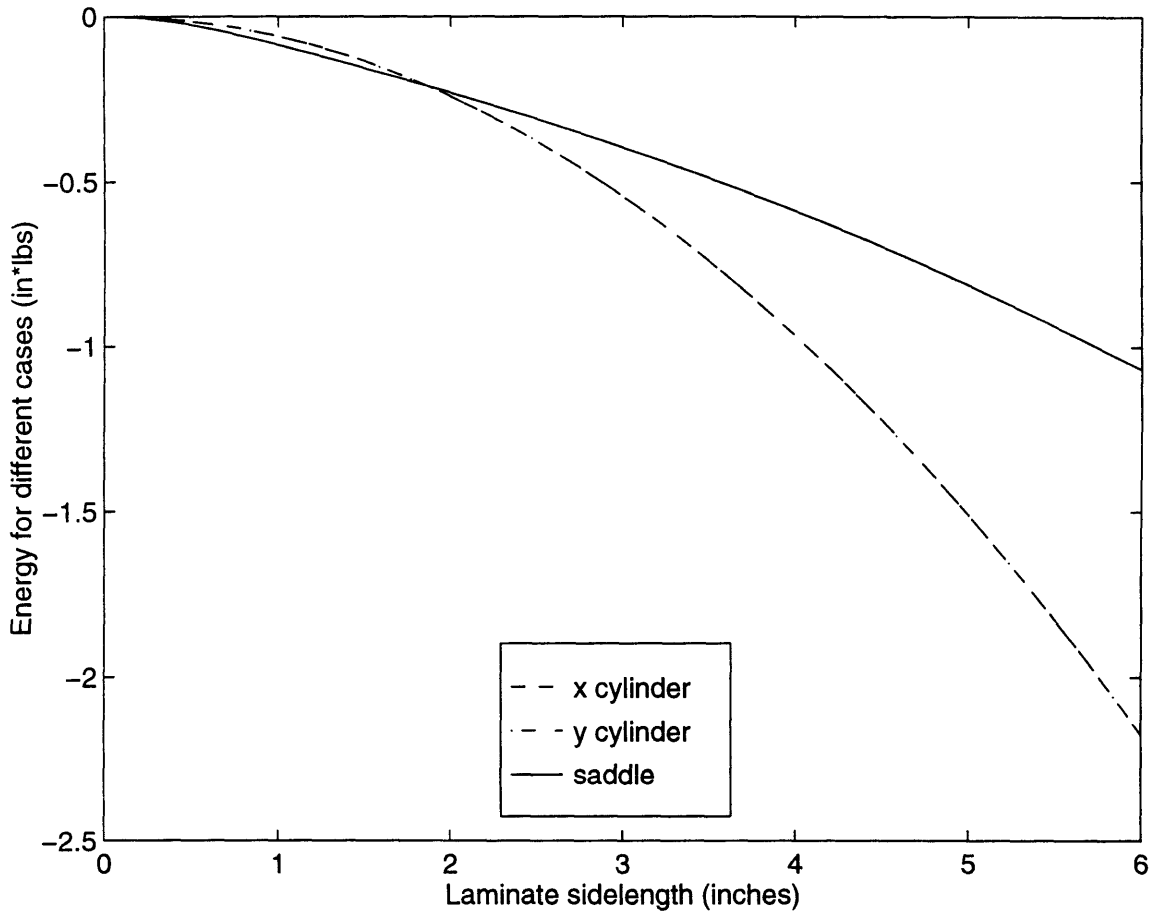

Figure 4.2 Laminate potential energy vs. sidelength for $[0_2/90_2]_T$ layup with zero shear assumption.

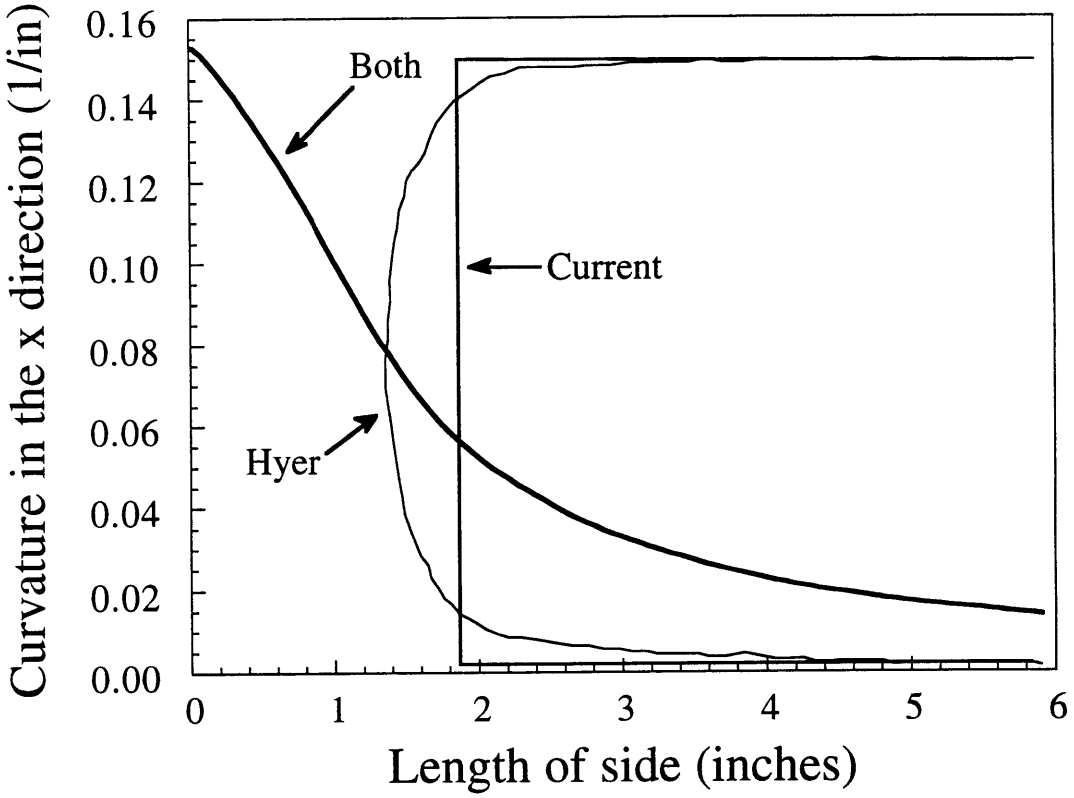

Figure 4.3 Comparison of solution techniques for laminate x curvature vs. sidelength for $[0_2/90_2]_T$ layup between Hyer and current work (assuming zero midplane shear).

because of large deformation effects. The dashed line represents the first cylindrical shape. The curvature remains constant at a value slightly below the CLPT solution. The other cylindrical shape has a constant curvature in the x direction of zero.

Figure 4.2 shows the calculated total potential energies for the three shapes. The energy is negative in all cases because Eq. 4.70 implies that the zero-energy reference state is that of constrained thermal deformations, and the laminate is relaxing from this state. The solid line is the energy of the saddle shape. The cylindrical shapes have the same potential energy, shown by the dashed line. The saddle shape has a lower potential energy until the laminate sidelength reaches 1.86 inches, after which the cylindrical shapes have lower potential energy. Therefore, it is assumed that the only stable shape for the laminate is a saddle until the sidelength reaches 1.86 inches. After this point, the cylindrical shapes are assumed to be stable, while the saddle shape is not. Since both cylindrical shapes have the same potential energy, neither of them is favored. Both cylindrical shapes will exist, and a laminate can be switched from one to the other by means of a snap-through.

Figure 4.3 shows Hyer's solution for the x curvature. Hyer found that the saddle shape was stable for a small sidelength, but that the stable solution bifurcated into two cylindrical shapes. The point of bifurcation for the $[0_2/90_2]_T$ layup was at a sidelength of 1.38 inches. After the bifurcation, the curvatures of the stable cylindrical shapes rapidly approached asymptotic values of zero for one and slightly below the CLPT value for the other.

A comparison of the results of the two methods is also shown in Figure 4.3. The saddle shape curvature solutions are identical. The solutions from the current work's method for the cylindrical shapes are identical to the asymptotes from Hyer's solution. Hyer's numerical technique gave a

bifurcation at 1.38 inches, after which the curvatures of the two cylindrical shapes went from values equal to saddle shape values to asymptotic values. The cylindrical curvatures reached values within 5% of the asymptotic values at a laminate sidelength of 1.97 inches. The technique of the current work did not include this transition behavior. Instead, the energies of the three assumed shapes are compared at each value of laminate sidelength. The change from saddle to cylindrical stable shape is predicted to be 1.86 inches in the current work. Thus, the solution technique of the current method predicts a change in stable shape which is within the transition region of Hyer's numerical technique. This result gives confidence in the solution technique of the current work.

A major difference between Hyer's method and that of the current work is Hyer's assumption that the shear deformation of the midplane is zero. This assumption has been removed in the current work. The effect of this difference can be seen in Figure 4.4, which is analogous to Figure 4.3. The laminate examined is the same as in the previous comparison– the only difference is the removal of the zero shear assumption. The curvatures and energies for the cylindrical solutions are identical to those considered previously. The removal of the zero shear assumption changes the behavior of the saddle shape solution, however. Allowing shear results in larger curvatures for a given laminate sidelength. Consequently, the sidelength at which the saddle shape becomes unstable is larger in the case where shear deformations are allowed, as can be seen by comparing Figures 4.3 and 4.4. When shear deformations are allowed, the saddle shape is stable up to a laminate sidelength of 2.82 inches, as compared to 1.86 inches for the case of zero shear. Thus there is a significant difference between solutions using Hyer's assumptions and the current work.

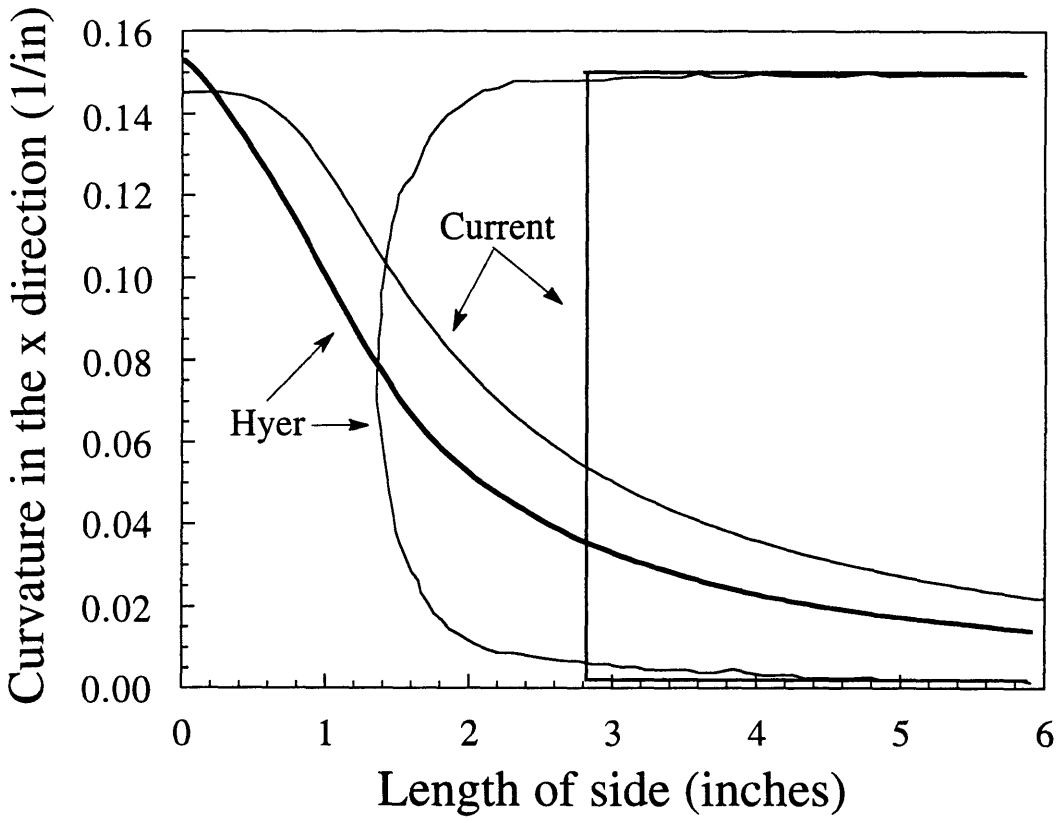

Figure 4.4 Comparison of solution methods for laminate x curvature vs. sidelength for $[0_2/90_2]_T$ layup between Hyer and current work.

CHAPTER 5

EXPERIMENTAL PROCEDURES

An experimental investigation was carried out to provide a quantitative verification of the analysis developed in Chapter 4, and to gain insights into the problem of laminate property variations. In this chapter the test matrix and the rationale behind it are presented. Manufacturing, pre-testing specimen preparation, and the experimental setup, including its calibration, are described. Finally, experimental procedures and data reduction methods are presented.

The experimental investigation considered eighteen different composite panels with sixteen different layups. Five specimens were manufactured from each of the panels. Specimens were progressively heated from room temperature to 100°C (212°F) in a thermal environment chamber. End displacements of the specimens, which were supported as cantilevered (clamped-free) beams, were measured with two laser displacement sensors. The change of end displacements with temperature provided values of the thermal bending coefficients.

5.1 TEST MATRIX

Ninety rectangular graphite/epoxy specimens were manufactured from eighteen graphite/epoxy panels with sixteen different layups. The layups were chosen after a parametric study using the analytical model was

conducted. Layups were selected that would allow examination of trends in laminate properties and their variations with changing layup angles, laminate thickness, ply grouping, and other factors. Table 5.1 is a matrix of all specimens manufactured.

The first six panels were unsymmetric laminates, which had non-zero mean W^T's, and were noticeably curved at room temperature. All six of these layups have been previously studied in published literature, and provide a comparison between the current and previous work. The first four layups were cross-ply laminates examined by Hyer [25, 26]. The other two unsymmetric layups were the same as two studied by Wong [27]. Wong's work was performed in the TELAC laboratory, and the laminates he studied were made with TELAC manufacturing methods.

The remainder of the specimens had symmetric layups, and thus were predicted to have zero mean $\mathbf{W^T}$. There was a distribution of W^T's around the zero point, however, because of the variations in material properties and processing variables.

The first of the symmetric panels examined were of the $[\pm\theta]_s$ family of laminates. These panels showed the effect of different ply angles on $\mathbf{W^T}$ distributions. The specific angles studied were 30°, 45°, and 60°.

Various laminates containing ±30° plies were the emphasis of the remaining panels. Studies were conducted with the VARBEND analysis developed in Chapter 4 prior to the beginning of testing, and these studies predicted that laminates in the ±30° family would show measurable differences in the distributions of thermal bending coefficients among layups to be tested. Three panels were used to study thickness and ply grouping effects. Four panels were used to study the results of including 0° and 90° plies in the layup. Finally, a total of three $[\pm 30]_s$ panels were made so that

Table 5.1 Experimental Test Matrix

Groups	Number of panels	Layup	Number of specimens
Unsymmetric (Hyer)	1	$[0_4/90_4]_T$	5
	1	$[0_2/90_2]_T$	5
	1	$[(0/90)_2]_T$	5
	1	$[0_3/90]_T$	5
Unsymmetric (Wong)	1	$[0/30]_T$	5
	1	$[0_{10}/30_{10}]_T$	5
Angle Ply	3	$[\pm30]_s$	15
	1	$[\pm45]_s$	5
	1	$[\pm60]_s$	5
Thickness	1	$[(\pm30)_2]_s$	5
	1	$[(\pm30)_4]_s$	5
	1	$[30_2/-30_2]_s$	5
Zeros	1	$[0/\pm30]_s$	5
	1	$[\pm30/0]_s$	5
	1	$[0/\pm30/90]_s$	5
	1	$[0_2/(\pm30)_2]_s$	5

variations between specimens cut from one panel could be compared with those between specimens taken from different panels.

The material system chosen for this investigation was AS4/3501-6 graphite/epoxy prepreg tape. This material system has been used extensively at TELAC, where considerable experience in manufacturing with it has been accumulated.

5.2 TEST SPECIMEN MANUFACTURE AND PREPARATION

All specimens were manufactured at TELAC using standard laboratory procedures. Panels measuring 14" x 12" (35.6 cm x 30.5 cm) were fabricated using standard hand layup techniques. The panels were manufactured in three batches of six panels each. The material used was 12" (30.5 cm) wide, 0.005" (0.127 mm) thick continuous AS4/3501-6 unidirectional prepreg tape manufactured by Hercules. All panels were manufactured from the same roll of material, which was spool #2A1 of prepreg lot #7683-4, manufactured on November 17, 1994. Layups were done on January 5, 9, and 11, 1995. The panels were cured in an autoclave within one day of layup according to the manufacturer's recommended cure cycle [40]. After the cure, the panels were immediately postcured at 177°C (350°F) for eight hours.

After postcure, the panels were cut into specimens using the cutting plan in Figure 5.1. The same cutting plan was used for all panels. The edges of the panels were not used because of the possibility of matrix washout effects. The cutting plan was designed such that specimens originated from different locations in the panel, so that variations in thicknesses and volume fraction with location would appear as random variations. All specimens were cut to 6" x 1" (15.24 cm x 2.54 cm) with a water-cooled

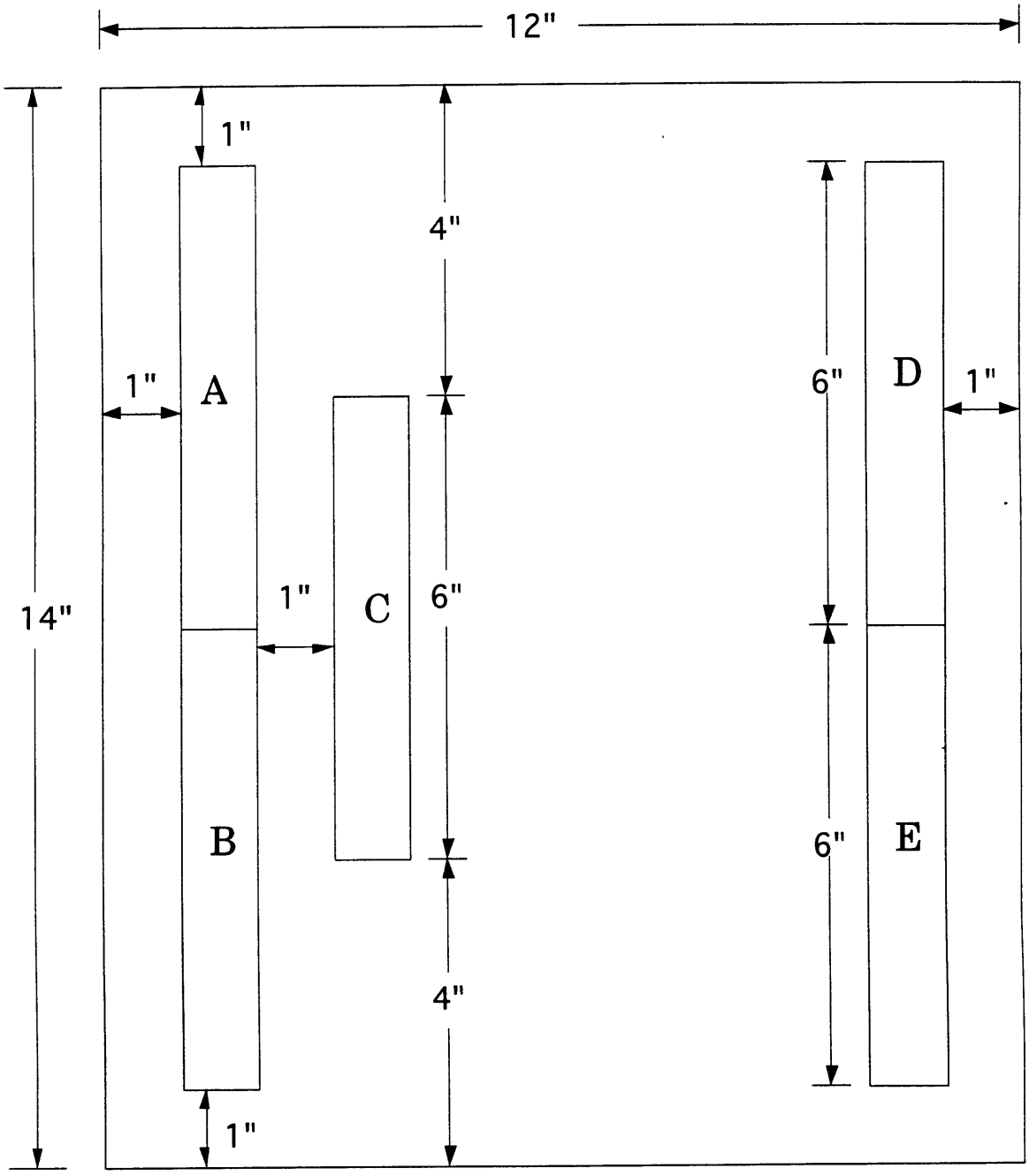

Figure 5.1 Specimen cutting plan.

diamond blade. In the case of some of the unsymmetric laminates, the curvature at room temperature after cure was too great to cut the laminate flat without the possibility of damaging the laminate. These laminates were supported by a section of PVC tube for all cutting. The bottom of a sacrificial PVC tube of the correct curvature was cut off so it would sit on the blade table, and an unsymmetric laminate was wrapped around it. The PVC supported the laminate in its stable room temperature shape, so the cutting process did not damage the laminate. A schematic of this technique is shown in Figure 5.2.

Some additional preparation steps were necessary before testing. In order to obtain specimen temperature data, Omega K-type thermocouples were attached to all specimens with RTV rubber adhesive. The thermocouples were attached at the middle of the width, 1.5" (38.1 mm) from the root end of the specimens. To eliminate moisture absorbed during cutting and other preparatory steps, specimens were desiccated in a postcure oven for 24 hours at 121°C (250°F). After bake-out, specimens were stored with desiccant in airtight containers. Immediately before testing, a small strip of white contact paper was attached to the free end of the specimens. The paper was thin enough so as not to affect the bending stiffness of the specimen. Its function was to provide a good surface for the lasers to reflect off of, since it was extremely difficult to take measurements directly off the surface of the graphite/epoxy specimens. The thermal expansion of the paper and its glue was calculated, and the expansion was found to be too small to affect the experimental results.

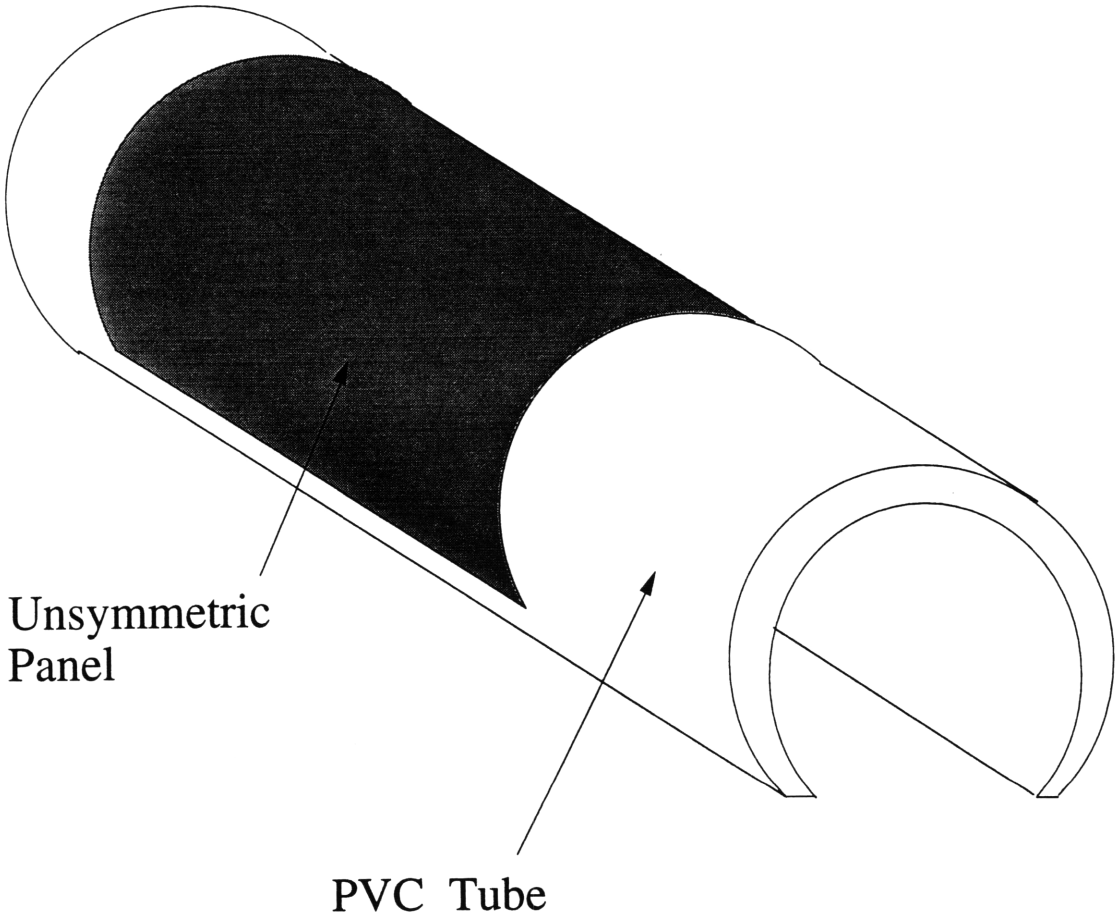

Figure 5.2 Unsymmetric specimen cutting technique.

5.3 EXPERIMENTAL SETUP

The specimens described in Section 5.2 were mounted in a thermal environment chamber. The specimens were clamped at one end and free to deform at the other. No mechanical loads or moments were applied. Tip displacements of the specimen were measured by two laser displacement sensors. Because of limits on their operating temperature, the laser sensors were mounted outside the chamber, and the laser beams traveled through an optical quality window. This section describes the experimental setup used. Equipment, data collection techniques, and calibrations are described. Typical raw data is also presented and discussed, and data reduction techniques are presented.

5.3.1 Equipment

Testing of all specimens was performed in a thermal environment chamber manufactured by Envirotronics, Inc. The chamber had a temperature range of -68°C to 177°C (-90°F to 350°F). The eight cubic foot volume chamber also included a gaseous nitrogen purge system for removal of humid air. The chamber temperature was regulated by a Chromalox controller, which could be programmed to a desired thermal profile. The profile used was a ramp with an initial slope of 4°C/minute (7.2°F/minute), and a hold at the set-point temperature. The commanded chamber temperature and actual specimen temperature data are shown in Figure 5.3. The specimen temperature is approximately three degrees Celsius below the chamber temperature in the steady state. This is most probably due to the fact that the control thermocouple is located near the chamber fan and heater, and quite far from the specimen. The measured specimen temperatures were used in all data reduction.

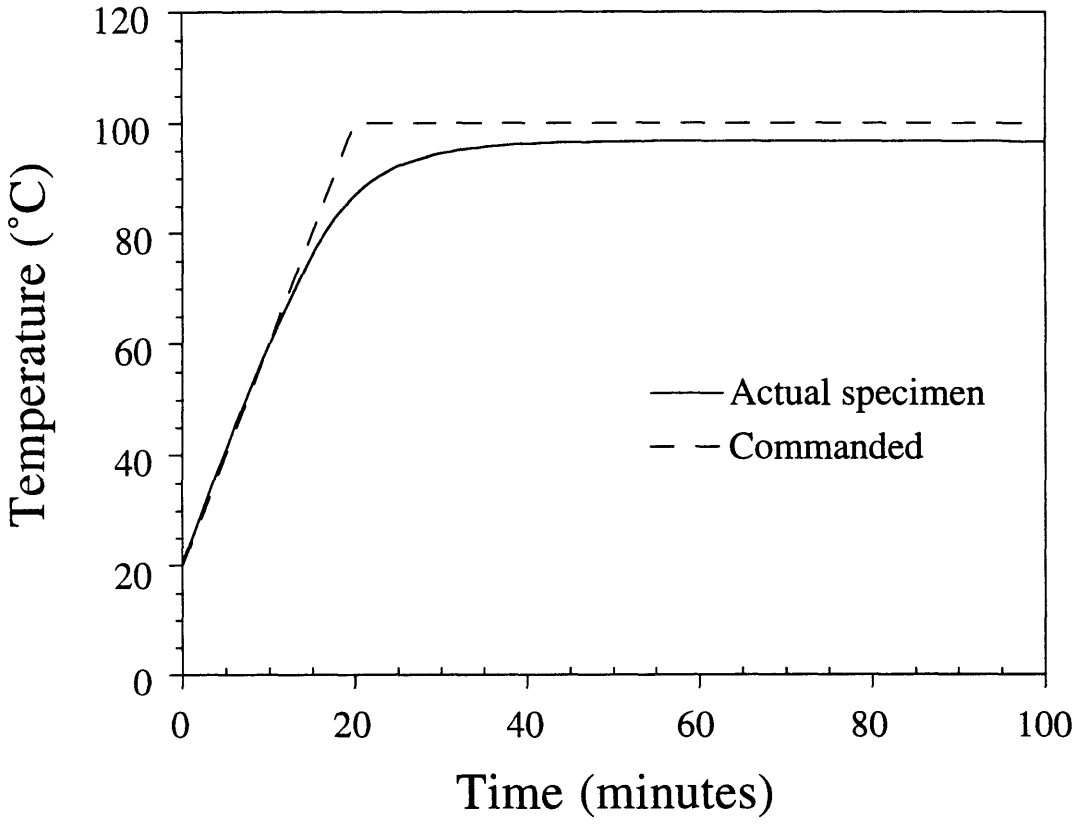

Figure 5.3 Commanded and actual specimen temperature profiles for ramp to 100°C.

A schematic of the complete specimen mounting and measurement setup used in the experiments is shown in Figure 5.4. A more detailed blown-up view is shown in Figure 5.5. Two laser displacement sensors were mounted outside the thermal chamber. The laser beams went through an optical window and reflected off the specimen, which was placed in a mount inside the thermal chamber. The specimen mount was attached to the optics mount with threaded rod. The displacements measured by the laser sensors as the specimen temperature changed were used to find the thermal bending coefficients. Components of the setup are discussed further in this subsection.

Two Keyence laser displacement sensors were used to measure tip deflections of the specimens. The laser displacement sensors work by triangulation. A diode laser projects a spot onto the specimen, and an offset sensor measures the angle to the spot, from which distance can be calculated. The manufacturer claims the laser sensors have a resolution of 10 μm (0.4 mils) over an operating range of 80 mm (3.15"). A controller paired with each sensor conditioned the output of the laser sensor to an analog output voltage proportional to the measured distance. The zero set-point and the slope of the voltage-displacement curve were adjustable. These settings were left constant throughout all experiments. Because the operating temperature range of the lasers was only 0 to 50°C (32 to 122°F), they could not be used inside the chamber. Consequently, the laser sensor heads were mounted on the outside of a port in the chamber wall.

The sensor heads of the lasers were attached to a mount made of G10 (an engineering plastic), shown in Figure 5.6. G10 was chosen as the laser mount material because of its low thermal conductivity, low CTE, high stiffness, and good machinability. The laser mount was attached with bolts

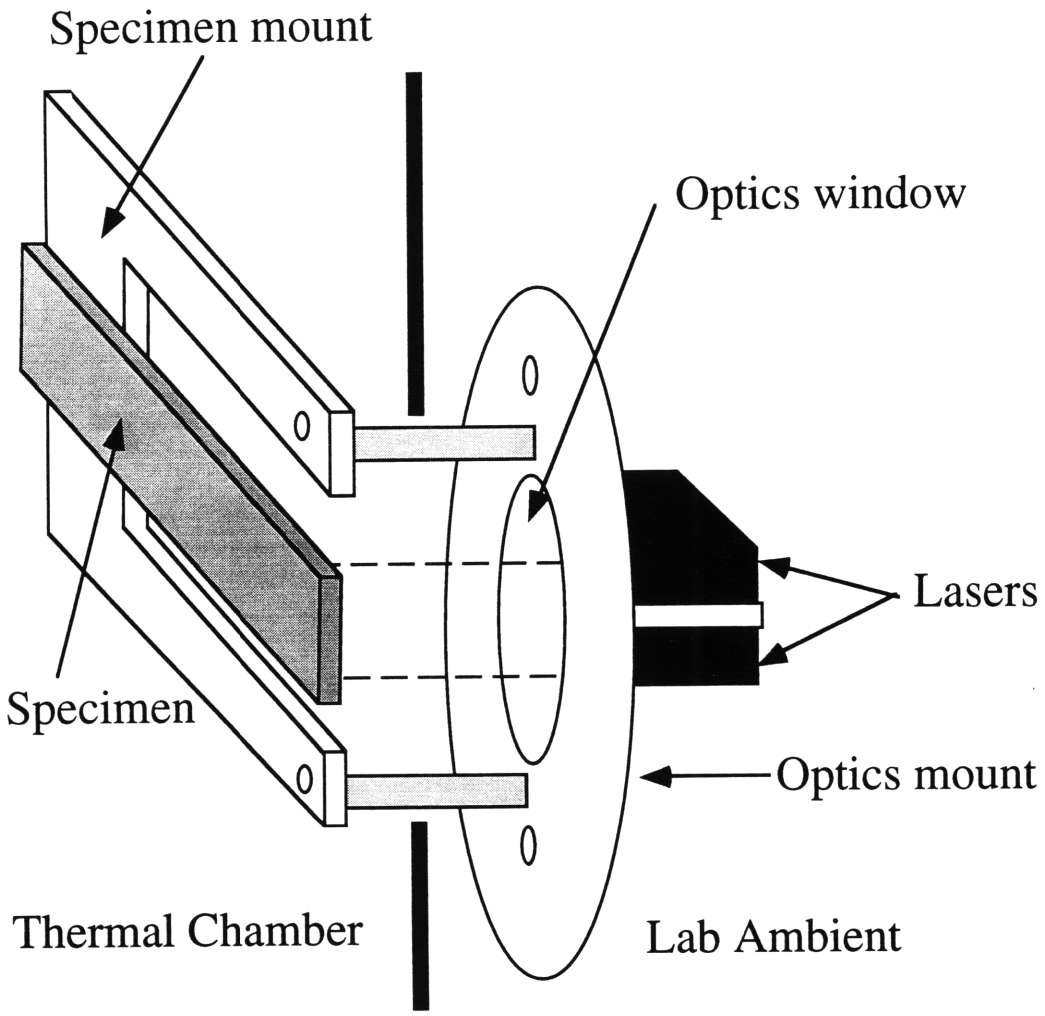

Figure 5.4 Experimental setup.

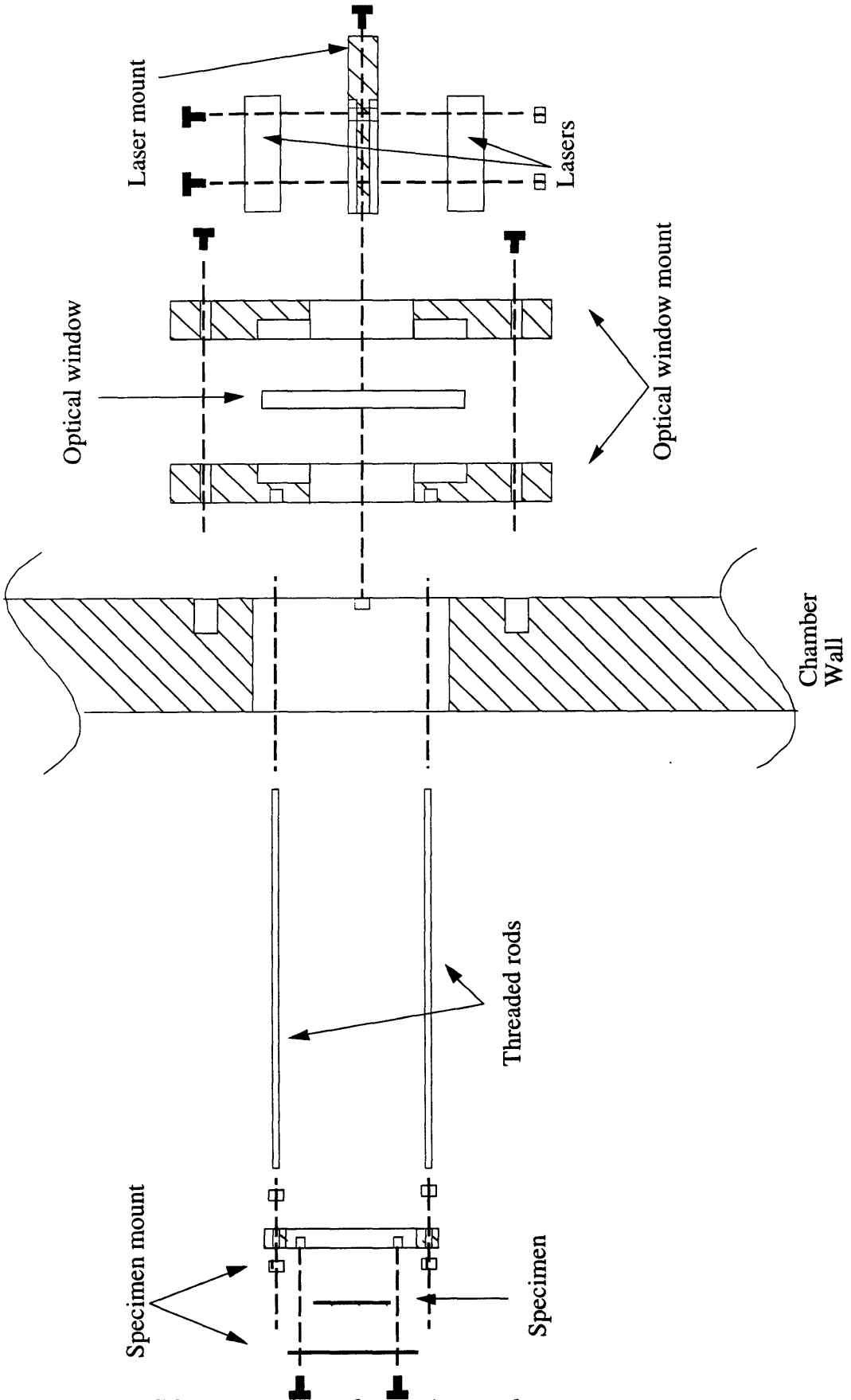

Figure 5.5 Blown-up view of experimental setup.

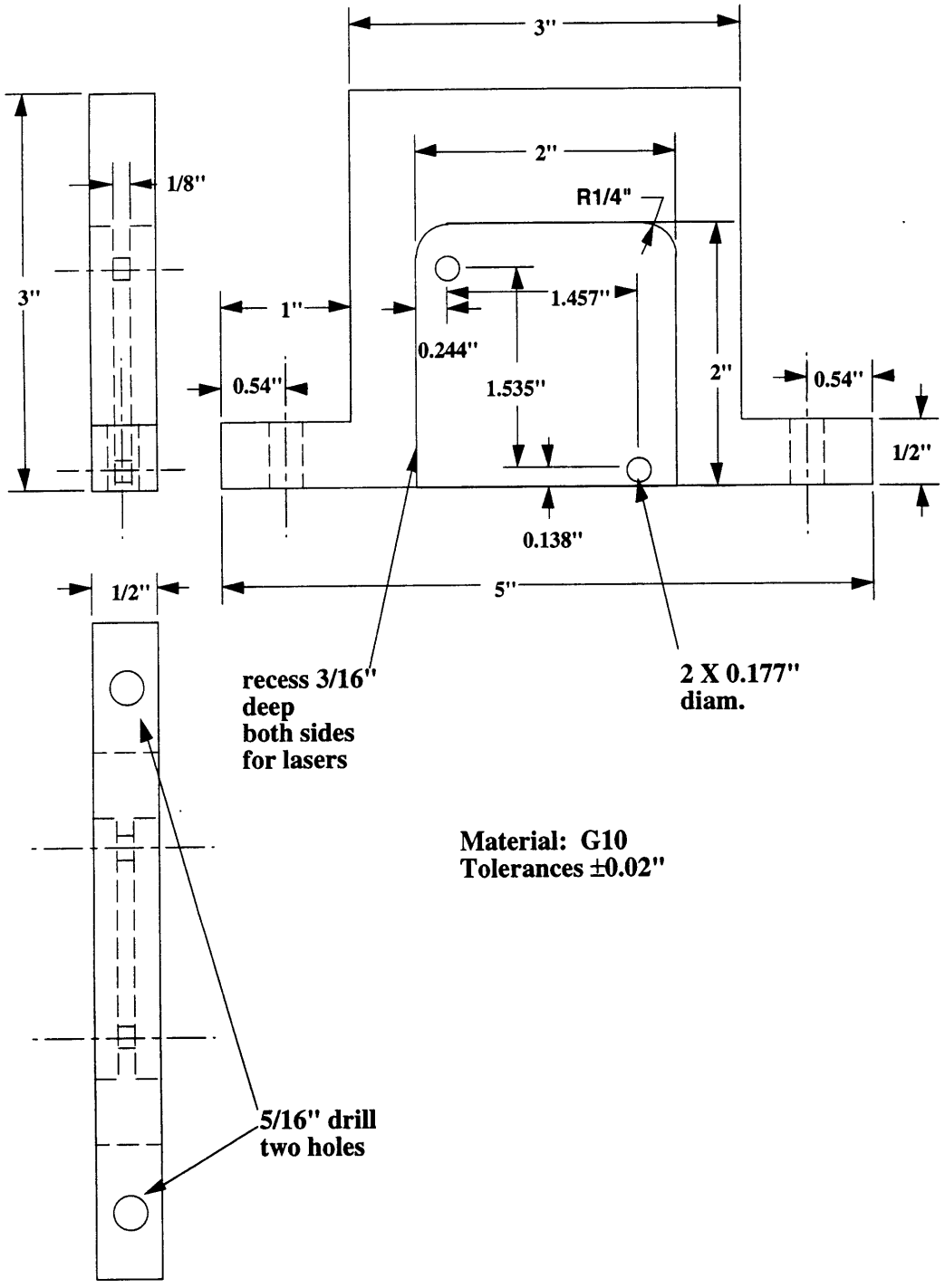

Figure 5.6 Laser mount.

which went through the laser mount and optics mount and screwed into threaded holes in the outside of the chamber wall.

The laser beams traveled through a Melles Griot optical quality window, which was mounted in an aluminum holder outside the chamber. The beams reflected off points on the specimen 1/16" (1.59 mm) from the free end of the specimen and 1/16" (1.59 mm) from each horizontal edge. A drawing of one of the identical halves of the optical window mount is shown in Figure 5.7.

Specimens were affixed in a U-shaped aluminum specimen mount, shown in Figure 5.8. The specimen mount was attached to the inside of the optical window mount with two 6" (15.24 cm) long 10-32 steel threaded rods, which screwed into holes drilled and tapped in the optical window mount. The attachment of the specimen mount was done by attaching the rods to the optical window mount instead of bolting directly to the inside of the chamber wall because of the relatively high CTE and long time constant of the chamber wall itself. The mounting system used decouples the experimental measurements from any motion of the chamber wall. The specimen mount was attached to the threaded rods with one nut on either side of the specimen mount on each rod.

One end of the specimens was clamped at the base of the U. Two holes were drilled and tapped in the specimen mount 2" (5.08 cm) apart. A rectangular aluminum piece 1" x 3" (2.54 cm x 7.62 cm) had clearance holes drilled in locations which aligned with the holes in the specimen mount. Two 4-40 screws went through the clearance holes and screwed into the specimen mount. There was enough clearance between the screws for the specimen root, which was clamped between the rectangular piece and the specimen

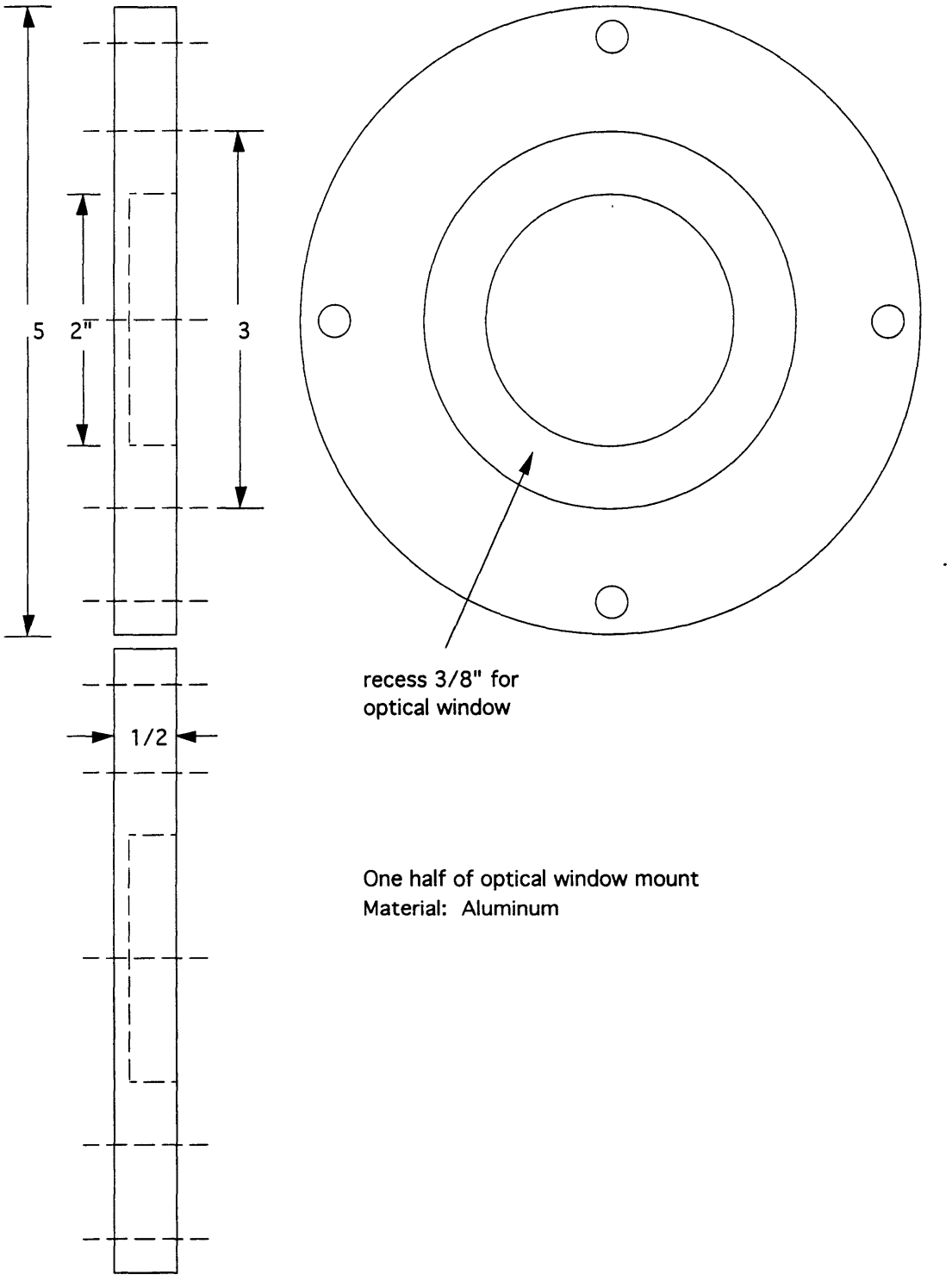

Figure 5.7 Optical window mount.

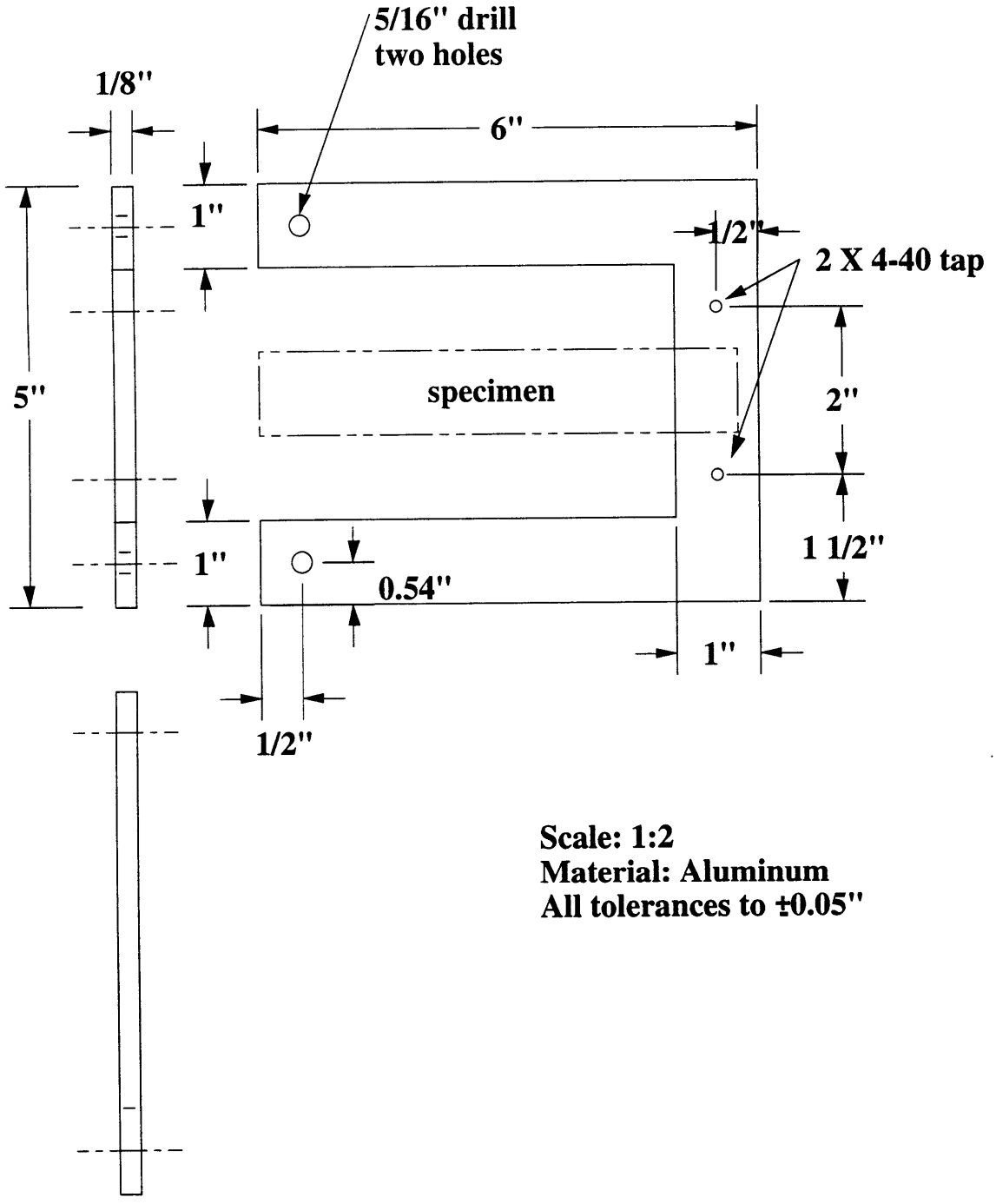

Figure 5.8 Specimen mount.

mount by the force of the screws. The other end of the specimen, where laser measurements were taken, was free to deflect in any way.

5.3.2 Data Collection

This subsection details the data collection procedures used. First, data collection is described for runs used to characterize the thermal environment of the chamber. Following that is a description of the data collection procedures for the data production runs. The latter tests generated experimental data for all specimens in the test matrix.

Each specimen had a K-type thermocouple attached with RTV rubber adhesive near the root. The output from these thermocouples was converted to a linearly proportional voltage with an Omega Model TAC-80K thermocouple signal conditioner placed outside the chamber at room temperature. The K-type thermocouple wire traveled out of the chamber through a port in the wall. During calibration runs to characterize the thermal environment of the chamber, ten J-type thermocouples were placed on the equipment at various locations described below. These J-type thermocouples were attached with flash tape. The wires placed inside the chamber exited the chamber through a port and were connected to a ten-channel Omega Model 199 J-type thermocouple signal conditioner, which remained outside the chamber at room temperature. The J-type signal conditioner displayed temperature directly. Temperature values were recorded manually by switching between channels on the J-type signal conditioner and writing the values in a laboratory notebook. The K-type thermocouple and laser outputs were in the form of proportional voltages, which were read with an Omega digital voltmeter with an A-B-C switch. Values were written in the laboratory notebook.

There were three different placement schemes used for the J-type thermocouples, as shown in Figure 5.9, where Nx denotes thermocouple number x for configuration N. N takes on values of A, B, and C, and x varies from 1 to 10. Finally, K denotes the placement of the K-type thermocouple. It is important to note that placements A and B were used with an earlier laser mount made of aluminum. Specimens used in these thermal characterization runs were made from aluminum, steel, and graphite/epoxy. There was no significant change in temperature data with specimen material.

The placements of the J-type thermocouples shown in Figure 5.9 was designed to give an accurate understanding of the thermal response of the test setup. Some placements were constant throughout all three placement scenarios. All three had thermocouples 1 and 2 on the laser sensor heads. These were used to determine the temperature of the laser sensors, which was important in data reduction, as will be explained in the next subsection. All placements also had thermocouple number 4 on the ambient side of the optical window mount, and 6,7, and 8 were always at various places on the threaded rods. These thermocouples showed the temperature gradient from the specimen temperature to the temperature outside the chamber. All placements had thermocouples 9 and 10 on the specimen mount, which allowed confirmation that the specimen and its mount were reaching the desired temperature. Placements A and C had thermocouple number 3 on the side of the laser mount. Thermocouple A5 was placed on the inside of the optical window mount, so the temperature gradient through the optical window mount could be examined. Thermocouples B3, B5, and C5 were placed on the specimen. In addition to the K-type thermocouple on the specimen, these thermocouples allowed confirmation that the specimen

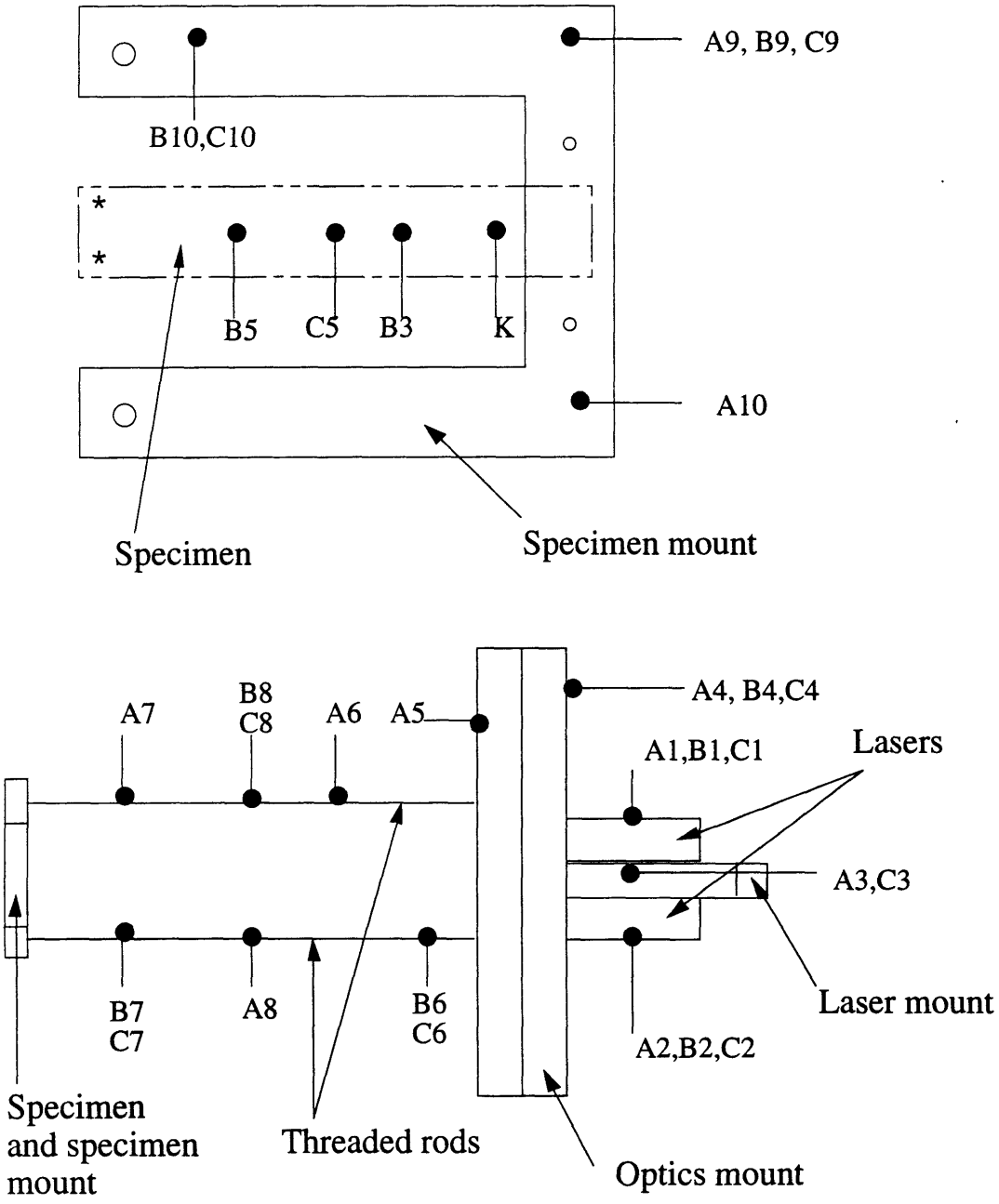

Figure 5.9 Placement of J-type thermocouples.

reached thermal equilibrium throughout its length at a consistent value. Results from these temperature tests are discussed in the next subsection.

During production runs, all but two of the J-type thermocouples were removed. The remaining thermocouples were C1 and C2 in Figure 5.9, which were mounted on the laser housings. These thermocouples remained attached to the J-type multi-channel signal conditioner, which stayed outside of the chamber at room temperature. The K-type thermocouple was attached to the specimen. Its wire left the chamber through a port, where it was connected to the Omega K-type signal conditioner. The output from the K-type signal conditioner as well as the two output voltages from the laser controllers were connected with BNC cable to an A-B-C switch. The output of this switch led to an Omega digital voltmeter. During testing, outputs from the K-type thermocouple signal conditioner and the laser sensors were read from the voltmeter and written in a laboratory notebook, and temperatures from the J-type thermocouples were read directly from the J-type signal conditioner and written in the laboratory notebook.

5.3.3 Thermal Calibration

The temperature data from the J-type thermocouple calibration runs clarified the thermal environment of the chamber and the thermal response of the test setup. Tables 5.2, 5.3, and 5.4 show thermocouple temperatures for typical runs with placements A, B, and C, respectively. In all three cases, the final chamber setpoint was 150°C (302°F). Measurements were taken until all thermocouples reached equilibrium temperatures.

Temperature values for a typical run with placement A are shown in Table 5.2. Thermocouples K, A9 and A10 reached equilibrium temperatures within 2°C (3.6°F) of the chamber setpoint. Thermocouples A6, A7, and A8

Table 5.2 Thermal Chamber Temperature Profile for Placement A

Time is in minutes

All temperatures are in °C

Time	K	A1	A2	A3	A4	A5	A6	A7	A8	A9	A10
0	23.4	24	24	24	23	24	24	25	24	25	26
15	19.2	25	25	24	24	24	24	22	22	21	21
30	20.9	25	25	25	24	24	23	23	23	23	23
45	47.8	26	26	25	25	27	38	44	45	50	50
60	48.3	27	27	27	27	30	41	46	47	50	51
75	48.3	28	28	28	28	30	41	47	47	50	51
90	48.4	29	29	28	29	31	41	47	47	50	51
105	48.3	30	30	29	30	32	41	47	47	50	51
120	48.4	31	30	30	30	32	42	47	47	50	51
135	48.4	31	30	29	30	32	42	47	47	50	51
150	96.4	32	31	31	32	38	67	84	83	98	99
165	98.6	35	34	34	36	42	71	88	87	100	100
180	98.7	37	36	36	38	44	72	88	88	100	100
195	98.7	38	38	37	39	45	73	89	88	100	100
210	98.8	39	38	38	40	45	73	89	88	100	100
225	99.8	39	39	38	40	46	73	89	88	100	100
240	143	39	39	38	40	46	74	89	88	100	100
255	148	39	39	38	41	52	95	123	120	145	146
270	148	41	41	40	44	56	101	129	126	148	149
285	148	43	43	42	46	57	103	130	127	149	150
300	148	44	44	41	47	58	104	130	127	149	149
315	148	45	44	42	47	59	104	130	128	150	150
330	148	44	45	42	48	60	104	130	128	150	150
345	148	43	45	42	48	59	104	131	128	149	150
360	148	46	46	43	48	59	104	131	128	149	150

Table 5.3 Thermal Chamber Temperature Profile for Placement B

Time is in minutes

All temperatures are in °C

Time	K	B1	B2	B3	B4	B5	B6	B7	B8	B9	B10
0	23.1	24	24	26	24	26	24	25	25	26	26
15	23.1	25	25	25	24	25	24	25	25	25	25
35	46.9	26	26	50	26	49	31	48	43	50	50
50	47.7	27	27	50	27	50	33	49	44	50	50
65	47.6	28	28	50	28	50	33	49	44	50	51
80	47.6	28	28	50	28	50	33	49	44	50	51
95	47.6	28	28	50	28	50	34	49	45	50	51
110	86.9	29	29	97	30	95	43	92	76	97	98
125	95.5	31	32	100	32	99	47	95	81	99	100
140	96.1	33	33	100	34	99	48	95	82	99	100
155	96.2	34	34	100	34	99	49	95	82	99	100
170	96.0	34	35	100	36	99	50	95	82	99	100
185	95.5	36	36	99	37	99	50	95	82	98	100
200	95.3	37	36	99	37	97	50	95	82	98	100
215	95.4	37	37	99	38	98	51	95	82	98	99
230	95.3	37	37	99	38	98	51	95	82	98	100
260	142	40	40	147	43	146	63	140	118	145	149
300	143	43	43	148	46	146	66	141	119	146	149
328	143	44	44	148	46	146	67	141	119	146	149
358	143	45	45	148	47	146	67	140	119	146	149
388	143	45	45	148	47	146	67	141	119	146	149

Table 5.4 Thermal Chamber Temperature Profile for Placement C

Time is in minutes

All temperatures are in °C

Time	K	C1	C2	C3	C4	C5	C6	C7	C8	C9	C10
0	22.4	24	24	24	23	25	24	24	24	25	25
15	21.9	26	26	25	24	24	24	24	24	24	24
30	22.3	27	28	25	24	24	24	24	24	25	25
45	22.4	29	28	26	25	25	25	25	25	25	25
60	22.5	29	29	27	25	25	25	25	25	25	25
80	22.7	29	30	27	26	25	26	25	25	25	25
92	22.5	30	30	27	26	25	26	25	25	25	25
105	22.5	30	30	27	26	25	26	25	25	25	25
120	47.5	30	30	27	27	49	32	48	42	49	50
135	48.2	30	30	27	28	50	33	49	44	50	50
150	48.2	31	31	28	29	50	34	49	44	50	51
165	48.1	31	31	28	29	50	34	49	45	50	50
180	47.7	31	31	28	30	50	35	49	45	50	50
195	47.7	31	31	28	30	50	35	49	45	50	50
210	95.8	31	31	28	32	97	44	93	77	97	99
225	97.3	32	32	28	34	99	48	95	81	99	100
240	97.3	32	32	29	36	99	50	96	82	99	100
255	97.2	33	33	30	37	99	51	96	82	99	100
270	97.2	34	34	30	38	99	51	96	83	99	100
285	97.2	34	34	31	38	99	52	96	83	99	100
300	97.2	34	34	31	39	99	52	96	83	99	100
315	143	35	34	30	40	144	60	137	113	144	147
330	145	35	35	31	43	147	64	141	118	146	149
345	145	36	36	32	45	147	66	141	120	147	150
360	145	36	36	32	46	147	67	142	120	146	150
420	145	36	37	34	48	147	69	142	121	146	150
487	145	37	37	33	47	147	68	141	119	146	149

show there is a gradient along the threaded rods from a high temperature at the specimen mount to a low at the optical window mount. This gradient increases as the chamber temperature increases. A5 and A4 show the gradient through the optical window mount, which reaches 11°C (52°F) when the chamber temperature is 150°C (302°F). Thermocouples A1, A2, and A3 are mounted on the laser sensor heads and the (early version, aluminum) laser mount outside the chamber, and all heated up significantly. The final temperatures of the laser sensor heads were both 46°C (115°F).

Temperature values for a typical run with placement B are shown in Table 5.3. Thermocouples B9 and B10 reach values near the chamber setpoint. Thermocouples B6, B7, B8, and B4 once again show the gradient along the threaded rods and through the optical window mount. Since B6 is closer to the optical window mount than A6 was, it indicates a lower temperature. Thermocouples B3 and B5 show that temperatures on the specimen are within 2°C (3.6°F). Finally, thermocouples B1 and B2 show that the lasers both heated up to a temperature of 45°C (113°F), which is very similar to the final results for A1 and A2.

Temperature values for a typical run with placement C are shown in Table 5.4. It is important to note that placement C had a laser mount made of G10, while the laser mount in placements A and B was made of aluminum. Since aluminum is much more thermally conductive than G10, the equilibrium temperatures of the lasers in placements A and B were much higher than those of C. Thermocouples C9 and C10 reach equilibrium values identical to those for placement B. The gradient along the threaded rods and through the optical window mount as measured by thermocouples C6, C7, C8, and C4 is also nearly identical to that shown for placement B. Thermocouples C5 and K show the specimen again is nearly uniform in

temperature. Thermocouples C1, C2, and C3 give the temperatures of the laser sensor heads and laser mount. While these temperatures are still well above room temperatures, they are approximately 10°C (40°F) below their equivalents in placements A and B because of the different laser mount material. The final laser temperatures are both 37°C (98.6°F). The runs with all three placements served to characterize the thermal environment throughout the experimental setup.

5.3.4 Measurement Calibration

In order to verify the analysis, the data collected in the experimental investigation had to be accurate to very small deformations. The predicted smallest standard deviation of the thermal bending coefficient for the specimens in the current study was predicted to be 2.82 $\mu in/in^2/°F$ (200 $\mu m/m^2/°C$) for the $[(\pm 30)_4]_s$ panel. The tests were performed over a temperature range of 75°C (135°F). Simple calculations based on the specimen geometry indicated a repeatable tip deflection resolution better than ±0.13 mm (±5.25 mils) was needed to observe this small a thermal bending coefficient.

Calibration tests of the lasers were performed on an optical bench. First, the lasers were mounted in a stationary position on the bench. A target attached to the end of a high-precision micrometer was moved back and forth along the lines of sights of the laser. Laser output voltages and distances were recorded to obtain the laser voltage-deflection conversion. Results from this test are shown in Figure 5.10, where the different symbols represent voltages from the different laser sensor heads. Laser 1 is the one located on top in Figure 5.4, and laser 2 the one on bottom. Figure 5.10 shows that both lasers exhibit extremely good linearity. The slope of the voltage versus

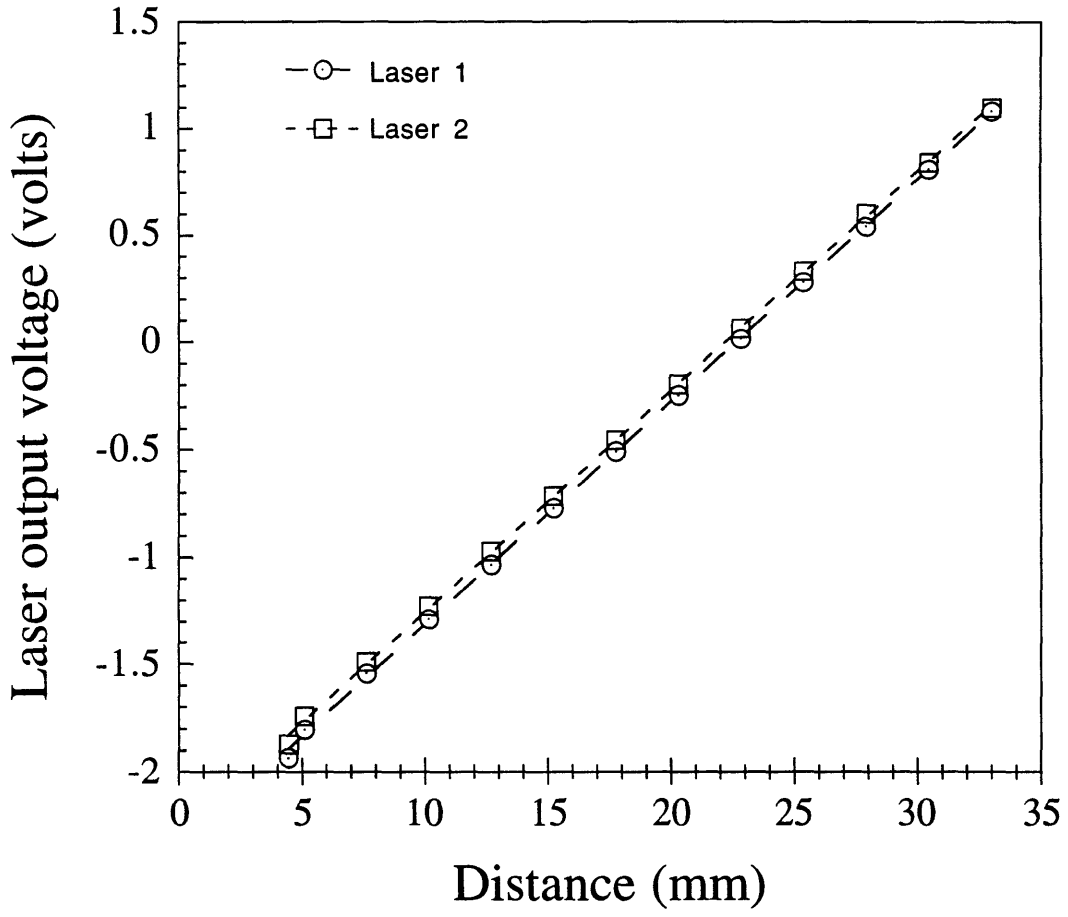

Figure 5.10 Laser output voltages versus distance to target on optical table.

distance line is 0.104 volts per millimeter (V/mm) (2.64 V/in) for laser 1, and 0.103 V/mm (2.62 V/in) for laser 2. Both have a standard error (from a least squares regression on the slopes [41]) of 0.48 millivolts per millimeter (mV/mm) (12.2 V/in). This standard error results in a measurement uncertainty of approximately 5 μm/mm, or 0.5%. The slope for both lasers is slightly different from the manufacturer's specification of 0.1 V/mm (2.54 V/in). The difference is of about the same magnitude as the measurement uncertainty. The laser voltage-distance slopes are adjustable. The adjustment is not simple, so the lasers were left at the setting which gave Figure 5.10 throughout all testing.

The second bench test verified that the presence of the optical glass in the complete experimental setup did not significantly alter the operation of the lasers. This was established by conducting these calibration tests on the optical bench at room temperature both with and without the optical glass in the path of the lasers.

Another test performed on the optical bench measured laser output voltage as a function of laser temperature. There was some change in the temperature of the laser sensor heads during the experiments, as seen in the thermal environment discussion above. Besides heating due to the increase in chamber temperature through the thermal path along the threaded rods and through the optical window and laser mounts, there was some self-heating of the lasers. This heating is due to heat produced by the operation of the electronics within the laser sensor heads. This self-heating caused the temperature of the laser heads to reach 26°C (79°F) while mounted on the optical bench, where external heating was zero. Increasing temperature causes a drift in the output voltages, which can be misinterpreted as specimen deformations.

The lasers, with thermocouples attached, were mounted on the optical bench, where they measured the distance to a stationary target. The lasers were heated with a hair dryer, and temperatures and output voltages were recorded. The hair dryer was used to heat the lasers for approximately 45 seconds and then turned off. Laser temperatures and laser output voltages remained constant over the next five minutes, so it was assumed that the lasers achieved a uniform equilibrium temperature, and cooled only very slowly in the ambient air. As can be seen in Figure 5.11, the laser output voltage increases with temperature. Note that the values and slopes of the curves in Figure 5.11 are different. The slope of the voltage versus temperature line is 4.5 mV/°C (2.5 mV/°F) for laser 1, and 6.1 mV/°C (3.4 mV/°F) for laser 2. Both slopes have a standard error of 0.55 mV/°C (0.31 mV/°F). Since the laser sensor heads undergo a temperature change of approximately 5°C (9°F) during a typical test, the uncertainty for the test is about 2.75 mV, which translates to about 0.03 mm (1.2 mils) using the voltage-distance calibration results above. Thermocouples were placed on the laser head housings for all of the specimen tests, and these readings were used to adjust the laser output voltages for laser temperature. Each laser's temperature-voltage curve was used separately in the data reduction to remove the voltage change due to heating, as will be explained further in Section 5.5.

During testing with the environmental chamber, the output voltage of each of the lasers as measured by the voltmeter varied ±1 millivolt around an average value while taking an equilibrium temperature reading. Using the voltage-displacement calibration results, this voltage uncertainty translates to a distance uncertainty of ±10 μm (±0.4 mils).

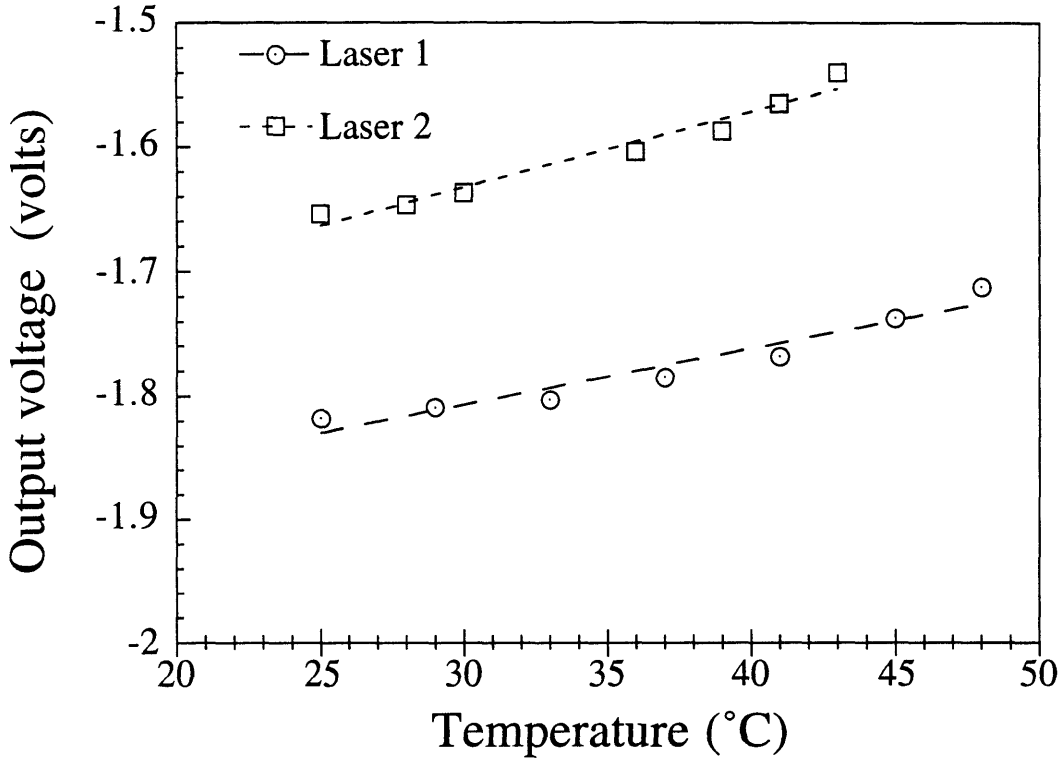

Figure 5.11 Laser output voltages versus temperature of laser sensor heads.

Several calibration tests using the entire test set-up were performed. An aluminum specimen with the same dimensions as the graphite/epoxy test specimens was placed in the specimen mount for these tests. It was assumed the aluminum specimen would have negligible curvature with temperature. The calibration tests were run with the same experimental procedure (detailed in the next section) as the production tests. The chamber was taken to temperatures of 25°C and 100°C (77°F and 212°F) at a rate of 4°C/minute (7.2 °F/minute). The chamber was held at these setpoint temperatures until the laser output voltage reached equilibrium. The chamber was then ramped up to the next temperature setpoint. Laser output voltages and temperatures of the specimen and laser sensor heads were recorded.

To test repeatability, the experimental procedures discussed in the next section were executed four times. The specimen was completely removed and then remounted between runs. Laser output voltages and temperatures were measured. Figure 5.11 was used to correct each laser's output for the effect of laser temperature change on the measurement. After this correction, there was still some change in laser output voltage with temperature. This voltage change was assumed to be the result of thermally induced deformations of the equipment.

The equilibrium laser output voltages at 25°C and 100°C (77°F and 212°F) from the aluminum specimen tests at approximately one hour after the beginning of the temperature ramp, adjusted for laser temperature change, were used to determine the deformation of the equipment. Table 5.5 shows equilibrium voltages from the four calibration runs. The data has been adjusted for the change of laser output voltage with laser temperature, and the initial voltages were taken to be zero. In all cases, there is an increase in adjusted voltage from 25°C to 100°C (77°F and 212°F). The average adjusted

Table 5.5 Equilibrium Data and Reduction for Calibration Runs

All values are in volts.
All values have been compensated for laser temperature change and zero point.

	Laser 1			Laser 2		
Run	25°C voltage	100°C voltage	voltage change	25°C voltage	100°C voltage	voltage change
1	.044	.071	.027	.030	.052	.022
2	.039	.066	.027	-.001	.016	.017
3	.036	.064	.028	.021	.044	.023
4	.053	.067	.014	.056	.068	.012
Average			0.024			0.019
Range			0.014			0.011

voltage change was 24 mV for laser 1, and 19 mV for laser 2. Using the laser voltage-distance calibration in Figure 5.10, these voltage changes translate to distance changes of 0.24 mm (9.4 mils) and 0.19 mm (7.5 mils) for laser 1 and laser 2, respectively. This deformation was subtracted from the deformation measured in the tests with the remainder of the specimens. The total range of the four calibration runs was 14 mV for laser 1, and 12 mV for laser 2. The measured uncertainties of the calibration voltages are thus +4/-10 mV for laser 1, and +4/-7 mV for laser 2. This means the displacements are known to +0.04/-0.10 mm (+1.6/-3.9 mils) for laser 1, and +0.04/-0.07 mm (+1.6/-2.8 mils) for laser 2.

The total uncertainty needs to be known to examine the validity of the experiment. The first source of uncertainty is the conversion from laser output voltage to distance. As mentioned above, the error in this calibration was 0.48 mV/mm (12.2 V/in) for both lasers, or 4.8 μm per mm of displacement. Since most total displacements are small, this uncertainty is very small compared to others. The next uncertainty source is the correction of laser voltage for laser sensor head temperature. During a typical test, this uncertainty is approximately 2.75 mV, or about 0.03 mm (1.2 mils), again a very small value. The distance resolution of the lasers was ±10 μm (±0.4 mils), which is very small compared to other uncertainties. The final source of uncertainty was the run-to-run variation of the equipment deformations. The observed run-to-run variation in simulated data production testing was +4/-10 mV, which translates to +0.04/-0.10 mm (+1.6/-3.9 mils). Summing all of the uncertainties gives a total uncertainty for the experiments of +0.07/-0.13 mm (+2.8/-5.1 mils). As mentioned above, the resolution needed in the experiments according to the analysis was ±0.13 mm (±5.25 mils). The similarity of the numbers means that the experimental setup could not

observe the smallest thermal bending coefficients predicted. Fortunately, the vast majority of the layups in the experimental test matrix have thermal bending coefficient standard deviations large enough that this problem does not arise. The $[(\pm 30)_4]_s$ layup, the $[0_2/(\pm 30)_2]_s$ and the $[0_{10}/30_{10}]_s$ layups are the only ones in the test matrix with thermal bending coefficient standard deviations small enough to be severely affected by the equipment-induced uncertainty.

5.4 EXPERIMENTAL PROCEDURES

In order to obtain the thermal bending coefficients of the test specimens, deflections were measured at different temperatures. Data was collected from a limited number of specimens at 25°C, 50°C, 100°C, and 150°C (77°F, 122°F, 212°F, and 302°F). These tests showed that the relation between temperature and displacement was linear. Therefore, in the remainder of the tests deflections were measured at only two temperatures: 25°C and 100°C (77°F and 212°F).

The specimen was attached to the specimen mount, and the chamber was purged with dry gaseous nitrogen to remove moisture. The chamber was set to 25°C (77°F) and turned on. Laser output voltage and temperatures of thermocouples K (on the specimen), C1 (on laser 1), and C2 (on laser 2) were recorded every fifteen minutes until an equilibrium laser output voltage within ±1 millivolt (mV) was reached. During this time, typically 45 minutes, there was some change in laser output voltage from the initial measurements due to the self-induced heating of the laser heads.

Once equilibrium was obtained, the controller was used to ramp the chamber temperature up to 100°C (212°F) at a rate of 4°C/minute

(7.2°F/minute). Laser voltage and temperature data were taken at the beginning of the temperature ramp, 15 minutes after the beginning of the temperature ramp, and at 5 minute intervals from 30 minutes to one hour after the beginning of the temperature ramp. Typically, at approximately 45 minutes after the beginning of the temperature ramp, laser output voltages and temperatures throughout the chamber reached equilibrium. The laser output voltages and temperatures recorded at this time were used in the data reduction procedures detailed in the next section.

At one hour after the beginning of the temperature ramp to 100°C (212°F), the controller was used to cool the chamber down to 25°C (77°F) at the rate of 4°C/minute (7.2°F/minute). After the chamber returned to 25°C (77°F), the specimen was removed and rebagged.

The raw data taken included output voltages from the laser sensors and thermocouple signal conditioners and times of readings. Values were written in a laboratory notebook for later entry into a Microsoft Excel spreadsheet for data reduction. Figure 5.12 shows raw laser output voltages versus time for a typical specimen. It is specimen C of the first $[\pm 30]_s$ panel. The complete set of raw data values for this specimen is given in Table 5.6.

5.5 DATA REDUCTION

This section describes the data reduction techniques used in the current work. Raw equilibrium laser output voltages for each laser sensor V_1 and V_2 at the two temperatures are subtracted to get the changes in laser voltages, as in Eqs. 5.1 and 5.2, where $V_i(j)$ is the output voltage of laser i at chamber temperature j.

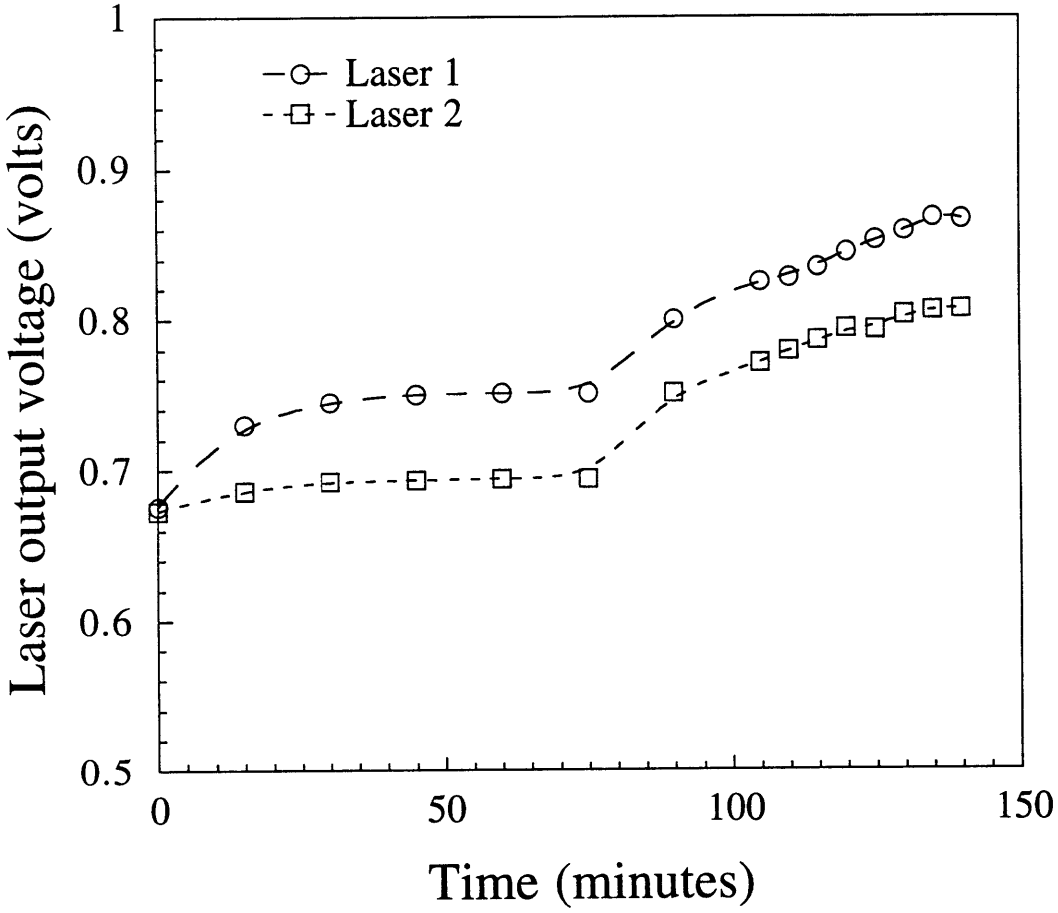

Figure 5.12 Typical raw specimen data.

Table 5.6 Typical Tabulated Raw Specimen Data

Time is in minutes

All temperatures are in °C

Laser voltages are in volts

Time	K Temp.	Laser 1 V	Laser 2 V	Laser 1 T	Laser 2 T
0	23.6	0.676	0.673	26	26
15	23.3	0.730	0.686	29	29
30	23.5	0.745	0.692	29	29
45	23.5	0.750	0.693	29	30
60	23.3	0.751	0.694	29	30
75	23.3	0.751	0.694	30	30
90	93.6	0.8	0.751	30	30
105	98.0	0.825	0.771	31	31
110	98.2	0.828	0.779	32	32
115	98.1	0.835	0.786	32	32
120	98.1	0.845	0.794	33	33
125	98.1	0.853	0.793	33	34
130	98.0	0.859	0.803	34	34
135	98.0	0.868	0.806	34	34
140	98.0	0.868	0.806	34	34

$$\Delta V_{1raw} = V_1(100^\circ C) - V_1(25^\circ C) \tag{5.1}$$

$$\Delta V_{2raw} = V_2(100^\circ C) - V_2(25^\circ C) \tag{5.2}$$

The laser voltage versus laser temperature curves are then used to correct for the voltage change due to heating of the lasers:

$$\Delta V_{1Tadj} = \Delta V_{1raw} - m_{1T}\left[T_1(100^\circ C) - T_1(25^\circ C)\right] \tag{5.3}$$

$$\Delta V_{2Tadj} = \Delta V_{2raw} - m_{2T}\left[T_2(100^\circ C) - T_2(25^\circ C)\right] \tag{5.4}$$

where m_{1T} and m_{2T} are the slopes of the laser voltage versus laser temperature curves for laser 1 and laser 2 respectively, and $T_i(j)$ is the temperature of laser i at chamber temperature j. The amount of displacement in the experimental setup is subtracted from this result to give the laser voltage change in Eqs. 5.5 and 5.6.

$$\Delta V_{1f} = \Delta V_{1Tadj} - \Delta V_{1equip} \tag{5.5}$$

$$\Delta V_{2f} = \Delta V_{2Tadj} - \Delta V_{2equip} \tag{5.6}$$

Next, the laser voltage versus distance curves are used to find the amount the specimen distance changes with temperature in Eqs. 5.7 and 5.8. In these equations m_{1D} and m_{2D} are the slopes of the laser voltage versus distance curves for laser 1 and laser 2 respectively, and ΔD_1 and ΔD_2 are the changes in distances as measured by the two lasers and corrected for laser temperatures and equipment deformation.

$$\Delta D_1 = \frac{\Delta V_{1f}}{m_{1D}} \tag{5.7}$$

$$\Delta D_2 = \frac{\Delta V_{2f}}{m_{2D}} \tag{5.8}$$

Two lasers are used in the experiments to enable identification of two elements of curvature. The average of the two distances gives curvature in the one direction, and the difference the curvature in the six direction, through Eqs. 5.9 and 5.10 respectively.

$$\kappa_1 = \frac{(\Delta D_1 + \Delta D_2)}{L^2} = W_1^T \Delta T \tag{5.9}$$

$$\kappa_6 = \frac{2(\Delta D_1 - \Delta D_2)}{LB} = W_6^T \Delta T \tag{5.10}$$

In these equations, L is the distance between the clamp and the laser spots, and B is the distance between laser spots (See Figure 5.13).

Specimens from one panel, with the layup $[0_3/90]_T$, could not be analyzed with Eq. 5.9. Specimens from this panel had dominant curvature in the y direction, while all other cross-ply unsymmetric specimens had dominant curvature in the x direction. The x axis is defined as along the length of the specimen as shown in Figure 5.13. In finding the experimental value for $\mathbf{W}_2^T$ for this panel, the data reduction technique is slightly altered. The equation for curvature becomes

$$\kappa_2 = \frac{(\Delta D_1 + \Delta D_2)}{B^2} = W_2^T \Delta T \tag{5.11}$$

It should be noted that Eq. 5.9 assumes that the curvature in the y direction is zero, just as Eq. 5.11 assumes that the curvature in the x direction is zero. This assumption puts some error into the reduction, but the amount is not large. For the majority of the specimens, a CLPT analysis indicates the error is of the order of B^2/L^2, or approximately 1/36. For the $[0_3/90]_T$ specimens the error cannot be established, as the large deformation analysis used indicates that the x direction curvature should be zero.

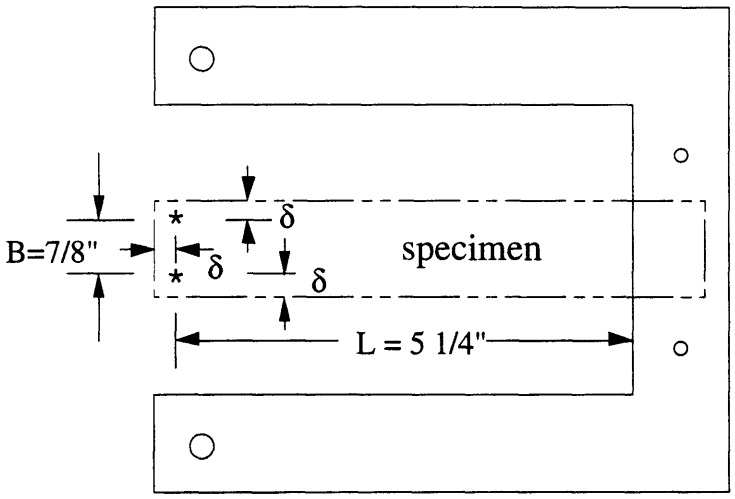

* denotes laser spot

$\delta = 1/16"$

Figure 5.13 Geometry used in curvature and W^T calculations.

Once the changes in curvatures are calculated, they are divided by the change in temperature. The results are the one and six elements of the thermal bending coefficient vector for all specimens, and the two element of the vector for the $[0_3/90]_T$ specimen. Means and standard deviations of the data taken from five specimens from each panel are calculated. Results from the experimental investigation and comparisons with model predictions are presented in Chapter 6.

5.5.1 Example Specimen Data Reduction

This subsection contains the step-by-step data reduction for an example specimen. The example specimen is specimen C of the first $[\pm 30]_s$ panel, for which raw data and a plot of the raw output laser voltages are presented in Table 5.6 and Figure 5.12, respectively.

Table 5.7 shows the data reduction and uncertainties for the example specimen in both metric and English units. The units of all voltages are millivolts. The units of the tip displacements (Δz) are millimeters in the metric system, and mils in the English system. The units of the thermal bending coefficients are $\mu m/m^2/°C$ in the metric system, and $\mu in/in^2/°F$ in the English system.

Voltages at the equilibrium temperatures 25°C and 100°C (77°F and 212°F) and the raw ΔV between them are shown for both lasers in the raw data row. Table 5.6 shows that the temperatures of the lasers are both 29°C (84°F) while the chamber is in thermal equilibrium at 25°C (77°F), and both laser temperatures are 34°C (93°F) while the chamber is in thermal equilibrium at 100°C (212°F). From these temperatures and the laser voltage-laser temperature calibration of Figure 5.11, the ΔV's are adjusted for the change due to the heating of the lasers. The temperature adjusted

Table 5.7 Typical Tabulated Specimen Data Reduction

	Laser 1				Laser 2				Thermal bending coefficient	
	25C	100C	ΔV	Δz	25C	100C	ΔV	Δz	W_1^T	W_6^T
Metric Units	mV	mV	mV	mm	mV	mV	mV	mm	μm/m²/°C	μm/m²/°C
Raw data	751	868	117		694	806	113			
Temp. adjusted			99				88			
Setup adjusted			75	0.721			69	0.675	1050	414
Uncertainty			+7 -13	+0.07 -0.13			+7 -13	+0.07 -0.13	±195	±1800
English Units				mil				mil	μin/in²/°F	μin/in²/°F
Setup adjusted				28.4				26.5	14.8	5.84
Uncertainty				+2.8 -5.2				+2.8 -5.2	±2.75	±25.4

ΔV's are shown in Table 5.7. The next step is to remove the voltage changes due to the thermal deformation of the test setup. This is accomplished by subtracting the average of the voltage changes of the calibration runs, which are given in Table 5.5. The resulting corrected ΔV's are 75 mV for laser 1, and 69 mV for laser 2. These voltage changes are converted to displacement changes by using the laser voltage-distance calibration of Figure 5.10. The displacement changes are 0.721 mm (28.4 mils) for laser 1, and 0.675 mm (26.5 mils) for laser 2. Finally, Eqs. 5.9 and 5.10 are used to calculate the bend and twist curvatures, which are divided by the specimen temperature change to yield the thermal bending coefficients W_1^T and W_6^T. The values for these coefficients are 1050 $\mu m/m^2/°C$ (14.8 $\mu in/in^2/°F$) and 414 $\mu m/m^2/°C$ (5.84 $\mu in/in^2/°F$), respectively. Note that the uncertainty is approximately 18% of the W_1^T value. The uncertainty dominates the W_6^T data. This is due to the fact that this specimen had a very low W_6^T value. The other specimens from this panel had much larger values of W_6^T, which put them beyond the uncertainty of the equipment. The final rows show adjusted mean values and uncertainties in English units, which will be used for most data presentation in the following chapter.

The $[0_3/90]_T$ panel has a different uncertainty. Comparing Eqs. 5.9 and 5.11 shows that the difference in uncertainties will be due to the differences in the denominator. The specimen width B is much smaller than the specimen length L (see Figure 5.13), which makes the uncertainty much larger. The calculated uncertainties for this panel are 7020 $\mu m/m^2/°C$ (210 $\mu in/in^2/°F$).

CHAPTER 6

RESULTS AND DISCUSSION

Experimental and analytical results are presented and discussed in this chapter. The experimentally measured thermal bending coefficients are presented and correlated with analytical predictions. Large-deformation analytical results are presented for those layups which do not follow CLPT predictions. Parametric studies are presented to examine the importance of various material property and geometry variations to dimensional stability.

6.1 EXPERIMENTAL RESULTS AND CORRELATIONS

6.1.1 Introduction

Experimental results are presented in this section. Raw data may be found in Appendix D, including specimen temperatures, laser output voltages, and laser sensor head temperatures. All data presented in this section is reduced to the x-direction bending and x-y twisting elements of the thermal bending coefficient vector (W_1^T and W_6^T) using the procedures outlined in Section 5.5.

Two types of graphs are presented in this section. The first type shows the experimental thermal bending coefficients W_1^T and W_6^T. All data is shown, one point per specimen. The second type of graph shows correlations of the experimental thermal bending coefficients data with the predictions of the CLPT-based analysis developed in Sections 4.1 and 4.2 and implemented

in the VARBEND computer program. This analysis will be referred to as the VARBEND analysis in the remainder of this document. In these graphs, the experimental data has been further reduced to mean and standard deviations. The +/- one standard deviation range of properties predicted by the analysis are represented by thick gray bars. The data is shown superimposed, with a symbol at the mean value, and +/- one standard deviation error bars. For the purposes of the present discussion, the term "interval" will be used for the mean thermal bending coefficient +/- one standard deviation. In all cases, the bend and twist thermal bending coefficients are plotted against laminate type. Groups of laminates are presented in each figure so trends can be examined.

The units of the thermal bending coefficients are those of curvature divided by temperature. From Eqs. 5.9–5.11, it can be seen that the units of the thermal bending coefficients are in/in^2/°F. The values of the thermal bending coefficients for the panels studied in the current work are very small, especially for the symmetric panels. Therefore, the y axes on all graphs in this section are labeled in micro-inches/in^2/°F, or μin/in^2/°F.

6.1.2 $[\pm 30]_s$ Panels

Three different panels were made with the $[\pm 30]_s$ layup, and five specimens were cut from each panel. The bend and twist thermal bending coefficients of specimens are shown for each panel individually, and also for all panels combined.

The W_1^T data are shown in Figure 6.1. The scatter in the data for each panel is readily visible. Each panel has a non-zero mean. All means are greater than zero. In addition to the difference between specimens within

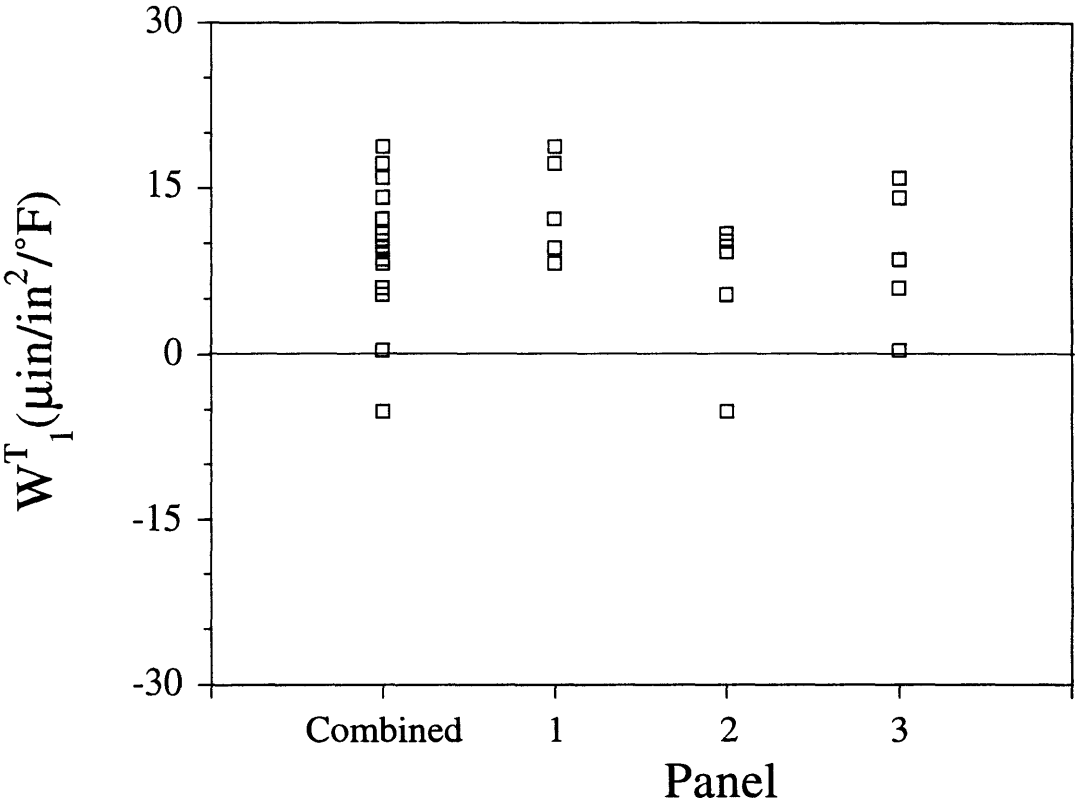

Figure 6.1 Experimental W_1^T values for $[\pm 30]_s$ panels.

each panel, there is a difference in mean W_1^T between panels. These differences are of approximately the same order.

A histogram for the combined W_1^T data is shown in Figure 6.2. It resembles a normal distribution, although the number of specimens is too small to draw any significant conclusions on the nature of the distribution.

Figure 6.3 shows correlations of W_1^T data with the VARBEND analysis for the $[\pm 30]_s$ panels. The predictions bracket the experimental data. The experimental standard deviations are much smaller than predicted. The experimental intervals vary from panel to panel, and from each panel to the combined interval, by less than one experimental standard deviation. The standard deviation for all panels combined is of the same order as the standard deviations for a single panel.

The W_6^T data for the $[\pm 30]_s$ panels are shown in Figure 6.4. There is much more scatter in this data than in Figure 6.1–note the difference in scales. All means are non-zero and positive. The differences within panels are similar to those between panels.

A histogram for the combined W_6^T data is shown in Figure 6.5. No conclusions can be drawn from this distribution.

Figure 6.6 shows correlations of W_6^T data with the VARBEND analysis for the $[\pm 30]_s$ panels. The predictions again bracket the experimental data. The experimental intervals are closer to the analytical predictions than was the case for the W_1^T correlation. The amount the intervals vary from panel to panel, and from each panel to combined data, is less than one experimental standard deviation. The standard deviation for all panels combined is of the same order as the standard deviations for a single panel.

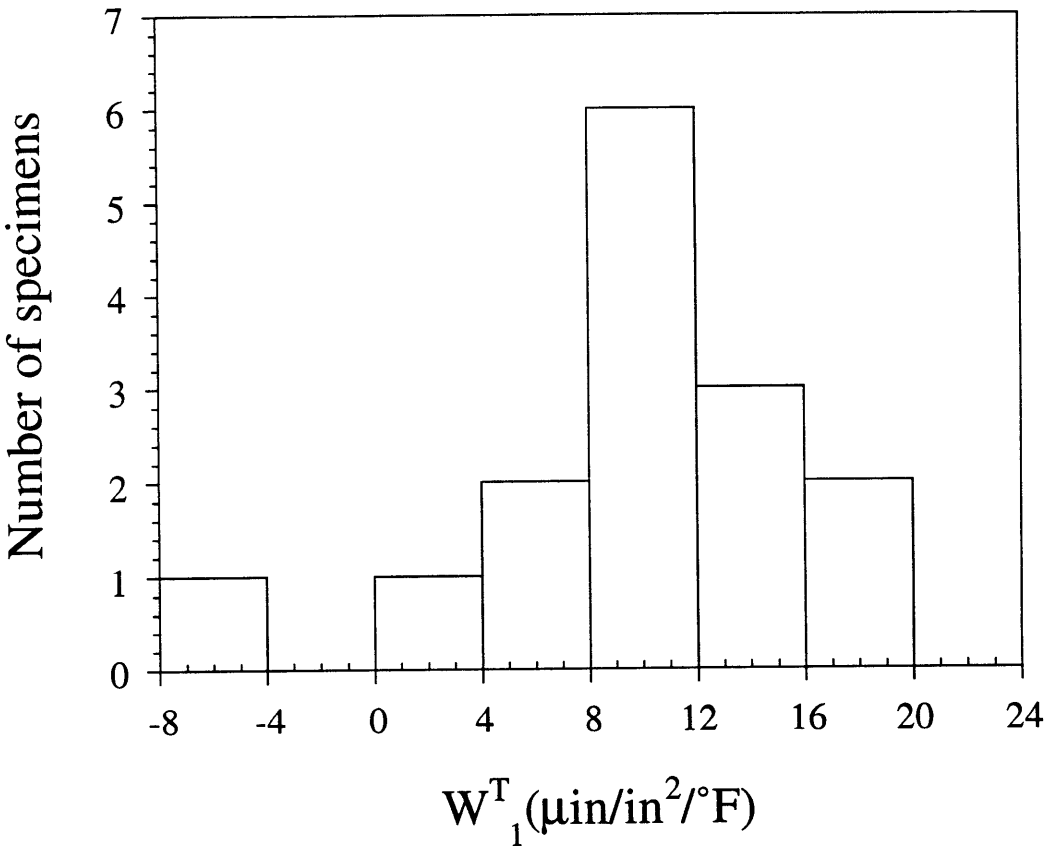

Figure 6.2 Histogram of W_1^T values for $[\pm 30]_s$ panels.

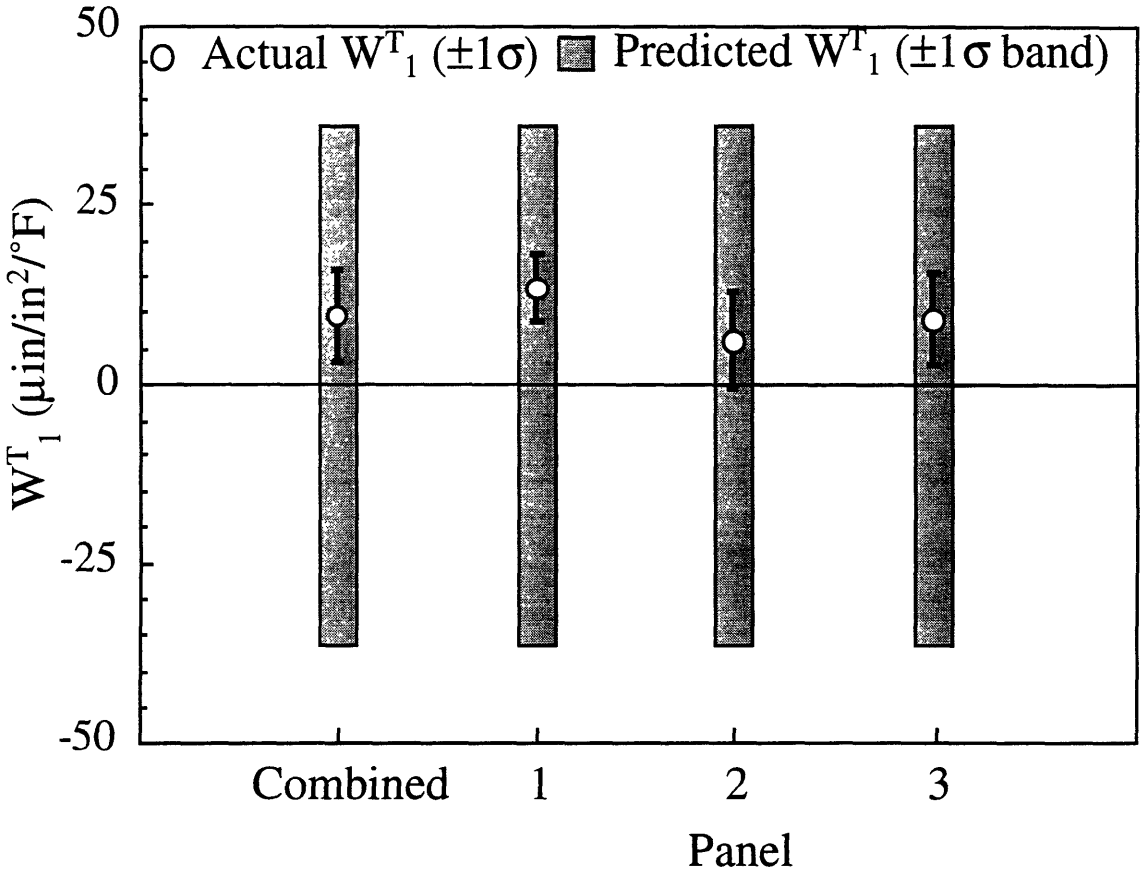

Figure 6.3 Correlation of W_1^T values for $[\pm 30]_s$ panels.

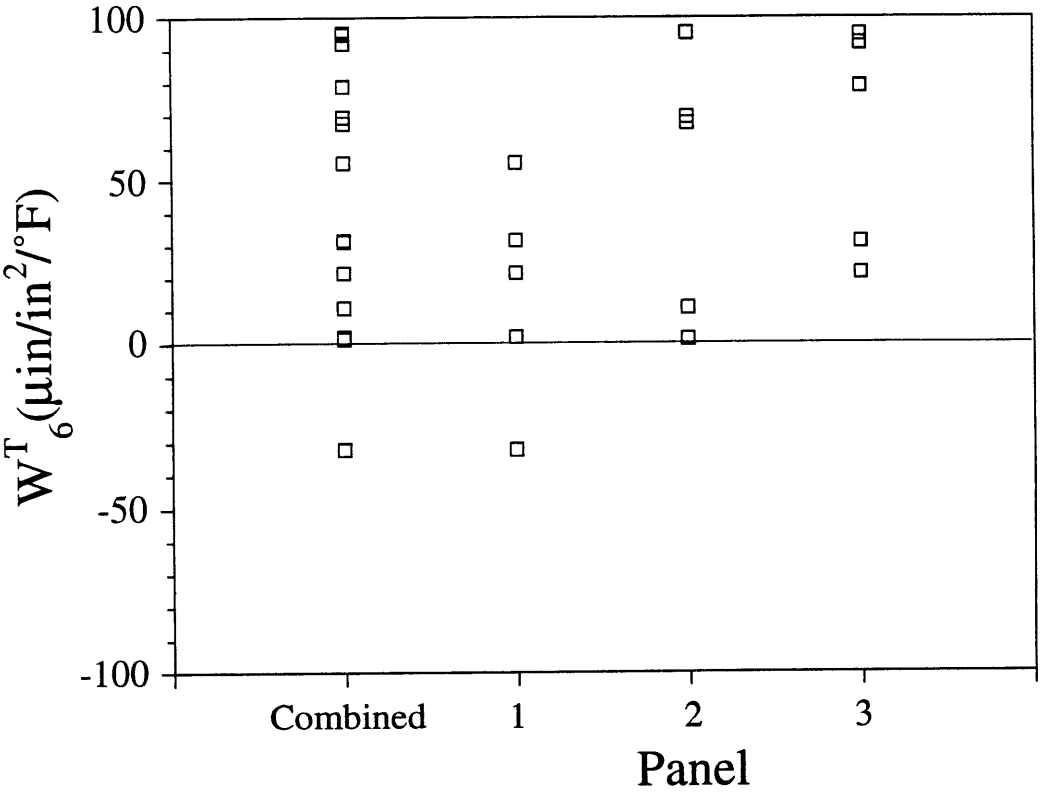

Figure 6.4 Experimental W_6^T values for $[\pm 30]_s$ panels.

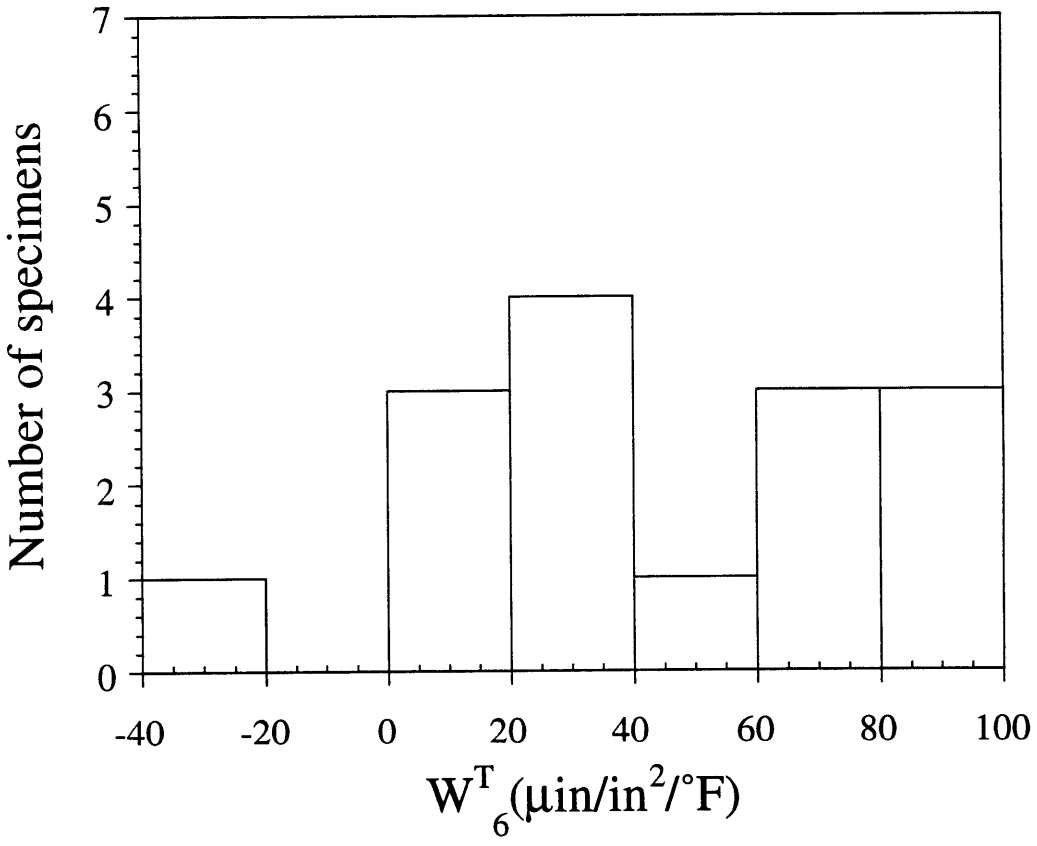

Figure 6.5 Histogram of W_6^T values for $[\pm 30]_s$ panels.

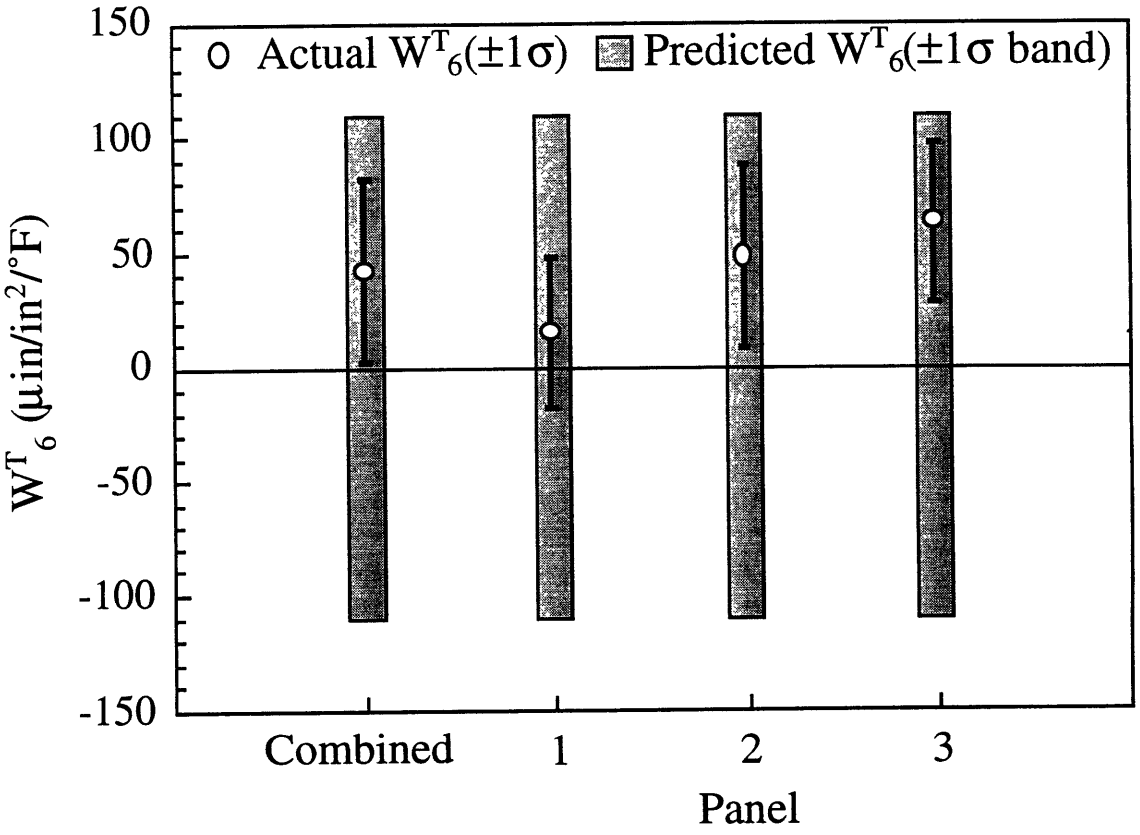

Figure 6.6 Correlation of W_6^T values for $[\pm 30]_s$ panels.

6.1.3 $[\pm\theta]_s$ Group

Data for bend and twist W^T for different angles in the $[\pm\theta]_s$ family of laminates are presented in Figures 6.7–6.10 along with correlation with the VARBEND analysis. The specific laminates examined are $[\pm30]_s$, $[\pm45]_s$, and $[\pm60]_s$.

The W_1^T data for panels from the $[\pm\theta]_s$ family are shown in Figure 6.7. There is more scatter in the panels with θ=45 and θ=60 than the θ=30 panels. All means are non-zero, but not all are positive.

Figure 6.8 shows correlations of W_1^T data with VARBEND analyses for the $[\pm\theta]_s$ panels. In this figure, it can be seen that the increase in scatter with increasing θ noted in the previous paragraph is predicted. The predictions bracket the experimental intervals. The experimental standard deviations are much smaller than the predicted standard deviations.

The W_6^T data for panels from the $[\pm\theta]_s$ family are shown in Figure 6.9. The distributions of the measured W_6^T for θ=45 and θ=60 are somewhat odd in this case. The standard deviations of these data are slightly larger than for the θ=30 layup. Each distribution has one point far removed from all the others, however. Without these out-liers, the scatters for θ=45 and θ=60 would be much smaller than for θ=30.

Figure 6.10 shows correlations of W_6^T data with VARBEND analyses for the $[\pm\theta]_s$ panels. The predicted standard deviations are all very similar, so no noticeable trend is expected. Thus the similar experimental standard deviations correlate well with analytical predictions. The predicted standard deviations bracket the experimental intervals. The magnitudes of the experimental standard deviations and the predicted standard deviations are very similar for W_6^T, in contrast to W_1^T, which had much smaller measured standard deviations than predicted.

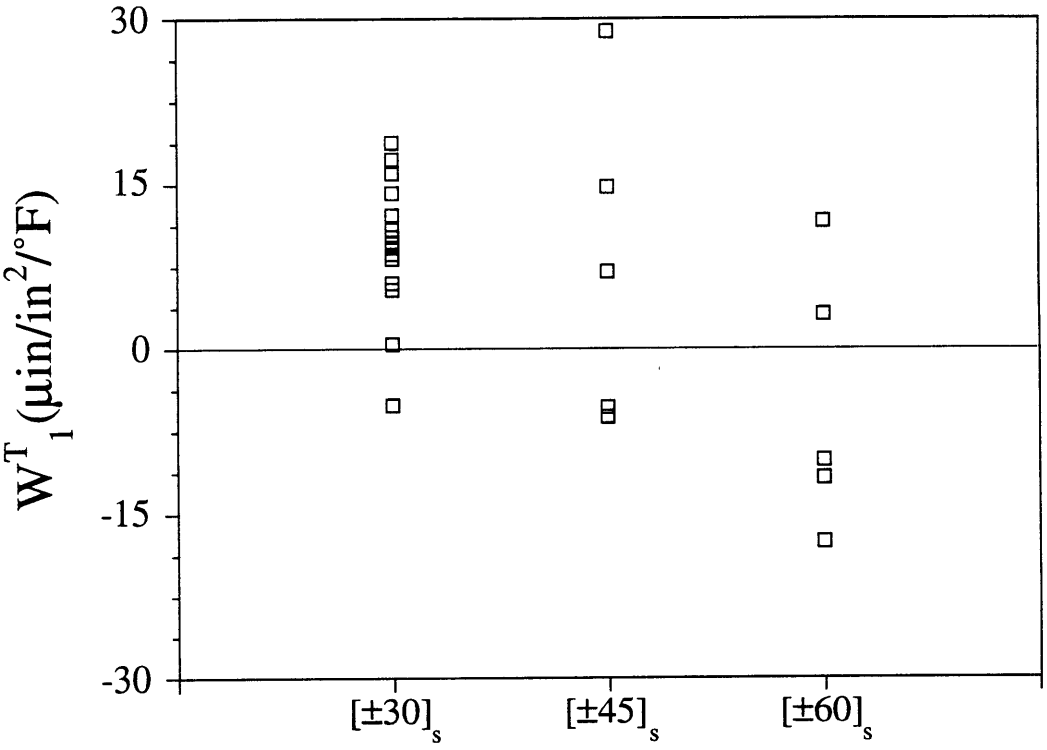

Figure 6.7 Experimental W_1^T values for $[\pm\theta]_s$ panels.

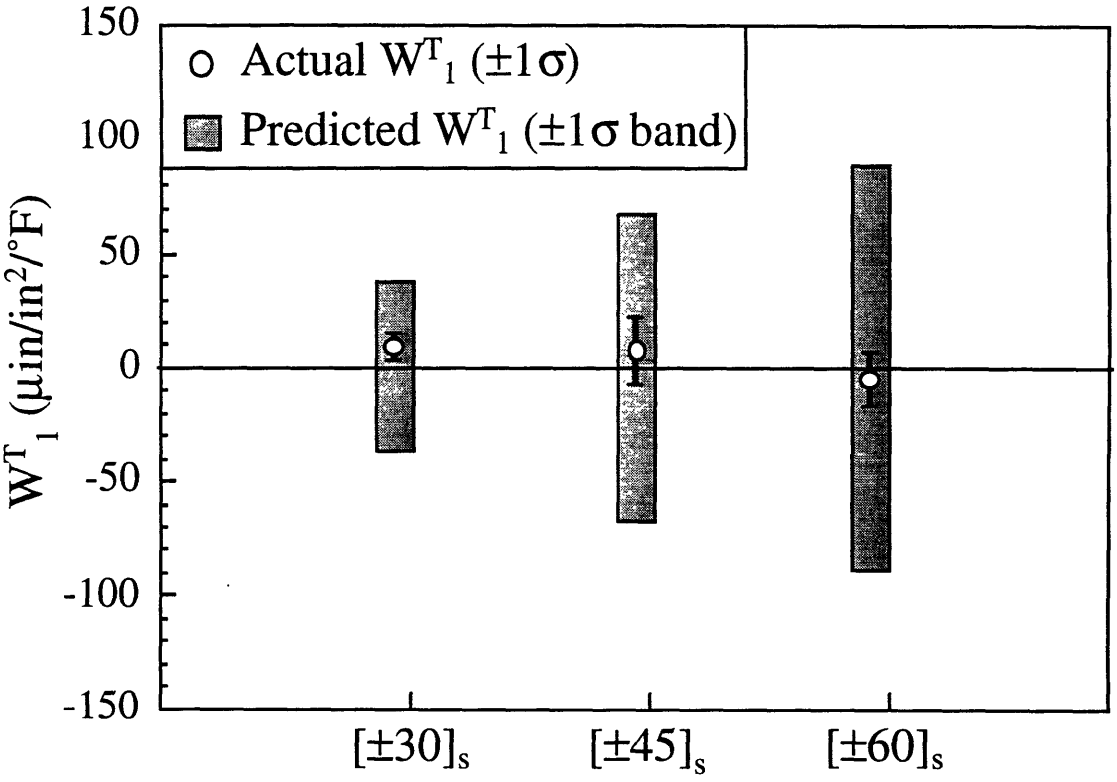

Figure 6.8 Correlation of W_1^T values for $[\pm\theta]_s$ laminates.

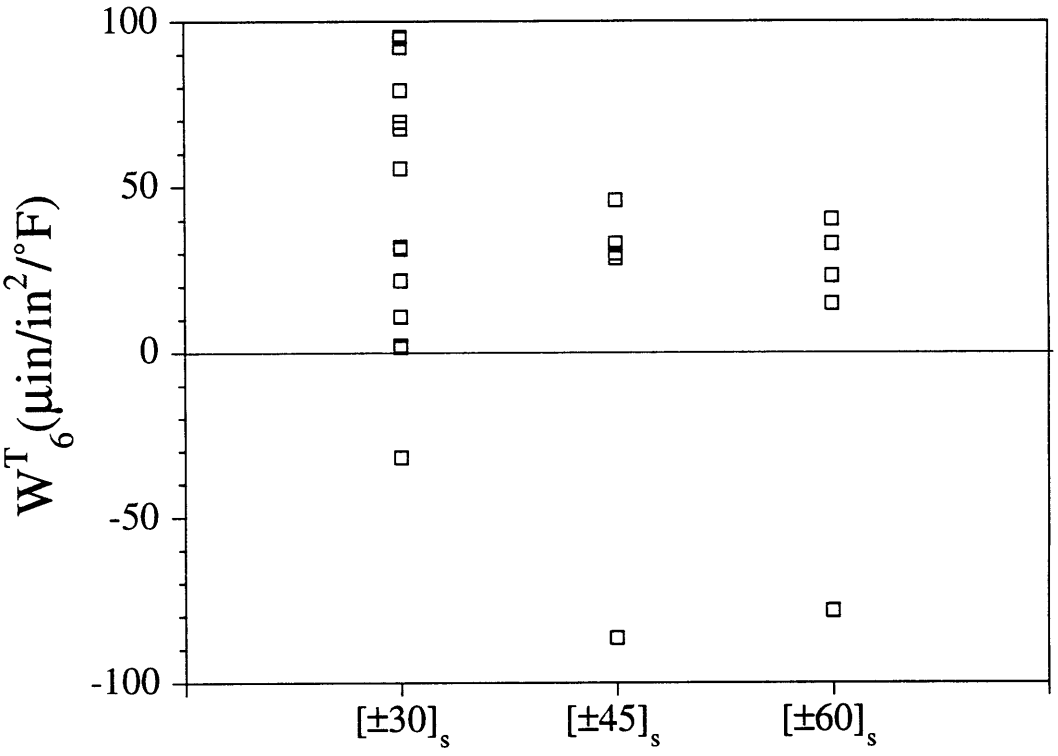

Figure 6.9 Experimental W_6^T values for $[\pm\theta]_s$ panels.

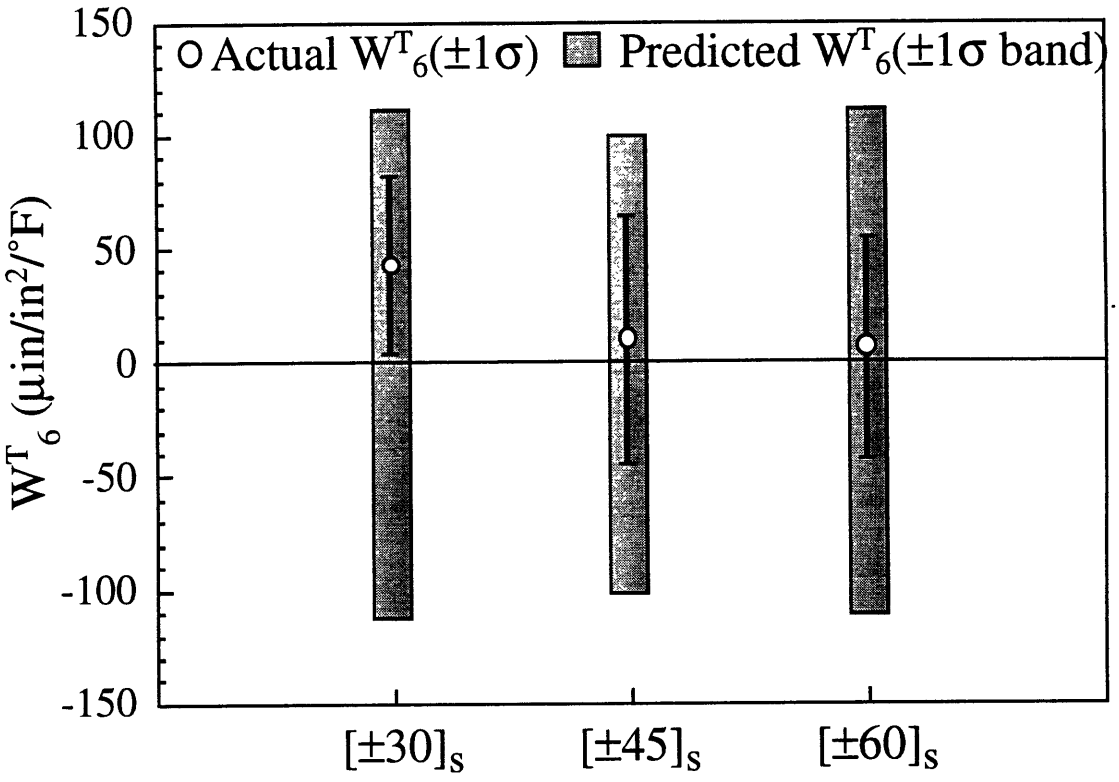

Figure 6.10 Correlation of W_6^T values for $[\pm\theta]_s$ laminates.

6.1.4 Thickness Group

Data for bend and twist W^T and correlations with VARBEND analyses for panels grouped to examine thickness trends are presented in Figures 6.11–6.14. The specific laminates examined are $[\pm 30]_s$, $[30_2/\text{-}30_2]_s$, $[(\pm 30)_2]_s$, and $[(\pm 30)_4]_s$.

The W_1^T data for panels in this group are shown in Figure 6.11. There is less scatter in the thicker panels than in the $[\pm 30]_s$ panels. All panels have a non-zero mean W_1^T. All mean W_1^T's are greater than zero.

Figure 6.12 shows correlations of W_1^T data with VARBEND analyses. The analysis predicts that the standard deviations decrease as thickness increases. This trend is seen in the experimental standard deviations, although it is not as strong in magnitude as the predicted trend. The intervals for the first three laminates in this group are bracketed by the predicted standard deviations. The mean value of the $[(\pm 30)_4]_s$ panel, however, lies just outside the predicted standard deviations. The experimental and predicted standard deviations for this layup still overlap. The experimentally measured standard deviations become very small for the thicker laminates, as predicted.

The W_6^T data for panels in this group are shown in Figure 6.13. The results are more ambiguous than those for W_1^T. As compared to the scatter of the $[\pm 30]_s$ panels, the scatter of the $[30_2/\text{-}30_2]_s$ panel is approximately the same, the scatter of the $[(\pm 30)_2]_s$ panel is smaller, and the scatter of the $[(\pm 30)_4]_s$ panel is larger. There are mean shifts away from zero for all panels. All of these mean shifts are positive.

Figure 6.14 shows correlations of W_6^T data with VARBEND analyses. The correlation in this case is poor. The VARBEND analysis predicts that the standard deviation of the thermal twist coefficient should decrease as

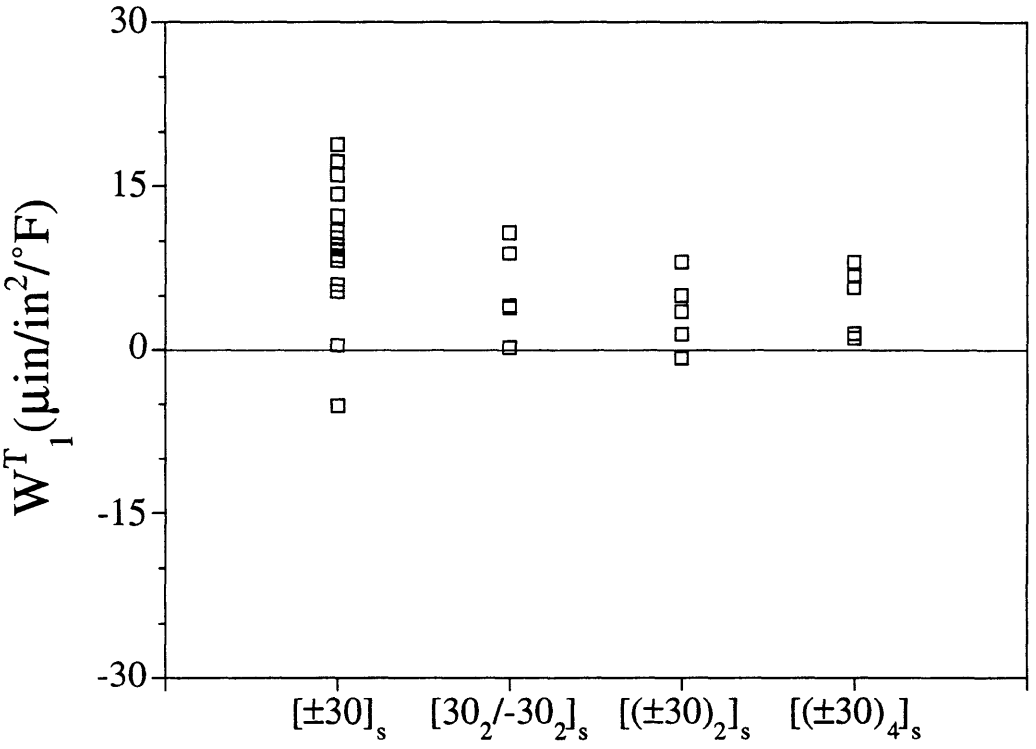

Figure 6.11 Experimental W_1^T values for panels with thickness and ply grouping variations.

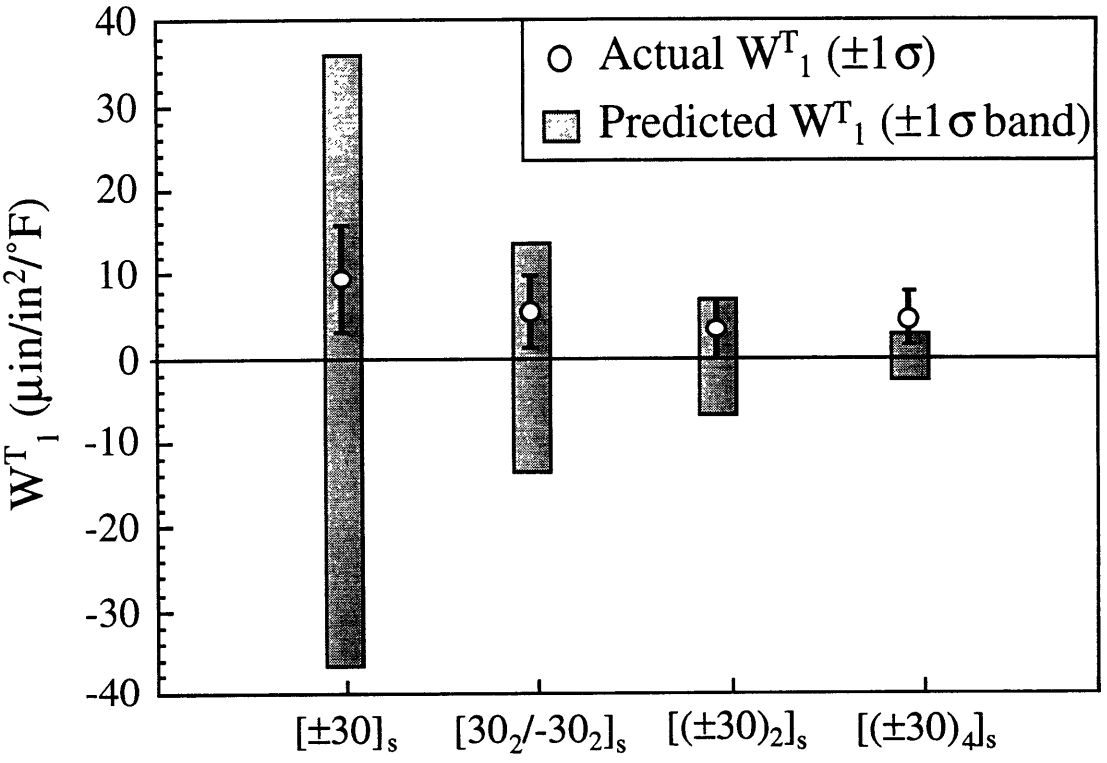

Figure 6.12 Correlation of W_1^T values for laminates with thickness and ply grouping variations.

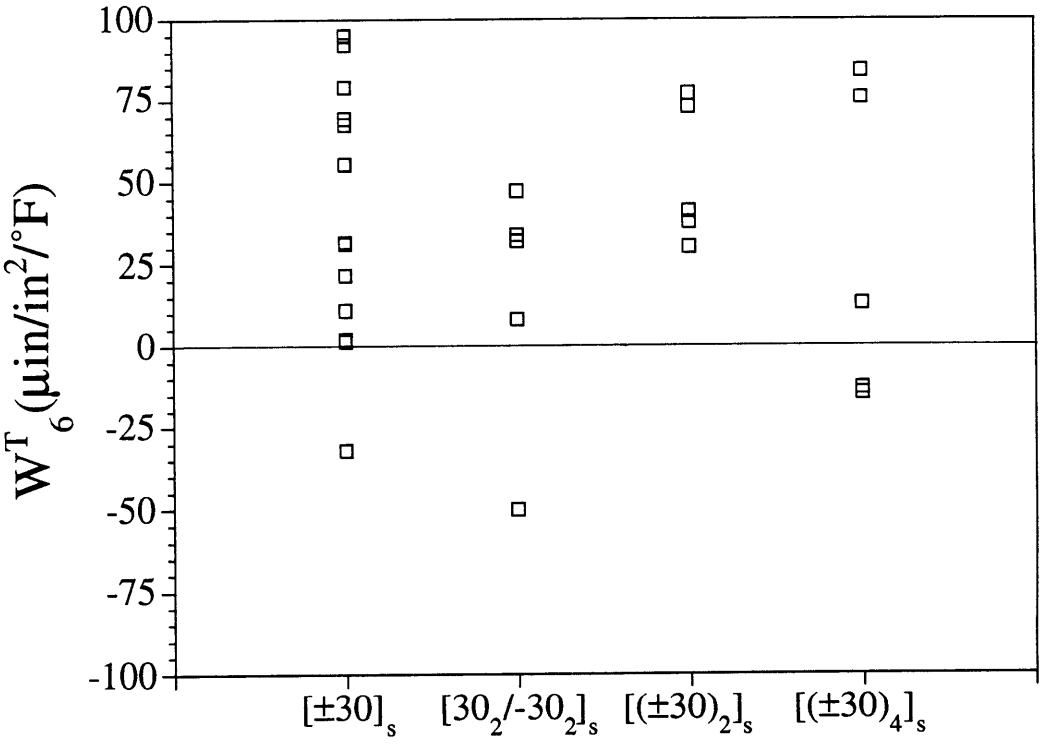

Figure 6.13 Experimental W_6^T values for panels with thickness and ply grouping variations.

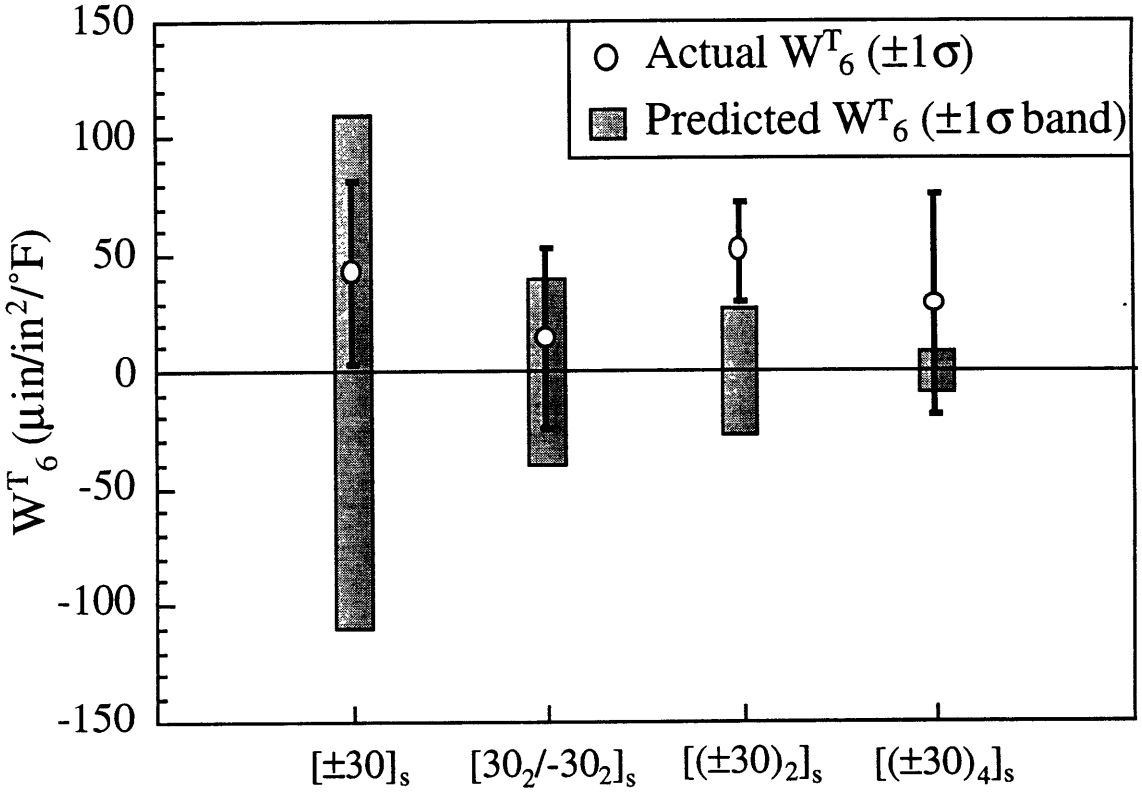

Figure 6.14 Correlation of W_6^T values for laminates with thickness and ply grouping variations.

thickness increases. The experimental data shows that the $[(\pm 30)_4]_s$ panel has the largest standard deviation in the group, instead of the smallest. This standard deviation is much larger than the prediction. The other experimental standard deviations follow the predicted trend. Another case of poor correlation is that the interval of the $[(\pm 30)_2]_s$ panel data falls entirely outside the predicted interval.

6.1.5 0° and 90° Ply Addition Group

Data for bend and twist W^T and correlations with VARBEND analyses for panels grouped to examine the effects of the addition of 0° and 90° plies to the $[\pm 30]_s$ family are presented in Figures 6.15–6.18. The specific laminates examined are $[\pm 30]_s$, $[\pm 30/0]_s$, $[0/\pm 30]_s$, $[0/\pm 30/90]_s$, and $[0_2/(\pm 30)_2]_s$.

The W_1^T data for panels in this group are shown in Figure 6.15. In most panels with additional plies, there is much less scatter than in the $[\pm 30]_s$ panels. The exception to this scatter reduction is $[0/\pm 30]_s$, which has more scatter. The means for all panels are non-zero and positive.

Figure 6.16 shows correlations of W_1^T data with VARBEND analyses. Much of the predicted trend is captured, but there are some discrepancies between the experiments and predictions. First is that the measured standard deviation of W_1^T of the $[0/\pm 30]_s$ panel is much greater than that of other panels which include 0° plies. Nevertheless, the experimental interval is almost entirely within the predicted interval for this panel. The second discrepancy is that there is a large mean shift in the $[0_2/(\pm 30)_2]_s$ panel, so that the entire experimental interval falls outside the predicted interval.

The W_6^T data for panels in this group are shown in Figure 6.17. There is less scatter in the panels with additional plies than in the $[\pm 30]_s$ panels. The amount of scatter reduction here is not as large as in Figure 6.15. There

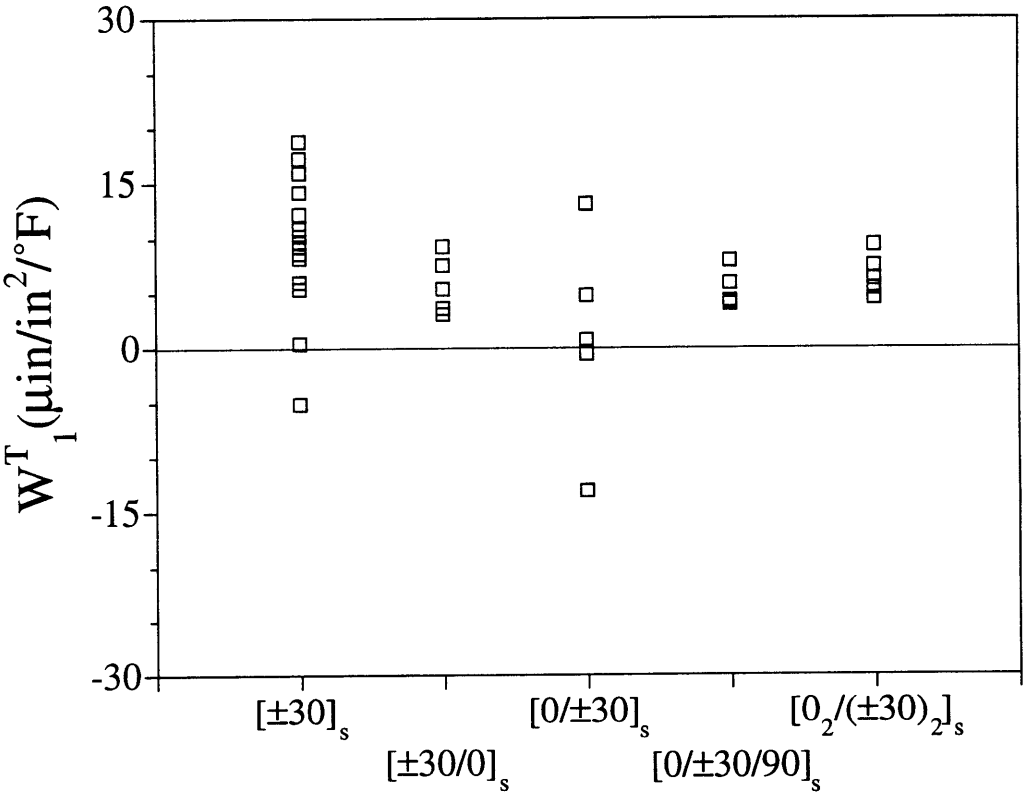

Figure 6.15 Experimental W_1^T values for panels with 0° and 90° ply additions.

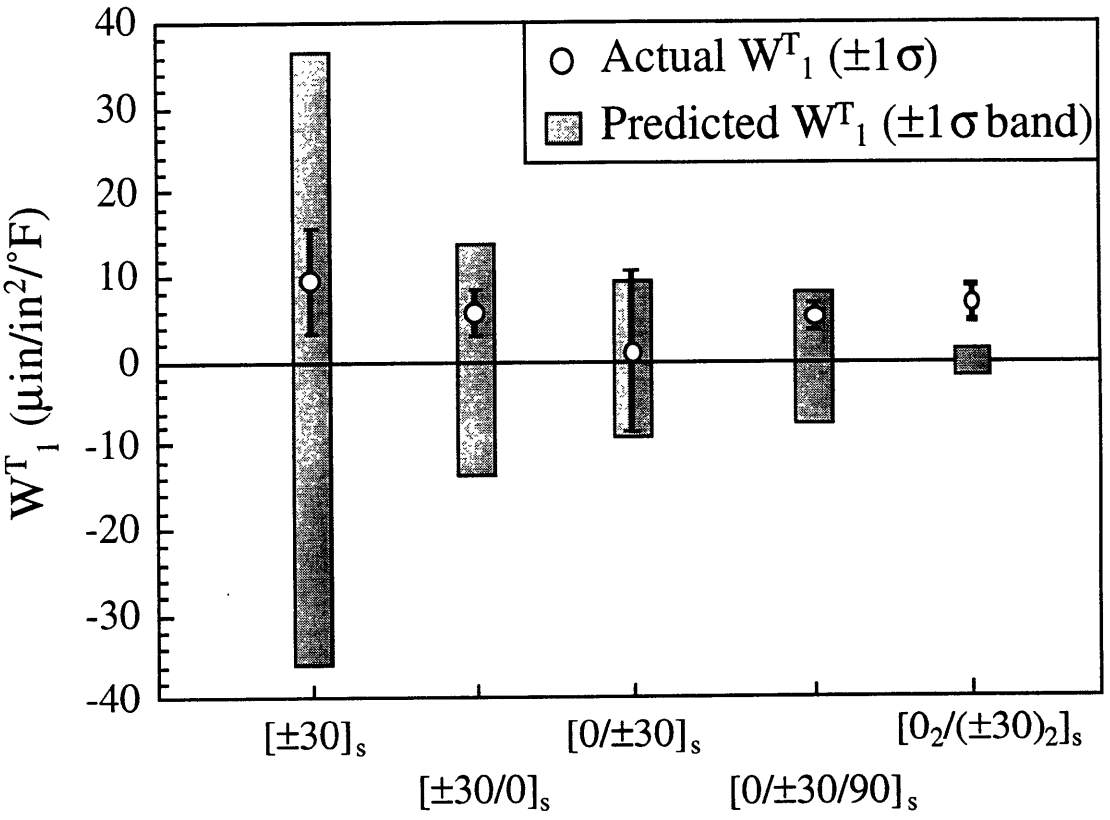

Figure 6.16 Correlation of W_1^T values for laminates with 0° and 90° ply additions.

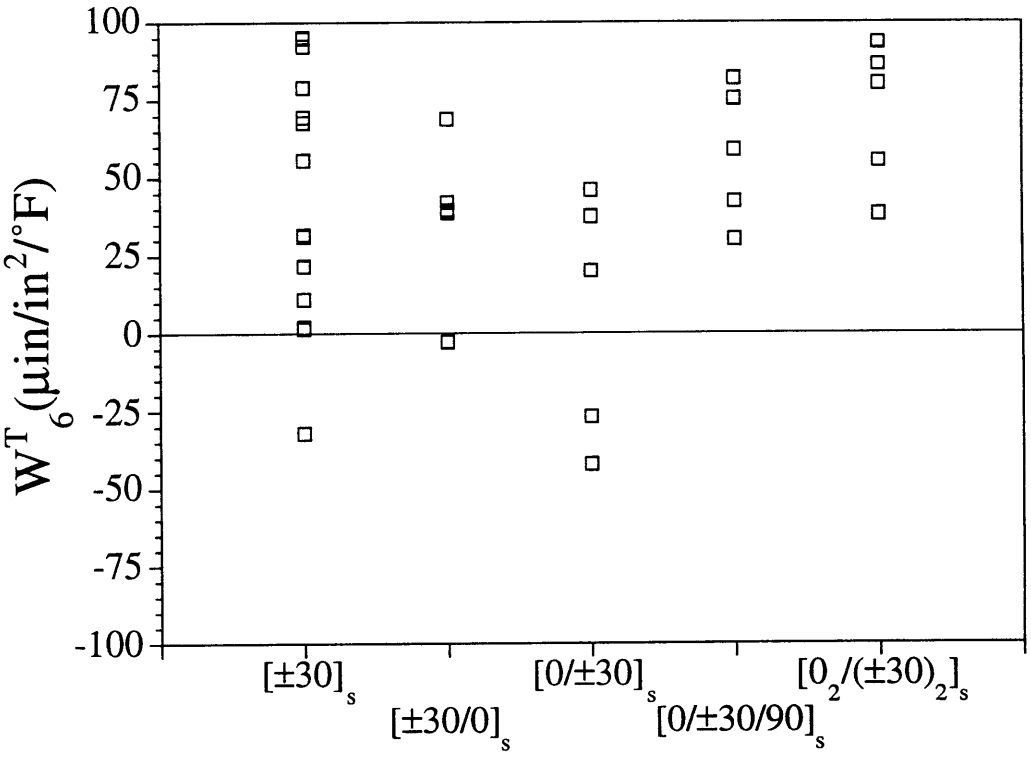

Figure 6.17 Experimental W_6^T values for panels with 0° and 90° ply additions.

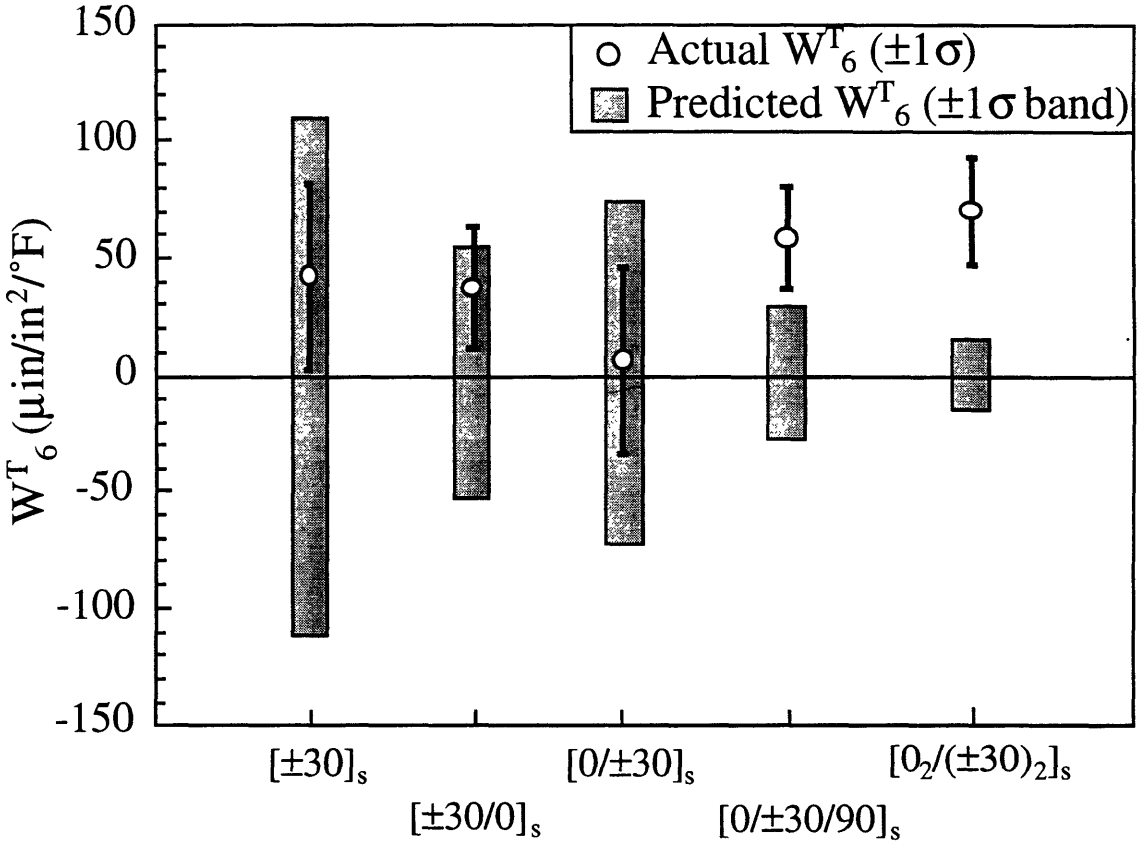

Figure 6.18 Correlation of W_6^T values for laminates with 0° and 90° ply additions.

are mean shifts away from zero in all panels. All of these mean shifts are positive.

Figure 6.18 shows correlations of W_6^T data with VARBEND analyses. Some of the predicted trend is captured in the experimental data. The experimental intervals for the $[\pm 30/0]_s$, $[0/\pm 30/90]_s$, and $[0_2/(\pm 30)_2]_s$ panels are all smaller than those for the $[\pm 30]_s$ and $[0/\pm 30]_s$ panels. The difference is not as large as predicted, however. The predicted reduction in interval size between the $[\pm 30]_s$ and $[0/\pm 30]_s$ panels is not seen in the experimental data. Also, there are large mean shifts for the $[0/\pm 30/90]_s$ and $[0_2/(\pm 30)_2]_s$ panels. These shifts are large enough to make the experimental intervals fall completely outside the predicted intervals for these panels. A similar mean shift effect was seen in W_1^T of the $[0_2/(\pm 30)_2]_s$ panel.

6.1.6 Unsymmetric Group

The remainder of the laminates are unsymmetric, so some elements of the $\mathbf{W}^T$ vector are expected to have non-zero means. Data for bend and twist W^T, and correlations with VARBEND analyses, are presented in Figures 6.19–6.24. The specific laminates examined are $[0_2/90_2]_T$, $[(0/90)_2]_T$, $[0_4/90_4]_T$, $[0_3/90]_T$, $[0/30]_T$, and $[0_{10}/30_{10}]_T$. The first four panels are cross-plies.

The W_1^T data for panels in this group (except the $[0_3/90]_T$ panel, for reasons to be explained below) are shown in Figure 6.19. Since these panels are unsymmetric, the thermal bending coefficients have a much greater magnitude than the symmetric panels–note the change in scale. There is still significant scatter in the W_1^T data.

Figure 6.20 shows correlations of W_1^T data with VARBEND analyses. The correlation is very good for some panels in this group. The experimental intervals for the $[(0/90)_2]_T$, $[0_4/90_4]_T$, and $[0_{10}/30_{10}]_T$ panels fall neatly within

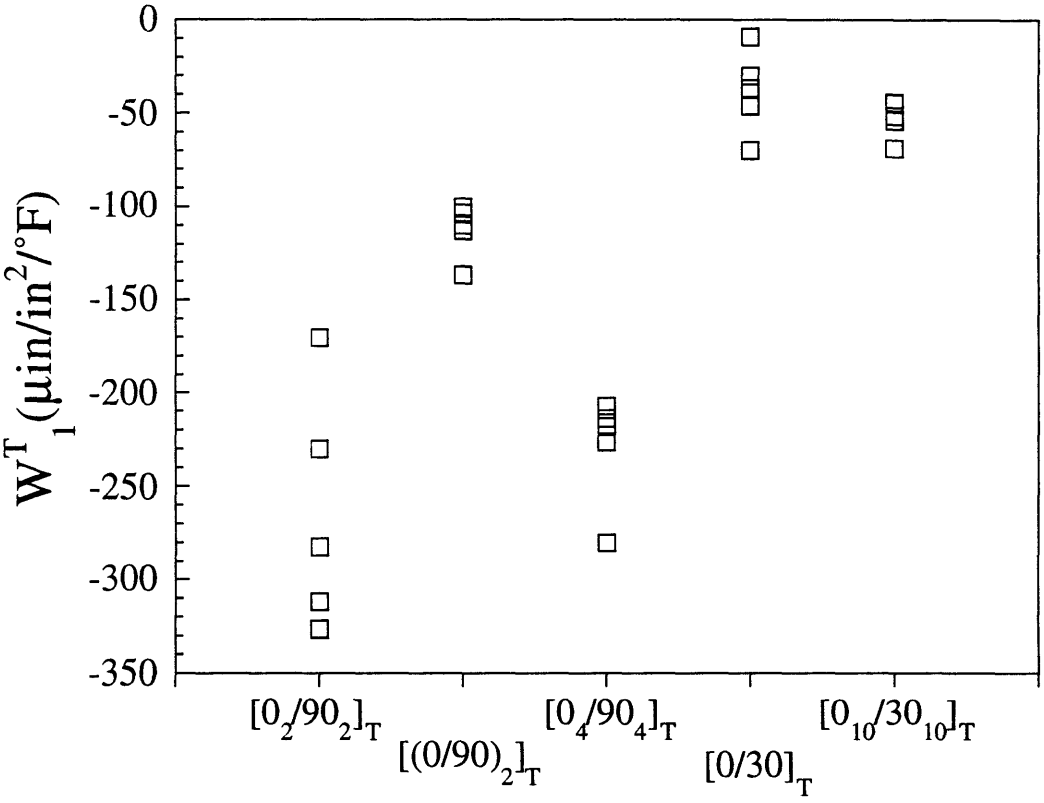

Figure 6.19 Experimental W_1^T values for unsymmetric panels.

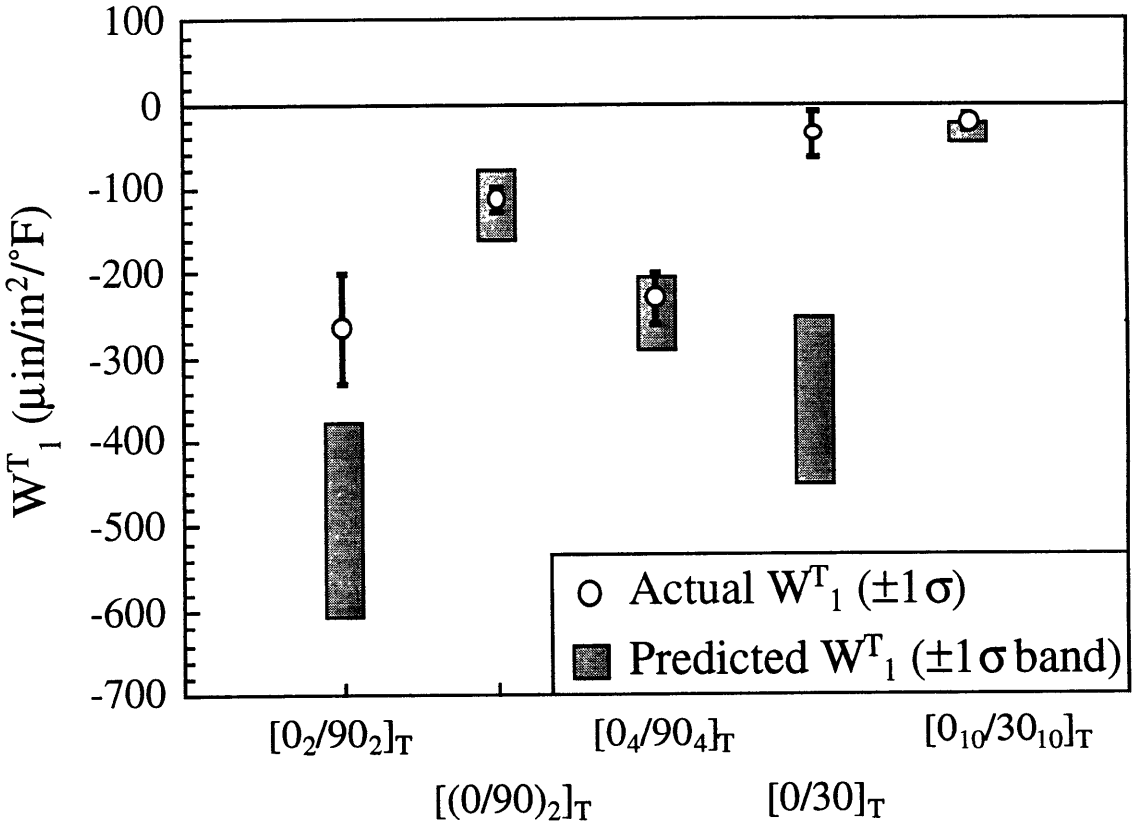

Figure 6.20 Correlation of W_1^T values for unsymmetric laminates.

their respective predicted intervals. The experimental interval size also agrees well with predictions. The interval size is smaller for the $[(0/90)_2]_T$ and $[0_4/90_4]_T$ panels than for the $[0_2/90_2]_T$ panel, as predicted. The interval size is smaller for the $[0_{10}/30_{10}]_T$ panel than for the $[0/30]_T$ panel, also as predicted. The experimentally determined means of two of the panels do not correlate with the analytical values. The entire experimental intervals for the $[0_2/90_2]_T$ and $[0/30]_T$ panels fall far outside the predicted intervals. The results for these panels are discussed further in Section 6.2, where they are correlated with the large-deformation model developed in Section 4.6.

The W_6^T data for panels in this group are shown in Figure 6.21. Note that data for the $[0_3/90]_T$ panel, which is not included in Figure 6.19, is included in this graph. There are positive mean shifts for the $[0/30]_T$, and $[0_{10}/30_{10}]_T$ panels. The means for the cross-ply panels vary around zero. There is a large scatter for all panels.

Figure 6.22 shows correlations of W_6^T data with VARBEND analyses. The correlation is very good for most panels in this group. The means and standard deviations for the cross-ply panels are all small, as predicted. The standard deviation for the $[0_{10}/30_{10}]_T$ panel is smaller than for the $[0/30]_T$ panel. There is one major discrepancy between experimental and predicted results. The mean W_6^T for the $[0/30]_T$ panel is much lower than the mean W_6^T predicted by the VARBEND analysis. The amount of this difference in means is large enough that the experimental interval lies far outside the predicted interval. This is due to large-deformation effects, and is discussed further in Section 6.2.

One unsymmetric cross-ply laminate was different from all the others, as discussed in Section 5.5. The specimens cut from the $[0_3/90]_T$ panel all had principal curvature in the y direction, while all others were curved in the x

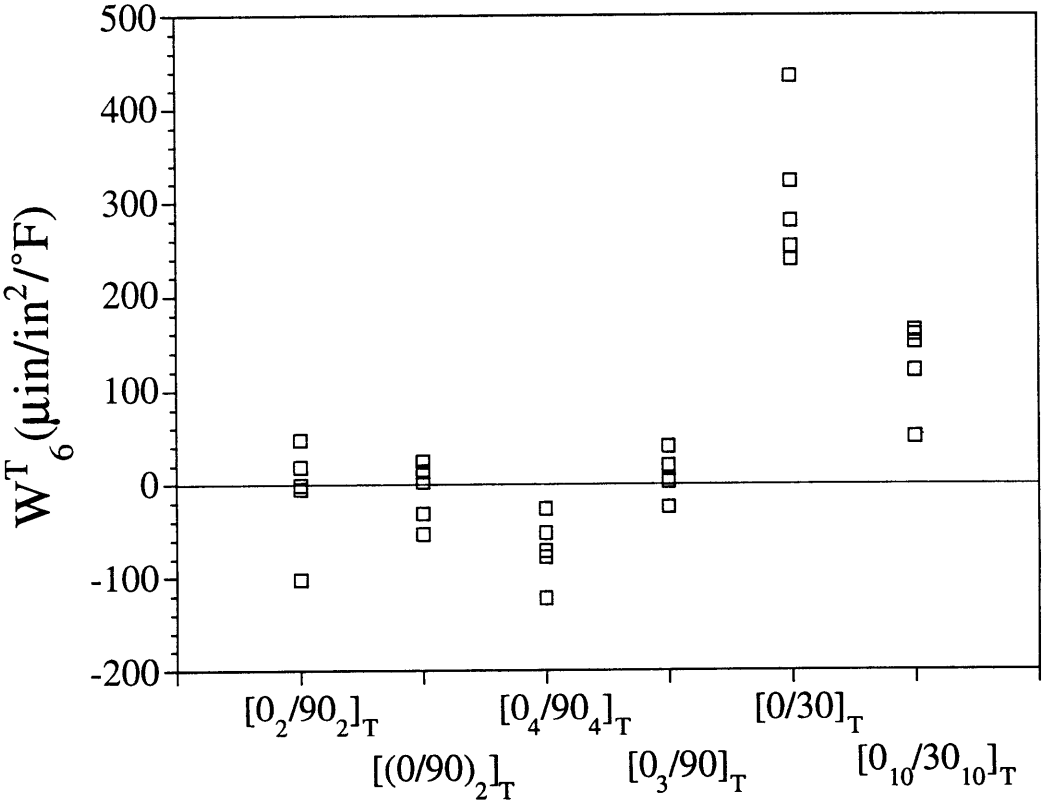

Figure 6.21 Experimental W_6^T values for unsymmetric panels.

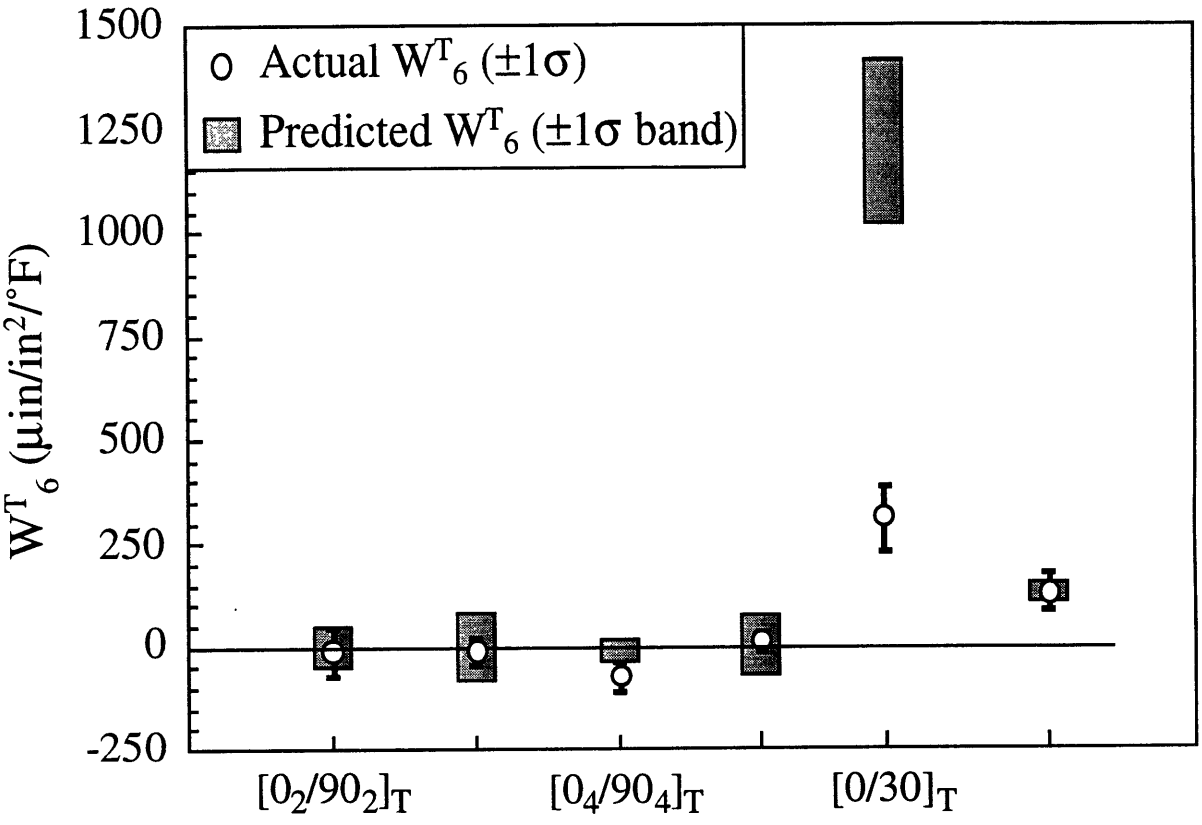

Figure 6.22 Correlation of W_6^T values for unsymmetric laminates.

direction. Because of this difference, it was impossible to measure W_1^T. Instead, W_2^T was measured. Data for this panel is plotted in Figure 6.23. There is a large mean value of W_2^T, and also a very large scatter.

Figure 6.24 shows the correlation of W_2^T data with the VARBEND analysis for the $[0_3/90]_T$ panel. The experimental standard deviation is much larger than the predicted standard deviation. The mean of the experimental data is just below the predicted interval.

6.1.7 Discussion of Correlation of Experiment and VARBEND Model

In general, the correlation between experimental and predicted values for the thermal bending coefficients is good. In most cases, the mean experimental values for the W^T's fall within one predicted standard deviation of the predicted mean. In many cases, the predicted interval completely brackets the measured data.

Most trends predicted by the VARBEND model are seen in the data. As a rule, the W_6^T standard deviations in the experimental data are larger than those of W_1^T, as predicted. The correlation with predicted trends among groups of panels is generally good. Most changes in measured W_1^T and W_6^T due to angle and thickness variations, and the additions of 0° and 90° plies, match predictions.

A notable difference between experiment and predictions is that the means are not always the same. The predicted means of W_1^T and W_6^T for symmetric specimens are zero. The non-zero mean values measured can be due to a few factors. The first is that, except for the $[\pm 30]_s$ layup, all specimens for each layup came from the same panel. Therefore, any differences from nominal values which were constant throughout a panel, such as a mislaid ply angle, would be the same for all specimens of a given

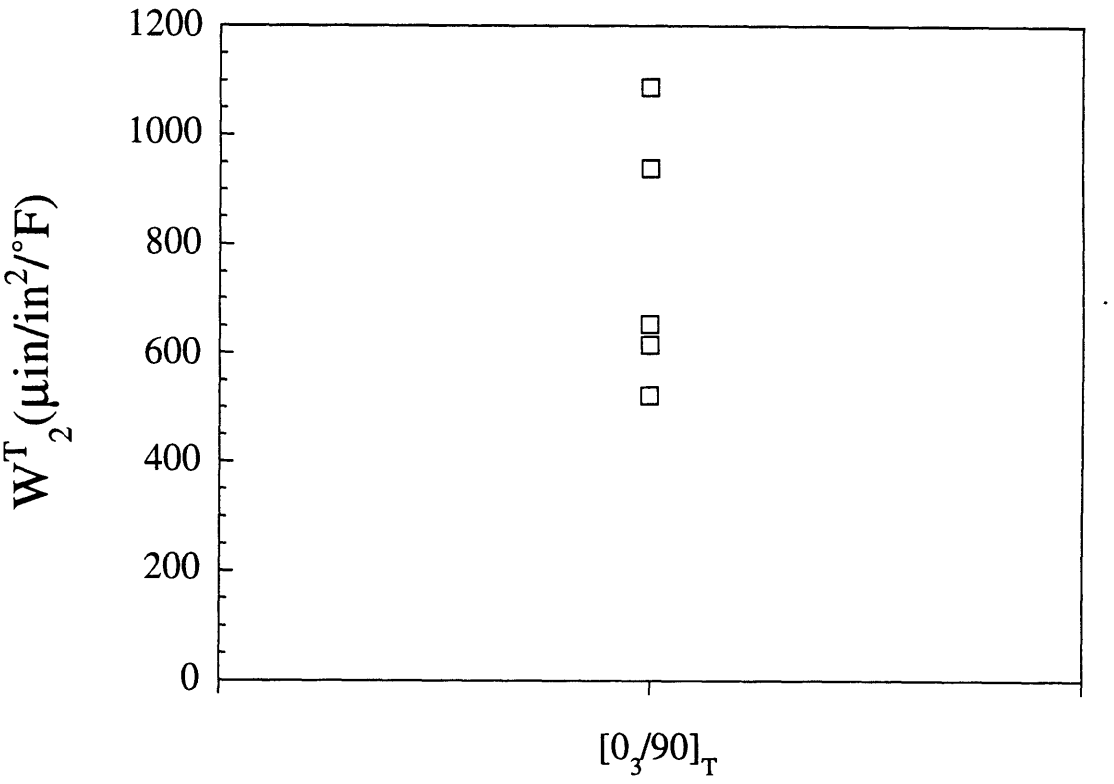

Figure 6.23 Experimental W_2^T values for $[0_3/90]_T$ panel.

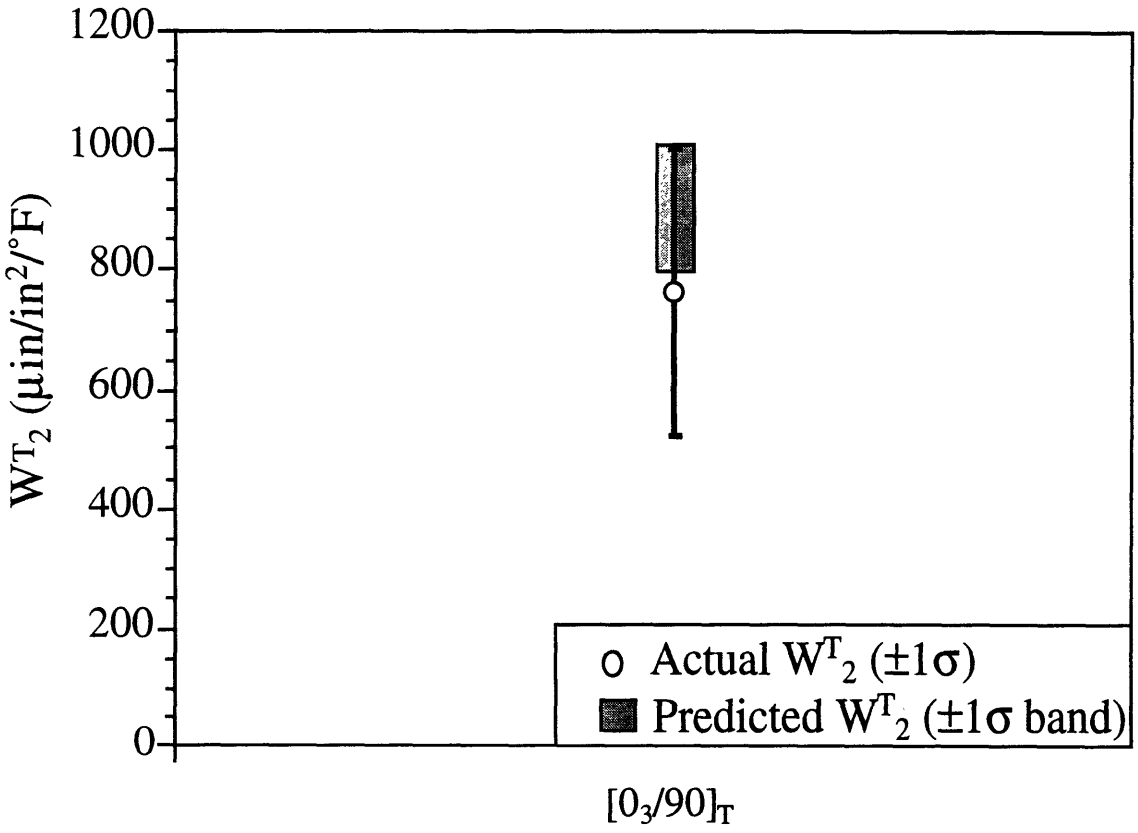

Figure 6.24 Correlation of W_2^T values for $[0_3/90]_T$ laminate.

panel. This would cause a shift in the mean. In addition, only five specimens were tested from each panel. Therefore, there is not a large confidence in the values of the means. A greater number of specimens from multiple panels for each layup would give greater confidence in the mean W^T values.

There is also a difference between experimental and predicted standard deviation values for many specimens. In most cases, the experimental standard deviations (especially for W_1^T) were lower than the predicted standard deviations. Most specimens for a given layup were from a single panel. This would tend to reduce the standard deviations. All panels were made from a single roll of prepreg provided by Hercules. This would also tend to decrease standard deviations, since batch-to-batch variations in material properties would not be included. There is also not a large confidence in the experimental standard deviations because of the small number of samples. A greater number of specimens from multiple panels for each layup would give greater confidence in the W^T standard deviation values.

Some of the correlations were not good for panels which were predicted to have a very small standard deviation. Part of the problem may be the uncertainties inherent in the experimental setup. As discussed in Chapter 5, the thermal deformation of the test setup contributed most to system uncertainty.

The data reduction equations (Eqs. 5.9 and 5.10) were used to find the worst case thermal bending coefficient uncertainty. For bending, assuming that the distance error spans the entire distance uncertainty range yields a worst case W_1^T error of 2.75 $\mu in/in^2/°F$. The smallest predicted standard deviation for the panels in the experimental study is 2.82 $\mu in/in^2/°F$ for the $[(\pm 30)_4]_s$ panel, and the smallest measured standard deviation was 1.70

$\mu in/in^2/°F$, for the $[0/\pm30/90]_s$ panel. Thus the scatter of the data in the case of the most stable laminates is probably due primarily to uncertainty of the measuring system. This could mean that the actual standard deviations are lower than those measured. Similarly, the worst case W_6^T error due to measurement uncertainty is 25.4 $\mu in/in^2/°F$, and the smallest predicted W_6^T is 8.67 $\mu in/in^2/°F$ (also for the $[(\pm30)_4]_s$ panel). The uncertainties are less critical for the majority of the panels, however, as typical measured values of the W^T's are much larger than the measurement uncertainty.

Throughout the experimental data, there is a bias towards positive thermal bending coefficients. The specimens were oriented such that positive W_1^T caused curving towards the side of the laminate that was adjacent to the cure plate during curing. The bias is thus likely to be due to a slight asymmetry in the cure process. This asymmetry could be due to thermal gradients through the thickness during cure, gradients in compaction and/or resin bleed, etc. Such asymmetry would cause a non-zero mean thermal bending coefficient. There is no clear explanation for the mean shift in the thermal twist coefficient.

Finally, some of the unsymmetric specimens exhibited behavior notably different from the VARBEND predictions. The reason for the discrepancies in these cases is that the specimens in question were in the large-deformation regime, and thus the thermal bending coefficients could not be accurately calculated using the small deformation assumptions used in CLPT and the VARBEND code. These specimens are discussed further in the next section.

6.2 CORRELATION WITH LARGE-DEFORMATION ANALYSIS

Some of the unsymmetric laminates have mean experimental W^T values significantly different from those predicted by the VARBEND analysis. As noted in Subsection 6.1.6, the entire W_1^T experimental intervals for the $[0_2/90_2]_T$ and $[0/30]_T$ panels fall far outside the predicted intervals. The correlations between the experiments and the VARBEND predictions are equally poor in W_6^T for the $[0/30]_T$ panel. In addition, the $[0_3/90]_T$ panel had dominant curvature in the y direction, as opposed to the dominant curvature in the x direction seen in all other cross-ply unsymmetric laminates in the current study. In this section, the large-deformation model developed in Section 4.6 is used to analyze the three panels which do not agree with the VARBEND analysis. Curvatures and stable shapes as functions of laminate dimension and temperature are presented for the $[0_2/90_2]_T$ and $[0/30]_T$ panels. Predictions of the large-deformation analysis are then compared to the experimental results.

6.2.1 $[0_2/90_2]_T$ Panel

This subsection presents the results of a large-deformation analysis of the $[0_2/90_2]_T$ laminate. This layup was also used as the example laminate of Subsection 4.6.4. In Chapter 4, properties of the T300/5208 graphite/epoxy material system were used in the analysis to enable a direct comparison with Hyer's results [25]. In this section, material properties in the analysis are those of the AS4/3501-6 graphite/epoxy material system used in the experiments of the current work.

The large-deformation analysis is first used to examine curvatures and stable shapes for the $[0_2/90_2]_T$ laminate as functions of laminate sidelength. The laminate is assumed to be square, and the temperature is assumed to be

room temperature. The laminate is loaded only by cooling from the stress-free temperature, which is assumed to be 350°F (177°C). Since the layup is a cross-ply, the principal curvature axes are coincident with the laminate axes, and the twist curvature is zero. The results are shown in Figures 6.25–6.27. Figures 6.25 and 6.26 show the calculated curvatures for the three assumed shapes in the x and y directions respectively. Figure 6.27 shows the calculated total potential energies.

In Figure 6.25, the solid line represents a saddle shape. At zero sidelength, the minimum energy solution for this shape is identical to the CLPT solution. The curvatures are smaller than predicted by CLPT for non-zero sidelength because of large deformation effects. The dashed line represents the first cylindrical shape. The curvature remains constant at a value slightly below the CLPT solution. The other cylindrical shape has a constant curvature in the x direction of zero. In Figure 6.26, the curvature of the first shape in the y direction is the negative of the curvature in the x direction of that shape. The first cylindrical shape gives zero curvature in the y direction. The curvature of the second cylindrical shape in the y direction remains constant at a value which is the negative of the curvature of the first cylindrical shape in the x direction.

Figure 6.27 shows the calculated total potential energies for the three shapes. The solid line is the energy of the saddle shape. The other shapes have exactly the same potential energy. The saddle shape has a lower potential energy until the laminate sidelength reaches 3.01 inches (76 mm), after which the cylindrical shapes have lower potential energy. Therefore, it is assumed that the only stable shape for the laminate is a saddle until the sidelength reaches 3.01 inches (76 mm). After this point, the cylindrical shapes are assumed to be stable, while the saddle shape is not. Since both

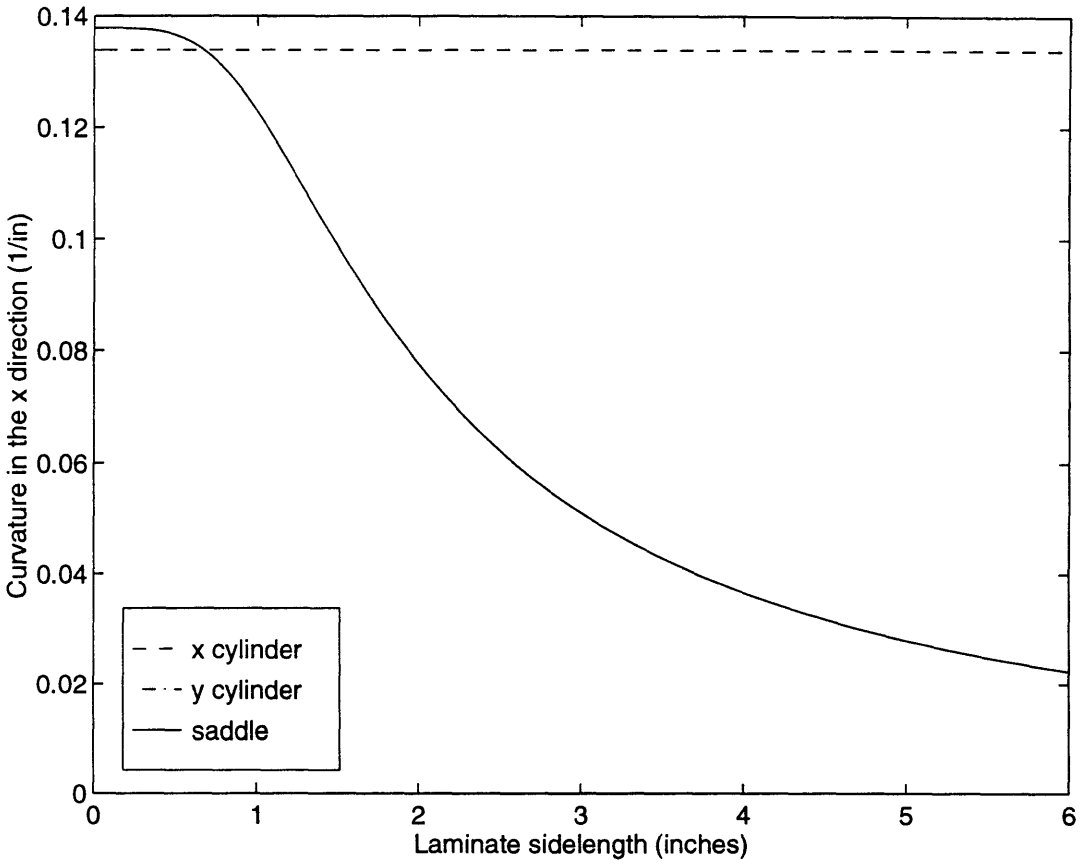

Figure 6.25 Laminate x curvature vs. sidelength for $[0_2/90_2]_T$ layup.

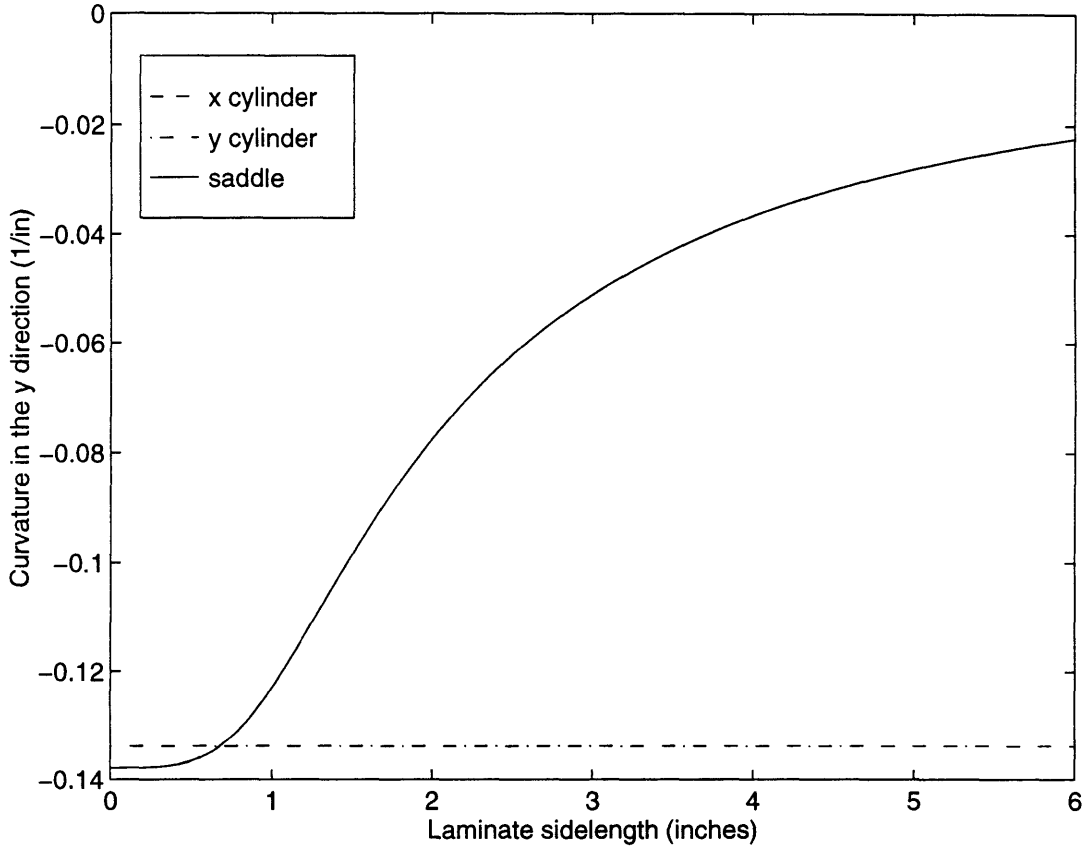

Figure 6.26 Laminate y curvature vs. sidelength for $[0_2/90_2]_T$ layup.

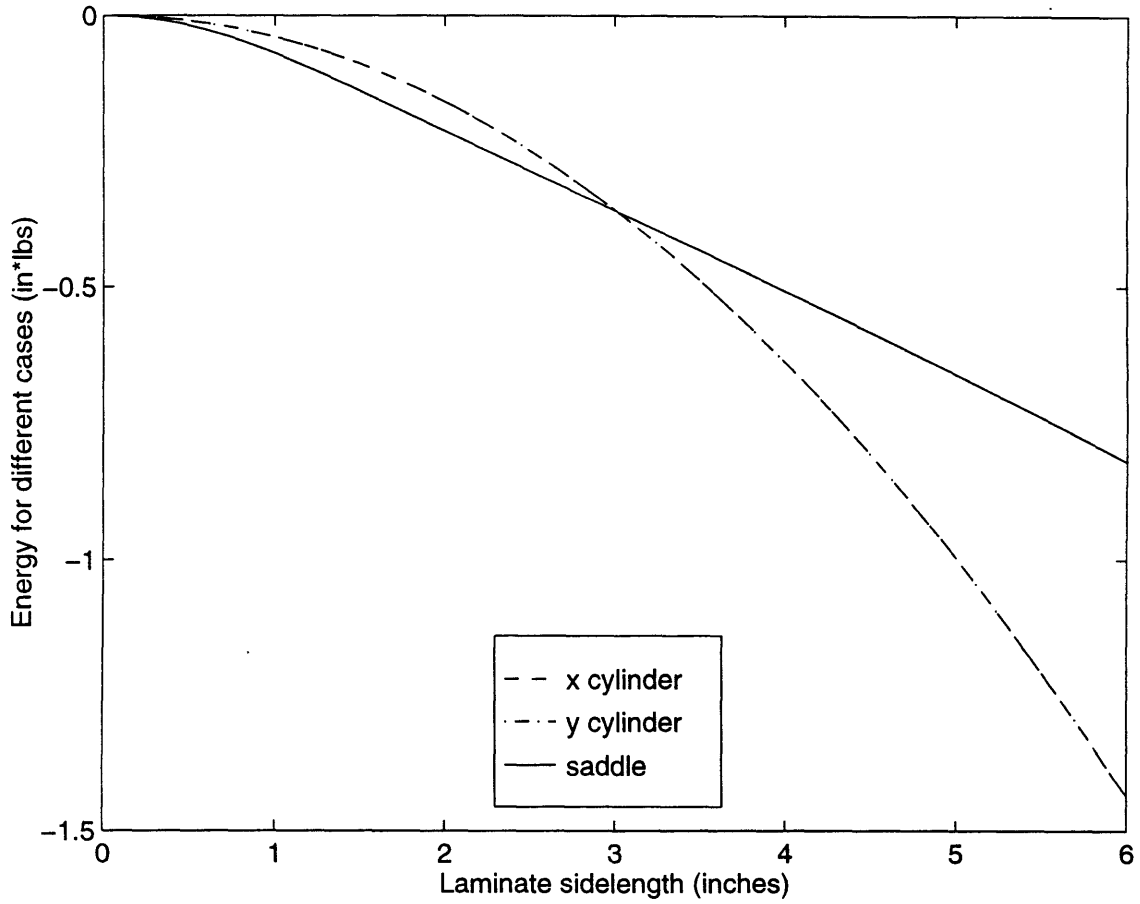

Figure 6.27 Laminate potential energy vs. sidelength for $[0_2/90_2]_T$ layup.

cylindrical shapes have the same potential energy, neither of them is favored. Both cylindrical shapes will exist, and a laminate can be switched from one to the other by means of a snap-through.

Curvature and stability are also examined as a function of the difference in temperature from the stress-free temperature. The laminate in this case is assumed to have the same dimensions as the experimental specimens. Figures 6.28 and 6.29 show the calculated curvatures for the three shapes in the x and y directions respectively, and Figure 6.30 shows the calculated total potential energies.

In Figure 6.28, the solid line represents the large-deformation saddle shape, the dashed line the non-zero x curvature cylindrical shape, and the dash-dot line the CLPT solution based on small deformations. All curvatures are shown versus the temperature difference from the stress-free temperature. The non-zero y curvature cylindrical shape has zero curvature in the x direction. For all temperatures, the first cylinder has a curvature slightly lower than the CLPT prediction. The saddle shape has a predicted curvature which becomes much less than the CLPT prediction as the temperature difference from the cure temperature becomes more negative. The curvatures in the y direction, shown in Figure 6.29, show similar trends. The curvature of the saddle shape in the y direction is the negative of the x curvature of the saddle shape.

Figure 6.30 shows the calculated total potential energies for the three shapes as functions of temperature difference from the stress-free temperature. All shapes have zero total potential energy at ΔT=0. For this laminate, both cylindrical shapes have the same energy. The saddle shape has the lowest total potential energy over the entire temperature range, so it

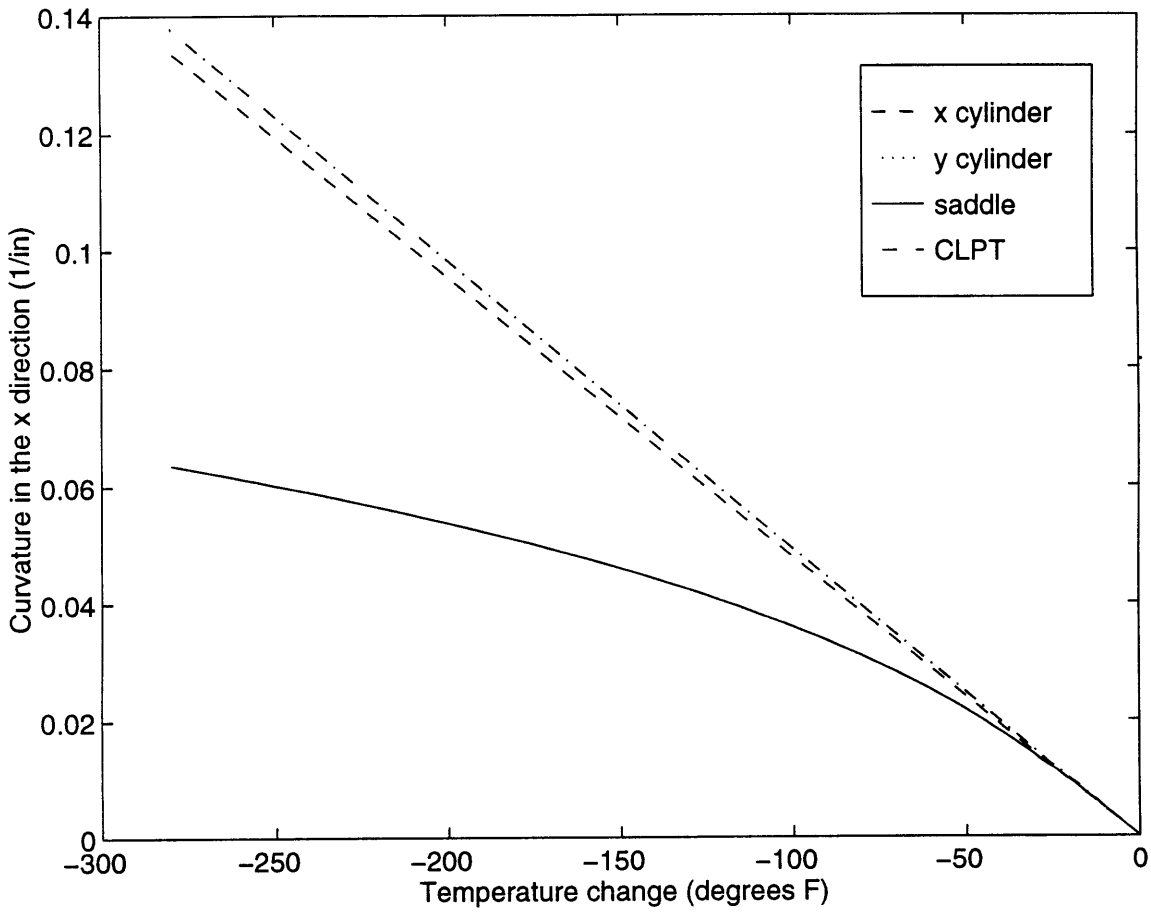

Figure 6.28 Laminate x curvature vs. temperature change for $[0_2/90_2]_T$ layup.

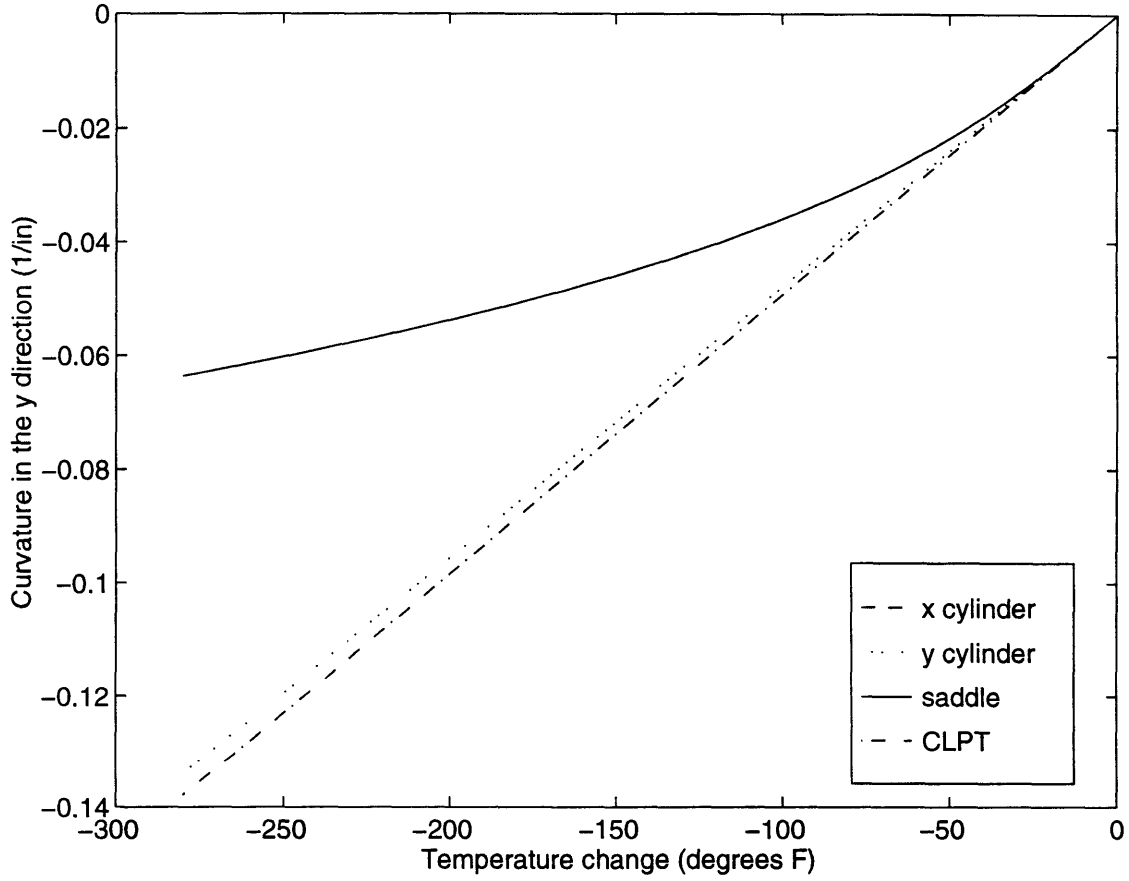

Figure 6.29 Laminate y curvature vs. temperature change for $[0_2/90_2]_T$ layup.

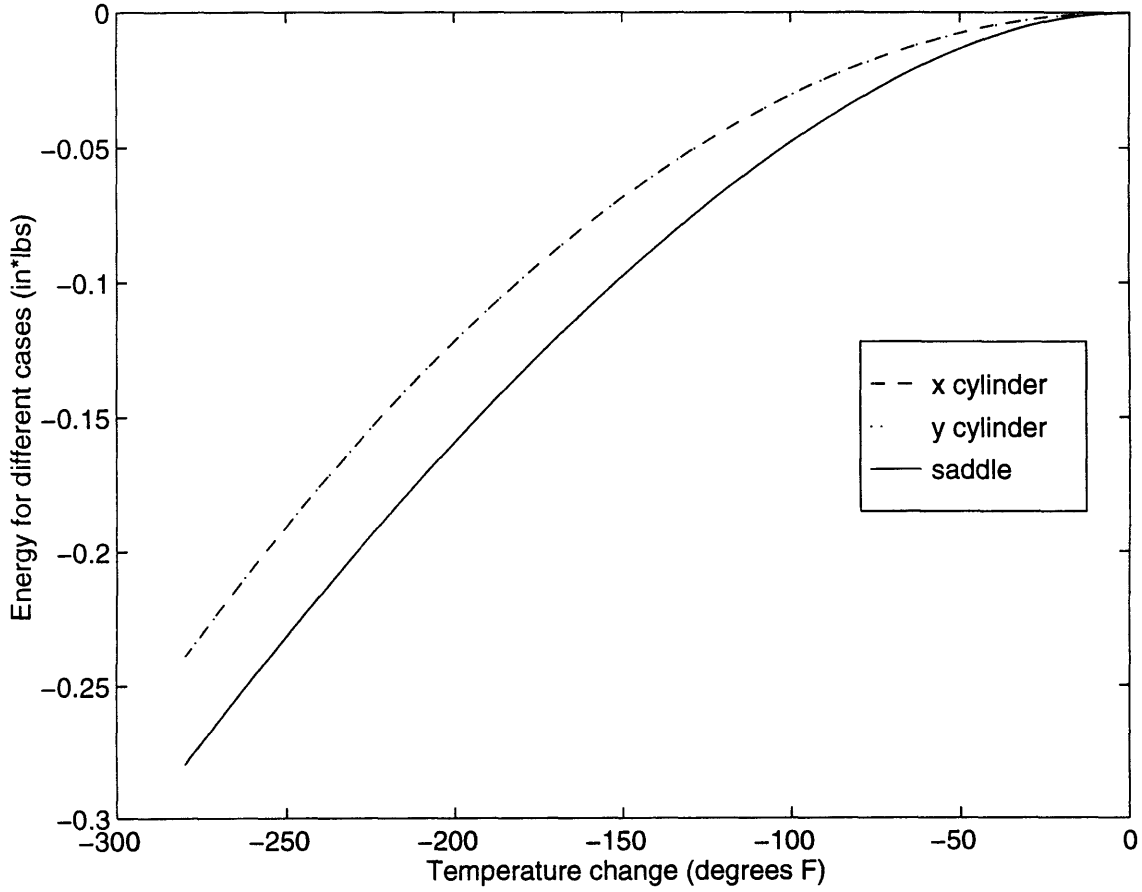

Figure 6.30 Laminate potential energy vs. temperature change for $[0_2/90_2]_T$ layup.

is the stable shape. The geometry of the specimen makes the cylindrical shapes unfavorable.

6.2.2 $[0/30]_T$ Panel

This subsection presents the results of the large-deformation analysis for a $[0/30]_T$ laminate. Experimental W^T data for this laminate differed significantly from VARBEND predictions in both bending and twisting. This laminate differs from the previous example in that twist curvatures are included.

The large-deformation analysis is first used to examine curvatures and stable shapes for the $[0/30]_T$ laminate as functions of laminate sidelength. The laminate is assumed to be square, and the temperature is assumed to be room temperature. The laminate is loaded only by cooling from the stress-free temperature, which is assumed to be 350°F (177°C). For this laminate, the principal curvature axes are at an angle of -37° relative to the laminate axes. This laminate has non-zero twist curvature with temperature. The results are shown in Figures 6.31–6.34. Figures 6.31 and 6.32 show the calculated curvatures for the three assumed shapes in the x and y directions respectively. Figure 6.33 shows the calculated x-y twist curvature. Figure 6.34 shows the calculated total potential energies.

In Figure 6.31, the solid line represents a saddle shape in laminate principal curvature axes. At zero sidelength, the minimum energy solution for this shape is identical to the CLPT solution. The curvatures are smaller than predicted by CLPT for non-zero sidelength because of large deformation effects. The amount by which the saddle shape solutions from the large-deformation and CLPT analyses differ increases rapidly with laminate sidelength. The dashed line represents the first cylindrical (in laminate

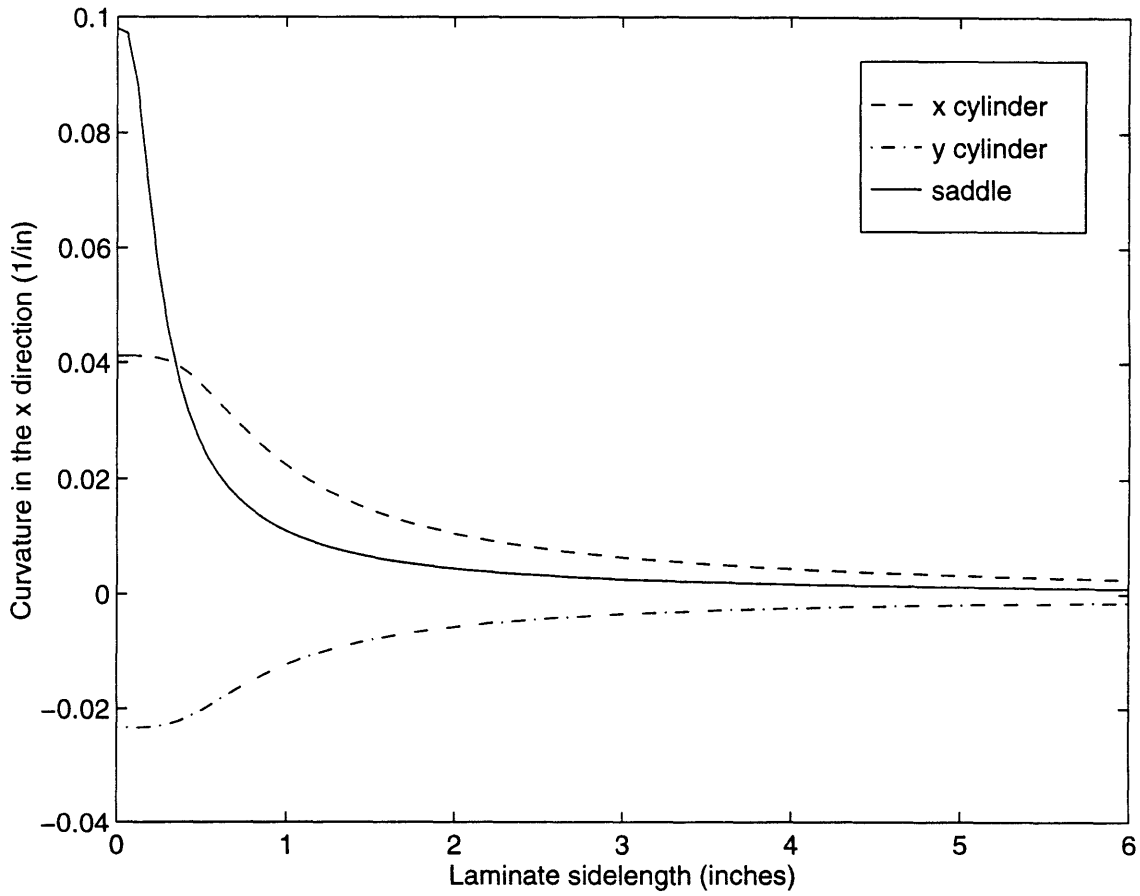

Figure 6.31 Laminate x curvature vs. sidelength for $[0/30]_T$ layup.

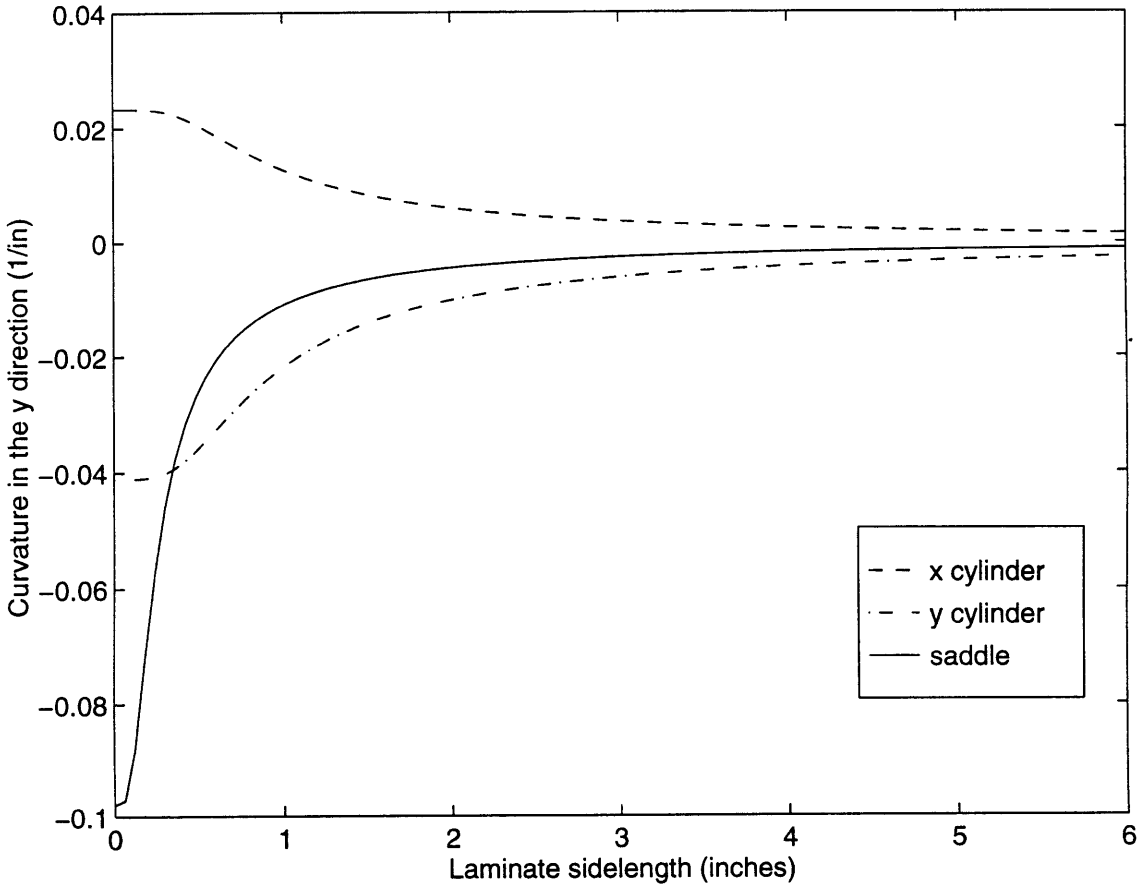

Figure 6.32 Laminate y curvature vs. sidelength for $[0/30]_T$ layup.

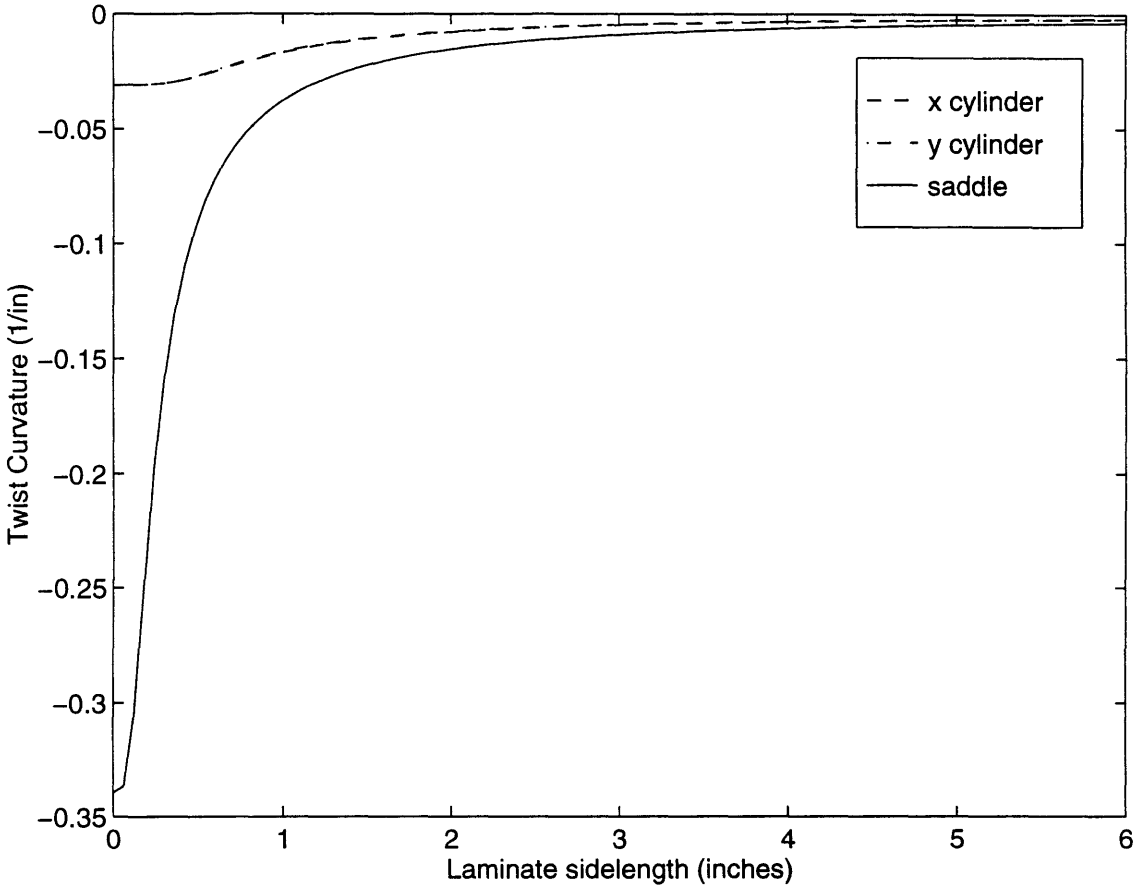

Figure 6.33 Laminate x-y twist curvature vs. sidelength for $[0/30]_T$ layup.

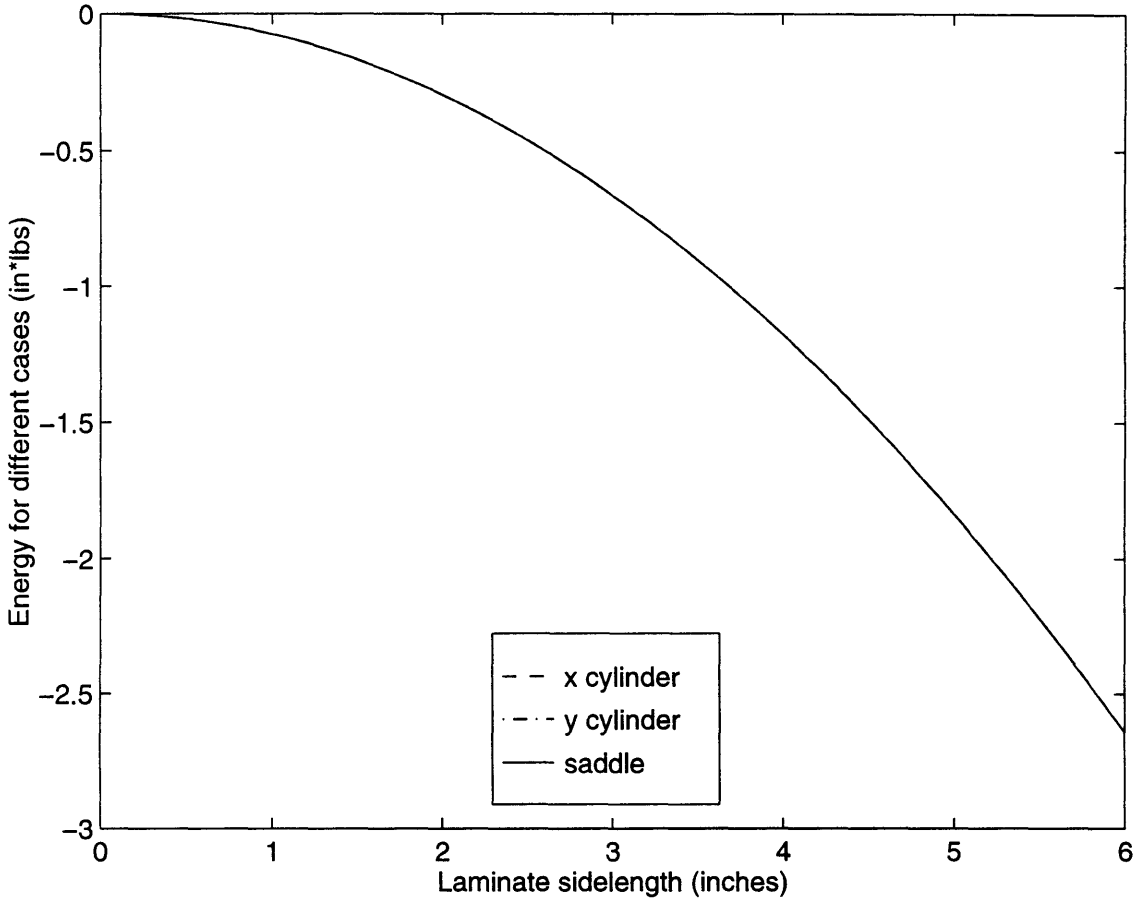

Figure 6.34 Laminate potential energy vs. sidelength for $[0/30]_T$ layup.

principal curvature axes) shape. The x curvature for this shape is much smaller than the saddle shape at zero sidelength. The decrease in curvature with sidelength is smaller than for the saddle shape, so this shape has the greatest x curvature over most of the graph. The dash-dot line represents the second cylindrical shape. The x curvature for this shape begins at a negative value and increases towards zero as laminate sidelength increases. In Figure 6.32, the curvature of the first shape in the y direction is the negative of the curvature in the x direction of that shape. The y curvature of the second shape is the negative of the x curvature of the third shape, and vice versa.

Figure 6.33 shows the calculated x-y twist curvature for the three shapes. The large-deformation saddle shape twist curvature is equal to the CLPT solution at zero sidelength, and rapidly goes towards zero. The two cylindrical shapes have the same values for twist curvature for all sidelengths. The twist curvatures for the cylindrical states are much closer to zero than the saddle shape at zero sidelength. The twist curvatures of the cylindrical shapes are always closer to zero than the twist curvatures of the saddle shape.

Figure 6.34 shows the calculated total potential energies for the three shapes. The total potential energies have very similar values. The differences cannot be seen on the scale of this graph. The saddle shape has a slightly lower potential energy for all sidelengths. Therefore, it was assumed that the stable shape for the laminate is a saddle in laminate principal curvature axes.

Curvature and stability are also examined as functions of the difference in temperature from the stress-free temperature for the $[0/30]_T$ laminate. The laminate in this case is assumed to have the same dimensions as the experimental specimens. Figures 6.35 and 6.36 show the calculated

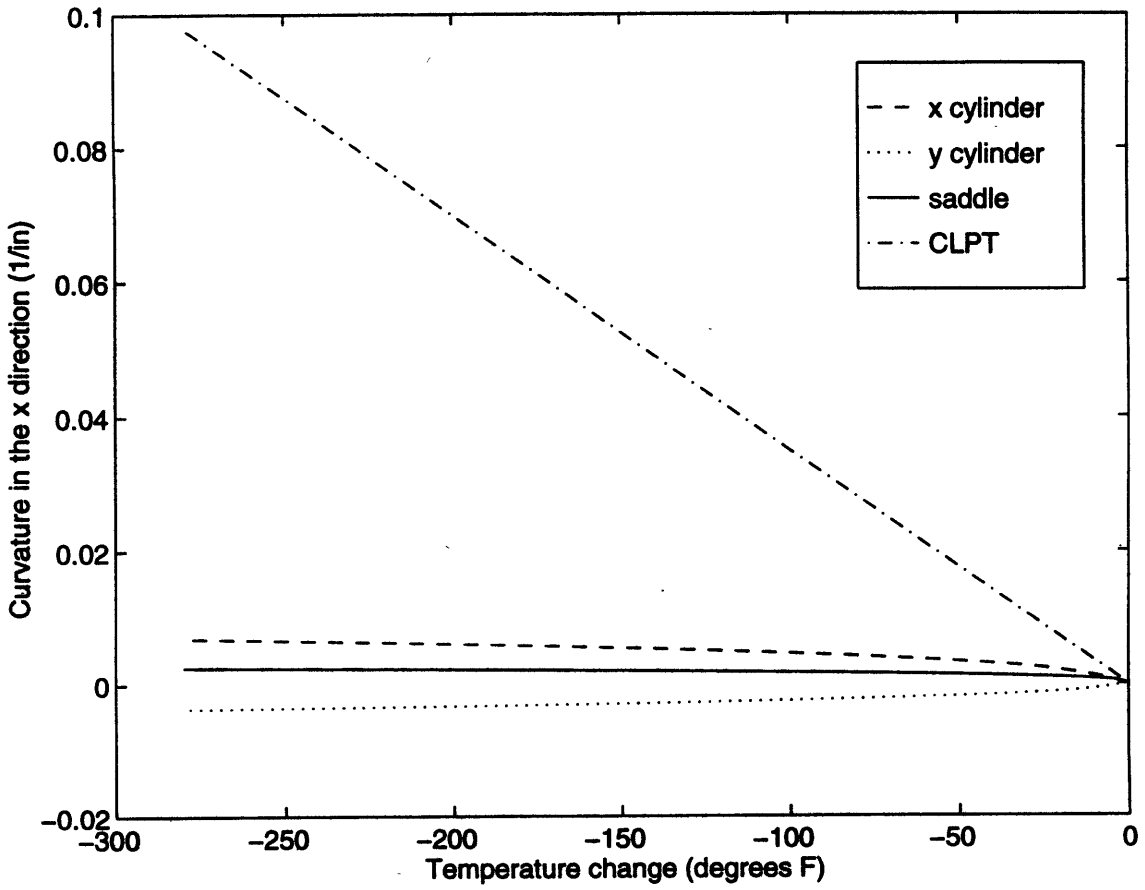

Figure 6.35 Laminate x curvature vs. temperature change for $[0/30]_T$ layup.

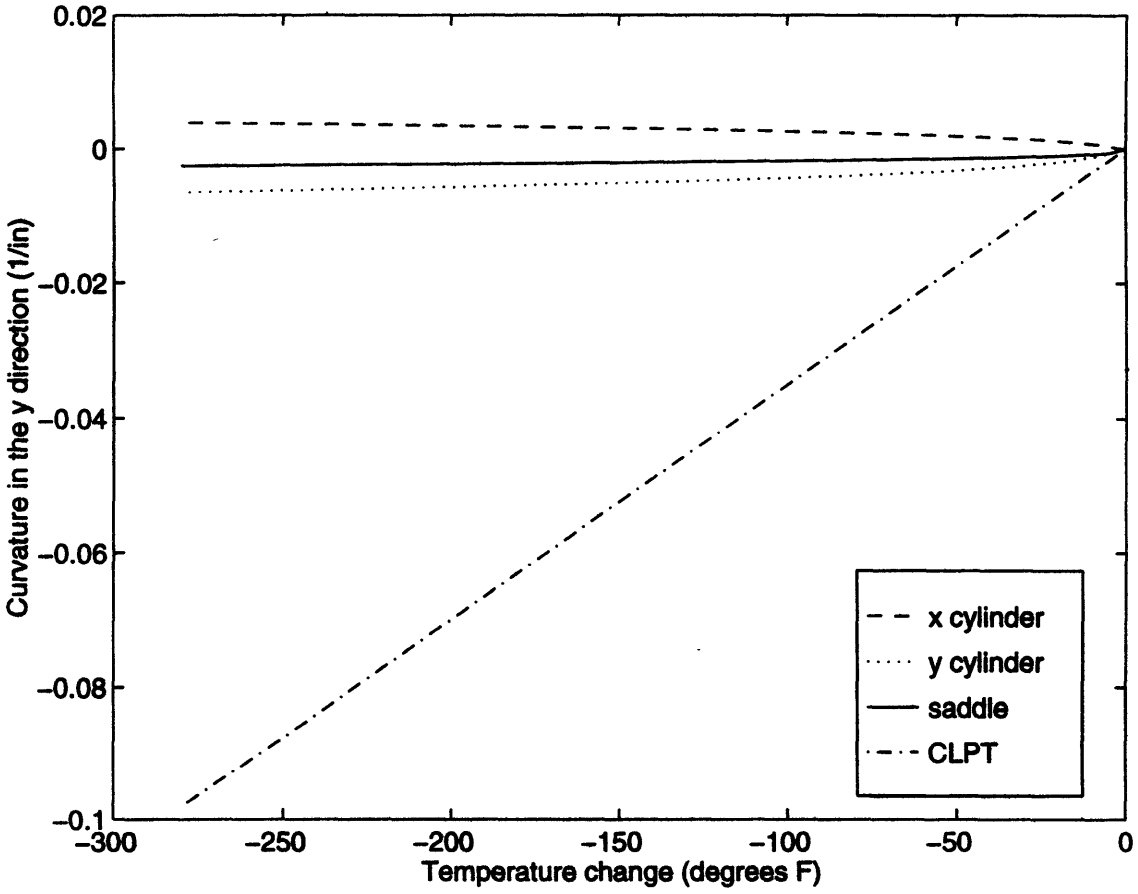

Figure 6.36 Laminate y curvature vs. temperature change for $[0/30]_T$ layup.

curvatures for the three shapes in the x and y directions respectively, and Figure 6.37 shows the calculated x-y twist curvature. Figure 6.38 shows the calculated total potential energies.

In Figure 6.35, the solid line represents the large-deformation saddle shape, the dashed line the non-zero x curvature cylindrical shape, and the dash-dot line the CLPT solution based on small deformations. All curvatures are shown versus the temperature difference from the stress-free temperature. For all temperatures, all three shapes have curvatures much smaller than the CLPT prediction. The saddle shape has smaller x curvature than the first cylindrical shape. The curvatures in the y direction, shown in Figure 6.36, show similar trends. The curvature of the saddle shape in the y direction is the negative of the x curvature of the saddle shape. The y curvature of the second shape is the negative of the x curvature of the third shape, and vice versa.

Figure 6.37 shows the calculated x-y twist curvature for the three shapes. The two cylindrical shapes have the same values for twist curvature for all temperatures. The twist for the cylindrical shapes is closer to zero than the twist for the large-deformation saddle shape. The calculated twist curvatures for all three shapes are approximately an order of magnitude lower than the CLPT solution. Thus large deformations have a very noticeable effect on the behavior of this laminate.

Figure 6.38 shows the calculated total potential energies for the three shapes as functions of temperature difference from the stress-free temperature. All three shapes are very close in total potential energy. The differences are too small to be seen on the scale of the graph. The saddle shape has the lowest total potential energy over the entire temperature range, so it is taken to be the stable shape.

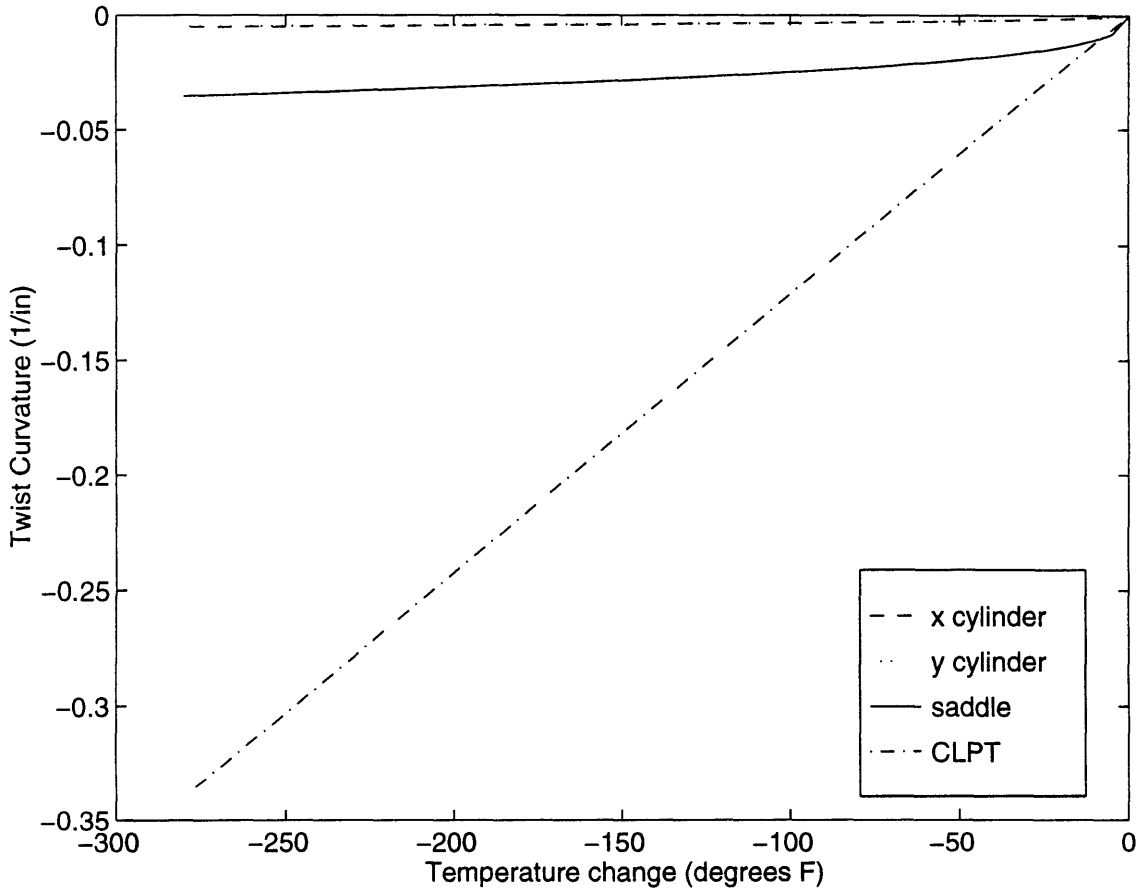

Figure 6.37 Laminate x-y twist curvature vs. temperature change for $[0/30]_T$ layup.

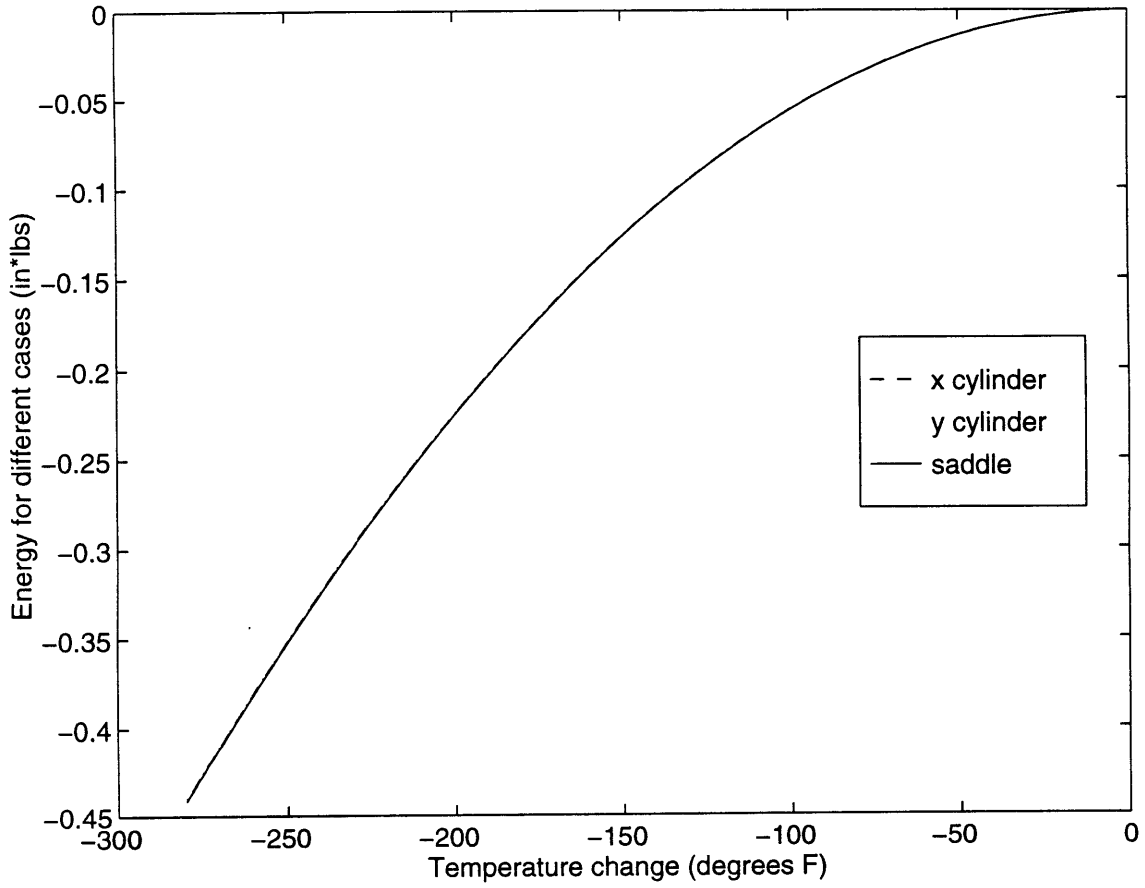

Figure 6.38 Laminate potential energy vs. temperature change for $[0/30]_T$ layup.

6.2.3 Correlation of Experiment and Large-Deformation Analysis

This subsection compares the results of the large-deformation analysis with experimental data. The large-deformation analysis does not calculate standard deviation information, so only means can be compared.

The first laminate which had large differences between experimental and VARBEND-predicted intervals was the layup $[0_2/90_2]_T$. The large-deformation analysis yields a value for W_1^T of -150 μin/in^2/°F (10600 μm/m^2/°C). This value is just outside of the experimental interval. The large-deflection prediction is closer to zero than the experimental mean. While the VARBEND analysis over-predicts W_1^T for the $[0_2/90_2]_T$ panel, the large-deformation analysis somewhat under-predicts it.

The next panel examined is $[0/30]_T$. The experimental data showed much smaller W_1^T and W_6^T means than the VARBEND analysis. The large-deformation analysis was used to re-predict the mean values for these thermal bending coefficients. The results are that the large-deformation model predicts a mean W_1^T of -5.5 μin/in^2/°F (-390 μm/m^2/°C), and a mean W_6^T of 53 μin/in^2/°F (3760 μm/m^2/°C). Just as for the $[0_2/90_2]_T$ panel, the large-deformation analysis under-predicts the measured thermal bending coefficients for the $[0/30]_T$ panel.

The modified correlation with experiment is shown in Figures 6.39 and 6.40. These figures are modified from Figures 6.20 and 6.22 respectively by using the means predicted by the large-deformation analysis. Since the large-deformation method does not provide standard deviation values, the predicted standard deviations used are from the VARBEND analysis.

The modifications in all cases bring about similar results. The means of all modified predictions are smaller in magnitude than the experimental means. There is some amount of overlap between experimental intervals and

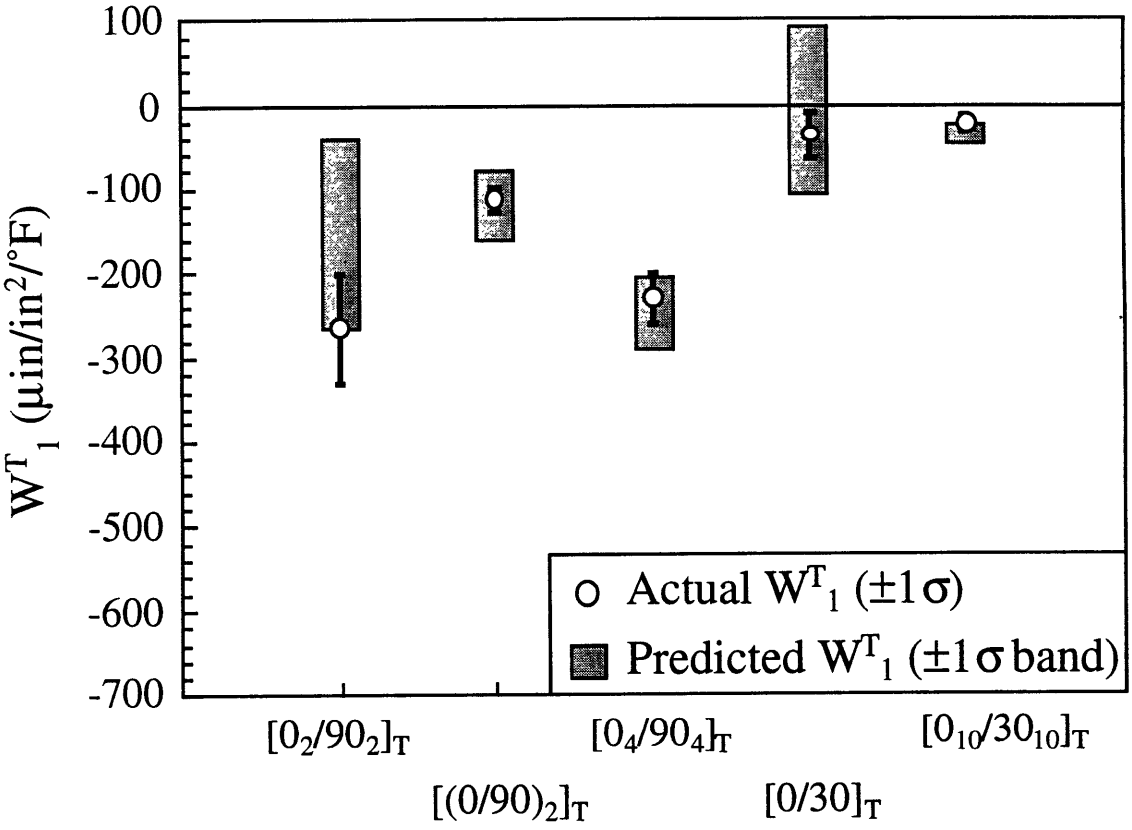

Figure 6.39 Correlation of W_1^T for unsymmetric laminates modified for large deformations.

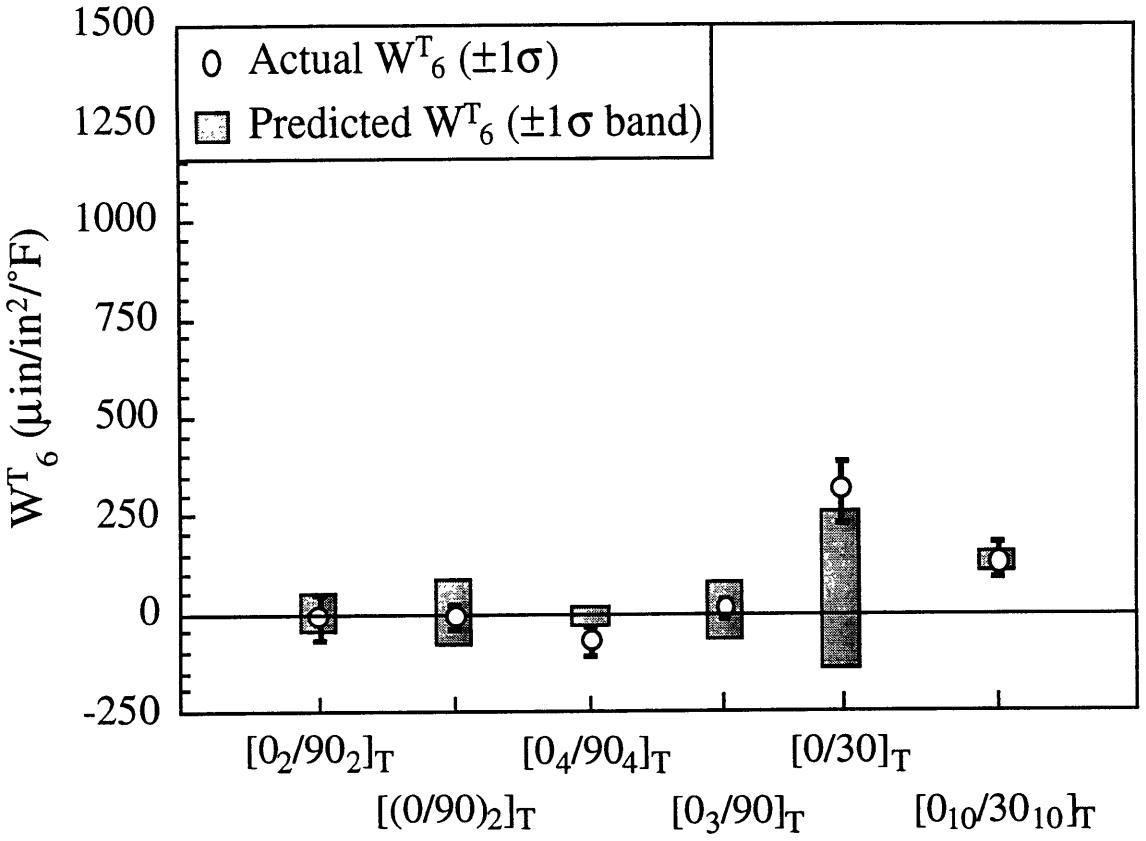

Figure 6.40 Correlation of W_6^T for unsymmetric laminates modified for large deformations.

modified predicted intervals. In the case of W_1^T for the $[0/30]_T$ panel, the interval predicted by the large-deformation analysis brackets the experimental interval. The large-deformation analyses greatly improved the correlations between the experiments and the analyses.

6.2.4 $[0_3/90]_T$ Panel

The final panel which exhibited behavior not predicted by the VARBEND analysis had the layup $[0_3/90]_T$. Specimens from this panel had dominant curvature in the y direction, while all other cross-ply unsymmetric specimens had dominant curvature in the x direction, where x is defined as along the length of the specimen as shown in Figure 5.7. The large-deformation analysis predicts that these specimens will have a right circular cylindrical shape, with curvature in the y direction. This prediction was verified in the experiments, as the specimens were seen to have a cylindrical shape, with dominant curvature in the y direction. The value for W_2^T predicted by the large-deformation model is approximately the same as the value predicted by the VARBEND model. The large-deformation model predicts zero mean values for W_1^T and W_6^T in this case.

6.3 VARBEND PARAMETRIC STUDY

This section presents a parametric study done using the analytical methodology developed in Sections 4.1 and 4.2 and implemented in the VARBEND computer code. Changes in the thermal bending coefficients with layup angles and grouping effects are examined. Also presented are sensitivity studies, which allow comparisons of the relative importance of input variables in determining laminate properties.

6.3.1 Layup Angle as a Parameter

Parametric studies of the effects of angle variations on the W^T's for some families of symmetric layups are presented in Figures 6.41 through 6.45. The mean W^T values are zero for symmetric laminates, so only standard deviations are shown. Predicted standard deviations vary continuously with layup angles. It can be seen in Figure 6.41 that of the $[\pm\theta]_s$ layups, the 45° layup is predicted to have minimum standard deviation in W_6^T, since the fibers are in the direction to give maximum resistance to twist. Twist standard deviation is symmetrical about this point. In bending, the standard deviations increase as the laminate differs from a unidirectional laminate, reaching a maximum at θ=35° for W_2^T and 55° for W_1^T.

Adding 0° plies to the $[\pm\theta]_s$ layup is predicted to reduce bending deformation variation, since fibers are along the direction of bending, acting as stiffeners. This reduction was much greater for the $[0/\pm\theta]_s$ layup than the $[\pm\theta/0]_s$ layup because of the greater effectiveness in bending stiffness of the outside plies. These effects can be seen in Figures 6.42 and 6.43. Note that W_6^T is not always decreased significantly by the addition of these plies.

Figure 6.44 shows the variations of the W^T's for the $[0/\pm\theta/90]_s$ layup. Bend and twist W^T variations are reduced for this layup. In Figure 6.45, the W^T's are shown for the $[0/\theta/90/-\theta]_s$ layup. The effect of the stacking order change is to reduce the variations in W_2^T and W_6^T, while having little effect on W_1^T.

6.3.2 Sensitivity Metrics

This subsection presents sensitivity metrics for some sample laminates and laminate properties. The relative importance of the individual ply

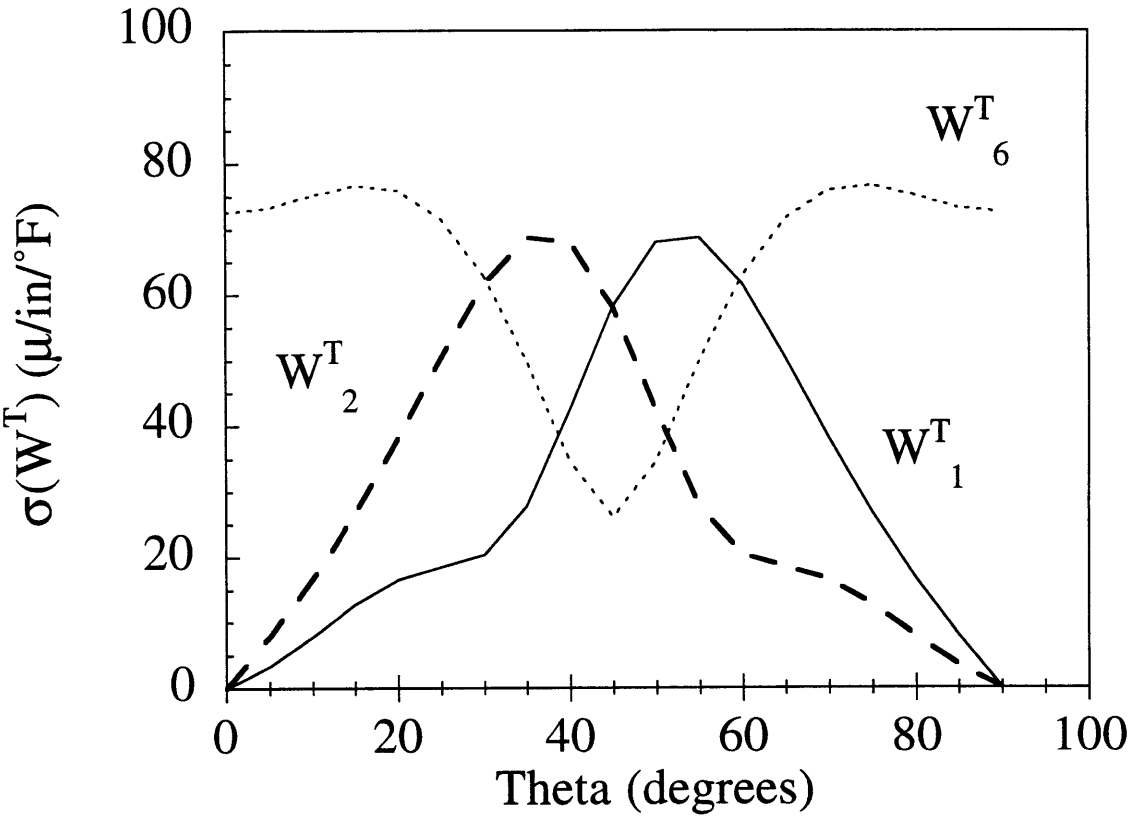

Figure 6.41 Predicted standard deviation of W^T's for $[\pm\theta]_s$ laminates.

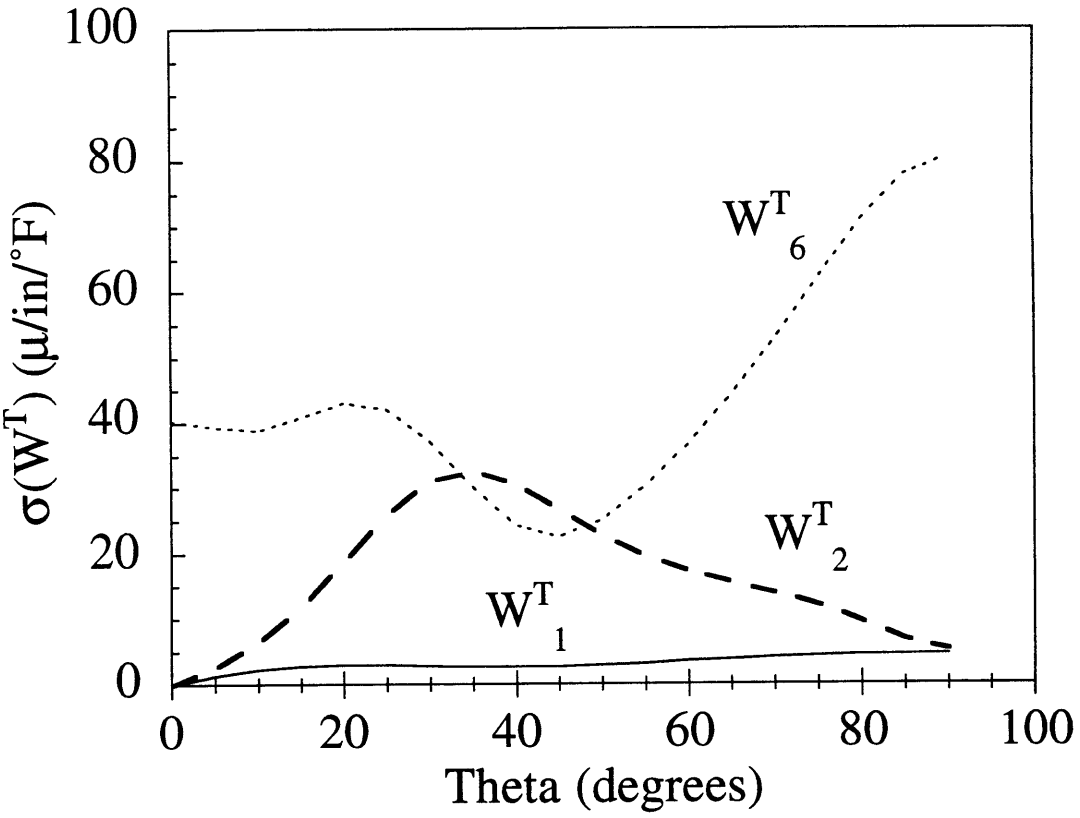

Figure 6.42 Predicted standard deviation of W^T's for $[0/\pm\theta]_s$ laminates.

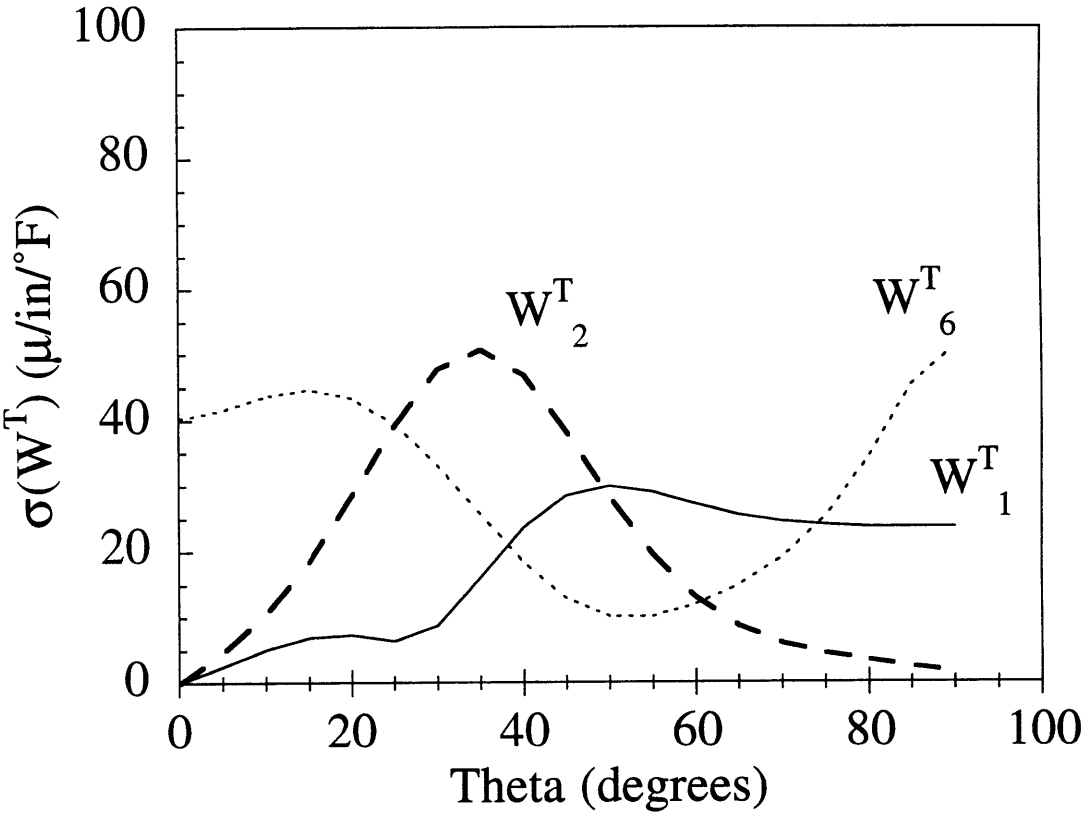

Figure 6.43 Predicted standard deviation of W^T's for $[\pm\theta/0]_s$ laminates.

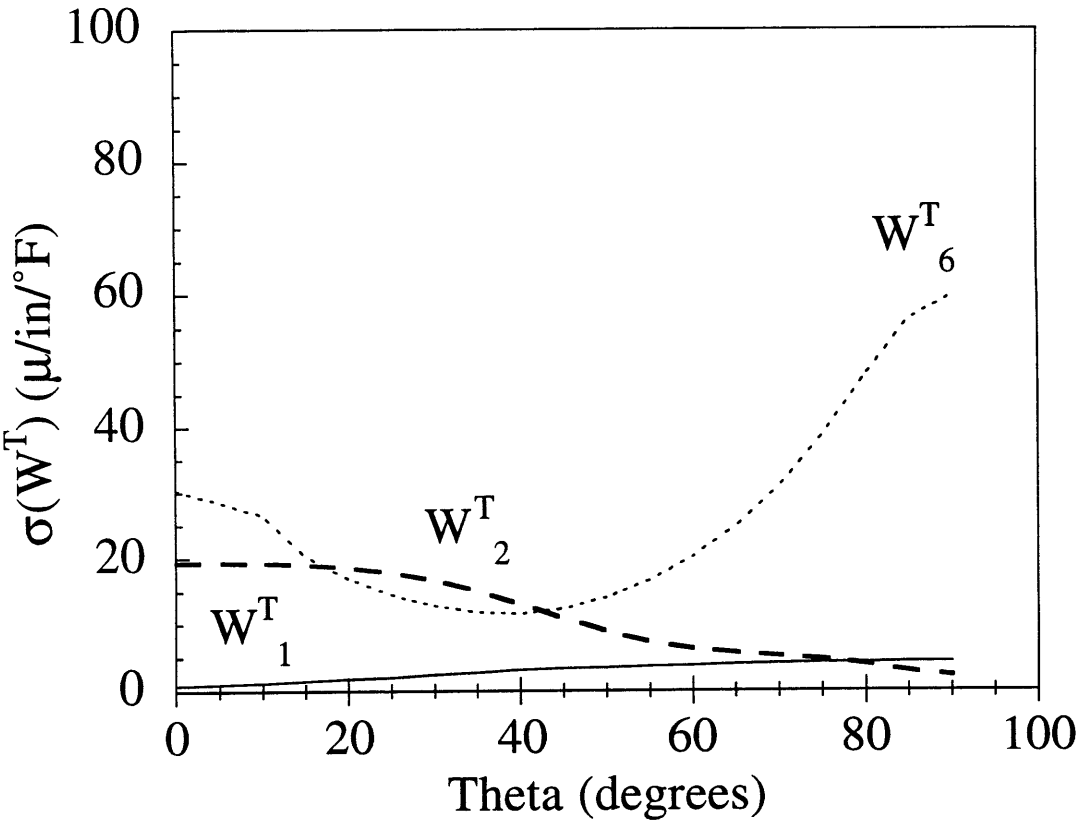

Figure 6.44 Predicted standard deviation of W^T's for $[0/\pm\theta/90]_s$ laminates.

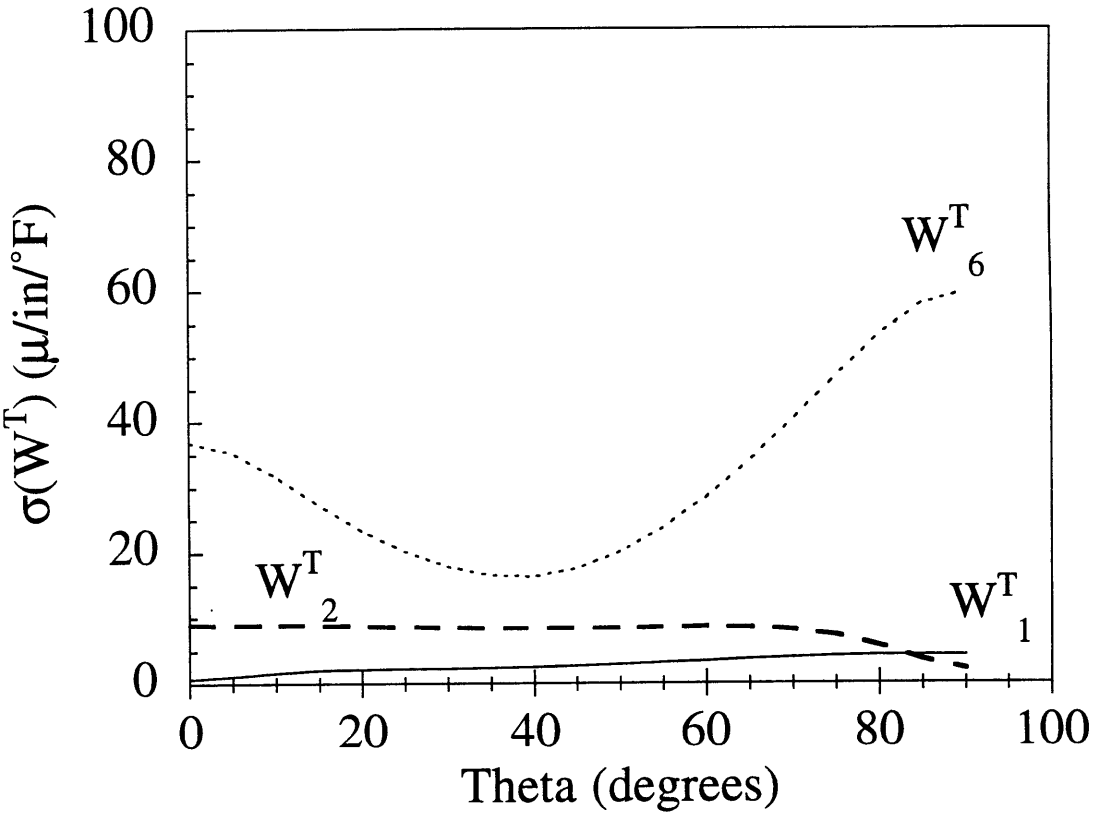

Figure 6.45 Predicted standard deviation of W^T's for $[0/\theta/90/-\theta]_s$ laminates.

material properties and geometric variables are examined. The effect of volume fraction variations, the inclusion of which is a new feature in the current work, is stressed.

The sensitivity metric examined in this section is the second metric presented in Section 4.5, which is repeated as Eq. 6.1 for the reader's convenience.

$$d_{ij}^{\sigma} = \frac{\partial Y_i}{\partial X_j} \hat{\sigma}_{Xj} \tag{6.1}$$

This sensitivity metric has units of the laminate property. It shows the contribution of the variation of input variable X_j to the variation of laminate variable Y_i (see Tables 4.1 and 4.2). Instead of presenting the effect of each individual ply thickness and angle, these factors are consolidated by statistically combining the effects of all plies, as in Eqs. 6.2 and 6.3.

$$d_{i(thickness)}^{\sigma} = \sqrt{\sum_{j=1}^{nply} (d_{ij}^{\sigma})^2} \tag{6.2}$$

$$d_{i(angle)}^{\sigma} = \sqrt{\sum_{j=nply}^{2nply} (d_{ij}^{\sigma})^2} \tag{6.3}$$

As mentioned in Chapter 4, the ordinary VARBEND method assumes the laminate is made from one material, and hence ply-by-ply material variations are not considered. In the VARBEND runs used to generate results shown in this section, each ply was specified as a separate (though identical) material. This had the effect of allowing ply-by-ply material variations. VARBEND treated the material properties in each ply as separate independent variables. The contributions of each material property for each ply are statistically combined using Eq. 6.4, where *nmatl* is the

number of materials used to specify the laminate, and m is an index of the material properties which takes on values 1, 2, ..., 9.

$$d^{\sigma}_{i(material\ property\ m)} = \sqrt{\sum_{j=1}^{nmatl} (d^{\sigma}_{i(2nply+(j-1)*9+(m-1))})^2} \tag{6.4}$$

The first laminate examined is $[\pm 30]_s$, the base laminate for much of the experimental portion of the current work. Values of the sensitivity metrics are given in Figures 6.46 and 6.47 for the laminate longitudinal CTE α_1 and x direction thermal bending coefficient W_1^T. Longitudinal CTE depends strongly on ply stiffnesses, CTE's, and volume fraction. In contrast, the factors that strongly affect W_1^T are thicknesses and ply angles.

The next laminate examined is $[(\pm 30)_4]_s$. Sensitivity plots are presented in Figures 6.48 and 6.49. The sensitivity plot for longitudinal laminate CTE is identical to that for the $[\pm 30]_s$ layup. This is expected, as stacking order and thickness should not affect in-plane properties. On the other hand, the sensitivities of W_1^T have changed notably. The material properties have become more important than the geometric variables. Ply shear modulus, CTE's, and volume fraction are the most important of the material properties.

The effect of adding 0° plies can be seen in the sensitivity plots for the $[0/\pm 30]_s$ layup shown in Figures 6.50 and 6.51. Both sensitivity plots show that ply thickness is the most important factor in the variation of α_1 and W_1^T.

The final laminate examined is $[(0/90)_2]_T$, an unsymmetric cross-ply laminate. Sensitivity metric values for this layup are given in Figures 6.52 and 6.53. For this layup, the most important parameter in both laminate properties examined is ply thickness. Some of the material properties are also important.

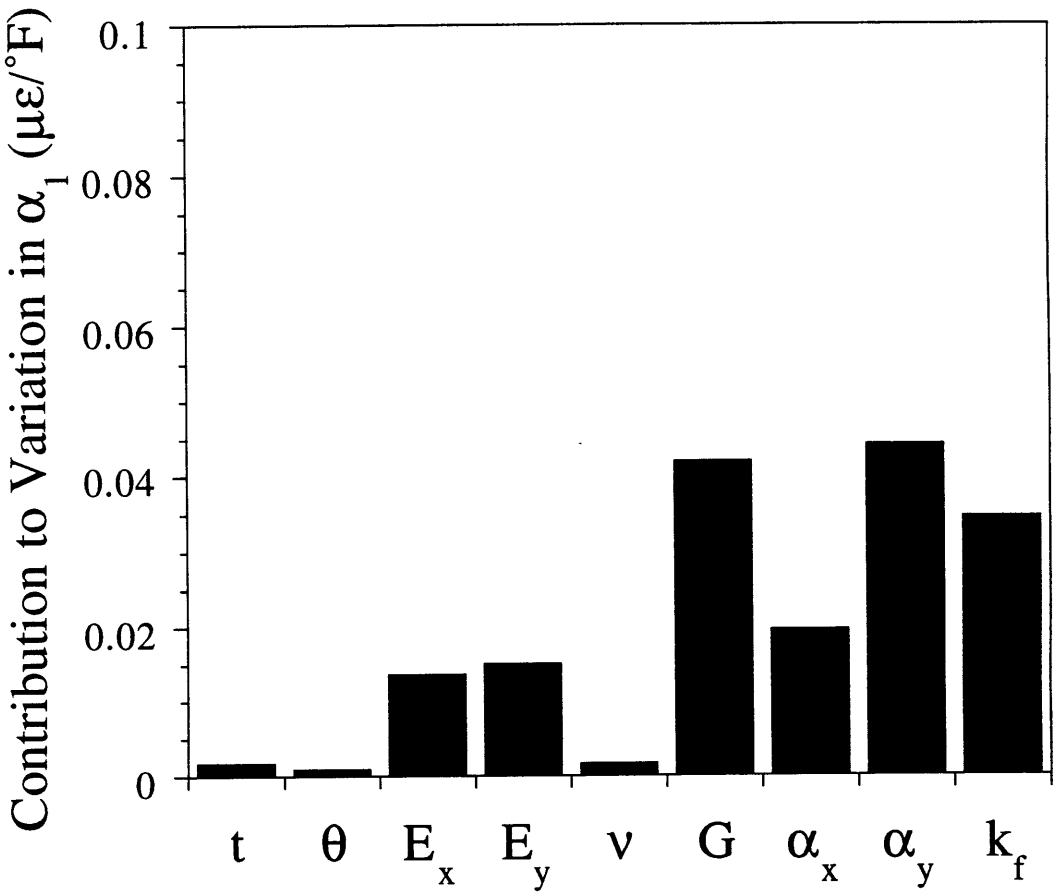

Figure 6.46 Sensitivity study for axial CTE (α_1) of $[\pm 30]_s$ laminate.

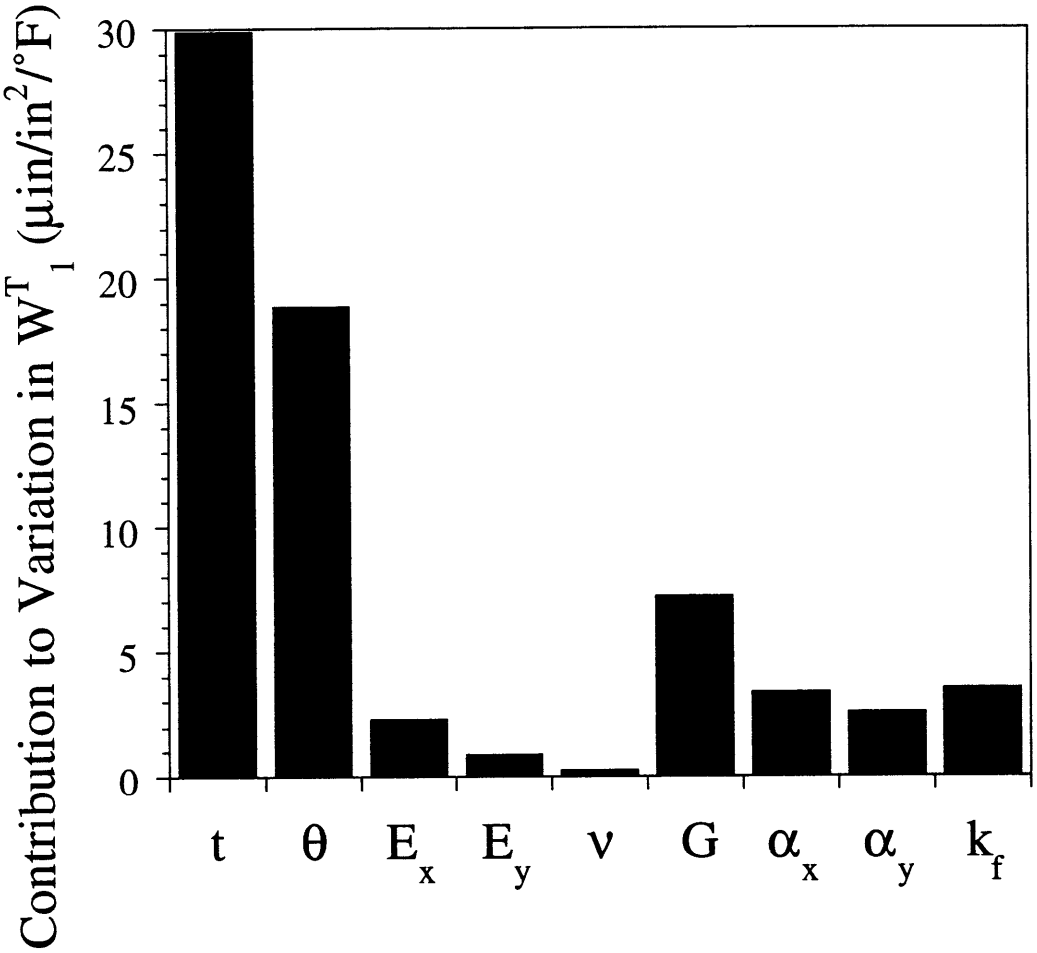

Figure 6.47 Sensitivity study for thermal bending coefficient W_1^T of $[\pm 30]_s$ laminate.

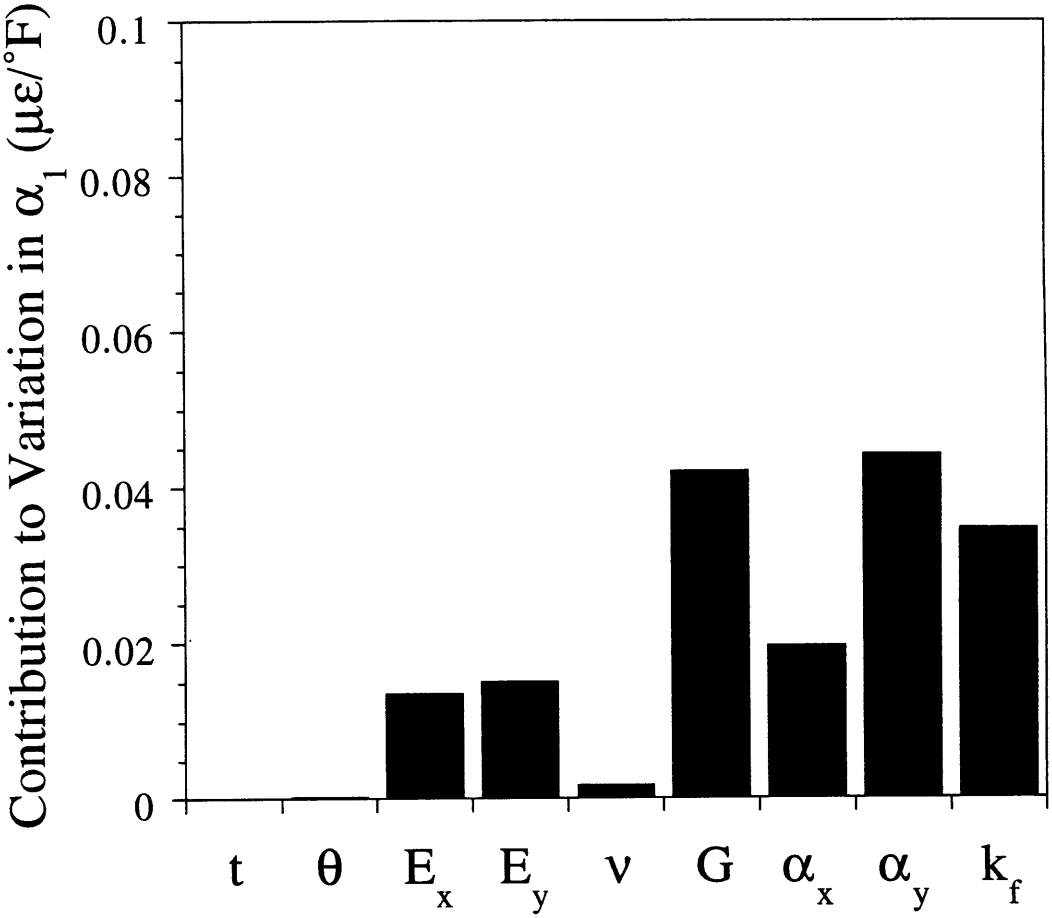

Figure 6.48 Sensitivity study for axial CTE (α_1) of $[(\pm 30)_4]_s$ laminate.

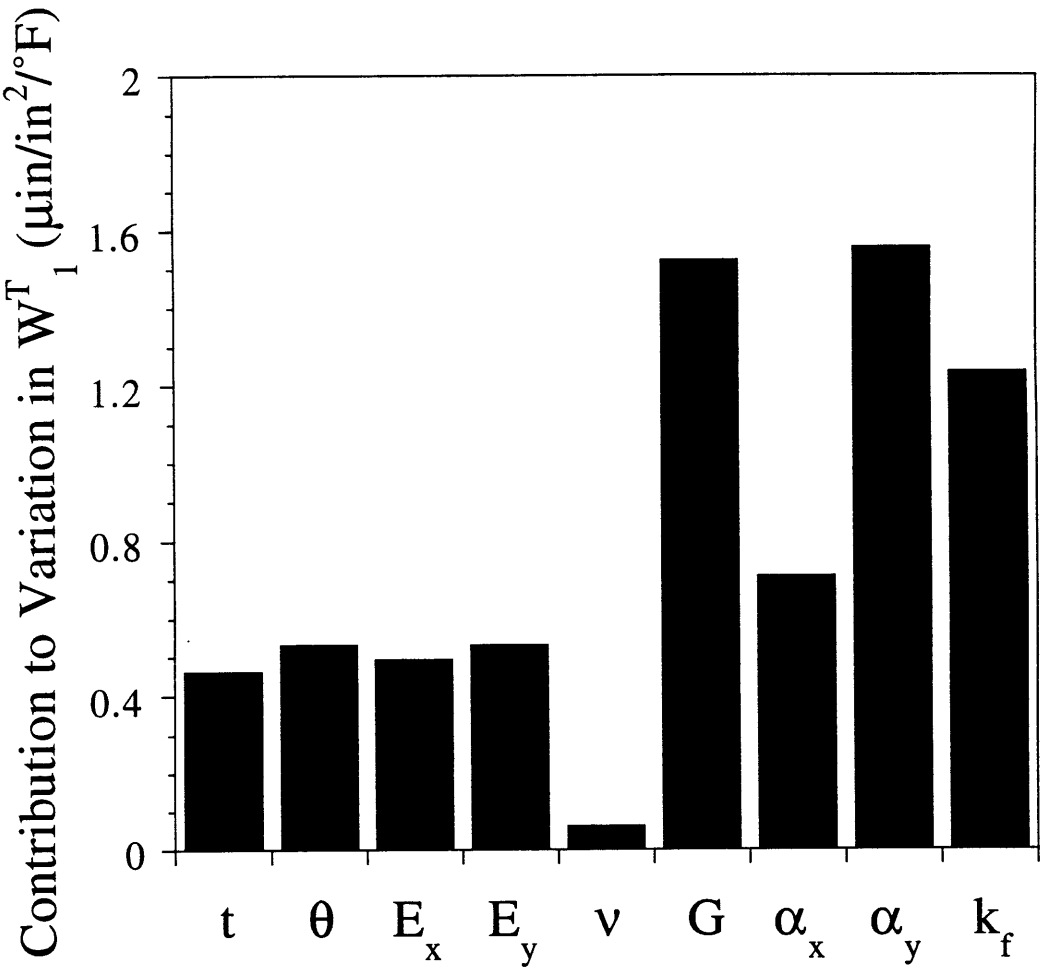

Figure 6.49 Sensitivity study for thermal bending coefficient W_1^T of $[(\pm 30)_4]_s$ laminate.

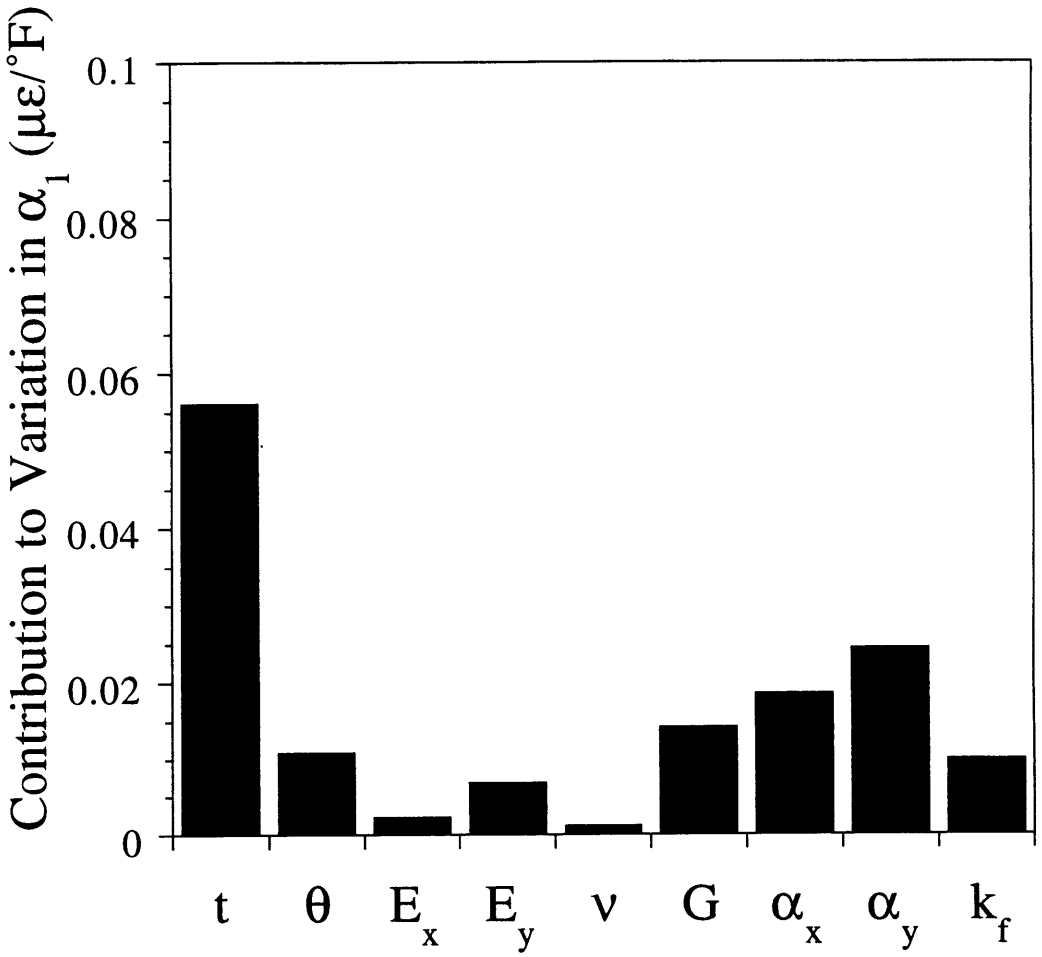

Figure 6.50 Sensitivity study for axial CTE (α_1) of $[0/\pm30]_s$ laminate.

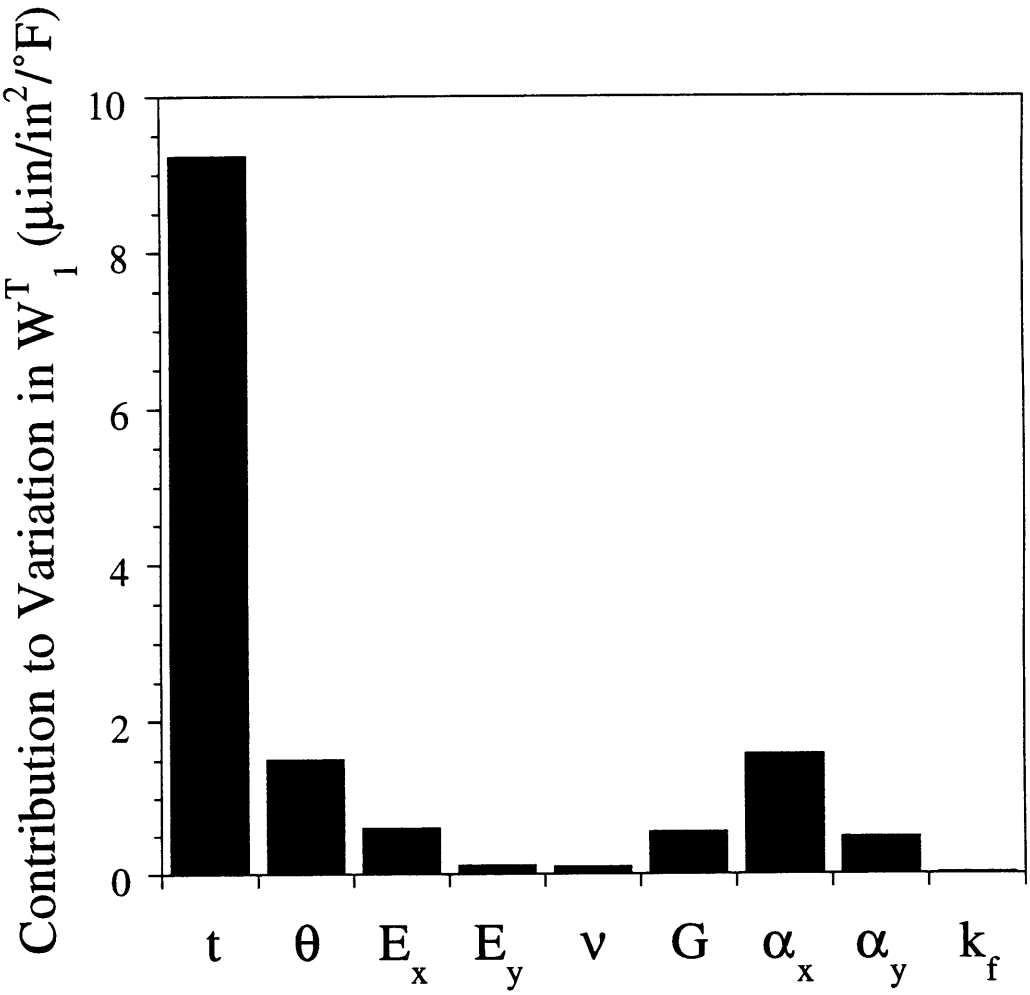

Figure 6.51 Sensitivity study for thermal bending coefficient W_1^T of $[0/\pm30]_s$ laminate.

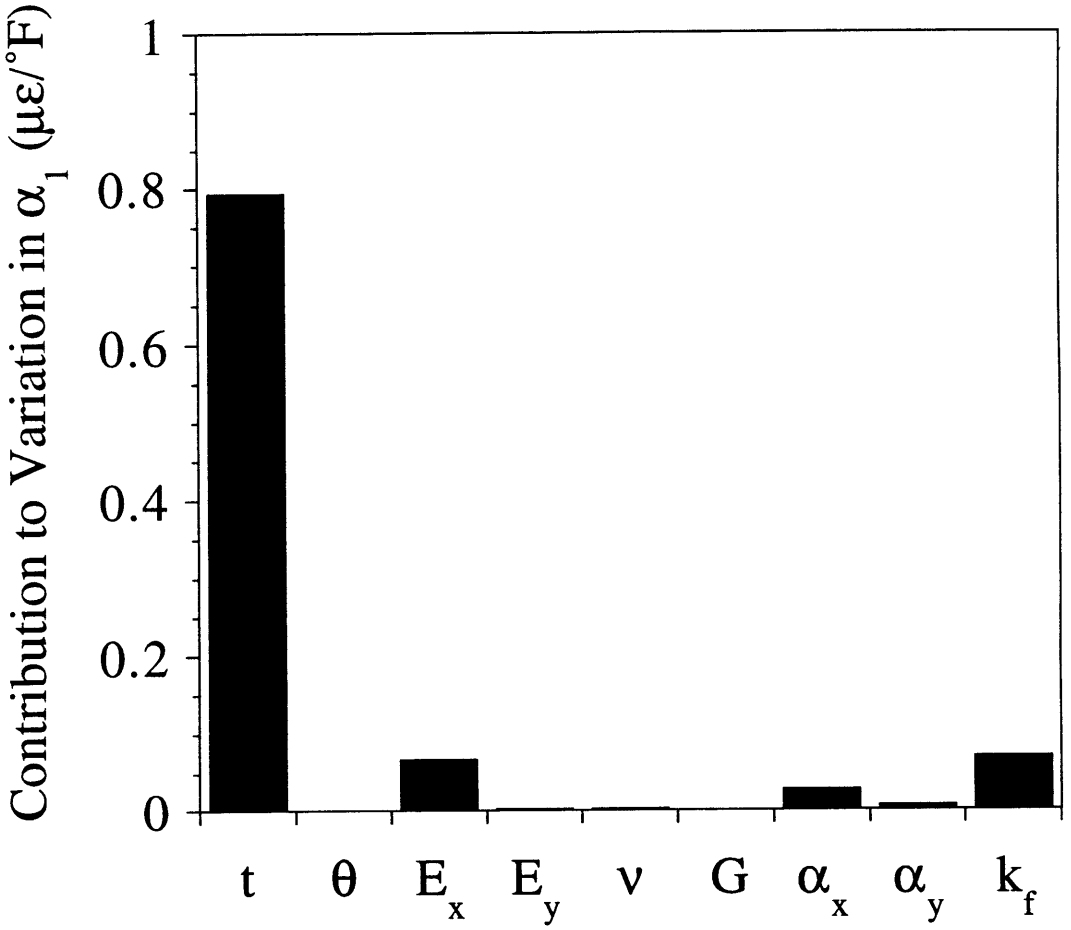

Figure 6.52 Sensitivity study for axial CTE (α_1) of $[(0/90)_2]_T$ laminate.

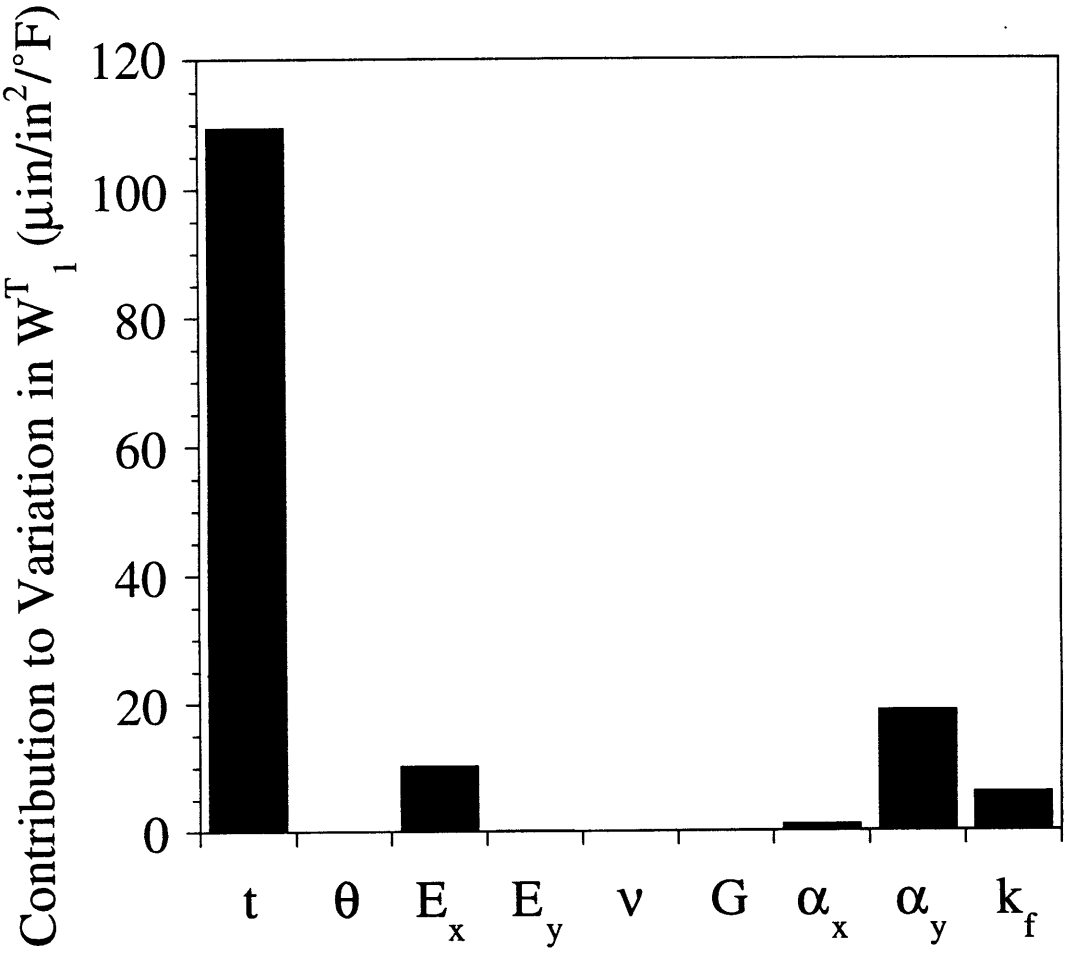

Figure 6.53 Sensitivity study for thermal bending coefficient W_1^T of $[(0/90)_2]_T$ laminate.

6.3.3 Discussion of Parametric Studies

The parametric studies presented in Section 6.3.1 illustrate the usefulness of the VARBEND analysis for preliminary design. The mean thermal bending coefficients in all layups studied in the section are equal to zero; therefore, the standard deviations of the W^T's are the performance metrics of interest. The results indicate that the distributions of laminate properties are a strong function of layup. In Figure 6.41, trade-offs in using different angles in the $[\pm\theta]_s$ layup can be seen. Unidirectional laminates, for example, have a very low standard deviation for W_1^T, but a high standard deviation for W_6^T. The θ=45 laminate has the minimum W_6^T standard deviation, but higher standard deviations in W_1^T and W_2^T. Figures 6.42–6.45 show the effects of adding 0° and 90° plies, and altering the stacking sequence, respectively. These figures show that changing the layup changes both the magnitudes of, and trends seen in, the W^T standard deviations.

The sensitivity analyses presented in Subsection 6.3.2 indicate which manufacturing parameters and material properties are important to controlling laminate property variations. The parameters controlling laminate property variations are extremely dependent on the layup and material used, and also on which laminate property is being examined. Examples of the relative importance of many input parameters is seen in Figures 6.46–6.53. The thicknesses and ply layup angles are especially important in determining the W_1^T distributions of the laminate studied, but all input parameters have a non-trivial influence on the W_1^T distribution for at least one of the laminates. Different input parameters were found to be important to the variations in α_1 and W_1^T of the same laminate. It is difficult to generalize the results of the sensitivity analyses. No one material property

or manufacturing parameter was found to dominate the variations in laminate properties for all layups.

CHAPTER 7

CONCLUSIONS AND RECOMMENDATIONS

The present work was conducted to investigate variations in laminate properties due to random variations in ply material properties and manufacturing parameters. Understanding these variations is critical to the design and construction of dimensionally stable composite structures. This understanding was achieved through a combination of analytical modeling and experimental verification. In this chapter, the findings of the current work are summarized, conclusions are drawn from the findings, and directions for future work are recommended.

The stated goals of the present work have been achieved. A FORTRAN code called VARBEND has been developed to predict variations in laminate properties. The code can be run quickly on a desktop computer. Experimental data on thermally induced bending was collected for a large number of specimens. The data was reduced and correlated with the analytical model. These correlations verified the analysis.

Large deformation effects were found to be important for some of the unsymmetric laminates studied. Their behavior is not predicted well by Classical Laminated Plate Theory (CLPT). The large-deformation analysis method of Hyer was extended to quantify these effects for general laminates. The correlation between the large-deformation analysis and experimental data for the unsymmetric specimens was very good. The development and

implementation of the general large-deformation analysis was a significant achievement in its own right.

Correlations between the analyses and the experimental data were good, with some interesting exceptions. The VARBEND analysis predicted zero means and non-zero standard deviations for the W^T's of symmetric laminates. The experiments had consistently non-zero mean values, which were probably due to asymmetries in the manufacturing process. These non-zero mean values were not considered in the analysis, but they were usually within one predicted standard deviation of the predicted value of zero. Some laminates had larger standard deviations than predicted. It was noted that these laminates were all very sensitive to ply thicknesses. Also, the standard deviations of some laminates were small enough that the data could not be considered meaningful due to the uncertainties in the thermal deformation of the test setup. Finally, the standard deviations of the thermal twist coefficient were usually larger relative to predictions than those of the thermal bend coefficients, for as-yet unknown reasons.

Parametric studies allowed investigations beyond the practical scope of the experimental portion of this project. Standard deviations of laminate properties were found to be complex functions of the material properties and manufacturing parameters. No generalizations could be made about laminate property standard deviations that would apply to all layups. The VARBEND code was also used for sensitivity studies. These studies were used to identify the relative importance of the ply material properties and manufacturing parameters to laminate property standard deviations. The relative importance of the parameters varied with the layup, material, and which laminate property was under consideration. Again the results cannot be generalized to identify parameters critical to all laminates. The

VARBEND code can, however, be used to identify which factors are the most important in determining the laminate property standard deviations for any specific laminate design.

Several recommendations can be made based on the current work. The first is that the VARBEND code should be used for the design of composite laminates. The code can be used in trades to minimize the standard deviations in the laminate properties of interest. The code can also be used to determine which material properties and manufacturing parameters are critical to control in order to keep the laminate property standard deviations within given limits. The code is nearly complete. Slight modifications and improvements, such as allowing correlations between materials on a ply-by-ply basis, and correlations between ply thicknesses, are recommended.

Further experimental work would be useful. The experimental setup should be examined and possibly redesigned to reduce the uncertainty in experimental data. In the current design, the uncertainties limited the ability to verify the analysis for very-low-standard-deviation laminates. A systematic examination of the sources of variations in laminate properties should also be undertaken. This was done on a limited basis in the current work–three panels of one layup were manufactured to compare variations within panels to those between panels. In addition, material batch-to-batch variations, variations among different material systems, and variations within small areas versus across entire large panels could be examined. Different laminate properties (such as tensile modulus) could also be tested.

Existing large corporate or other limited distribution ply property databases should be used as inputs into the analysis. Such databases generally contain a large number of points; therefore, there is a great deal of confidence in the means and standard deviations. No modification of such

data is needed for it to be used as inputs into the VARBEND code. Also, if large distributions of *laminate* properties are available, they could be used for further verification of the analytical model.

The analysis developed in the present investigation works. It can be used to design laminates for minimum standard deviations in important laminate properties. The code can also be used to find approximate standard deviations of candidate laminates in preliminary design trades. Finally, the VARBEND code can be used to focus on which factors are critical to control if one wishes to maintain a low standard deviation of a specific laminate property in a specific design. The VARBEND code can be run quickly and easily, and can save expensive and time-consuming testing, design iteration, and rework.

REFERENCES

1. Bowles, D. and Tenney, D., "Composite Tubes for the Space Station Truss Structure", SAMPE Journal, May/June, 1987, pp. 49-56.

2. Tompkins, S. S., Bowles, D. E., Slemp, W. S., and Teichman, L. A., "Response of Composite Materials to the Space Station Orbit Environment", *AIAA/NASA Space Station Symposium*, Williamsburg VA, 1988.

3. Jones, R., Lukez, R., Peterson, B., Batty, J. C., and Redd, F. J., "Extended Thermal Cycle Testing of Graphite/Epoxy Composite Struts for Space Station Applications", *SAMPE Quarterly*, Vol. 21, No. 1, October, 1989, pp. 34-38.

4. Thompson, D. F. and Babel, H. W., "Material Applications on the Space Station: Key Issues and the Approach to their Solution", *SAMPE Quarterly*, Vol. 21, No. 1, October, 1989, pp. 27-33.

5. Tompkins, S. S., Funk, J. G., Bowles, D. E., Towell, T. W., and Connell, J. W., "Composite Materials for Precision Space Reflector Panels", *SPIE International Symposium and Exhibition on Optical Engineering and Photonics*, Orlando, Florida, 1992.

6. Brent, D. N. and Lou, M. C., "Thermal and Mechanical Stability of the WF/PC II Optical Alignment", AIAA-94-1738-CP, 1993.

7. Telcamp, A. R. and Derby, E. A., "Design Considerations for Composite Materials Used in the MARS Observer Camera", *SPIE*, Orlando, FL, 1990.

8. Krumweide, G. C., *Attacking Dimensional Instability Problems in Graphite/Epoxy Structures*. March 24, 1992, Composite Optics, Inc.

9. Shapery, R. A., "Thermal Expansion Coefficients of Composite Materials Based on Energy Principles", *Journal of Composite Materials*, Vol. 2, No. 3, 1968, pp. 380-404.

10. Ishiwaka, T., Fukunaga, K., and Kobayashi, S., "Thermal Expansion Coefficient of Unidirectional Composites", *Journal of Composite Materials*, Vol. 12, 1978, pp. 153-168.

11. Ishiwaka, T., Fukunaga, H., and Ono, K., "Graphite-epoxy Laminates with Almost Null Coefficient of Thermal Expansion Under a Wide Temperature Range", *Journal of Materials Science*, Vol. 24, 1989, pp. 2011-2017.

12. Strife, J. R. and Prewo, K. M., "The Thermal Expansion Behavior of Unidirectional and Bidirectional Kevlar/Epoxy Composites", *Journal of Composite Materials*, Vol. 13, October, 1979, pp. 264-277.

13. Chamis, C. C., "Simplified Composite Micromechanics Equations for Hygral, Thermal, and Mechanical Properties", *SAMPE Quarterly*, Vol. 15, April, 1984, pp. 14-23.

14. Rosen, B. W. and Hashin, Z., "Effective Thermal Expansion Coefficients and Specific Heats of Composite Materials", *International Journal of Engineering Science*, Vol. 8, 1970, pp. 157-173.

15. Hashin, Z., "Analysis of Properties of Fiber Composites with Anisotropic Constituents", *Journal of Applied Mechanics*, Vol. 46, September, 1979, pp. 543-550.

16. Bowles, D. E. and Tompkins, S. S., "Prediction of Coefficients of Thermal Expansion for Unidirectional Composites", *Journal of Composite Materials*, Vol. 23, April, 1989, pp. 370-387.

17. Rogers, K. F., Phillips, L. N., Kingston-Lee, D. M., Yates, B., Overy, M. J., Sargent, J. P., and McCalla, B. A., "The Thermal Expansion of Carbon-Fibre Reinforced Plastics Part 1. The influence of Fibre Type and Orientation", *Journal of Materials Science*, Vol. 12, 1977, pp. 718-734.

18. Rogers, Phillips, Kingston-Lee, Yates, Overy, Sargent, and McCalla, "The Thermal Expansion of Carbon-Fibre Reinforced Plastics Part 2. The influence of fibre volume fraction", *Journal of Materials Science*, Vol. 13, 1978, pp. 433-440.

19. Tompkins, S. S., Bowles, D. E., and Kennedy, W. R., "A Laser Interferometer Dilatometer for Thermal Expansion Measurements of Composites", *Proceedings of the 10th International Congress on Experimental Mechanics*, Montreal Canada, 1984, pp. 367-376.

20. Bowles, D. E., Post, D., Herakovich, C. T., and Tenney, D. R., "Moire Interferometry for Thermal Expansion of Composite Materials", *SAMPE Journal*, Vol. 21, No. 12, December, 1981, pp. 441-448.

21. Wolff, E. G., "Measurement Techniques for Low Expansion Materials", *Nations SAMPE Technical Conference Series*, 1977.

22. Doxsee, L. E. and Springer, G. S., "Measurements of Temperature Induced Deformations in Composite Cylindrical Shells", *Journal of Composite Materials*, Vol. 25, October, 1991, pp. 1340-1350.

23. Timoshenko, S., "Analysis of Bi-Metal Thermostats", *Journal of the Optical Society of America*, September, 1925, pp. 233-255.

24. Hyer, M. W., "Some Observations on the Cured Shape of Thin Unsymmetric Laminates", *Journol of Composite Materials*, Vol. 15, March, 1981, pp. 175-194.

25. Hyer, M. W., "Calculations of the Room-Temperature Shapes of Unsymmetric Laminates", *Journal of Composite Materials*, Vol. 15, July, 1981, pp. 296-310.

26. Hyer, M. W., "The Room-Temperature Shapes of Four-Layer Unsymmetric Cross-Ply Laminates", *Journal of Composite Materials*, Vol. 16, July, 1982, pp. 318-340.

27. Wong, M., "The Effects of Fabrication and Moisture on the Curvatures of Thin Unsymmetric Graphite/Epoxy Laminates", Massachusetts Institute of Technology, SM Thesis, 1982.

28. Tompkins, S. S. and Funk, J. G., "Sensitivity of the Coefficient of Thermal Expansion of Selected Graphite Reinforced Composite Laminates to Lamina Thermoelastic Properties", *SAMPE Quarterly*, April, 1992, pp. 55-61.

29. Hinckley, C. M., "Statistical Evaluation of the Variations in Laminate Composite Properties Resulting from Ply Misalignment", *SPIE Proceedings*, Orlando, FL, 1990.

30. McManus, H. L., "Probabilistic Methods for the Calculation of Laminate Properties", *American Society for Composites 7th Technical Conference on Composite Materials*, University Park PA, 1992.

31. Hedgepeth, J. M., "Influence of Fabrication Tolerances on the Surface Accuracy of Large Antenna Structures", *AIAA Journal*, Vol. 20, May, 1982, pp. 680-686.

32. Sable, W. W., "A Probabilistic Model of the Thermal Dimensional Stability of Composite Structural Components", *SPIE International*

Symposium and Exhibition on Optical Engineering and Photonics, Orlando FL, 1992.

33. Jones, R. M., *Mechanics of Composite Materials*, Hemisphere Publishing, 1975.

34. Tsai, S. S., *Theory of Composites Design*, Think Composites, Dayton, Ohio, 1992.

35. Hoel, P. G., *Introduction to Mathematical Statistics*, Second ed. John Wiley & Sons, Inc., New York, NY, 1954, pp. 331.

36. Hines, W. W. and Montgomery, D. C., *Probability and Statistics in Engineering and Management Science*, John Wiley & Sons, New York, NY, 1980.

37. Brownlee, K. A., *Statistical Theory and Methodology in Science and Engineering*, John Wiley & Sons, Inc., New York, NY, 1960, pp. 570.

38. Mendenhall, W. and Sincich, T., *Statistics for the Engineering and Computer Sciences*, Dellen Publishing Company, Santa Clara, California, 1984, pp. 884.

39. *Matlab*. 1994, The Mathworks, Inc.: Natick, MA.

40. Lagace, P. A., Brewer, J. C., and Varnerin, C., "TELAC Manufacturing Course Notes", TELAC Report 88-4B, Massachusetts Institute of Technology, 1990.

41. Hogg, R. V. and Tanis, E. A., *Probability and Statistical Inference*, 3rd ed. Macmillan Publishing Company, New York, NY, 1988, pp. 658.

APPENDIX A

COUPLE.M MANUAL AND SCRIPT

COUPLE.M- A Computer Code for Prediction of Material Correlation Coefficients

INTRODUCTION

Couple.m is a simple, easy to use Matlab script that will calculate the expected statistics of the stiffnesses and hygrothermal properties of a composite ply, given the means and standard deviations of fiber stiffnesses and hygrothermal properties, matrix stiffnesses and hygrothermal properties, and fiber volume fraction. It uses random number generators, micromechanical relations, and simple statistics to calculate material correlation coefficients for a given material system. Other statistics are also calculated, including means, standard deviations, and covariances for ply stiffnesses and hygrothermal properties.

GENERATION OF FIBER AND MATRIX PROPERTIES

The program generates sets of fiber stiffnesses and hygrothermal properties, matrix stiffnesses and hygrothermal properties, and fiber volume fractions. This is done in Matlab with the 'random' command, which generates random numbers from a given type of distribution. In the random command, the first argument is the distribution type, the second is the mean value, the third is the standard deviation, and the last two arguments denote how many numbers are generated. In couple.m, each step in the overall loop generates one value for each input variable, and standard deviations are assumed to be 2% of the mean values. All the inputs are independent normally distributed random variables. The entire loop is repeated a large number of times to insure that normal distributions are in fact achieved.

PLY PROPERTIES

The sets of input variables are combined to form sets of ply properties. The micromechanical relations developed by Chamis are used to calculate the ply stiffnesses and hygrothermal properties. The sets of ply properties are all stored in a large matrix, which is used to calculate the statistics, including the matrix of correlation coefficients.

STATISTICS

Several statistical metrics are calculated by the program. Each ply stiffness and hygrothermal property X_j has a mean $\overline{X}_j$ calculated by

$$\overline{X}_j = \frac{\sum_{i=1}^{n} X_{ij}}{n}$$

where X_{ij} is the ith generated value for X_j, and n is the number of sets of ply properties generated. The next statistic is the standard deviation, $\hat{\sigma}_{Xj}$:

$$\hat{\sigma}_{Xj} = \sqrt{\frac{\sum_{i=1}^{n} (X_{ij} - \overline{X}_j)^2}{n-1}}$$

The covariance is also calculated by couple.m, through the equation

$$s_{xy} = \frac{\sum_{i=1}^{n} (X_{ij} - \overline{X}_j)(X_{ik} - \overline{X}_k)}{n}$$

Finally, the material correlation coefficients are calculated from

$$c_{jk} = \frac{\sum_{i=1}^{n} (X_{ij} - \overline{X}_j)(X_{ik} - \overline{X}_k)}{\sqrt{\sum_{i=1}^{n} (X_{ij} - \overline{X}_j)^2 \sum_{i=1}^{n} (X_{ik} - \overline{X}_k)^2}}$$

The material correlation coefficients matrix is the ultimate goal of the script. It is used as an input to VARBEND to account for coupling between ply material properties when calculating standard deviations of laminate engineering properties. For more details, see Reference 3.

OUTPUT

The screen outputs of the script are the 9 by 9 covariance matrix **b**, the 9 by 9 correlation coefficient matrix **c**, the 9 element standard deviation vector **d**, and the 9 element vector of ply property means **e**. All generated numbers are of course available in Matlab's memory for further calculations.

NOTES

1) The number of ply properties generated can be changed. Care should be taken to make sure the number is large enough to form the correct distribution. The number used in the development was 100,000, which resulted in the correct distributions of fiber, matrix, and ply properties.
2) The correlation coefficients are dimensionless, so the units used for means and standard deviations of fiber and matrix properties should not change the correlation coefficient matrix. Other statistics do have units, however. All inputs must be in the same system of units.
3) The example in the attached listing uses the properties of AS4 fibers and 3501-6 epoxy matrix. While similar material systems will yield similar results, radically different material systems require running the script with the appropriate inputs.

APPENDIX A REFERENCES

1. McManus, H. L., "Probabilistic Methods for the Calculation of Laminate Properties", *Proceedings of the ASC 7th Technical Conference on Composite Materials*, Technomic, Lancaster PA, October 1992. (also in the *Journal of Reinforced Plastics and Composites*, Vol. 12, No. 6, June 1993, pp. 712-722).

2 Abernathy, E and McManus, H.L., "Effects of Material and Manufacturing Variations on Dimensionally Stable Composite Structure"; *Proceedings of the ASC 10th Technical Conference on Composite Materials*, Technomic, Santa Monica CA, October 1995.

3. Abernathy, E., "Probabilistic Design and Analysis of Dimensionally Stable Composite Structures", MIT, SM Thesis, 1995.

```
% Program to find correlation coefficients for laminates using random
% numbers within normal distributions
% filename ->  couple.m
% This version uses English units
% Correlation coefficients are unitless, so unit system doesn't matter
% for it.  Does matter for all other info, however.

clear
m=100000   % How many random #'s to use for each variable

for k=1:m

prog=k                % See how far we are

% Get vectors of random numbers for all matrix and fiber properties
% (including volume fraction).  Do this with 'random' command,
% where 'Normal' is the type of distribution, the next entry
% is mean, the middle is std. dev, and the last 2 are M and N to
% create an MxN matrix of random numbers in the distribution

% MAKE SURE MEANS AND STD. DEV.'S ARE ALL FILLED OUT CORRECTLY
% The standard dev's below are 2 percent of the mean value

Ef1(k)=random('Normal',31.0E6,6.2E5,1,1);              %Long. fiber modulus
Ef2(k)=random('Normal',2.0E6,4E4,1,1);                 %Trans. fiber modulus
NUf(k)=random('Normal',0.20,0.004,1,1);                %Fiber Poisson ratio
Gf(k)=random('Normal',2.0E6,4.0E4,1,1);                %Fiber shear modulus
CTEf1(k)=random('Normal',-0.55E-6,1.1E-8,1,1);         %Long. fiber CTE
CTEf2(k)=random('Normal',5.6E-6,11.2E-8,1,1);          %Trans. fiber CTE
Em(k)=random('Normal',0.5076E6,1.02E4,1,1);            %Matrix modulus
NUm(k)=random('Normal',0.35,0.007,1,1);                %Matrix Poisson ratio
Gm(k)=random('Normal',1.894E5,4E3,1,1);                %Matrix shear modulus
CTEm(k)=random('Normal',6.9E-5,14E-7,1,1);             %Matrix CTE
CMEm(k)=random('Normal',0.33,0.0066,1,1);              %Matrix CME
VF(k)=random('Normal',0.62,0.0124,1,1);                %Volume Fraction

% Check to make sure volume fraction is  within real-life bounds
if VF(k)<0.0
           VF(k)=0.0;
end
if VF(k)>1.0
           VF(k)=1.0;
end

VM(k)=1-VF(k);
sc(k)=sqrt(VF(k));

% Use micromechanics to find ply properties at each step from
% the fiber and matrix properties

E1(k)=VF(k)*Ef1(k)+(1-VF(k))*Em(k);
E2(k)=Em(k)/(1-sc(k)*(1-(Em(k)/Ef2(k))));
NU(k)=VF(k)*NUf(k)+VM(k)*NUm(k);
G(k)=Gm(k)/(1-sc(k)*(1-(Gm(k)/Gf(k))));
CTE1(k)=(CTEf1(k)*Ef1(k)*VF(k)+CTEm(k)*Em(k)*VM(k))/E1(k);
CTE2(k)=CTEf2(k)*sc(k)+(1-sc(k))*(1+(VF(k)*NUm(k)*Ef1(k))/E1(k))*CTEm(k);
CME1(k)=VM(k)*Em(k)*CMEm(k)/E1(k);
CME2(k)=(1-sc(k))*(1+(sc(k)*(1-sc(k))*Em(k))/(sc(k)*E2(k)+(1-sc(k))*Em(k))) *CMEm(k);

end

% Do transposes to make variables columns rather than rows
E1t=E1';
E2t=E2';
```

```
NUt=NU';
Gt=G';
CTE1t=CTE1';
CTE2t=CTE2';
CME1t=CME1';
CME2t=CME2';
VFt=VF';

% Form matrix where columns are ply variables, and rows are observations
% This will be an m by 9 matrix
a=[E1t E2t NUt Gt CTE1t CTE2t CME1t CME2t VFt];
% Calculate covariance matrix (9 by 9)
b=cov(a)

% Calculate correlation coefficients matrix (9 by 9)
c=corrcoef(a)

% Calculate standard deviations of all columns (1 by 9)
% Can use this to check c given b above from
%    If b is the covariance matrix, b = COV(a), then CORRCOEF(a) is
%    the matrix whose (i,j)'th element is b(i,j)/SQRT(b(i,i)*b(j,j)).

d=std(a)

% Calculate means of all columns (1 by 9)
e=mean(a)
```

APPENDIX B

VARBEND MANUAL AND CODE

VARBEND- A Computer Code for Sensitivity Analysis of Composite Laminates

INTRODUCTION

VARBEND is a simple, easy to use computer program that will calculate the expected means and standard deviations of the engineering properties of a composite laminate, given the means and standard deviations of layup variables and ply material properties. It also calculates the sensitivity of laminate properties to layup and ply variables, which can be useful in determining which parameters are the most important to control for a specific application's design requirements.

INPUT

The inputs are ASCII text files, which must be in the same folder as the program.

The first, the **main input file**, should be of the following format:

```
NPLY
```
(number of plies)
```
MATNUM   T          TSD        ANG        ANGSD
```
(material number, thickness, standard deviation of thickness, angle in degrees, and standard deviation of angle- repeat for each ply)
```
E11      E11SD      E22        E22SD      NU12     NU12SD    G        GSD
ALPHA1   ALPHA1SD   ALPHA2     ALPHA2SD   BETA1    BETA1SD   BETA2    BETA2SD      VF    VFSD
```
(unidirectional material properties for material 1, followed by their standard deviations. The properties are axial and transverse moduli, Poisson's ratio, shear modulus, axial and transverse thermal expansion coefficients, axial and transverse moisture expansion coefficients, and volume fraction. Repeat the entire set for each material.)
```
ANGLE CORRELATION FLAG
```
(flag as to whether there are angle correlations: 1 if yes, 0 if no. If the flag is set to zero, no further input is needed.)
```
ANGLE CORRELATION MATRIX
```

(The angle correlation matrix. It should be a symmetric matrix with the number of rows and columns equal to the number of plies. There should be ones on the diagonal, and values should be between -1 and 1. Correlations are dimensionless. Each line of input should be a row of the matrix.)

The second input file usually needed is the **material coupling coefficient file** which contains the coupling matrix c_{ij}. The material correlation coefficient matrix is specific to the material system used. The file **couplematrix** included with the VARBEND program contains the material correlation coefficient matrix for the AS4/3501-6 material system. The correlation matrix for different material systems can be calculated using COUPLE.M [3].

The inputs are FORTRAN free field- a value must be provided for each item, and items are separated by blanks. If the data required on a single line does not fit, you can continue to another line without needing any special continuation character. End all lines including the last one with a carriage return. The units used for material properties do not matter, as long as they are consistent.

NOTES:

1) If using metric units, ply thicknesses should be given in METERS, not millimeters as they are usually reported. Also, ply angles should be in degrees, not radians.
2) To neglect volume fraction variations, whether for a composite ply or for some other purpose (e.g. honeycomb core, aluminum facesheet), simply use a volume fraction standard deviation for that material of zero.
3) To neglect angle correlations, simply enter a zero on a line by itself after the material properties. The same effect can be achieved by entering the identity matrix for the angle correlation matrix.

OUTPUT

The results are the mean laminate engineering properties, and their standard deviations. The mean laminate engineering properties are calculated from the mean inputs using Classical Laminated Plate Theory (CLPT). In addition to the laminate stiffnesses and hygrothermal properties, laminate volume fraction and bending coefficients are calculated. The laminate volume fraction is the average of the ply volume fractions. The thermal and hygral bending coefficients $\mathbf{W}^T$ and $\mathbf{W}^H$ are the out-of-plane analogs to the in-plane coefficients of thermal expansion and coefficients of hygral expansion. When multiplied by the temperature difference from the stress-free temperature, $\mathbf{W}^T$ yields the laminate curvature. Similarly, $\mathbf{W}^H$ gives laminate curvature when multiplied by moisture content.

$$\boldsymbol{\kappa}^T = \mathbf{W}^T \Delta T$$

$$\mathbf{W}^{\mathbf{T}} = \mathbf{b}^{*\mathrm{T}} \sum \overline{\mathbf{Q}}_k \overline{\boldsymbol{\alpha}}_k t_k + \mathbf{d}^{*} \sum \overline{\mathbf{Q}}_k \overline{\boldsymbol{\alpha}}_k t_k \bar{z}_k$$

$$\boldsymbol{\kappa}^{\mathbf{H}} = \mathbf{W}^{\mathbf{H}} \Delta H$$

$$\mathbf{W}^{\mathbf{H}} = \mathbf{b}^{*\mathrm{T}} \sum \overline{\mathbf{Q}}_k \overline{\boldsymbol{\beta}}_k t_k + \mathbf{d}^{*} \sum \overline{\mathbf{Q}}_k \overline{\boldsymbol{\beta}}_k t_k \bar{z}_k$$

A complete derivation of the bending coefficients is presented in Reference 3. The laminate standard deviations are calculated from the formula:

$$\sigma_{Yi}^2 = \sum_{j=1}^{n} \sum_{k=1}^{n} \frac{\partial Y_i}{\partial X_j} \frac{\partial Y_i}{\partial X_k} c_{jk} \sigma_{Xj} \sigma_{Xk}$$

where Y_i is the ith laminate property, X_j is the jth ply material or layup variable, σ_{Xj} is the standard deviation of the jth ply material or layup variable, σ_{Yi} is the standard deviation of the ith laminate property, and c_{jk} is the correlation coefficient between X_j and X_k. If the standard deviation of volume fraction is zero, all input variables become independent, so c_{jk} is 1 if $j=k$, and $c_{jk}(j \neq k)=0$. Non-zero volume fraction standard deviations invalidate the independent ply property assumption, for volume fraction couples the material properties.

The means and standard deviations of laminate properties are printed to the screen. More detailed calculations are printed to the file VAR.OUT. In addition to a repetition of the input data and the screen output, VAR.OUT contains the individual derivatives

$$\text{DERIVATIVE} = d_{ij} = \frac{\partial Y_i}{\partial X_j}$$

which are useful for calculations but difficult to compare or interpret. Therefore, VAR.OUT contains two additional sensitivity metrics. The first is SIGMAi, the contribution of the variation of input variable X_j to the variation of laminate variable Y_i:

$$\text{SIGMA}_\text{i} = d_{ij}^{\sigma} = \frac{\partial Y_i}{\partial X_j} \sigma_{Xj}$$

A final metric is dimensionless, and show the proportional change in laminate property for a given proportional change in the ply variable:

$$\text{PERCENT} = \bar{d}_{ij} = \frac{\partial Y_i}{\partial X_j} \frac{\overline{X}_j}{\overline{Y}_i}$$

This metric is useful in that in can be used to compare any sensitivities with each other, but is meaningless if the mean of the laminate or ply variable is zero.

SAMPLE SESSION

The problem considered is a quasi-isotropic layup, [0/±45/90]s, made of the AS4/3501-6 material system with standard deviations typical of the material. The angle correlation matrix is included, but is simply the identity matrix, so there is no angle coupling. The input files, screen output, and portions of the file VAR.OUT are included. User input is in **bold**.

INPUT FILE (in a text file named **quasiinput**)

```
8
1 .0052 0.001   0 2
1 .0052 0.001  45 2
1 .0052 0.001 -45 2
1 .0052 0.001  90 2
1 .0052 0.001  90 2
1 .0052 0.001 -45 2
1 .0052 0.001  45 2
1 .0052 0.001   0 2
21.847E6 .61287E6 1.351E6 2.93427E4 .2451 .004 0.78042E6 2.776E4
-0.29383E-6 0.02453E-6 1.2627E-5 0.49255E-6 .0023 1.7493E-4 0.0571 0.0034 0.62 0.0143
1
1.0 0.0 0.0 0.0 0.0 0.0 0.0 0.0
0.0 1.0 0.0 0.0 0.0 0.0 0.0 0.0
0.0 0.0 1.0 0.0 0.0 0.0 0.0 0.0
0.0 0.0 0.0 1.0 0.0 0.0 0.0 0.0
0.0 0.0 0.0 0.0 1.0 0.0 0.0 0.0
0.0 0.0 0.0 0.0 0.0 1.0 0.0 0.0
0.0 0.0 0.0 0.0 0.0 0.0 1.0 0.0
0.0 0.0 0.0 0.0 0.0 0.0 0.0 1.0
```

MATERIAL COUPLING COEFFICIENT FILE
(in a text file named **couplematrix**)

```
1.0 0.5486 -0.3738 0.6355 -0.6571 -0.5404 -0.8091 -0.6606 0.6968
0.5486 1.0 -0.4252 0.6978 -0.4715 -0.5773 -0.5866 -0.7334 0.7691
-0.3738 -0.4252 1.0 -0.5089 0.3848 0.4270 0.4867 0.5166 -0.5425
0.6355 0.6978 -0.5089 1.0 -0.6529 -0.6638 -0.8061 -0.8475 0.8981
-0.6571 -0.4715 0.3848 -0.6529 1.0 0.8086 0.7586 0.6781 -0.7254
-0.5404 -0.5773 0.4270 -0.6638 0.8086 1.0 0.6710 0.7065 -0.7501
-0.8091 -0.5866 0.4867 -0.8061 0.7586 0.6710 1.0 0.9250 -0.8860
-0.6606 -0.7334 0.5166 -0.8475 0.6781 0.7065 0.9250 1.0 -0.9397
0.6968 0.7691 -0.5425 0.8981 -0.7254 -0.7501 -0.8860 -0.9397 1.0
```

SCREEN OUTPUT

```
 Input file name, or HELP if you need it
quasiinput
 Input name of file with material coupling matrix
couplematrix

MEAN ENGINEERING CONSTANTS FOR LAMINATE-
  E11 =   8.3717E+06   E22 =   8.3717E+06
  V12 =   3.0088E-01   G   =   3.2177E+06
  ALPHA1 =   6.1708E-07   ALPHA2 =   6.1708E-07   ALPHA12 =  -2.6875E-15
  BETA1  =   6.1634E-03   BETA2  =   6.1634E-03   BETA12  =   0.0000E+00
  VF  =   7.0000E-01
  WT1    =   0.0000E+00   WT2    =   0.0000E+00   WT6     =   0.0000E+00
  WH1    =   0.0000E+00   WH2    =   0.0000E+00   WH6     =   0.0000E+00

STANDARD DEVIATIONS-
  E11 =   6.7032E+05   E22 =   6.6679E+05
  V12 =   2.9248E-02   G   =   2.2214E+05
  ALPHA1 =   1.6407E-07   ALPHA2 =   1.6336E-07   ALPHA12 =   2.5552E-07
  BETA1  =   9.6183E-04   BETA2  =   9.5967E-04   BETA12  =   1.0837E-03
  VF  =   1.4300E-02
  WT1    =   9.6324E-06   WT2    =   3.0989E-05   WT6     =   2.8591E-05
  WH1    =   4.0853E-02   WH2    =   1.3143E-01   WH6     =   1.2126E-01

MORE DETAILED OUTPUT IN FILE VAR.OUT

STOP
```

In the above, the laminate engineering constants are as follows:

E11	Axial modulus
E22	Transverse modulus
V12	Poisson's ratio
G	Shear modulus
ALPHAij	Coefficient of thermal expansion (CTE)
BETAij	Coefficient of moisture expansion (CME)
WTi	Thermal bending coefficient
WHi	Hygral bending coefficient

OUTPUT FILE

```
        LAMINATE-

   PLY     MATERIAL      THICKNESS      SD         ANGLE        SD
    1          1          0.0052      0.0010       0.00       2.00
    2          1          0.0052      0.0010      45.00       2.00
    3          1          0.0052      0.0010     -45.00       2.00
    4          1          0.0052      0.0010      90.00       2.00
    5          1          0.0052      0.0010      90.00       2.00
    6          1          0.0052      0.0010     -45.00       2.00
    7          1          0.0052      0.0010      45.00       2.00
    8          1          0.0052      0.0010       0.00       2.00

        MATERIAL PROPERTIES AND SD'S FOR MATERIAL  1-
        E11          2.1847E+07     6.1287E+05
        E22          1.3510E+06     2.9343E+04
        NU           2.4510E-01     4.0000E-03
```

G	7.8042E+05	2.7760E+04
ALPHA1	-2.9383E-07	2.4530E-08
ALPHA2	1.2627E-05	4.9255E-07
BETA1	2.3000E-03	1.7493E-04
BETA2	5.7100E-02	3.4000E-03
VOLFRAC	6.2000E-01	1.4300E-02

MEAN ENGINEERING CONSTANTS FOR LAMINATE-

E11 =	8.3717E+06	E22 =	8.3717E+06		
V12 =	3.0088E-01	G =	3.2177E+06		
ALPHA1 =	6.1708E-07	ALPHA2 =	6.1708E-07	ALPHA12 =	-2.6875E-15
BETA1 =	6.1634E-03	BETA2 =	6.1634E-03	BETA12 =	0.0000E+00
VF =	6.2000E-01				
WT1 =	0.0000E+00	WT2 =	0.0000E+00	WT6 =	0.0000E+00
WH1 =	0.0000E+00	WH2 =	0.0000E+00	WH6 =	0.0000E+00

STANDARD DEVIATIONS-

E11 =	6.7032E+05	E22 =	6.6679E+05		
V12 =	2.9248E-02	G =	2.2214E+05		
ALPHA1 =	1.6407E-07	ALPHA2 =	1.6336E-07	ALPHA12 =	2.5552E-07
BETA1 =	9.6183E-04	BETA2 =	9.5967E-04	BETA12 =	1.0837E-03
VF =	1.4300E-02				
WT1 =	9.6324E-06	WT2 =	3.0989E-05	WT6 =	2.8591E-05
WH1 =	4.0853E-02	WH2 =	1.3143E-01	WH6 =	1.2126E-01

FACTORS AFFECTING LAMINATE E11
(MEAN VALUE = 8.372E+06 EXPECTED SD = 6.703E+05)

	VARIABLE PROPERTIES				LAMINATE SENSITIVITY*		
PROPERTY			MEAN	SD	DERIVATIVE	SIGMAi	PERCENT
T	PLY	1	5.200E-03	1.000E-03	3.273E+08	3.273E+05	0.20333
ANGLE	PLY	1	0.000E+00	2.000E+00	1.325E+01	2.650E+01	N/A
T	PLY	2	5.200E-03	1.000E-03	-9.791E+07	-9.791E+04	-0.06081
ANGLE	PLY	2	4.500E+01	2.000E+00	-4.082E+04	-8.165E+04	-0.21943
T	PLY	3	5.200E-03	1.000E-03	-9.834E+07	-9.834E+04	-0.06109
ANGLE	PLY	3	-4.500E+01	2.000E+00	4.083E+04	8.165E+04	-0.21945
T	PLY	4	5.200E-03	1.000E-03	-1.256E+08	-1.256E+05	-0.07802
ANGLE	PLY	4	9.000E+01	2.000E+00	5.605E-01	1.121E+00	0.00001
T	PLY	5	5.200E-03	1.000E-03	-1.256E+08	-1.256E+05	-0.07802
ANGLE	PLY	5	9.000E+01	2.000E+00	5.605E-01	1.121E+00	0.00001
T	PLY	6	5.200E-03	1.000E-03	-9.834E+07	-9.834E+04	-0.06109
ANGLE	PLY	6	-4.500E+01	2.000E+00	4.083E+04	8.165E+04	-0.21945
T	PLY	7	5.200E-03	1.000E-03	-9.791E+07	-9.791E+04	-0.06081
ANGLE	PLY	7	4.500E+01	2.000E+00	-4.082E+04	-8.165E+04	-0.21943
T	PLY	8	5.200E-03	1.000E-03	3.273E+08	3.273E+05	0.20333
ANGLE	PLY	8	0.000E+00	2.000E+00	1.325E+01	2.650E+01	N/A
E11	MATL	1	2.185E+07	6.129E+05	3.337E-01	2.045E+05	0.87072
E22	MATL	1	1.351E+06	2.934E+04	3.123E-01	9.164E+03	0.05040
NU	MATL	1	2.451E-01	4.000E-03	-7.684E+03	-3.074E+01	-0.00022
G	MATL	1	7.804E+05	2.776E+04	8.462E-01	2.349E+04	0.07888
ALPHA1	MATL	1	-2.938E-07	2.453E-08	0.000E+00	0.000E+00	0.00000
ALPHA2	MATL	1	1.263E-05	4.926E-07	0.000E+00	0.000E+00	0.00000
BETA1	MATL	1	2.300E-03	1.749E-04	0.000E+00	0.000E+00	0.00000
BETA2	MATL	1	5.710E-02	3.400E-03	0.000E+00	0.000E+00	0.00000
VOLFRA	MATL	1	6.200E-01	1.430E-02	1.193E+07	1.706E+05	0.88378

* DERIVATIVE = change in laminate property with change in variable property
(units of laminate property / units of variable property)
SIGMAi = expected variation in laminate property due to variation in variable property alone (units of laminate property)
(= VARIABLE PROPERTY SD * DERIVATIVE)
PERCENT = percent change in laminate property with 1% change in variable property (meaningless if mean of either is 0.0)
(= DERIVATIVE * VARIABLE PROP. MEAN / LAMINATE PROP. MEAN)

... repeated for all laminate stiffness properties ...

FACTORS AFFECTING LAMINATE ALPHA1
(MEAN VALUE = 6.171E-07 EXPECTED SD = 1.641E-07)

	VARIABLE PROPERTIES				LAMINATE SENSITIVITY*		
	PROPERTY		MEAN	SD	DERIVATIVE	SIGMAi	PERCENT
T	PLY	1	5.200E-03	1.000E-03	-6.101E-05	-6.101E-08	-0.51414
ANGLE	PLY	1	0.000E+00	2.000E+00	-3.583E-12	-7.165E-12	N/A
T	PLY	2	5.200E-03	1.000E-03	-3.783E-07	-3.783E-10	-0.00319
ANGLE	PLY	2	4.500E+01	2.000E+00	1.083E-08	2.166E-08	0.78966
T	PLY	3	5.200E-03	1.000E-03	-1.405E-07	-1.405E-10	-0.00118
ANGLE	PLY	3	-4.500E+01	2.000E+00	-1.083E-08	-2.165E-08	0.78959
T	PLY	4	5.200E-03	1.000E-03	5.978E-05	5.978E-08	0.50372
ANGLE	PLY	4	9.000E+01	2.000E+00	2.476E-13	4.952E-13	0.00004
T	PLY	5	5.200E-03	1.000E-03	5.978E-05	5.978E-08	0.50372
ANGLE	PLY	5	9.000E+01	2.000E+00	2.476E-13	4.952E-13	0.00004
T	PLY	6	5.200E-03	1.000E-03	-1.405E-07	-1.405E-10	-0.00118
ANGLE	PLY	6	-4.500E+01	2.000E+00	-1.083E-08	-2.165E-08	0.78959
T	PLY	7	5.200E-03	1.000E-03	-3.783E-07	-3.783E-10	-0.00319
ANGLE	PLY	7	4.500E+01	2.000E+00	1.083E-08	2.166E-08	0.78966
T	PLY	8	5.200E-03	1.000E-03	-6.101E-05	-6.101E-08	-0.51414
ANGLE	PLY	8	0.000E+00	2.000E+00	-3.583E-12	-7.165E-12	N/A
E11	MATL	1	2.185E+07	6.129E+05	-3.820E-14	-2.341E-08	-1.35250
E22	MATL	1	1.351E+06	2.934E+04	6.174E-13	1.811E-08	1.35161
NU	MATL	1	2.451E-01	4.000E-03	6.284E-07	2.514E-09	0.24961
G	MATL	1	7.804E+05	2.776E+04	3.464E-22	9.615E-18	0.00000
ALPHA1	MATL	1	-2.938E-07	2.453E-08	9.295E-01	2.280E-08	-0.44259
ALPHA2	MATL	1	1.263E-05	4.926E-07	7.050E-02	3.472E-08	1.44259
BETA1	MATL	1	2.300E-03	1.749E-04	0.000E+00	0.000E+00	0.00000
BETA2	MATL	1	5.710E-02	3.400E-03	0.000E+00	0.000E+00	0.00000
VOLFRA	MATL	1	6.200E-01	1.430E-02	-3.239E-06	-4.632E-08	-3.25474

* DERIVATIVE = change in laminate property with change in variable property
(units of laminate property / units of variable property)
SIGMAi = expected variation in laminate property due to variation in variable property alone (units of laminate property)
(= VARIABLE PROPERTY SD * DERIVATIVE)
PERCENT = percent change in laminate property with 1% change in variable property (meaningless if mean of either is 0.0)
(= DERIVATIVE * VARIABLE PROP. MEAN / LAMINATE PROP. MEAN)

... repeated for all laminate hygrothermal properties ...

FACTORS AFFECTING LAMINATE WT1
(MEAN VALUE = 0.000E+00 EXPECTED SD = 9.632E-06)

	VARIABLE PROPERTIES				LAMINATE SENSITIVITY*		
	PROPERTY		MEAN	SD	DERIVATIVE	SIGMAi	PERCENT
T	PLY	1	5.200E-03	1.000E-03	-6.292E-03	-6.292E-06	N/A
ANGLE	PLY	1	0.000E+00	2.000E+00	9.663E-08	1.933E-07	N/A
T	PLY	2	5.200E-03	1.000E-03	-1.101E-03	-1.101E-06	N/A
ANGLE	PLY	2	4.500E+01	2.000E+00	6.989E-07	1.398E-06	N/A
T	PLY	3	5.200E-03	1.000E-03	-1.703E-03	-1.703E-06	N/A
ANGLE	PLY	3	-4.500E+01	2.000E+00	-4.192E-07	-8.385E-07	N/A
T	PLY	4	5.200E-03	1.000E-03	2.293E-18	2.293E-21	N/A
ANGLE	PLY	4	9.000E+01	2.000E+00	-1.383E-08	-2.766E-08	N/A
T	PLY	5	5.200E-03	1.000E-03	2.491E-18	2.491E-21	N/A
ANGLE	PLY	5	9.000E+01	2.000E+00	1.383E-08	2.766E-08	N/A

```
T       PLY   6    5.200E-03  1.000E-03     1.703E-03   1.703E-06      N/A
ANGLE   PLY   6   -4.500E+01  2.000E+00     4.192E-07   8.385E-07      N/A
T       PLY   7    5.200E-03  1.000E-03     1.101E-03   1.101E-06      N/A
ANGLE   PLY   7    4.500E+01  2.000E+00    -6.989E-07  -1.398E-06      N/A
T       PLY   8    5.200E-03  1.000E-03     6.292E-03   6.292E-06      N/A
ANGLE   PLY   8    0.000E+00  2.000E+00    -9.663E-08  -1.933E-07      N/A
E11     MATL  1    2.185E+07  6.129E+05    -1.629E-27  -9.986E-22      N/A
E22     MATL  1    1.351E+06  2.934E+04     1.431E-26   4.199E-22      N/A
NU      MATL  1    2.451E-01  4.000E-03    -3.794E-19  -1.518E-21      N/A
G       MATL  1    7.804E+05  2.776E+04    -6.358E-26  -1.765E-21      N/A
ALPHA1  MATL  1   -2.938E-07  2.453E-08     1.282E-15   3.144E-23      N/A
ALPHA2  MATL  1    1.263E-05  4.926E-07     1.175E-15   5.787E-22      N/A
BETA1   MATL  1    2.300E-03  1.749E-04     0.000E+00   0.000E+00      N/A
BETA2   MATL  1    5.710E-02  3.400E-03     0.000E+00   0.000E+00      N/A
VOLFRA  MATL  1    6.200E-01  1.430E-02    -1.126E-19  -1.610E-21      N/A

 * DERIVATIVE = change in laminate property with change in variable property
              (units of laminate property / units of variable property)
   SIGMAi     = expected variation in laminate property due to variation in
              variable property alone (units of laminate property)
              ( = VARIABLE PROPERTY SD * DERIVATIVE)
   PERCENT    = percent change in laminate property with 1% change in
              variable property (meaningless if mean of either is 0.0)
              ( = DERIVATIVE * VARIABLE PROP. MEAN / LAMINATE PROP. MEAN)

             ...  repeated for all laminate bending coefficients  ...
```

APPENDIX B REFERENCES

1. McManus, H. L., "Probabilistic Methods for the Calculation of Laminate Properties", *Proceedings of the ASC 7th Technical Conference on Composite Materials*, Technomic, Lancaster PA, October 1992. (also in the *Journal of Reinforced Plastics and Composites*, Vol. 12, No. 6, June 1993, pp. 712-722).

2 Abernathy, E and McManus, H.L., "Effects of Material and Manufacturing Variations on Dimensionally Stable Composite Structure"; *Proceedings of the ASC 10th Technical Conference on Composite Materials*, Technomic, Santa Monica CA, October 1995.

3. Abernathy, E., "Probabilistic Design and Analysis of Dimensionally Stable Composite Structures", MIT, SM Thesis, 1995.

```
C*********************************************************************
C
C                       V A R B E N D
C
C     CODE FOR SENSITIVITY ANALYSIS OF COMPOSITE LAMINATES
C
C          c 1995 Erik Abernathy and Hugh L. McManus
C            Massachusetts Institute of Technology
C               Rm 33-311, 77 Massachusetts Ave.
C              Cambridge MA 02139  (617) 253-0672
C
C*********************************************************************
C
C                     Version 1.1  10-12-95
C                     WRITTEN IN MPW FORTRAN
C                c 1988,1989 Language Systems Corp.
C
C*********************************************************************
C
C
C Permission to use, copy and modify this software and its documentation
C for internal purposes only and without fee is hereby granted provided
C that the above copyright notice and this permission appear on all copies
C of the code and supporting documentation.  For any other use of this
C software, in original or modified form, including but not limited to,
C adaptation as the basis of a commercial software or hardware product, or
C distribution in whole or in part, specific prior permission and/or the
C appropriate license must be obtained from MIT.  This software is provided
C "as is" without any warranties whatsoever, either express or implied,
C including but not limited to the implied warranties of merchantability
C and fitness for a particular purpose.  This software is a research
C program, and MIT does not represent that it is free of errors or bugs or
C suitable for any particular task.
C
C
C*********************************************************************
C
C    compile this code with variables initially set to zero !!
C
C*********************************************************************
C
      IMPLICIT REAL*8 (A-H,O-Z)
      REAL*8 N,M,E,K,NT,MT,NBAR,MBAR
      LOGICAL YESNO
      CHARACTER*80 LINE
      CHARACTER*60 ISTR,DESC,FNAME,FNAMEA
      CHARACTER*20 FTYPE
      CHARACTER*10 PER
      CHARACTER*7 NAME
      CHARACTER*7 ENAME
      CHARACTER*4 NTYP, help, yes, no, quit
      COMMON /STRESS/ESTAR(3),SIGMA(3),SIGSTR(3),EPS(3),ALF(3),
     +               AL(3),EPT(3),BET(3),BE(3)
      COMMON /MNEK/M(3),N(3),E(3),K(3),NT(3),MT(3),NBAR(3),MBAR(3)
      COMMON /STUFF/NLAY,T(100),ANG(100),MATER(100),DELTAT,
     +              A(3,3),B(3,3),D(3,3),AP(3,3),BP(3,3),DP(3,3),
     +              Q(3,3),QQ(3,3),THICK,DELTAM,BPT(3,3)
      COMMON /WORDS/HELP,YES,NO,QUIT
      COMMON /MATR/CONST(4,30),TP(30),DESC(30),NMATR,
     +             ALFA1(30),ALFA2(30),STRENG(5,30),BETA(2,30),VFPLY(30)
      COMMON /FAIL/IFAIL(30),FACMAX,ULT(5),FTYPE(5)
      COMMON /PARSE/ISTR,IP,JTABL(10,14)
C
C
```

```
      COMMON /VAR/NX,XX(200),SD(200),ITYP(200),IN1(200),IN2(200),
     +NAME(11),NTYP(2)
      DIMENSION ETA0(17),ETA1(17),ETA2(17),
     +          DEDX(200,17),SIG(200,17),SUMS(17)
      DIMENSION CC(9,9)
      DIMENSION AA(200,200)
      DATA HELP/'HELP'/,YES/'YES '/,NO/'NO  '/,QUIT/'QUIT'/
      DATA NAME/'T','ANGLE','E11','E22','NU','G','ALPHA1'
     +,'ALPHA2','BETA1','BETA2','VOLFRAC'/
      DATA NTYP/'PLY','MATL'/
C
    1 TYPE *,' Input file name, or HELP if you need it'
      READ(5,802)FNAME
      IF (FNAME .EQ. 'HELP' .OR. FNAME .EQ. 'help') THEN
        OPEN(UNIT=1,FILE='VARHELP',STATUS='OLD',ERR=5,READONLY)
        DO 2 I = 1, 10000
          READ(1,809,ERR=3,END=3)LINE
    2     WRITE(6,810)LINE
    3   CLOSE(1,ERR=1)
        GO TO 1
    5   TYPE *,' TOO BAD, THERE IS NO HELP (call x23726)'
        GO TO 1
      ENDIF
      OPEN(UNIT=2,FILE=FNAME,STATUS='OLD',ERR=666)
      OPEN(UNIT=7,FILE='VAR.OUT',STATUS='NEW')
      READ(2,*,ERR=667)NLAY
      NX = 1
      NMATR = 1
      DO 10 I = 1, NLAY
        READ(2,*,ERR=668) MATER(I),XX(NX),SD(NX),XX(NX+1),SD(NX+1)
        IF(MATER(I) .GT. NMATR)NMATR = MATER(I)
        XX(NX+1) = XX(NX+1) * .0174532925
        SD(NX+1) = SD(NX+1) * .0174532925
        ITYP(NX) = 1
        ITYP(NX+1) = 1
        IN1(NX) = 1
        IN1(NX+1) = 2
        IN2(NX) = I
        IN2(NX+1) = I
   10   NX = NX + 2
      DO 20 I = 1, NMATR
        READ(2,*,ERR=669) (XX(J),SD(J),J=NX,NX+3)
        READ(2,*,ERR=670) (XX(J),SD(J),J=NX+4,NX+8)
        DO 15 J = 1,9
          JJ = NX + J - 1
          ITYP(JJ) = 2
          IN1(JJ) = J
   15     IN2(JJ) = I
   20   NX = NX + 9
      NX = NX - 1
      READ(2,*,ERR=22,IOSTAT=MALICE) NFLAG
   22 IF(MALICE .GT. 0) GOTO 671
      IF(NFLAG .EQ. 1) THEN
         DO 25 I=1,NLAY
            READ(2,*,ERR=672) (AA(I,J), J=1,NLAY)
   25 END DO
      ENDIF
      DO 30 I = 1, NX
   30   CALL STORE(I,XX(I))
      WRITE(7,804)(I,MATER(I),T(I),SD(2*I-1),
     +  ANG(I)/.0174532925,SD(2*I)/.0174532925,I=1,NLAY)
      DO 31 I = 1, NMATR
        WRITE(7,805) I
        JJ = 2*NLAY + (I-1)*9
```

```
   31   WRITE(7,806)(NAME(J+2),XX(JJ+J),SD(JJ+J),J=1,9)
        CALL MCLAMS(ETA0)
        IF(ETA0(5) .NE. 0.)THEN
          IF(ABS(ETA0(7)/ETA0(5)) .LT. 1.D-9)ETA0(7) = 0.
        ENDIF
        IF(ETA0(8) .NE. 0.)THEN
          IF(ABS(ETA0(10)/ETA0(8)) .LT. 1.D-9)ETA0(10) = 0.
        ENDIF
        DO 35 L=1,6
           IF(ABS(ETA0(L+11)) .LT. 1.D-15)ETA0(L+11)=0.
   35 END DO
        DO 100 I = 1, NX
        IF(SD(I) .NE. 0.)THEN
C    IF IN1(I) .EQ. 9 TESTS IF THE CURRENT I IS A VOLUME FRACTION
C    IF SO, CALCULATE EFFECTS OF VF CHANGING ALL PLY MATERIAL PROPERTIES
C    IF NOT, PROCEED AS IN THE ORIGINAL VAR PROGRAM
          IF (IN1(I) .EQ. 9) THEN
            CALL COUPLE(CC)
            DO 40 L=(I-8),I
   40         CALL STORE(L,XX(L)+CC((L-I+9),9)*SD(L))
            CALL MCLAMS(ETA1)
            DO 45 L=(I-8),I
   45         CALL STORE(L,XX(L)-CC((L-I+9),9)*SD(L))
            CALL MCLAMS(ETA2)
            DO 46 L=(I-8),I
   46         CALL STORE(L,XX(L))
          ELSE
              CALL STORE(I,XX(I)+SD(I))
              CALL MCLAMS(ETA1)
              CALL STORE(I,XX(I)-SD(I))
              CALL MCLAMS(ETA2)
          ENDIF
          CALL STORE(I,XX(I))
          DO 50 J = 1, 17
            DEDX(I,J) = (ETA1(J) - ETA2(J)) / (2. * SD(I))
   50       SIG(I,J) = DEDX(I,J) * SD(I)
        ENDIF
  100 CONTINUE
        DO 110 J=1,17
           DO 106 I=1,NX
              IF(SD(I) .NE. 0.)THEN
                 DO 104 L=1,NX
                    IF(SD(L) .NE. 0.)THEN
                       IF(I .EQ. L) THEN
                          SUMS(J)=SUMS(J)+SIG(I,J)**2
                       ELSE IF(ITYP(I) .EQ. 2) THEN
                          IF(IN2(I) .EQ. IN2(L))THEN
                             IF(ITYP(L) .EQ. 2)THEN
                                SUMS(J)=SUMS(J)+SIG(I,J)*SIG(L,J)*CC(IN1(I),IN1(L))
                             ENDIF
                          ENDIF
                       ELSE IF (NFLAG .EQ. 1) THEN
                          IF(IN1(I) .EQ. 2) THEN
                             IF(IN1(L) .EQ. 2) THEN
                                SUMS(J)=SUMS(J)+SIG(I,J)*SIG(L,J)*AA(IN2(I),IN2(L))
                             ENDIF
                          ENDIF
                       ENDIF
                    ENDIF
  104            END DO
              ENDIF
  106      END DO
  110 SUMS(J) = SQRT(SUMS(J))
        WRITE(6,800)ETA0
```

```
      WRITE(6,801)SUMS
      WRITE(6,803)
      WRITE(7,800)ETA0
      WRITE(7,801)SUMS
      DO 150 I = 1, 17
        IF(I .LE. 6) THEN
          ENAME = NAME(I+2)
        ELSE IF(I. EQ. 7) THEN
          ENAME = 'ALPHA12'
        ELSE IF(I .EQ. 10) THEN
          ENAME = 'BETA12'
C ADD ENAME FOR VOLUME FRACTION
        ELSE IF(I .EQ. 11) THEN
          ENAME = 'VOLFRAC'
C
C ADD ENAMES FOR CURVATURES
        ELSE IF(I .EQ. 12) THEN
          ENAME = 'WT1'
        ELSE IF(I .EQ. 13) THEN
          ENAME = 'WT2'
        ELSE IF(I .EQ. 14) THEN
          ENAME = 'WT6'
        ELSE IF(I .EQ. 15) THEN
          ENAME = 'WH1'
        ELSE IF(I .EQ. 16) THEN
          ENAME = 'WH2'
        ELSE IF(I .EQ. 17) THEN
          ENAME = 'WH6'
C
        ELSE
          ENAME = NAME(I+1)
        ENDIF
        WRITE(7,807)ENAME,ETA0(I),SUMS(I)
        DO 140 J = 1, NX
        IF(SD(J) .NE. 0.) THEN
          FAC = 1.
          IF(ITYP(J) .EQ. 1) THEN
            NI = IN1(J)
            IF(NI.EQ.2) FAC = 1./.0174532925
          ELSE
            NI = IN1(J) + 2
          ENDIF
          IF(ETA0(I) .NE. 0. .AND. XX(J) .NE. 0.)THEN
            WRITE(PER,811)DEDX(J,I)*XX(J)/ETA0(I)
          ELSE
            PER = '     N/A  '
          ENDIF
          WRITE(7,808)NAME(NI),NTYP(ITYP(J)),IN2(J),XX(J)*FAC,
     +      SD(J)*FAC,DEDX(J,I)/FAC,SIG(J,I),PER
        ENDIF
  140   CONTINUE
      WRITE(7,812)
  150 CONTINUE
      STOP
  666 TYPE *,' CAN''T OPEN INPUT FILE!!'
      TYPE *,' VAR looks for an input file in the current'
      TYPE *,' default directory.  If you type NAME, it will'
      TYPE *,' look for NAME.DAT.  If the file is not in the'
      TYPE *,' default directory, or is not a .DAT file, type a full'
      TYPE *,' file spec. (e.g. UD3:[MCMANUS.MCLAM.VAR]TEST.DAT)'
      TYPE *,' DON''T use clip commands like *ADD- just the file name'
      TYPE *,' Type HELP instead of a file name and you will get help'
      TYPE *,' on input file format and other info about VAR'
      STOP
```

```
  667 TYPE *,' INPUT ERROR!! Reading first line of input file!'
      STOP
  668 TYPE *,' INPUT ERROR!! Reading input for ply',I,'!'
      STOP
  669 TYPE *,' INPUT ERROR!! Reading stiffnesses for material',I,'!'
      STOP
  670 TYPE *,' INPUT ERROR!! Reading hygrothermals for material',I,'!'
      STOP
  671 TYPE *,' INPUT ERROR!! Reading flag for angle correlation coefficients!'
      STOP
  672 TYPE *,' INPUT ERROR!! Reading angle correlation coefficients!'
      TYPE *,' Recall that the angle correlation coefficient matrix'
      TYPE *,' should be a symmetric matrix, with ones on the diagonals,'
      TYPE *,' and with the number of rows and number of columns'
      TYPE *,' equal to the number of plies in the laminate'
      STOP
  800 FORMAT(/' MEAN ENGINEERING CONSTANTS FOR LAMINATE-'
     +/'   E11 = ',1PE12.4,'   E22 = ',1PE12.4,
     +/'   V12 = ',1PE12.4,'   G   = ',1PE12.4,
     +/'   ALPHA1 = ',1PE12.4,'   ALPHA2 = ',1PE12.4,
     +'   ALPHA12 = ',1PE12.4,
     +/'   BETA1  = ',1PE12.4,'   BETA2  = ',1PE12.4,
     +'   BETA12  = ',1PE12.4,
C ADD VOLUME FRACTION, CURVATURES TO OUTPUT
     +/'   VF  = ',1PE12.4,
     +/'   WT1    = ',1PE12.4,'   WT2    = ',1PE12.4,
     +'   WT6    = ',1PE12.4,
     +/'   WH1    = ',1PE12.4,'   WH2    = ',1PE12.4,
     +'   WH6    = ',1PE12.4)
C
  801 FORMAT(/' STANDARD DEVIATIONS-'
     +/'   E11 = ',1PE12.4,'   E22 = ',1PE12.4,
     +/'   V12 = ',1PE12.4,'   G   = ',1PE12.4,
     +/'   ALPHA1 = ',1PE12.4,'   ALPHA2 = ',1PE12.4,
     +'   ALPHA12 = ',1PE12.4,
     +/'   BETA1  = ',1PE12.4,'   BETA2  = ',1PE12.4,
     +'   BETA12  = ',1PE12.4,
C ADD VOLUME FRACTION, CURVATURES TO OUTPUT
     +/'   VF  = ',1PE12.4,
     +/'   WT1    = ',1PE12.4,'   WT2    = ',1PE12.4,
     +'   WT6    = ',1PE12.4,
     +/'   WH1    = ',1PE12.4,'   WH2    = ',1PE12.4,
     +'   WH6    = ',1PE12.4)
C
  802 FORMAT(A60)
  803 FORMAT(/' MORE DETAILED OUTPUT IN FILE VAR.OUT')
  804 FORMAT(10X,'LAMINATE-'//
     +'    PLY     MATERIAL      THICKNESS     SD         ANGLE'
     +,'        SD'
     +/(3X,I3,8X,I3,10X,F6.4,5X,F6.4,6X,F6.2,5X,F6.2))
  805 FORMAT(/10X,'MATERIAL PROPERTIES AND SD''S FOR MATERIAL',I3'-')
  806 FORMAT(10X,A7,5X,1PE11.4,5X,1PE10.4)
  807 FORMAT(/'     FACTORS AFFECTING LAMINATE ',A7/
     +'      (MEAN VALUE = ',1PE10.3,'    EXPECTED SD = ',1PE10.3,')'//
     +'             VARIABLE PROPERTIES                  LAMIN'
     +,'ATE SENSITIVITY*'/
     +'     PROPERTY         MEAN       SD         DERIVATIVE'
     +,'    SIGMAi      PERCENT')
  808 FORMAT(1X,A6,1X,A4,I3,3X,2(1PE10.3,1X),4X,1PE10.3,2X,1PE10.3,
     +1X,A10)
  809 FORMAT(A80)
  810 FORMAT(1X,A80)
  811 FORMAT(F10.5)
  812 FORMAT(/'  * DERIVATIVE = change in laminate property ',
```

```
     +'with change in variable property',
     +       /'                 (units of ',
     +'laminate property / units of variable property)',
     +       /'    SIGMAi     = expected variation in laminate ',
     +'property due to variation in ',
     +       /'                 variable property alone ',
     +'(units of laminate property)',
     +       /'                 ( = VARIABLE PROPERTY SD * ',
     +'DERIVATIVE)',
     +       /'    PERCENT    = percent change in laminate ',
     +'property with 1% change in ',
     +       /'                 variable property',
     +' (meaningless if mean of either is 0.0)',
     +       /'                 ( = DERIVATIVE * VARIABLE PROP. ',
     +'MEAN / LAMINATE PROP. MEAN)')
  814 FORMAT(10X,A6,5X,1PE11.4)
  816 FORMAT(/10X,'IN LOOP TO GET SUMS AROUND 48')

      END
C
      SUBROUTINE STORE(IX,X)
C
C   c 1992 Hugh L. McManus
C
      IMPLICIT REAL*8 (A-H,O-Z)
      REAL*8 N,M,E,K,NO,NT,MT,NBAR,MBAR
      LOGICAL YESNO
      CHARACTER*60 ISTR,DESC,FNAME,FNAMEA
      CHARACTER*20 FTYPE
      COMMON /STRESS/ESTAR(3),SIGMA(3),SIGSTR(3),EPS(3),ALF(3),
     +               AL(3),EPT(3),BET(3),BE(3)
      COMMON /MNEK/M(3),N(3),E(3),K(3),NT(3),MT(3),NBAR(3),MBAR(3)
      COMMON /STUFF/NLAY,T(100),ANG(100),MATER(100),DELTAT,
     +              A(3,3),B(3,3),D(3,3),AP(3,3),BP(3,3),DP(3,3),
     +              Q(3,3),QQ(3,3),THICK,DELTAM,BPT(3,3)
      COMMON /WORDS/HELP,YES,NO,QUIT
      COMMON /MATR/CONST(4,30),TP(30),DESC(30),NMATR,
     +             ALFA1(30),ALFA2(30),STRENG(5,30),BETA(2,30),VFPLY(30)
      COMMON /FAIL/IFAIL(30),FACMAX,ULT(5),FTYPE(5)
      COMMON /PARSE/ISTR,IP,JTABL(10,14)
      COMMON /VAR/NX,XX(200),SD(200),ITYP(200),IN1(200),IN2(200),
     +NAME(11),NTYP(2)
      IF(ITYP(IX) .EQ. 1)THEN
        IF(IN1(IX) .EQ. 1)THEN
          T(IN2(IX)) = X
        ELSE
          ANG(IN2(IX)) = X
        ENDIF
      ELSE
        IF(IN1(IX) .LE. 4) THEN
          CONST(IN1(IX),IN2(IX)) = X
        ELSE IF(IN1(IX) .EQ. 5) THEN
          ALFA1(IN2(IX)) = X
        ELSE IF(IN1(IX) .EQ. 6) THEN
          ALFA2(IN2(IX)) = X
        ELSE IF(IN1(IX) .EQ. 9) THEN
          VFPLY(IN2(IX)) = X
        ELSE
          BETA(IN1(IX)-6,IN2(IX)) = X
        ENDIF
      ENDIF
      RETURN
      END
C
```

```
      SUBROUTINE MCLAMS(ETA)
C
C   c 1992 Hugh L. McManus
C
      IMPLICIT REAL*8 (A-H,O-Z)
      REAL*8 N,M,E,K,NO,NT,MT,NBAR,MBAR
      LOGICAL YESNO
      CHARACTER*60 ISTR,DESC,FNAME,FNAMEA
      CHARACTER*20 FTYPE
      COMMON /STRESS/ESTAR(3),SIGMA(3),SIGSTR(3),EPS(3),ALF(3),
     +               AL(3),EPT(3),BET(3),BE(3)
      COMMON /MNEK/M(3),N(3),E(3),K(3),NT(3),MT(3),NBAR(3),MBAR(3)
      COMMON /STUFF/NLAY,T(100),ANG(100),MATER(100),DELTAT,
     +              A(3,3),B(3,3),D(3,3),AP(3,3),BP(3,3),DP(3,3),
     +              Q(3,3),QQ(3,3),THICK,DELTAM,BPT(3,3)
      COMMON /WORDS/HELP,YES,NO,QUIT
      COMMON /MATR/CONST(4,30),TP(30),DESC(30),NMATR,
     +             ALFA1(30),ALFA2(30),STRENG(5,30),BETA(2,30),VFPLY(30)
      COMMON /FAIL/IFAIL(30),FACMAX,ULT(5),FTYPE(5)
      COMMON /PARSE/ISTR,IP,JTABL(10,14)
      COMMON /VAR/NX,XX(200),SD(200),ITYP(200),IN1(200),IN2(200),
     +NAME(11),NTYP(2)
      DIMENSION ALFL(3),BETS(3),WT(3),WH(3)
      DIMENSION ETA(17)
      VF =0.
      CALL MATMAK
      E11 = 1. / (AP(1,1) * THICK)
      E22 = 1. / (AP(2,2) * THICK)
      G = 1. / (AP(3,3) * THICK)
      V12 = - AP(1,2) / AP(1,1)
      V21 = - AP(1,2) / AP(2,2)
      DO 3 I=1,NLAY
    3 VF = VF+T(I)*VFPLY(MATER(I))
      VF = VF/THICK
      DELTAT = 1.
      DELTAM = 0.
      CALL THRMAK
      CALL MATKLG(ALFL,AP,NT,BP,MT)
C
C ADDED TO CALCULATE WT(CURVATURE DUE TO TEMPERATURE)
      CALL MATKLG(WT,BPT,NT,DP,MT)
C
      DELTAT = 0.
      DELTAM = 1.
      CALL THRMAK
      CALL MATKLG(BETS,AP,NT,BP,MT)
C
C ADDED TO CALCULATE WH (CURVATURE DUE TO MOISTURE)
      CALL MATKLG(WH,BPT,NT,DP,MT)
C
      ETA(1) = E11
      ETA(2) = E22
      ETA(3) = V12
      ETA(4) = G
      ETA(11) = VF
      DO 10 I = 1, 3
        ETA(4+I) = ALFL(I)
        ETA(7+I) = BETS(I)
C
C ADD CURVATURES TO ETA MATRIX
        ETA(11+I) = WT(I)
   10   ETA(14+I) = WH(I)
  100 FORMAT(/' VOLUME FRACTION IS ',1PE12.4)
C
```

```
      RETURN
      END

      SUBROUTINE MATFOO(X,A,Y)
C
C     c 1992 Hugh L. McManus
C
      IMPLICIT REAL*8 (A-H,O-Z)
      DIMENSION X(3),A(3,3),Y(3)
      DO 1 I=1,3
      X(I)=0.
      DO 1 J=1,3
    1 X(I)=X(I)+A(I,J)*Y(J)
      RETURN
      END

      SUBROUTINE MOHR(X,Y,THETA,F)
C
C     c 1992 Hugh L. McManus
C
      IMPLICIT REAL*8 (A-H,O-Z)
      DIMENSION X(3),Y(3)
      CS=COS(THETA)
      SN=SIN(THETA)
      CS2=CS**2
      SN2=SN**2
      CSSN=CS*SN
      X(1)=Y(1)*CS2+Y(2)*SN2+F*Y(3)*CSSN
      X(2)=Y(1)*SN2+Y(2)*CS2-F*Y(3)*CSSN
      X(3)=2.*(Y(2)-Y(1))*CSSN/F+(CS2-SN2)*Y(3)
      RETURN
      END


      SUBROUTINE THRMAK
C
C     c 1992 Hugh L. McManus
C
      IMPLICIT REAL*8 (A-H,O-Z)
      CHARACTER*60 DESC
      REAL*8 M,N,E,K,NT,MT,NBAR,MBAR
      COMMON /STUFF/NLAY,T(100),ANG(100),MATER(100),DELTAT,
     +              A(3,3),B(3,3),D(3,3),AP(3,3),BP(3,3),DP(3,3),
     +              Q(3,3),QQ(3,3),THICK,DELTAM,BPT(3,3)
      COMMON /STRESS/ESTAR(3),SIGMA(3),SIGSTR(3),EPS(3),ALF(3),
     +               AL(3),EPT(3),BET(3),BE(3)
      COMMON /MATR/CONST(4,30),TP(30),DESC(30),NMATR,
     +             ALFA1(30),ALFA2(30),STRENG(5,30),BETA(2,30),VFPLY(30)
      COMMON /MNEK/M(3),N(3),E(3),K(3),NT(3),MT(3),NBAR(3),MBAR(3)
      DO 1 I=1,3
      NT(I)=0.
    1 MT(I)=0.
      TOP=THICK/2.
      DO 3 I=1,NLAY
      BOTTOM=TOP-T(I)
      AL(1)=ALFA1(MATER(I))
      AL(2)=ALFA2(MATER(I))
      AL(3)=0.
      CALL MOHR(ALF,AL,(-ANG(I)),1.D0)
      BE(1)=BETA(1,MATER(I))
      BE(2)=BETA(2,MATER(I))
      BE(3)=0.
      CALL MOHR(BET,BE,(-ANG(I)),1.D0)
      CALL QMAK(I)
```

```
      DO 2 J=1,3
      FACA=Q(J,1)*ALF(1)+Q(J,2)*ALF(2)+Q(J,3)*ALF(3)
      FACB=Q(J,1)*BET(1)+Q(J,2)*BET(2)+Q(J,3)*BET(3)
      FAC = FACA*DELTAT + FACB*DELTAM
      NT(J)=NT(J)+FAC*(TOP-BOTTOM)
    2 MT(J)=MT(J)+FAC*(TOP**2-BOTTOM**2)
    3 TOP=BOTTOM
      DO 4 I=1,3
    4 MT(I)=MT(I)/2.
      RETURN
      END



      SUBROUTINE MATMAK
C
C   c 1992 Hugh L. McManus
C
      IMPLICIT REAL*8 (A-H,O-Z)
      COMMON /STUFF/NLAY,T(100),ANG(100),MATER(100),DELTAT,
     +              A(3,3),B(3,3),D(3,3),AP(3,3),BP(3,3),DP(3,3),
     +              Q(3,3),QQ(3,3),THICK,DELTAM,BPT(3,3)
      COMMON /MATR/CONST(4,30),TP(30),DESC(30),NMATR,
     +             ALFA1(30),ALFA2(30),STRENG(5,30),BETA(2,30),VFPLY(30)
      THICK=0.
      DO 1 J=1,3
      DO 1 K=1,3
      A(J,K)=0.
      B(J,K)=0.
    1 D(J,K)=0.
      DO 2 I=1,NLAY
    2 THICK=THICK+T(I)
      TOP=THICK/2
      DO 100 I=1,NLAY
      CALL QMAK(I)
      FACA=T(I)
      BOTTOM=TOP-FACA
      FACB=(TOP**2-BOTTOM**2)/2.
      FACD=(TOP**3-BOTTOM**3)/3.
      TOP=BOTTOM
      DO 99 J=1,3
      DO 99 K=1,3
      A(J,K)=A(J,K)+Q(J,K)*FACA
      B(J,K)=B(J,K)+Q(J,K)*FACB
   99 D(J,K)=D(J,K)+Q(J,K)*FACD
  100 CONTINUE
      CALL MATINV(AP,A)
      CALL MATMLT(QQ,B,AP)
      CALL MATMLT(Q,QQ,B)
      CALL MATSUB(Q,D,Q)
      CALL MATINV(DP,Q)
      CALL MATMLT(Q,AP,B)
      CALL MATMLT(BP,Q,DP)
      CALL MATNEG(BP)
      CALL MATMLT(Q,BP,QQ)
      CALL MATSUB(AP,AP,Q)
C  CALCULATE BPT(=TRANSPOSE(BP) FOR CALCULATION OF BENDING PARAMETERS)
      CALL MATNEG(DP)
      CALL MATMLT(BPT,DP,QQ)
      CALL MATNEG(DP)
      CALL CLEAN(BPT,3)
C
      CALL CLEAN(A,3)
      CALL CLEAN(AP,3)
```

```
      CALL CLEAN(B,3)
      CALL CLEAN(BP,3)
      CALL CLEAN(D,3)
      CALL CLEAN(DP,3)
      RETURN
      END


      SUBROUTINE CLEAN(A,N)
C
C     c 1992 Hugh L. McManus
C
      IMPLICIT DOUBLE PRECISION (A-H,O-Z)
      DIMENSION A(N,N)
      DMAX=0.
      DO 1 I = 1, N
        DO 1 J = 1, N
          IF(ABS(A(I,J)).GT. DMAX) DMAX = ABS(A(I,J))
    1 CONTINUE
      DMIN = DMAX * 1.E-7
      DO 2 I = 1, N
        DO 2 J = 1, N
          IF(ABS(A(I,J)) .LT. DMIN) A(I,J) = 0.0
    2 CONTINUE
      RETURN
      END

      SUBROUTINE QMAK(I)
C
C     c 1992 Hugh L. McManus
C
      IMPLICIT REAL*8 (A-H,O-Z)
      CHARACTER*60 DESC
      CHARACTER*20 FTYPE
      COMMON /STUFF/NLAY,T(100),ANG(100),MATER(100),DELTAT,
     +              A(3,3),B(3,3),D(3,3),AP(3,3),BP(3,3),DP(3,3),
     +              Q(3,3),QQ(3,3),THICK,DELTAM,BPT(3,3)
      COMMON /MATR/CONST(4,30),TP(30),DESC(30),NMATR,
     +             ALFA1(30),ALFA2(30),STRENG(5,30),BETA(2,30),VFPLY(30)
      COMMON /FAIL/IFAIL(30),FACMAX,ULT(5),FTYPE(5)
      IF(IFAIL(I).NE.1)GO TO 2
        DO 1 J=1,3
        DO 1 K=1,3
    1     Q(J,K) = 1.E-20
        RETURN
    2 M=MATER(I)
      DENOM=1-CONST(2,M)*CONST(3,M)**2/CONST(1,M)
      Q11=CONST(1,M)/DENOM
      Q22=CONST(2,M)/DENOM
      Q12=CONST(3,M)*Q22
      Q66=CONST(4,M)
      CS=COS(ANG(I))
      SN=SIN(ANG(I))
      C2=CS*CS
      S2=SN*SN
      C4=C2*C2
      S4=S2*S2
      C2S2=C2*S2
      TEMP1=2.*(Q12+2.*Q66)*C2S2
      TEMP2=(Q11-Q12-2.*Q66)*SN*CS
      TEMP3=(Q12-Q22+2.*Q66)*SN*CS
      Q(1,1)=Q11*C4+TEMP1+Q22*S4
      Q(1,2)=(Q11+Q22-4.*Q66)*C2S2+Q12*(S4+C4)
      Q(2,2)=Q11*S4+TEMP1+Q22*C4
```

```
      Q(1,3)=TEMP2*C2+TEMP3*S2
      Q(2,3)=TEMP2*S2+TEMP3*C2
      Q(3,3)=(Q11+Q22-2.*(Q12+Q66))*C2S2+Q66*(S4+C4)
      Q(2,1)=Q(1,2)
      Q(3,1)=Q(1,3)
      Q(3,2)=Q(2,3)
      RETURN
      END

      SUBROUTINE MATINV(AINV,A)
C
C     c 1992 Hugh L. McManus
C
      IMPLICIT DOUBLE PRECISION (A-H,O-Z)
      DIMENSION A(3,3),AINV(3,3)
      DET=DETERM(A)
      AINV(1,1)=(A(2,2)*A(3,3)-A(2,3)*A(3,2))/DET
      AINV(1,2)=(A(1,3)*A(3,2)-A(1,2)*A(3,3))/DET
      AINV(1,3)=(A(1,2)*A(2,3)-A(1,3)*A(2,2))/DET
      AINV(2,1)=(A(3,1)*A(2,3)-A(2,1)*A(3,3))/DET
      AINV(2,2)=(A(1,1)*A(3,3)-A(1,3)*A(3,1))/DET
      AINV(2,3)=(A(1,3)*A(2,1)-A(1,1)*A(2,3))/DET
      AINV(3,1)=(A(2,1)*A(3,2)-A(2,2)*A(3,1))/DET
      AINV(3,2)=(A(1,2)*A(3,1)-A(1,1)*A(3,2))/DET
      AINV(3,3)=(A(1,1)*A(2,2)-A(1,2)*A(2,1))/DET
      RETURN
      END

      SUBROUTINE MATMLT(AB,A,B)
C
C     c 1992 Hugh L. McManus
C
      IMPLICIT DOUBLE PRECISION (A-H,O-Z)
      DIMENSION AB(3,3),A(3,3),B(3,3)
      DO 1 I=1,3
      DO 1 J=1,3
      AB(I,J)=0.
      DO 1 K=1,3
    1 AB(I,J)=AB(I,J)+A(I,K)*B(K,J)
      RETURN
      END

      SUBROUTINE MATSUB(AMB,A,B)
C
C     c 1992 Hugh L. McManus
C
      IMPLICIT DOUBLE PRECISION (A-H,O-Z)
      DIMENSION AMB(3,3),A(3,3),B(3,3)
      DO 1 I=1,3
      DO 1 J=1,3
    1 AMB(I,J)=A(I,J)-B(I,J)
      RETURN
      END

      FUNCTION DETERM(A)
      IMPLICIT DOUBLE PRECISION (A-H,O-Z)
      DIMENSION A(3,3)
      DETERM=A(2,1)*(A(1,3)*A(3,2)-A(1,2)*A(3,3))+
     +       A(2,2)*(A(1,1)*A(3,3)-A(1,3)*A(3,1))+
     +       A(2,3)*(A(1,2)*A(3,1)-A(1,1)*A(3,2))
      RETURN
      END

      SUBROUTINE MATOUT(A)
```

```
C
C    c 1992 Hugh L. McManus
C
      IMPLICIT DOUBLE PRECISION (A-H,O-Z)
      DIMENSION A(3,3)
      TYPE 1,((A(I,J),J=1,3),I=1,3)
    1 FORMAT(//3(/10X,3(1PE11.4,4X)))
      RETURN
      END

      SUBROUTINE MATNEG(A)
C
C    c 1992 Hugh L. McManus
C
      IMPLICIT DOUBLE PRECISION (A-H,O-Z)
      DIMENSION A(9)
      DO 1 I=1,9
    1 A(I)=-A(I)
      RETURN
      END

      SUBROUTINE MATKLG(X,A,Y,B,Z)
C
C    c 1992 Hugh L. McManus
C
      IMPLICIT DOUBLE PRECISION (A-H,O-Z)
      DIMENSION A(3,3),B(3,3),X(3),Y(3),Z(3)
      DO 1 I=1,3
      X(I)=0
      DO 1 J=1,3
    1 X(I)=X(I)+A(I,J)*Y(J)+B(I,J)*Z(J)
      RETURN
      END

      SUBROUTINE COUPLE(CC)
C
C
      IMPLICIT DOUBLE PRECISION (A-H,O-Z)
      CHARACTER*60 ISTR,DESC,FNAME,FNAMEA
      COMMON /STUFF/NLAY,T(100),ANG(100),MATER(100),DELTAT,
     +              A(3,3),B(3,3),D(3,3),AP(3,3),BP(3,3),DP(3,3),
     +              Q(3,3),QQ(3,3),THICK,DELTAM,BPT(3,3)
      COMMON /MATR/CONST(4,30),TP(30),DESC(30),NMATR,
     +             ALFA1(30),ALFA2(30),STRENG(5,30),BETA(2,30),VFPLY(30)
      COMMON /VAR/NX,XX(200),SD(200),ITYP(200),IN1(200),IN2(200),
     +NAME(11),NTYP(2)
      DIMENSION CC(9,9)

    1 TYPE *,' Input name of file with material coupling matrix'
      READ(5,300)FNAMEA
      OPEN(UNIT=3,FILE=FNAMEA,STATUS='OLD',ERR=100)
      DO 10 I=1,9
      READ(3,*,ERR=200) (CC(I,J),J=1,9)
   10 END DO

      RETURN
  100 TYPE *,' CAN''T OPEN MATERIAL COUPLING MATRIX FILE!!'
      TYPE *,' VAR looks for an input file in the current'
      TYPE *,' default directory.  If you type NAME, it will'
      TYPE *,' look for NAME.DAT.  If the file is not in the'
      TYPE *,' default directory, or is not a .DAT file, type a full'
      TYPE *,' file spec. (e.g. UD3:[MCMANUS.MCLAM.VAR]TEST.DAT)'
      TYPE *,' DON''T use clip commands like *ADD- just the file name'
      TYPE *,' Type HELP instead of a file name and you will get help'
```

```
    TYPE *,' on input file format and other info about VAR'
    STOP
200 TYPE *,' INPUT ERROR!! Reading material coupling matrix file!'
    STOP
300 FORMAT(A60)


    END
```

APPENDIX C

LARGEDEF.M SCRIPT

This appendix contains the Matlab script which implements the large-deformation analysis developed in Section 4.6. The script uses symbolic mathematical manipulations in the solution. The manufacturing parameters and material properties in the script below are for a square $[0/30]_T$ laminate made of AS4/3501-6 graphite/epoxy. These parameters can be changed to a variety of layups and material systems without invalidating the method.

The script was run with Matlab Version 4.2 on the Athena computer network at MIT. Symbolic manipulations were carried out by an embedded Maple V Release 3 kernel. Most of the development used a Sun Sparc Classic computer. However, this computer could not perform some of the symbolic algebra for laminates which were not cross-plies. A Sun Sparc 5 succeeded in running the code at a significant increase in speed. The final runs were on a Silicon Graphics Indy workstation. This computer had no problems with the script, and was by far the fastest computer used.

```
% Program to perform laminate stability analysis
% Do loop on laminate sidelength
% Filename is largedef.m


clear all

deltaM=0;    %moisture content(%)
deltaT=-280;   % temperature change in degrees F


% Initialize matrices to zero
A=[0 0 0;0 0 0;0 0 0];
B=[0 0 0;0 0 0;0 0 0];
D=[0 0 0;0 0 0;0 0 0];
NT=[0;0;0];
MT=[0;0;0];
NH=[0;0;0];
MH=[0;0;0];

%                                                    MANUFACTURING VARIABLES
n=2; % number of plies
t=[.0052 .0052]; %thickness of each ply in inches
theta=[0 30]; % rotation in degrees for all plies
%                                                    MANUFACTURING VARIABLES

h=sum(t(:));   %h is total laminate thickness
% Compute upper height(zku) and lower height(zkl) for each ply
zku(1)=h/2;

for j=2:n
        zku(j)=zku(j-1)-t(j-1); % upper height of each ply
end

for i=1:n
        zkl(i)=zku(i)-t(i); % lower height of each ply
end


M=[0;0;0]; % applied running moment
N=[0;0;0]; % applied running load


for k=1:n                    % Loop on number of plies

%                                                          MATERIAL PROPERTIES
        % ep is ply engineering properties EL,ET,vLT,GLT
        ep=[20.59E6 1.42E6 .30 0.87E6];  %Eng props for AS4/3501-6 (psi)
        alpha=[-.167E-6;15.6E-6;0]; % CTE
        beta=[0;0;0]; % CME
%                                                          MATERIAL PROPERTIES

        EL=ep(1,1);
        ET=ep(1,2);
        NU=ep(1,3);
        G=ep(1,4);
        ang=theta(k)*pi/180;   %convert theta to radians

        %compute q matrix (unrotated ply)
        q11=EL/(1-NU^2*(ET/EL));
        q12=NU*ET/(1-NU^2*2*(ET/EL));
        q22=ET/(1-NU^2*(ET/EL));
        q66=G;
        q=[q11 q12 0;q12 q22 0;0 0 q66];
```

```
        stiff=inv(q);

        % Rotate q matrix to get Q matrix (Qbar)
        co=cos(ang);
        s=sin(ang);
        Q11(k)=q11*co^4+2*(q12+2*q66)*s^2*co^2+q22*s^4;
        Q12(k)=(q11+q22-4*q66)*s^2*co^2+q12*(s^4+co^4);
        Q22(k)=q11*s^4+2*(q12+2*q66)*s^2*co^2+q22*co^4;
        Q16(k)=(q11-q12-2*q66)*s*co^3+(q12-q22+2*q66)*s^3*co;
        Q26(k)=(q11-q12-2*q66)*s^3*co+(q12-q22+2*q66)*s*co^3;
        Q66(k)=(q11+q22-2*q12-2*q66)*s^2*co^2+q66*(s^4+co^4);
        Q=[Q11(k) Q12(k) Q16(k);Q12(k) Q22(k) Q26(k);Q16(k) Q26(k) Q66(k)];
        TR=[co^2 s^2 2*s*co; s^2 co^2 -2*s*co; -s*co s*co (co^2-s^2)];
        R=[1 0 0;0 1 0;0 0 2];
        %Calculate A,B,D matrices
        A=A+Q*t(k);
        B=B+Q*0.5*(zku(k)^2-zkl(k)^2);
        D=D+Q*(1/3)*(zku(k)^3-zkl(k)^3);
        alphabar=R*inv(TR)*inv(R)*alpha; %rotate CTE for each ply
        a11(k)=alphabar(1);
           a22(k)=alphabar(2);
        a12(k)=alphabar(3);
        betabar=R*inv(TR)*inv(R)*beta; %rotate CmE for each ply
        NT=NT+Q*alphabar*deltaT*t(k); %thermal stress for laminate
        MT=MT+Q*0.5*alphabar*deltaT*(zku(k)^2-zkl(k)^2); %lam thermal
                                                                    %moments
        NH=NH+Q*betabar*deltaM*t(k); %hygral stress for laminate
        MH=MH+Q*0.5*betabar*deltaM*(zku(k)^2-zkl(k)^2); %lam hygral
                                                                  %moments
end



ABBD=[A B;B D];
abbd=(ABBD)^(-1);
EK=abbd*[N+NT+NH;M+MT+MH];     %laminate strain/curvature matrix
WT=abbd*[NT;MT];
WH=abbd*[NH;MH];
if deltaT ~= 0
        WT = WT/deltaT;
end
if deltaM ~= 0
        WH = WH/deltaM;
end
curvt=[WT(4,1);WT(5,1);WT(6,1)];
curvh=[WH(4,1);WH(5,1);WH(6,1)];

L='L';

Lx=L;
Ly=L;


lambda=curvt(1,1)/curvt(2,1);

% Calculate angle of rotation between axis systems
phi2=atan((2*EK(6,1))/(EK(4,1)-EK(5,1)));
phi=phi2/2;
cp=cos(phi2);
sp=sin(phi2);

CM=0.5*(EK(4,1)+EK(5,1));
RM=sqrt((((EK(4,1)-EK(5,1))/2))^2+(EK(6,1))^2);
k1=CM+RM;
```

```
k2=CM-RM;

T=deltaT;


%                                        ASSUMED STRAIN/CURVATURE VECTOR
ek=sym('[d+c^2*y^2/2+a*c*x*y;e+c^2*x^2/2+b*c*x*y;a*c*x^2/2+\
        b*c*y^2/2+(a*b+c^2)*x*y/2+f;a;b;c]');


% Find expression for strain energy density
ek=simple(ek);
ekt = transpose(ek);
ektabbd=symop(ekt,'*',ABBD);
ektabbd=simple(ektabbd);
energy = symop(0.5,'*',ektabbd,'*',ek,'-',ekt,'*',[NT;MT]);
energy=simple(energy);


%  Calculate laminate total potential energy
% MADE INTEGRALS JUST IN TERMS OF L
tozy=int(energy,'y','-L/2','L/2');
energytot=int(tozy,'x','-L/2','L/2');
energytot=simple(energytot);


ap='ap';
bp='bp';

cm0=symop(ap,'+',bp);
cm0=symop(cm0,'/',2);
rm0=symop(ap,'-',bp);
rm0=symop(rm0,'/',2);

% Put energytot in terms of ap, bp and find first derivatives
a0=symop(cm0,'+',rm0,'*',cp);
b0=symop(cm0,'-',rm0,'*',cp);
c0=symop(rm0,'*',sp);
enerdiff=subs(energytot,a0,'a');
enerdiff=subs(enerdiff,b0,'b');
enerdiff=subs(enerdiff,c0,'c');
enerdiff=simple(enerdiff);
ed1=diff(enerdiff,'ap');
ed2=diff(enerdiff,'bp');
ed4=diff(enerdiff,'d');
ed5=diff(enerdiff,'e');
ed6=diff(enerdiff,'f');



% Solve for d,e,f, in terms of ap,bp

f=solve(ed6,'f');
f=simple(f);
ed5s=subs(ed5,f,'f');
ed5s=simple(ed5s);
e=solve(ed5s,'e');
e=simple(e);
ed4s=subs(ed4,f,'f');
ed4s=subs(ed4s,e,'e');
ed4s=simple(ed4s);
d=solve(ed4s,'d');
d=simple(d);
```

```
% Put enerdiff in terms of just ap,bp
et2=subs(enerdiff,f,'f');
et2=simple(et2);
et2 = subs(et2,e,'e');
et2si=simple(et2);
etotsub = subs(et2si,d,'d');
etotsub=simple(etotsub);


u=1001;

% Initialize vectors
leng=zeros(1,u);
aa1=zeros(1,u);
aa2=zeros(1,u);
aa3=zeros(1,u);
bb1=zeros(1,u);
bb2=zeros(1,u);
bb3=zeros(1,u);
cc1=zeros(1,u);
cc2=zeros(1,u);
cc3=zeros(1,u);
dd1=zeros(1,u);
dd2=zeros(1,u);
dd3=zeros(1,u);
ee1=zeros(1,u);
ee2=zeros(1,u);
ee3=zeros(1,u);
ff1=zeros(1,u);
ff2=zeros(1,u);
ff3=zeros(1,u);
ene1=zeros(1,u);
ene2=zeros(1,u);
ene3=zeros(1,u);


for l=2:u      % loop on laminate sidelength

        prog=l

        g=.006;

        leng(l)=(l-1)*g;
        v=leng(l);
        Ll=subs(L,v,'L');
        Ll=numeric(Ll);
        etotsubl=subs(etotsub,v,'L');
        ed1l=subs(ed1,v,'L');
        ed2l=subs(ed2,v,'L');
        ed4l=subs(ed4,v,'L');
        ed5l=subs(ed5,v,'L');
        ed6l=subs(ed6,v,'L');
        dl=subs(d,v,'L');
        el=subs(e,v,'L');
        fl=subs(f,v,'L');



% CASE 1:   bprime=0


% Put in assumed shape (bp=0) and solve for ap
bp1=0;
```

```
etot1=subs(etotsubl,bp1,'bp');
deda=diff(etot1,'ap');
apcase1=solve(deda,'ap');
ap1a=sym(apcase1,1,1);
ap1a=numeric(ap1a);
ap1=ap1a;

% Find constants for this case
a1=subs(a0,bp1,'bp');
a1=subs(a1,ap1,'ap');
a1=eval(a1);
b1=subs(b0,bp1,'bp');
b1=subs(b1,ap1,'ap');
b1=eval(b1);
c1=subs(c0,bp1,'bp');
c1=subs(c1,ap1,'ap');
c1=eval(c1);
d1=subs(dl,ap1,'ap');
d1=subs(d1,bp1,'bp');
d1=numeric(d1);
e1=subs(el,ap1,'ap');
e1=subs(e1,d1,'d');
e1=subs(e1,bp1,'bp');
e1=numeric(e1);
f1=subs(fl,ap1,'ap');
f1=subs(f1,d1,'d');
f1=subs(f1,e1,'e');
f1=subs(f1,bp1,'bp');
f1=numeric(f1);



% CASE 2:   aprime=0


% Put in assumed shape (ap=0) and solve for bp
ap2=0;
etot2=subs(etotsubl,ap2,'ap');
dedb=diff(etot2,'bp');
bpcase2=solve(dedb,'bp');
bp2a=sym(bpcase2,1,1);
bp2a=numeric(bp2a);
bp2=bp2a;


% Find constants for  Case 2
a2=subs(a0,bp2,'bp');
a2=subs(a2,ap2,'ap');
a2=eval(a2);
b2=subs(b0,bp2,'bp');
b2=subs(b2,ap2,'ap');
b2=eval(b2);
c2=subs(c0,bp2,'bp');
c2=subs(c2,ap2,'ap');
c2=eval(c2);
d2=subs(dl,ap2,'ap');
d2=subs(d2,bp2,'bp');
d2=numeric(d2);
e2=subs(el,ap2,'ap');
e2=subs(e2,d2,'d');
e2=subs(e2,bp2,'bp');
e2=numeric(e2);
```

```
f2=subs(fl,ap2,'ap');
f2=subs(f2,d2,'d');
f2=subs(f2,e2,'e');
f2=subs(f2,bp2,'bp');
f2=numeric(f2);



%CASE 3:   bprime=lambda(aprime)

% Put in assumed shape (bp=lambda*ap) and solve for ap
bp3=symop(lambda,'*',ap);
etot3=subs(etotsubl,bp3,'bp');
etot3=simple(etot3);
deda3=diff(etot3,'ap');
apcase3=solve(deda3,'ap');
ap3a=sym(apcase3,1,1);
ap3a=numeric(ap3a);
ap3=ap3a;
bp3=subs(bp3,ap3,'ap');
bp3=numeric(bp3);

% Find constants for this case
a3=subs(a0,bp3,'bp');
a3=subs(a3,ap3,'ap');
a3=eval(a3);
b3=subs(b0,bp3,'bp');
b3=subs(b3,ap3,'ap');
b3=eval(b3);
c3=subs(c0,bp3,'bp');
c3=subs(c3,ap3,'ap');
c3=eval(c3);
d3=subs(dl,ap3,'ap');
d3=subs(d3,bp3,'bp');
d3=numeric(d3);
e3=subs(el,ap3,'ap');
e3=subs(e3,d3,'d');
e3=subs(e3,bp3,'bp');
e3=numeric(e3);
f3=subs(fl,ap3,'ap');
f3=subs(f3,d3,'d');
f3=subs(f3,e3,'e');
f3=subs(f3,bp3,'bp');
f3=numeric(f3);



% Find center of Mohr's circle of principal curvature
cm1=0.5*(ap1+bp1);
cm2=0.5*(ap2+bp2);
cm3=0.5*(ap3+bp3);

cm=[cm1 cm2 cm3];

% Find radius of Mohr's circle of principal curvature
rm1=0.5*(ap1-bp1);
rm2=0.5*(ap2-bp2);
rm3=0.5*(ap3-bp3);

rm=[rm1 rm2 rm3];

% Find numbers for total potential energies for all 3 cases
```

```
etot1=subs(etotsubl,bp1,'bp');
en1=subs(etot1,ap1,'ap');
en1=numeric(en1);
etot2=subs(etotsubl,ap2,'ap');
en2=subs(etot2,bp2,'bp');
en2=numeric(en2);
en3=subs(etot3,ap3,'ap');
en3=numeric(en3);


% Put constants into results vectors
aa1(l)=a1;
aa2(l)=a2;
aa3(l)=a3;
bb1(l)=b1;
bb2(l)=b2;
bb3(l)=b3;
cc1(l)=c1;
cc2(l)=c2;
cc3(l)=c3;
dd1(l)=d1;
dd2(l)=d2;
dd3(l)=d3;
ee1(l)=e1;
ee2(l)=e2;
ee3(l)=e3;
ff1(l)=f1;
ff2(l)=f2;
ff3(l)=f3;

ene1(l)=en1;
ene2(l)=en2;
ene3(l)=en3;



end     % end for loop on laminate sidelength


%Initial values for results vectors
leng(1)=0;
aa1(1)=aa1(2);
aa2(1)=aa2(2);
aa3(1)=EK(4);
bb1(1)=bb1(2);
bb2(1)=bb2(2);
bb3(1)=EK(5);
cc1(1)=cc1(2);
cc2(1)=cc1(2);
cc3(1)=EK(6);


ene1(1)=0;
ene2(1)=0;
ene3(1)=0;


%                                                                    MAKE PLOTS

figure(1)
plot(leng,aa1,'--',leng,aa2,'-.',leng,aa3)
grid
title('Curvature in the x direction (1/in) ')
xlabel('Length of side, inches')
```

```
ylabel('Curvature x')

figure(2)
plot(leng,bb1,'--',leng,bb2,'-.',leng,bb3)
grid
title('Curvature in the y direction (1/in) ')
xlabel('Length of side, inches')
ylabel('Curvature y')


figure(3)
plot(leng,cc1,'--',leng,cc2,'-.',leng,cc3)
grid
title('Twist Curvature  (1/in) ')
xlabel('Length of side, inches')
ylabel('Twist Curvature ')


figure(4)
plot(leng,ene1,'--',leng,ene2,'-.',leng,ene3)
grid
title('Energy for different cases')
xlabel('Length of side, inches')
ylabel('Energy')
```

APPENDIX D

RAW EXPERIMENTAL DATA

This appendix presents raw experimental data for all specimens in the experimental test matrix. The data is presented in tabular form identical to that of Table 5.6. Each column of the tables represents a variable, and each row represents an observation. The first column is the amount of time since the beginning of the test in minutes. The second column is the temperature measured by the K-type thermocouple in °C. The third and fourth columns are output voltages for laser 1 and laser 2, respectively, in volts. Columns five and six are the temperatures measured by the J-type thermocouples attached to laser 1 and laser 2, respectively, in °C.

Table D.1 $[\pm 30]_s$ A Panel 1

Time	K Temp.	Laser 1 V	Laser 2 V	Laser 1 T	Laser 2 T
0	23.6	.370	0.673	29	28
15	23.3	0.730	0.686	28	28
30	23.5	0.745	0.692	29	29
45	92.0	0.750	0.693	29	28
60	95.0	0.751	0.694	29	28
75	97.0	0.751	0.694	30	29
80	97.6	0.8	0.751	30	29
85	97.9	0.825	0.771	31	30
90	98.0	0.828	0.779	31	30
95	98.1	0.835	0.786	31	31
100	98.1	0.845	0.794	31	31
105	98.1	0.853	0.793	32	32
110	98.1	0.859	0.803	32	32
115	98.1	0.868	0.806	32	32
120	98.1	0.868	0.806	32	32

Table D.2 $[\pm 30]_s$ B Panel 1

Time	K Temp.	Laser 1 V	Laser 2 V	Laser 1 T	Laser 2 T
0	23.6	.708	.723	26	27
15	23.0	.77	.730	28	29
30	23.2	.794	.736	29	29
45	23.4	.796	.735	29	29
60	23.4	.799	.733	29	29
75	95.1	.810	.770	29	29
90	98.0	.827	.797	30	30
95	98.2	.837	.807	31	31
100	98.3	.837	.801	31	31
105	98.2	.852	.816	32	32
110	98.0	.852	.815	32	32
115	98.1	.860	.822	33	33
120	98.1	.872	.827	33	33

Table D.3 $[\pm 30]_s$ C Panel 1

Time	K Temp.	Laser 1 V	Laser 2 V	Laser 1 T	Laser 2 T
0	23.6	0.676	0.673	26	26
15	23.3	0.730	0.686	29	29
30	23.5	0.745	0.692	29	29
45	23.5	0.750	0.693	29	30
60	23.3	0.751	0.694	29	30
75	23.3	0.751	0.694	30	30
90	93.6	0.8	0.751	30	30
105	98.0	0.825	0.771	31	31
110	98.2	0.828	0.779	32	32
115	98.1	0.835	0.786	32	32
120	98.1	0.845	0.794	33	33
125	98.1	0.853	0.793	33	34
130	98.0	0.859	0.803	34	34
135	98.0	0.868	0.806	34	34
140	98.0	0.868	0.806	34	34

Table D.4 $[\pm 30]_s$ D Panel 1

Time	K Temp.	Laser 1 V	Laser 2 V	Laser 1 T	Laser 2 T
0	23.9	.669	.708	27	28
15	23.6	.705	.704	29	29
30	23.2	.726	.702	30	29
45	23.4	.727	.703	30	30
60	23.4	.785	.789	30	31
75	95.1	.812	.814	30	32
90	98.0	.823	.818	32	33
95	98.2	.825	.815	33	33
100	98.3	.834	.820	33	33
105	98.2	.842	.820	33	33
110	98.0	.844	.830	34	34
115	98.1	.850	.832	34	34
120	98.1	.850	.834	34	35

Table D.5 $[\pm 30]_s$ E Panel 1

Time	K Temp.	Laser 1 V	Laser 2 V	Laser 1 T	Laser 2 T
0	23.5	.645	.636	27	27
15	23.2	.689	.66	29	29
30	23.2	.714	.682	30	30
45	23.3	.715	.683	30	30
60	23.3	.735	.695	30	30
75	97.0	.749	.709	31	31
80	97.9	.765	.790	32	32
85	97.8	.766	.739	32	32
90	97.8	.773	.745	33	32
95	97.8	.774	.744	33	33
100	97.8	.785	.746	33	33
105	97.8	.789	.751	34	34

Table D.6 $[\pm 30]_s$ A Panel 2

Time	K Temp.	Laser 1 V	Laser 2 V	Laser 1 T	Laser 2 T
0	21.4	.910	.914	26	26
15	24.3	.966	.644	29	29
30	23.5	.997	.971	29	29
45	23.0	1.016	.988	29	30
60	23.0	1.025	.999	29	30
75	23.1	1.024	1.001	30	30
90	91.8	.040	1.035	30	30
105	96.2	.068	.047	31	31
110	96.7	.069	.050	32	32
115	96.8	.084	.063	32	32
120	96.8	.090	.077	33	33
125	96.8	.089	.080	33	34
130	96.8	.092	.088	34	34
135	96.8	.092	.089	34	34
140	96.8	.103	.110	34	34

Table D.7 $[\pm 30]_s$ B Panel 2

Time	K Temp.	Laser 1 V	Laser 2 V	Laser 1 T	Laser 2 T
0	22.9	.835	.830	27	27
15	23.1	.858	.852	28	28
30	23.2	.871	.867	28	28
45	23.2	.882	.877	29	29
60	23.2	.884	.884	29	29
75	23.3	.888	.885	30	29
90	91.6	.914	.862	30	30
105	96.8	.950	.913	31	31
110	97.0	.945	.910	32	32
115	96.7	.957	.916	32	32
120	97.0	.962	.916	33	33
125	97.0	.965	.922	33	33
130	98.0	.975	.928	34	34
135	98.0	.974	.927	34	34

Table D.8 $[\pm 30]_s$ C Panel 2

Time	K Temp.	Laser 1 V	Laser 2 V	Laser 1 T	Laser 2 T
0	23.2	.741	.773	27	27
15	23.0	.800	.797	29	29
30	23.0	.822	.811	30	29
45	23.0	.822	.821	30	30
60	23.0	.828	.828	30	30
75	23.0	.829	.823	30	30
90	92.6	.854	.875	31	30
105	96.8	.870	.895	31	30
110	96.9	.877	.906	32	32
115	97.0	.881	.903	32	32
120	97.0	.884	.904	33	32
125	96.9	.888	.910	33	33
130	96.9	.896	.915	34	33
135	96.9	.900	.912	34	33

Table D.9 $[\pm 30]_s$ D Panel 2

Time	K Temp.	Laser 1 V	Laser 2 V	Laser 1 T	Laser 2 T
0	23.1	.904	.837	27	26
15	23.2	.918	.863	28	28
30	23.2	.928	.880	28	28
45	23.1	.936	.892	29	28
60	23.2	.941	.898	29	29
75	23.2	.944	.901	30	29
90	92.5	1.002	.857	31	30
105	97.1	1.010	.880	32	31
110	97.2	1.004	.902	33	32
115	97.3	1.022	.927	33	33
120	97.3	1.024	.938	33	33
125	97.2	1.030	.960	33	34
130	97.2	1.039	.975	34	34
135	97.1	1.040	.977	34	34

Table D.10 $[\pm 30]_s$ E Panel 2

Time	K Temp.	Laser 1 V	Laser 2 V	Laser 1 T	Laser 2 T
0	23.5	.858	.928	27	27
15	23.0	.928	.948	29	29
30	23.0	.948	.963	30	30
45	23.0	.955	.971	30	30
60	23.0	.954	.970	30	30
75	92.9	.937	.909	30	30
90	96.9	.944	.933	30	30
95	97.0	.947	.934	30	30
100	97.0	.953	.943	31	31
105	97.1	.957	.949	31	31
110	97.0	.958	.948	31	31
115	97.0	.967	.954	31	32
120	97.0	.968	.955	31	32

Table D.11 $[\pm 30]_s$ A Panel 3

Time	K Temp.	Laser 1 V	Laser 2 V	Laser 1 T	Laser 2 T
0	23.5	.797	.875	27	27
15	23.0	.859	.864	29	29
30	23.0	.874	.875	30	30
45	23.0	.884	.870	30	30
60	23.0	.885	.870	30	30
75	96.8	.948	.944	30	30
90	95.9	.954	.940	31	30
95	96.8	.964	.958	31	30
100	97.0	.964	.961	31	31
105	97.0	.967	.963	31	31
110	97.0	.974	.967	31	31
115	97.0	.980	.966	31	32
120	97.1	.982	.968	31	32

Table D.12 $[\pm 30]_s$ B Panel 3

Time	K Temp.	Laser 1 V	Laser 2 V	Laser 1 T	Laser 2 T
0	23.7	.695	.741	26	26
15	23.0	.739	.740	28	28
30	23.0	.746	.746	29	29
45	23.0	.756	.746	28	29
60	23.0	.747	.747	29	29
75	92.9	.773	.729	29	29
90	95.9	.774	.734	29	30
95	97.1	.788	.737	30	31
100	97.1	.786	.743	31	31
105	98.2	.788	.745	31	32
110	97.1	.793	.748	32	32
115	97.1	.798	.756	32	32
120	97.1	.798	.757	32	32

Table D.13 $[\pm 30]_s$ C Panel 3

Time	K Temp.	Laser 1 V	Laser 2 V	Laser 1 T	Laser 2 T
0	23.2	.828	.854	26	27
15	22.7	.863	.853	28	29
30	23.0	.868	.865	28	29
45	23.0	.866	.862	29	29
60	93.1	.922	.875	29	30
75	97.0	.914	.880	30	30
80	97.0	.917	.879	30	31
85	97.1	.927	.890	31	31
90	97.1	.932	.890	31	31
95	97.2	.933	.891	31	32
100	97.0	.944	.897	31	32
105	97.1	.951	.900	31	32

Table D.14 $[\pm 30]_s$ D Panel 3

Time	K Temp.	Laser 1 V	Laser 2 V	Laser 1 T	Laser 2 T
0	23.5	.876	.883	28	28
15	23.0	.905	.881	28	28
30	23.1	.920	.879	29	29
45	23.0	.922	.878	29	29
60	91.8	.992	.910	30	30
75	96.9	1.018	.950	30	31
80	97.0	1.016	.951	31	31
85	97.1	1.026	.955	31	31
90	97.1	1.028	.967	32	31
95	97.1	1.035	.978	32	32
100	97.1	1.031	.958	32	32
105	97.1	1.028	1958	32	32

Table D.15 $[\pm 30]_s$ E Panel 3

Time	K Temp.	Laser 1 V	Laser 2 V	Laser 1 T	Laser 2 T
0	23.1	.697	.665	25	25
15	20.7	.718	.661	27	27
30	22.4	.736	.673	28	28
45	22.9	.748	.679	29	29
60	23.0	.755	.681	29	29
75	93.7	.758	.705	29	29
90	96.7	.789	.727	30	30
95	97.1	.812	.737	30	31
100	97.1	.812	.738	30	31
105	97.1	.814	.741	31	32
110	97.1	.813	.755	31	32
115	97.2	.820	.754	32	32
120	97.1	.820	.761	32	32

Table D.16 $[\pm 45]_s$ A

Time	K Temp.	Laser 1 V	Laser 2 V	Laser 1 T	Laser 2 T
0	23.5	.789	.819	27	27
15	23.1	.788	.804	29	29
30	23.2	.800	.805	30	30
45	23.3	.800	.804	30	30
60	91.5	.746	.732	30	30
75	97.3	.770	.763	31	31
80	97.6	.778	.775	32	32
85	97.7	.789	.780	32	32
90	97.7	.787	.786	33	32
95	97.6	.794	.795	33	33
100	97.7	.798	.797	33	33
105	97.6	.807	.806	34	34

Table D.17 $[\pm 45]_s$ B

Time	K Temp.	Laser 1 V	Laser 2 V	Laser 1 T	Laser 2 T
0	23.0	1.140	1.198	28	29
15	23.0	1.255	1.210	29	29
30	23.1	1.275	1.221	30	30
45	23.3	1.277	1.221	30	30
60	95.0	1.271	1.242	30	30
75	97.8	1.190	1.245	31	31
80	97.9	1.255	1.245	31	31
85	98.2	1.273	1.245	31	32
90	98.1	1.207	1.255	32	32
95	98.0	1.215	1.253	32	32
100	98.0	1.207	1.257	32	33
105	97.8	1.207	1.261	32	33

Table D.18 $[\pm 45]_s$ C

Time	K Temp.	Laser 1 V	Laser 2 V	Laser 1 T	Laser 2 T
0	23.6	.658	.613	27	27
15	23.2	.651	.612	27	27
30	23.2	.660	.612	29	29
45	23.3	.659	.606	30	30
60	95.5	.690	.625	30	30
75	94.5	.707	.645	31	31
80	97.9	.709	.652	32	32
85	97.8	.714	.661	32	32
90	97.8	.713	.664	33	32
95	97.9	.720	.666	33	33
100	97.9	.726	.675	33	33
105	97.9	.728	.679	34	34

Table D.19 $[\pm 45]_s$ D

Time	K Temp.	Laser 1 V	Laser 2 V	Laser 1 T	Laser 2 T
0	23.7	.698	.654	27	27
15	22.8	.716	.654	29	29
30	23.2	.705	.658	30	29
45	23.3	.708	.653	30	30
60	95.5	.837	.782	31	30
75	94.5	.854	.805	31	31
80	97.9	.857	.812	32	32
85	97.8	.859	.814	32	32
90	97.8	.871	.817	32	32
95	97.8	.882	.824	32	33
100	97.8	.889	.824	33	33
105	97.8	.893	.827	33	34

Table D.20 $[\pm 45]_s$ E

Time	K Temp.	Laser 1 V	Laser 2 V	Laser 1 T	Laser 2 T
0	23.6	.755	.707	27	27
15	23.2	.777	.716	28	29
30	23.2	.773	.711	29	29
45	23.3	.773	.707	29	29
60	23.4	.774	.706	29	29
75	91.6	.884	.816	29	29
90	97.7	.867	.804	30	30
95	97.9	.871	.799	30	31
100	97.7	.867	.799	30	31
105	97.7	.863	.798	31	31
110	97.7	.858	.798	31	31
115	97.6	.858	.797	31	31
120	97.6	.859	.795	31	32

Table D.21 $[\pm 60]_s$ A

Time	K Temp.	Laser 1 V	Laser 2 V	Laser 1 T	Laser 2 T
0	23.0	.408	.347	27	27
15	23.1	.406	.349	28	29
30	23.2	.405	.405	30	30
45	23.3	.450	.413	30	30
60	92.1	.450	.414	30	30
75	97.2	.455	.415	31	31
80	97.9	.460	.440	32	32
85	97.8	.455	.428	32	32
90	97.8	.460	.435	33	32
95	97.8	.465	.435	33	33
100	97.8	.465	.435	33	33
105	97.8	.465	.438	34	34

Table D.22 $[\pm 60]_s$ B

Time	K Temp.	Laser 1 V	Laser 2 V	Laser 1 T	Laser 2 T
0	23.5	.670	.662	27	27
15	23.1	.705	.656	29	29
30	23.2	.711	.660	30	30
45	23.3	.712	.654	30	30
60	95.5	.700	.590	31	31
75	94.5	.701	.593	31	31
80	97.6	.652	.599	32	32
85	97.8	.645	.603	32	32
90	97.8	.644	.605	33	32
95	97.8	.648	.612	33	33
100	97.8	.657	.612	33	33
105	97.8	.658	.613	34	33

Table D.23 $[\pm 60]_s$ C

Time	K Temp.	Laser 1 V	Laser 2 V	Laser 1 T	Laser 2 T
0	23.8	.545	.479	27	27
15	23.1	.548	.474	29	29
30	23.3	.548	.472	30	30
45	23.3	.548	.469	30	31
60	95.8	.569	.487	30	30
75	97.6	.569	.495	31	31
80	97.7	.571	.503	32	31
85	97.7	.577	.503	32	32
90	97.6	.584	.507	33	32
95	97.7	.579	.507	33	33
100	97.7	.586	.508	34	33
105	97.7	.586	.512	34	34

Table D.24 $[\pm 60]_s$ D

Time	K Temp.	Laser 1 V	Laser 2 V	Laser 1 T	Laser 2 T
0	23.5	.921	.897	27	27
15	23.2	.922	.889	29	29
30	23.2	.919	.883	29	30
45	23.3	.917	.879	29	30
60	91.0	.855	.810	30	31
75	97.5	.832	.816	31	31
80	97.9	.834	.809	31	32
85	97.8	.834	.888	31	32
90	97.8	.833	.881	32	32
95	97.7	.841	.793	33	32
100	97.8	.843	.785	33	32
105	97.8	.844	.782	34	33

Table D.25 $[\pm 60]_s$ E

Time	K Temp.	Laser 1 V	Laser 2 V	Laser 1 T	Laser 2 T
0	23.4	.426	.360	29	27
15	23.0	.432	.360	29	29
30	23.0	.468	.394	30	30
45	23.0	.464	.394	30	30
60	94.0	.399	.345	30	30
75	97.1	.387	.328	31	31
80	97.9	.383	.327	31	31
85	97.8	.387	.330	32	32
90	97.8	.390	.333	32	32
95	97.8	.388	.330	33	32
100	97.8	.390	.327	33	32
105	97.8	.395	.334	33	32

Table D.26 $[30_2/\text{-}30_2]_s$ A

Time	K Temp.	Laser 1 V	Laser 2 V	Laser 1 T	Laser 2 T
0	21.5	.769	.722	28	27
15	23.1	.788	.742	28	28
30	23.1	.801	.754	29	28
45	23.2	.809	.765	29	29
60	23.2	.810	.763	29	29
75	91.3	.789	.775	29	29
90	97.0	.808	.794	30	30
95	97.2	.812	.803	31	31
100	97.3	.822	.803	32	31
105	97.3	.824	.804	32	32
110	97.2	.833	.805	33	32
115	97.1	.833	.808	33	33
120	97.1	.844	.811	34	33

Table D.27 $[30_2/-30_2]_s$ B

Time	K Temp.	Laser 1 V	Laser 2 V	Laser 1 T	Laser 2 T
0	22.5	.664	.642	27	27
15	22.9	.733	.685	28	28
30	22.7	.750	.698	29	28
45	22.9	.759	.706	29	29
60	23.1	.760	.704	30	29
75	91.4	.773	.717	30	30
90	96.8	.784	.746	31	31
95	96.9	.790	.747	32	31
100	96.9	.805	.748	32	32
105	96.9	.803	.747	33	32
110	96.9	.808	.756	33	33
115	96.9	.813	.758	33	33
120	96.9	.822	.759	34	33

Table D.28 $[30_2/-30_2]_s$ C

Time	K Temp.	Laser 1 V	Laser 2 V	Laser 1 T	Laser 2 T
0	23.2	.769	.760	28	27
15	23.1	.810	.771	28	28
30	23.0	.827	.772	29	28
45	23.1	.830	.781	29	29
60	23.1	.830	.779	29	29
75	92.3	.830	.784	30	29
90	97.0	.848	.806	30	30
95	97.1	.849	.807	31	31
100	97.1	.860	.810	32	32
105	97.1	.864	.821	32	32
110	97.1	.867	.822	33	33
115	97.1	.876	.822	34	33
120	97.1	.877	.822	34	33

Table D.29 $[30_2/-30_2]_s$ D

Time	K Temp.	Laser 1 V	Laser 2 V	Laser 1 T	Laser 2 T
0	23.4	.728	.775	28	27
15	23.1	.833	.787	29	29
30	23.1	.852	.795	30	29
45	23.0	.859	.793	30	30
60	23.1	.858	.795	30	30
75	93.4	.877	.865	30	30
90	97.0	.878	.886	31	31
95	97.1	.883	.897	32	32
100	97.1	.895	.902	33	32
105	97.1	.895	.904	33	33
110	97.1	.897	.906	33	33
115	97.1	.897	.908	33	33
120	97.1	.911	.912	34	34

Table D.30 $[30_2/-30_2]_s$ E

Time	K Temp.	Laser 1 V	Laser 2 V	Laser 1 T	Laser 2 T
0	21.5	.731	.700	28	27
15	22.8	.756	.709	28	28
30	23.1	.768	.718	29	28
45	23.0	.773	.728	29	29
60	23.0	.774	.730	29	29
75	92.3	.801	.763	29	29
90	96.8	.824	.780	30	30
95	96.8	.822	.782	31	31
100	96.9	.831	.781	32	31
105	96.9	.836	.789	32	32
110	96.8	.842	.799	33	33
115	96.8	.851	.801	34	33
120	96.8	.850	.803	34	34

Table D.31 $[(\pm 30)_2]_s$ A

Time	K Temp.	Laser 1 V	Laser 2 V	Laser 1 T	Laser 2 T
0	23.6	.811	.844	27	27
15	23.0	.870	.85.	29	29
30	23.0	.893	.856	30	29
45	23.1	.895	.856	30	30
60	92.6	.887	.854	30	31
75	97.0	.910	.871	31	32
80	97.2	.916	.874	32	32
85	97.2	.924	.881	32	32
90	97.2	.923	.888	32	33
95	97.2	.932	.889	33	33
100	97.1	.944	.897	33	33
105	97.2	.934	.898	33	33

Table D.32 $[(\pm 30_2)]_s$ B

Time	K Temp.	Laser 1 V	Laser 2 V	Laser 1 T	Laser 2 T
0	21.7	.653	.664	25	25
15	22.9	.711	.679	27	27
30	23.1	.726	.692	28	28
45	23.2	.735	.704	28	28
60	23.4	.739	.710	29	29
75	91.7	.741	.708	29	29
90	97.1	.720	.673	30	30
95	97.2	.742	.707	31	31
100	97.3	.746	.715	31	32
105	97.3	.749	.724	32	32
110	97.2	.758	.725	32	32
115	97.1	.759	.725	33	33
120	97.1	.770	.733	33	33

Table D.33 $[(\pm 30)_2]_s$ C

Time	K Temp.	Laser 1 V	Laser 2 V	Laser 1 T	Laser 2 T
0	21.5	.770	.727	28	27
15	23.1	.781	.749	28	28
30	23.1	.791	.754	29	28
45	23.2	.789	.755	29	29
60	23.2	.814	.765	29	29
75	91.3	.840	.766	29	29
90	97.0	.842	.776	30	30
95	97.2	.844	.785	31	31
100	97.3	.848	.786	32	31
105	97.3	.848	.790	32	32
110	97.2	.850	.796	33	32
115	97.1	.849	.764	33	33
120	97.1	.850	.795	34	33

Table D.34 $[(\pm 30)_2]_s$ D

Time	K Temp.	Laser 1 V	Laser 2 V	Laser 1 T	Laser 2 T
0	23.7	.675	.690	28	27
15	23.1	.729	.706	28	28
30	23.1	.744	.710	29	28
45	23.1	.753	.714	29	29
60	23.2	.753	.713	29	29
75	91.0	.805	.750	30	29
90	97.0	.810	.749	31	30
95	97.2	.824	.752	31	31
100	97.3	.829	.753	31	31
105	97.3	.830	.763	32	32
110	97.2	.838	.762	32	32
115	97.2	.840	.772	33	33
120	97.2	.848	.775	33	33

Table D.35 $[(\pm 30)_2]_s$ E

Time	K Temp.	Laser 1 V	Laser 2 V	Laser 1 T	Laser 2 T
0	23.5	.717	..686	27	27
15	23.2	.770	.723	29	29
30	23.2	.790	.730	30	30
45	23.1	.793	.731	30	30
60	94.5	.794	.739	30	30
75	97.1	.803	.739	31	31
80	97.2	.815	.759	32	32
85	97.3	.815	.762	32	32
90	97.3	.819	.758	33	32
95	97.3	.827	.766	33	33
100	97.2	.825	.764	33	33
105	97.2	.830	.766	34	34

Table D.36 $[(\pm 30)_4]_s$ A

Time	K Temp.	Laser 1 V	Laser 2 V	Laser 1 T	Laser 2 T
0	23.8	.701	.692	27	28
15	23.0	.747	.711	28	29
30	23.0	.759	.716	29	29
45	23.0	.761	.715	29	29
60	92.7	.784	.776	30	30
75	96.8	.780	.780	31	31
80	97.1	.792	.785	31	31
85	97.1	.794	.784	31	31
90	97.1	.802	.790	31	32
95	97.1	.803	.788	31	32
100	97.0	.803	.792	31	32
105	97.0	.800	.794	31	32

Table D.37 $[(\pm 30)_4]_s$ B

Time	K Temp.	Laser 1 V	Laser 2 V	Laser 1 T	Laser 2 T
0	23.0	.718	.724	26	27
15	23.2	.785	.751	27	28
30	23.0	.812	.766	28	29
45	23.0	.814	.765	29	29
60	92.2	.808	.793	29	29
75	96.9	.821	.795	30	30
80	96.9	.822	.795	30	30
85	97.0	.823	.793	31	31
90	97.0	.825	.796	31	31
95	97.0	.826	.800	32	31
100	970	.829	.809	32	31
105	97.0	.832	.816	32	32

Table D.38 $[(\pm 30)_4]_s$ C

Time	K Temp.	Laser 1 V	Laser 2 V	Laser 1 T	Laser 2 T
0	23.9	.750	.754	27	27
15	23.2	.768	.764	28	29
30	23.2	.776	.762	29	29
45	23.2	.777	.765	29	29
60	91.2	.779	.748	29	30
75	97.1	.785	.757	30	31
80	97.2	.797	.765	31	31
85	97.3	.810	.763	31	31
90	97.3	.808	.768	31	32
95	97.3	.814	.770	31	32
100	97.2	.818	.777	32	32
105	97.2	.819	.780	32	33

Table D.39 $[(\pm 30)_4]_s$ D

Time	K Temp.	Laser 1 V	Laser 2 V	Laser 1 T	Laser 2 T
0	23.5	.800	.754	27	27
15	23.2	.819	.757	29	28
30	23.2	.828	.761	29	29
45	23.1	.828	.762	29	29
60	94.5	.838	.810	30	29
75	97.1	.848	.832	30	30
80	97.2	.859	.837	31	31
85	97.3	.862	.845	31	31
90	97.3	.862	.844	32	32
95	97.3	.869	.845	32	32
100	97.2	.869	.847	32	32
105	97.2	.874	.858	32	33

Table D.40 $[(\pm 30)_4]_s$ E

Time	K Temp.	Laser 1 V	Laser 2 V	Laser 1 T	Laser 2 T
0	22.8	.795	.796	29	27
15	23.1	.805	.798	29	29
30	23.1	.808	.805	30	30
45	23.1	.809	.804	30	30
60	93.2	.845	.820	30	30
75	97.1	.868	.821	31	31
80	97.2	.875	.833	32	32
85	97.3	.876	.835	32	33
90	97.3	.876	.852	33	34
95	97.3	.886	.860	34	34
100	97.2	.888	.860	34	34
105	97.2	.895	.861	35	35

Table D.41 $[\pm 30/0]_s$ A

Time	K Temp.	Laser 1 V	Laser 2 V	Laser 1 T	Laser 2 T
0	23.2	.595	.609	26	27
15	23.2	.598	.611	28	29
30	23.1	.603	.620	29	29
45	23.2	.608	.622	29	29
60	23.1	.610	.626	30	30
75	97.8	.648	.663	32	31
90	97.9	.651	.662	32	32
95	97.8	.656	.669	33	32
100	97.7	.660	.675	33	32
105	97.7	.664	.681	33	33
110	98.0	.666	.685	34	33
115	97.9	.671	.690	34	34
120	97.9	.672	.690	34	34

Table D.42 $[\pm 30/0]_s$ B

Time	K Temp.	Laser 1 V	Laser 2 V	Laser 1 T	Laser 2 T
0	23.6	.660	.671	24	24
15	23.0	.685	.700	27	27
30	23.2	.694	.716	28	28
45	23.4	.698	.723	29	29
60	23.4	.700	.725	29	29
75	95.1	.715	.767	29	29
90	98.0	.721	.776	30	30
95	98.2	.726	.780	31	31
100	98.3	.727	.788	31	32
105	98.2	.730	.789	32	32
110	98.0	.733	.792	32	32
115	98.1	.736	.794	33	33
120	98.1	.739	.797	33	33

Table D.43 $[\pm 30/0]_s$ C

Time	K Temp.	Laser 1 V	Laser 2 V	Laser 1 T	Laser 2 T
0	23.0	.835	.786	26	27
15	23.2	.842	.803	28	28
30	23.1	.849	.816	28	28
45	23.1	.854	.824	28	28
60	23.2	.855	.825	29	29
75	95.1	.892	.840	29	29
90	97.1	.900	.845	30	30
95	97.1	.906	.845	30	31
100	97.3	.909	.856	31	31
105	97.2	.910	.850	31	32
110	97.2	.922	.862	32	32
115	97.2	.922	.870	33	33
120	97.2	.926	.875	33	33

Table D.44 $[\pm 30/0]_s$ D

Time	K Temp.	Laser 1 V	Laser 2 V	Laser 1 T	Laser 2 T
0	23.0	.788	.817	26	27
15	23.1	.838	.834	28	29
30	23.2	.858	.842	29	29
45	23.1	.873	.841	29	29
60	23.1	.868	.840	29	29
75	93.0	.879	.868	29	29
90	97.0	.906	.856	30	30
95	97.1	.900	.865	31	31
100	97.3	.908	.867	31	31
105	97.3	.904	.874	32	32
110	97.2	.904	.876	32	32
115	97.2	.909	.880	33	33
120	97.3	.915	.885	33	33

Table D.45 $[\pm 30/0]_s$ E

Time	K Temp.	Laser 1 V	Laser 2 V	Laser 1 T	Laser 2 T
0	23.6	.722	.809	26	27
15	23.0	.772	.812	27	27
30	23.2	.782	.811	28	28
45	23.4	.796	.834	28	28
60	23.4	.793	.855	29	29
75	95.1	.826	.861	29	30
90	98.0	.839	.862	30	30
95	98.2	.844	.874	30	31
100	98.3	.848	.878	30	31
105	98.2	.856	.880	30	31
110	98.0	.852	.882	31	31
115	98.1	.858	.883	31	31
120	98.1	.860	.886	31	31

Table D.46 $[0/\pm 30]_s$ A

Time	K Temp.	Laser 1 V	Laser 2 V	Laser 1 T	Laser 2 T
0	23.6	.910	.898	31	31
15	23.0	.900	.899	30	30
30	23.2	.903	.888	30	30
45	23.4	.897	.893	30	30
60	23.4	.930	.911	30	30
75	96.1	.925	.690	30	30
90	98.0	.930	.692	30	30
95	98.1	.919	.690	31	30
100	98.1	.921	.700	31	31
105	98.0	.940	.700	32	31
110	98.1	.950	.702	32	32
115	98.0	.959	.702	33	32
120	98.0	.955	.708	33	32

Table D.47 $[0/\pm30]_s$ B

Time	K Temp.	Laser 1 V	Laser 2 V	Laser 1 T	Laser 2 T
0	24.0	.848	.839	29	29
15	23.0	.860	.840	29	29
30	23.2	.860	.843	29	29
45	23.3	.857	.852	29	29
60	23.4	.863	.849	29	29
75	97.0	.884	.847	29	29
90	98.0	.895	.868	30	30
95	98.2	.893	.870	31	31
100	98.2	.909	.870	31	31
105	98.2	.902	.874	32	31
110	98.2	.925	.877	32	32
115	98.2	.920	.880	32	32
120	98.2	.918	.882	32	33

Table D.48 $[0/\pm30]_s$ C

Time	K Temp.	Laser 1 V	Laser 2 V	Laser 1 T	Laser 2 T
0	23.6	.628	.660	26	28
15	23.4	.639	.668	28	29
30	23.4	.644	.675	29	30
45	23.4	.646	.678	30	30
60	23.4	.648	.698	30	30
75	94.1	.658	.713	30	30
90	98.0	.669	.715	31	31
95	98.0	.671	.719	31	31
100	98.0	.675	.719	32	32
105	98.0	.675	.719	32	32
110	98.0	.679	.724	32	32
115	98.0	.680	.724	32	32
120	98.0	.683	.723	32	33

Table D.49 $[0/\pm30]_s$ D

Time	K Temp.	Laser 1 V	Laser 2 V	Laser 1 T	Laser 2 T
0	23.6	.720	.666	28	28
15	23.0	.735	.676	28	29
30	23.2	.651	.686	29	29
45	23.4	.655	.688	30	30
60	23.4	.657	.691	30	30
75	96.3	.661	.688	30	30
90	98.0	.667	.690	31	30
95	98.0	.670	.696	31	31
100	98.0	.675	.700	31	31
105	98.0	.680	.707	32	32
110	98.0	.680	.708	32	32
115	97.9	.682	.73	33	32
120	97.9	.685	.716	33	33

Table D.50 $[0/\pm30]_s$ E

Time	K Temp.	Laser 1 V	Laser 2 V	Laser 1 T	Laser 2 T
0	23.9	.594	.614	26	27
15	23.0	.628	.651	28	28
30	23.3	.634	.660	29	29
45	23.4	.637	.665	29	29
60	23.4	.635	.665	29	29
75	95.0	.631	.660	30	30
90	98.0	.640	.669	30	30
95	98.0	.643	.673	31	31
100	98.0	.647	.677	31	31
105	98.0	.648	.678	31	31
110	98.0	.649	.685	31	32
115	98.0	.650	.688	32	32
120	98.0	.656	.691	32	32

Table D.51 $[0/\pm30/90]_s$ A

Time	K Temp.	Laser 1 V	Laser 2 V	Laser 1 T	Laser 2 T
0	23.9	.782	.774	28	28
15	23.0	.780	.772	28	28
30	23.3	.783	.770	28	28
45	23.4	.782	.767	28	28
60	23.4	.795	.760	29	29
75	95.0	.810	.782	29	30
90	97.0	.817	.790	30	30
95	97.0	.818	.790	30	31
100	97.0	.822	.800	30	31
105	97.0	.825	.805	30	31
110	97.0	.822	.813	30	31
115	97.0	.832	.813	31	31
120	97.0	.835	.814	31	32

Table D.52 $[0/\pm30/90]_s$ B

Time	K Temp.	Laser 1 V	Laser 2 V	Laser 1 T	Laser 2 T
0	23.1	.834	.846	26	27
15	23.1	.886	.846	28	28
30	23.2	.890	.860	29	28
45	23.2	.900	.859	29	29
60	23.3	.900	.860	29	29
75	92.0	.930	.878	30	30
90	97.0	.930	.878	30	30
95	97.2	.958	.904	31	31
100	97.3	.965	.907	32	32
105	97.3	.965	.908	32	32
110	97.3	.970	.915	33	33
115	97.3	.972	.917	33	33
120	97.3	.970	.916	33	33

Table D.53 $[0/\pm30/90]_s$ C

Time	K Temp.	Laser 1 V	Laser 2 V	Laser 1 T	Laser 2 T
0	23.1	.870	.850	27	27
15	23.1	.879	.879	27	27
30	23.3	.888	.888	28	28
45	23.3	.892	.900	28	28
60	23.3	.896	.901	29	28
75	92.3	.910	.881	30	29
90	96.9	.934	.896	30	30
95	97.0	.935	.910	31	30
100	97.1	.944	.913	31	31
105	97.1	.955	.925	31	31
110	97.1	.950	.925	31	32
115	97.1	.955	.929	32	32
120	97.1	.961	.936	32	32

Table D.54 $[0/\pm30/90]_s$ D

Time	K Temp.	Laser 1 V	Laser 2 V	Laser 1 T	Laser 2 T
0	23.0	.914	.938	28	27
15	23.2	.964	.972	29	28
30	23.3	.983	.979	29	29
45	23.3	.996	.998	29	29
60	23.3	1.002	.999	30	30
75	91.2	.997	1.003	30	30
90	96.6	1.002	1.027	30	30
95	97.0	1.016	1.030	32	31
100	97.1	1.023	1.037	32	32
105	97.1	1.029	1.040	33	32
110	97.1	1.031	1.043	33	33
115	97.1	1.035	1.053	33	33
120	97.1	1.040	1.057	34	33

Table D.55 $[0/\pm30/90]_s$ E

Time	K Temp.	Laser 1 V	Laser 2 V	Laser 1 T	Laser 2 T
0	23.4	.780	.790	26	27
15	23.0	.784	.794	28	28
30	23.2	.814	.814	29	29
45	23.2	.826	.825	29	29
60	23.1	.860	.830	29	29
75	90.8	.859	.857	30	30
90	96.9	.898	.854	30	30
95	97.1	.912	.857	31	31
100	97.0	.918	.859	31	31
105	97.2	.920	.870	31	31
110	97.1	.926	.878	31	32
115	97.0	.930	.885	32	32
120	97.0	.940	.895	32	32

Table D.56 $[0_2/(\pm30)_2]_s$ A

Time	K Temp.	Laser 1 V	Laser 2 V	Laser 1 T	Laser 2 T
0	23.4	.780	.790	26	27
15	23.0	.784	.794	28	28
30	23.2	.814	.814	29	29
45	23.2	.826	.825	29	29
60	23.1	.860	.830	29	29
75	90.8	.859	.857	30	30
90	96.9	.898	.854	30	30
95	97.1	.912	.857	31	31
100	97.0	.918	.859	31	31
105	97.2	.920	.870	31	31
110	97.1	.926	.878	31	32
115	97.0	.930	.885	32	32
120	97.0	.940	.895	32	32

Table D.57 $[0_2/(\pm 30)_2]_s$ B

Time	K Temp.	Laser 1 V	Laser 2 V	Laser 1 T	Laser 2 T
0	23.0	.793	.803	28	27
15	23.1	.800	.815	29	28
30	23.1	.855	.830	30	30
45	23.1	.873	.837	30	30
60	23.1	.873	.839	30	30
75	92.1	.906	.873	31	31
90	97.3	.916	.881	31	32
95	97.4	.919	.878	31	32
100	97.4	.926	.883	32	32
105	97.4	.928	.884	32	32
110	97.3	.930	.889	33	33
115	97.2	.933	.888	33	33
120	97.2	.934	.891	33	33

Table D.58 $[0_2/(\pm 30)_2]_s$ C

Time	K Temp.	Laser 1 V	Laser 2 V	Laser 1 T	Laser 2 T
0	22.9	.803	.773	27	27
15	23.2	.831	.795	28	28
30	23.0	.838	.799	29	29
45	23.1	.845	.805	29	29
60	23.1	.846	.806	29	29
75	89.0	.855	.811	30	29
90	95.2	.863	.822	30	30
95	95.5	.900	.828	31	31
100	95.6	.904	.831	31	31
105	95.7	.902	.834	32	32
110	95.7	.906	.840	32	32
115	95.8	.909	.846	33	33
120	95.7	.909	.864	33	33

Table D.59 $[0_2/\pm30_2]_s$ D

Time	K Temp.	Laser 1 V	Laser 2 V	Laser 1 T	Laser 2 T
0	23.2	.739	.740	26	27
15	23.1	.810	.770	28	29
30	23.1	.823	.800	29	29
45	23.1	.845	.808	29	29
60	23.1	.846	.810	30	29
75	97.1	.880	.825	31	30
90	97.1	.911	.838	32	31
95	97.3	.921	.836	32	32
100	97.3	.934	.841	33	32
105	97.3	.940	.851	33	33
110	97.3	.939	.861	33	33
115	97.3	.949	.860	33	33
120	97.3	.948	.861	34	33

Table D.60 $[0_2/\pm30_2]_s$ E

Time	K Temp.	Laser 1 V	Laser 2 V	Laser 1 T	Laser 2 T
0	23.4	.715	.777	26	27
15	23.0	.783	.794	28	28
30	23.2	.809	.804	29	29
45	23.2	.819	8.110	29	29
60	23.1	.830	.810	29	29
75	90.8	.829	.810	30	30
90	96.9	.841	.825	30	30
95	97.1	.871	.826	31	31
100	97.0	.872	.835	31	31
105	97.2	.882	.834	31	31
110	97.1	.881	.836	31	32
115	97.0	.888	.840	32	32
120	97.0	.895	.839	32	32

Table D.61 $[0_2/90_2]_T$ A

Time	K Temp.	Laser 1 V	Laser 2 V	Laser 1 T	Laser 2 T
0	23.3	-1.870	-1.976	28	27
15	23.4	-1.878	-1.933	28	28
30	23.2	-1.889	-1.940	29	29
45	23.2	-1.900	-1.957	29	29
60	23.1	-1.901	-1.957	29	30
75	93.3	-.600	-.680	30	30
90	97.2	-.530	-.589	31	31
95	97.4	-.559	-.602	31	31
100	97.3	-.518	-.573	32	32
105	97.3	-.515	-.572	32	32
110	97.2	-.508	-.568	33	33
115	97.2	-.505	-.560	33	33
120	97.2	-.502	-.558	33	33

Table D.62 $[0_2/90_2]_T$ B

Time	K Temp.	Laser 1 V	Laser 2 V	Laser 1 T	Laser 2 T
0	23.5	-1.230	-1.300	27	27
15	23.2	-1.234	-1.336	28	28
30	23.2	-1.236	-1.338	29	29
45	94.0	.250	.183	30	30
60	97.3	.300	.216	31	31
65	97.2	.302	.214	31	31
70	97.4	.290	.203	32	31
75	97.3	.282	.204	32	32
80	97.4	.873	.196	33	33
85	97.3	.273	.192	33	33
90	97.3	.269	.188	33	33

Table D.63 $[0_2/90_2]_T$ C

Time	K Temp.	Laser 1 V	Laser 2 V	Laser 1 T	Laser 2 T
0	*	-.506	-.545	28	27
15	*	-.517	-.593	30	30
30	*	-.541	-.612	30	30
45	*	-.554	-.631	30	31
60	*	-.547	-.627	30	31
75	*	.592	.547	31	31
90	*	.607	.560	32	31
95	*	.596	.547	32	32
100	*	.590	.527	33	32
105	*	.570	.520	33	33
110	*	.556	.507	33	33
115	*	.540	.504	33	33
120	*	.525	.500	34	34

* Broken K thermocouple

Table D.64 $[0_2/90_2]_T$ D

Time	K Temp.	Laser 1 V	Laser 2 V	Laser 1 T	Laser 2 T
0	23.4	-1.122	-1.204	26	27
15	23.0	-1.071	-1.169	28	28
30	23.2	-1.083	-1.186	29	29
45	23.2	-1.073	-1.183	29	29
60	23.1	-1.073	-1.183	29	29
75	94.4	-.500	-.514	30	30
90	96.9	-.550	-.378	30	30
95	97.1	-.520	-.360	31	31
100	97.1	-.8518	-.353	31	31
105	97.2	-.516	-.356	31	31
110	97.1	-.516	-.353	31	32
115	97.1	-.512	-.350	32	32
120	97.1	-.513	-.350	32	32

Table D.65 $[0_2/90_2]_T$ E

Time	K Temp.	Laser 1 V	Laser 2 V	Laser 1 T	Laser 2 T
0	23.4	-2.10	-2.00	26	27
15	23.0	-2.08	-1.987	27	27
30	23.2	-2.06	-1.969	28	28
45	23.2	-2.05	-1.958	29	28
60	23.1	-2.05	-1.956	29	29
75	90.8	-.571	-.394	30	30
90	96.9	-.512	-.388	31	31
95	97.1	-.505	-.310	31	31
100	97.0	-.503	-.301	32	31
105	97.2	-.502	-.300	32	32
110	97.1	-.498	-.298	33	32
115	97.0	-.499	-.298	33	33
120	97.0	-.497	-.297	33	33

Table D.66 $[(0/90)_2]_T$ A

Time	K Temp.	Laser 1 V	Laser 2 V	Laser 1 T	Laser 2 T
0	23.1	.390	.619	27	27
15	23.3	.383	.619	28	28
30	23.5	.384	.621	29	29
45	94.7	.978	1.256	30	30
60	97.1	1.021	1.305	30	30
65	97.3	1.027	1.308	30	30
70	97.3	1.033	1.314	31	31
75	97.3	1.036	1.324	31	31
80	97.2	1.037	1.327	31	31
85	97.1	1.041	1.330	32	32
90	97.2	1.044	1.341	32	32

Table D.67 $[(0/90)_2]_T$ B

Time	K Temp.	Laser 1 V	Laser 2 V	Laser 1 T	Laser 2 T
0	23.2	.306	.503	27	27
15	23.2	.301	.496	28	28
30	23.2	.299	.498	29	29
45	94.0	.815	1.044	30	30
60	97.6	.845	1.076	31	31
65	97.6	.847	1.079	31	31
70	97.6	.849	1.079	31	31
75	97.6	.851	1.082	32	32
80	97.6	.855	1.089	32	32
85	97.6	.853	1.087	32	32
90	97.6	.857	1.089	32	33

Table D.68 $[(0/90)_2]_T$ C

Time	K Temp.	Laser 1 V	Laser 2 V	Laser 1 T	Laser 2 T
0	21.6	.700	.956	29	29
15	23.1	.676	.944	29	29
30	23.3	.667	.937	29	29
45	23.3	.665	.938	29	29
60	95.8	1.143	1.484	30	30
75	97.3	1.148	1.485	31	31
80	97.2	1.143	1.485	32	32
85	97.3	1.140	1.478	32	32
90	97.1	1.138	1.479	33	33
95	97.0	1.135	1.472	33	33
100	97.0	1.133	1.469	34	33
105	97.0	1.130	1.468	34	33

Table D.69 $[(0/90)_2]_T$ D

Time	K Temp.	Laser 1 V	Laser 2 V	Laser 1 T	Laser 2 T
0	21.6	.567	.808	24	24
15	23.1	.560	.812	26	26
30	23.3	.556	.815	27	27
45	23.3	.556	.815	28	28
60	95.8	1.109	1.374	29	29
75	97.3	1.115	1.380	31	31
80	97.2	1.112	1.373	32	31
85	97.3	1.110	1.380	32	32
90	97.1	1.109	1.383	33	32
95	97.0	1.108	1.380	33	33
100	97.0	1.108	1.382	33	33
105	97.0	1.109	1.385	34	33

Table D.70 $[(0/90)_2]_T$ E

Time	K Temp.	Laser 1 V	Laser 2 V	Laser 1 T	Laser 2 T
0	23.6	.452	.721	26	27
15	23.2	.431	.701	27	27
30	23.4	.423	.700	28	28
45	23.2	.420	.693	29	28
60	23.2	.420	.691	29	29
75	94.2	.937	1.210	30	30
90	97.1	.936	1.214	31	31
95	97.2	.932	1.215	31	31
100	97.2	.931	1.211	32	31
105	97.2	.930	1.207	32	32
110	97.1	.928	1.202	33	32
115	97.0	.926	1.199	33	33
120	97.0	.923	1.195	33	33

Table D.71 $[0_4/90_4]_T$ A

Time	K Temp.	Laser 1 V	Laser 2 V	Laser 1 T	Laser 2 T
0	23.0	-1.055	-1.009	26	27
15	23.4	-1.048	-.998	26	27
30	23.5	-1.045	-.992	27	28
45	23.3	-1.040	-.986	28	28
60	23.5	-1.039	-.986	29	29
75	94.1	.175	.324	29	29
90	97.0	.242	.409	30	29
95	97.0	.255	.429	30	30
100	97.0	.260	.437	31	30
105	97.0	.268	.449	31	31
110	97.0	.270	.447	31	31
115	97.0	.275	.452	32	32
120	97.0	.278	.457	32	32

Table D.72 $[0_4/90_4]_T$ B

Time	K Temp.	Laser 1 V	Laser 2 V	Laser 1 T	Laser 2 T
0	23.4	-.738	-.626	27	27
15	23.2	-.739	-.615	28	28
30	23.2	-.739	-.616	29	29
45	94.7	.260	.472	30	30
60	97.4	.295	.510	31	31
65	97.3	.298	.514	31	31
70	97.3	.298	.509	32	31
75	97.3	.300	.512	32	32
80	97.3	.301	.510	33	32
85	97.3	.301	.509	33	33
90	97.3	.302	.511	33	33

Table D.73 $[0_4/90_4]_T$ C

Time	K Temp.	Laser 1 V	Laser 2 V	Laser 1 T	Laser 2 T
0	23.7	-.389	-.221	27	27
15	23.2	-.395	-.214	29	28
30	23.2	-.396	-.213	29	29
45	94.6	.553	.781	30	30
60	97.3	.594	.832	31	30
65	97.4	.598	.832	32	31
70	97.4	.601	.843	32	32
75	97.3	.604	.844	33	32
80	97.3	.608	.838	33	33
85	97.3	.608	.840	33	33
90	97.3	.610	.839	34	34

Table D.74 $[0_4/90_4]_T$ D

Time	K Temp.	Laser 1 V	Laser 2 V	Laser 1 T	Laser 2 T
0	23.1	-.726	-.618	27	27
15	23.1	-.723	-.611	29	29
30	23.2	-.725	-.613	29	29
45	94.0	.297	.489	30	30
60	97.2	.348	.546	31	31
65	97.3	.350	.544	32	32
70	97.3	.352	.549	32	32
75	97.3	.352	.548	33	33
80	97.1	.351	.548	33	33
85	97.2	.353	.547	33	33
90	97.3	.351	.552	34	34

Table D.75 $[0_4/90_4]_T$ E

Time	K Temp.	Laser 1 V	Laser 2 V	Laser 1 T	Laser 2 T
0	23.2	-.485	-.350	27	27
15	23.2	-.493	-.340	29	29
30	23.2	-.495	-.339	30	29
45	94.5	.484	.703	30	30
60	97.3	.523	.743	31	31
65	97.3	.525	.749	32	31
70	97.2	.524	.750	32	32
75	97.2	.527	.755	33	32
80	97.2	.526	.750	33	33
85	97.2	.528	.752	33	33
90	97.2	.528	.753	34	34

Table D.76 $[0_3/90]_T$ A

Time	K Temp.	Laser 1 V	Laser 2 V	Laser 1 T	Laser 2 T
0	*	1.306	1.552	27	27
15	*	1.307	1.561	29	29
30	*	1.307	1.563	30	29
45	*	1.383	1.641	30	30
60	*	1.393	1.642	31	30
65	*	1.395	1.644	31	31
70	*	1.396	1.650	32	31
75	*	1.395	1.654	32	32
80	*	1.397	1.668	32	32
85	*	1.395	1.675	33	32
90	*	1.395	1.668	33	33

* Failure of K-type thermocouple- no temperature data

Table D.77 $[0_3/90]_T$ B

Time	K Temp.	Laser 1 V	Laser 2 V	Laser 1 T	Laser 2 T
0	23.1	1.290	1.478	27	27
15	23.2	1.295	1.498	29	29
30	23.1	1.292	1.498	29	29
45	94.1	1.356	1.616	29	29
60	97.1	1.360	1.625	30	30
65	97.2	1.367	1.635	31	31
70	97.1	1.369	1.628	31	31
75	97.2	1.370	1.627	32	32
80	97.1	1.372	1.625	32	32
85	97.1	1.372	1.624	33	33
90	97.0	1.375	1.633	33	33

Table D.78 $[0_3/90]_T$ C

Time	K Temp.	Laser 1 V	Laser 2 V	Laser 1 T	Laser 2 T
0	23.2	1.330	1.423	27	28
15	23.2	1.386	1.439	29	29
30	23.2	1.408	1.444	30	29
45	92.4	1.411	1.442	30	30
60	97.1	1.528	1.557	31	30
65	97.0	1.552	1.575	31	31
70	97.1	1.564	1.589	32	31
75	97.1	1.572	1.601	32	32
80	97.0	1.581	1.610	33	32
85	97.0	1.583	1.608	33	33
90	97.0	1.596	1.607	34	33

Table D.79 $[0_3/90]_T$ D

Time	K Temp.	Laser 1 V	Laser 2 V	Laser 1 T	Laser 2 T
0	23.0	1.1191	1.434	28	28
15	23.3	1.188	1.454	29	29
30	23.2	1.186	1.465	29	29
45	94.0	1.358	1.634	30	30
60	97.0	1.335	1.630	32	31
65	97.1	1.328	1.627	32	32
70	97.0	1.328	1.626	33	32
75	97.1	1.327	1.626	33	33
80	97.1	1.324	1.630	33	33
85	97.0	1.324	1.631	33	33
90	97.0	1.322	1.633	33	33

Table D.80 $[0_3/90]_T$ E

Time	K Temp.	Laser 1 V	Laser 2 V	Laser 1 T	Laser 2 T
0	23.2	1.364	1.600	26	26
15	23.2	1.367	1.613	28	28
30	23.2	1.370	1.615	29	29
45	94.5	1.467	1.750	29	29
60	97.3	1.458	1.740	30	30
65	97.3	1.460	1.740	31	31
70	97.2	1.459	1.739	31	31
75	97.2	1.464	1.738	32	32
80	97.2	1.463	1.736	32	32
85	97.2	1.461	1.737	32	32
90	97.2	1.460	1.738	33	32

Table D.81 $[0/30]_T$ A

Time	K Temp.	Laser 1 V	Laser 2 V	Laser 1 T	Laser 2 T
0	23.4	.440	1.119	26	26
15	23.2	.461	1.142	28	28
30	23.1	.461	1.141	29	29
45	91.8	.432	.950	29	29
60	96.8	.422	.928	30	30
65	96.9	.419	.925	31	31
70	97.0	.418	.928	31	31
75	97.0	.417	.926	32	32
80	97.1	.419	.928	32	32
85	97.0	.419	.930	32	32
90	97.0	.418	.923	32	32

Table D.82 $[0/30]_T$ B

Time	K Temp.	Laser 1 V	Laser 2 V	Laser 1 T	Laser 2 T
0	23.3	.829	1.300	26	26
15	23.1	.890	1.306	26	27
30	23.3	.892	1.309	27	28
45	91.9	.850	1.070	28	28
60	96.9	.817	1.073	29	29
65	96.9	.815	1.076	29	29
70	97.0	.809	1.066	30	30
75	97.0	.813	1.079	30	30
80	97.0	.808	1.080	30	30
85	97.0	.818	1.079	30	31
90	97.0	.820	1.080	31	31

Table D.83 $[0/30]_T$ C

Time	K Temp.	Laser 1 V	Laser 2 V	Laser 1 T	Laser 2 T
0	23.5	.645	1.255	27	27
15	23.0	.634	1.262	28	28
30	23.0	.633	1.261	28	28
45	93.3	.532	.975	29	29
60	96.9	.530	.955	30	30
65	96.9	.530	.953	30	30
70	97.0	.527	.956	30	31
75	97.0	.524	.958	30	31
80	97.0	.527	.964	31	31
85	97.0	.525	.964	31	32
90	97.0	.526	.969	31	32

Table D.84 $[0/30]_T$ D

Time	K Temp.	Laser 1 V	Laser 2 V	Laser 1 T	Laser 2 T
0	23.4	.752	1.624	27	26
15	23.1	.744	1.633	29	27
30	23.3	.742	1.630	29	28
45	91.8	.585	1.150	30	29
60	96.8	.581	1.158	31	30
65	96.9	.585	1.160	31	31
70	97.0	.584	1.159	31	32
75	97.0	.588	1.157	32	32
80	97.1	.589	1.159	32	33
85	97.0	.591	1.160	33	33
90	97.0	.592	1.160	33	33

Table D.85 $[0/30]_T$ E

Time	K Temp.	Laser 1 V	Laser 2 V	Laser 1 T	Laser 2 T
0	23.2	.466	1.114	26	26
15	23.2	.481	1.149	28	28
30	23.1	.483	1.154	29	29
45	91.8	.393	1.153	29	29
60	96.9	.370	.850	30	30
65	97.0	.375	.835	31	31
70	97.0	.381	.835	31	31
75	97.0	.377	.835	32	32
80	97.1	.380	.841	32	32
85	97.0	.379	.840	32	32
90	97.0	.380	.841	32	32

Table D.86 $[0_{10}/30_{10}]_T$ A

Time	K Temp.	Laser 1 V	Laser 2 V	Laser 1 T	Laser 2 T
0	23.2	.307	.608	30	30
15	23.2	.398	.612	30	30
30	23.1	.400	.613	30	30
45	91.9	.563	.768	30	30
60	97.0	.582	.777	31	31
65	97.2	.584	.780	31	31
70	97.3	.592	.790	31	32
75	97.2	.596	.795	32	32
80	97.1	.601	.800	32	32
85	97.0	.602	.812	32	33
90	97.0	.604	.810	33	33

Table D.87 $[0_{10}/30_{10}]_T$ B

Time	K Temp.	Laser 1 V	Laser 2 V	Laser 1 T	Laser 2 T
0	23.2	.382	.572	30	30
15	23.2	.395	.601	30	30
30	23.1	.394	.600	30	30
45	91.8	.627	.762	30	30
60	96.9	.645	.775	31	31
65	97.0	.640	.780	31	31
70	97.0	.652	.778	31	32
75	97.0	.660	.782	32	32
80	97.1	.657	.791	32	32
85	97.0	.659	.792	32	33
90	97.0	.658	.793	33	33

Table D.88 $[0_{10}/30_{10}]_T$ C

Time	K Temp.	Laser 1 V	Laser 2 V	Laser 1 T	Laser 2 T
0	23.2	.337	.600	30	29
15	23.2	.354	.613	30	30
30	23.1	.355	.615	30	30
45	91.8	.570	.771	30	30
60	96.9	.575	.782	31	31
65	97.0	.583	.780	31	31
70	97.0	.600	.786	31	32
75	97.0	.602	.786	32	32
80	97.1	.610	.785	33	33
85	97.0	.612	.788	34	33
90	97.0	.605	.790	34	34

Table D.89 $[0_{10}/30_{10}]_T$ D

Time	K Temp.	Laser 1 V	Laser 2 V	Laser 1 T	Laser 2 T
0	23.2	.202	.273	29	30
15	23.2	.204	.293	30	30
30	23.1	.203	.292	30	30
45	91.8	.478	.522	30	30
60	96.9	.495	.585	30	31
65	97.0	.515	.642	31	31
70	97.0	.513	.656	31	32
75	97.0	.520	.656	31	32
80	97.1	.522	.658	32	32
85	97.0	.521	.661	32	33
90	97.0	.520	.662	32	33

Table D.90 $[0_{10}/30_{10}]_T$ E

Time	K Temp.	Laser 1 V	Laser 2 V	Laser 1 T	Laser 2 T
0	23.2	.405	.597	30	30
15	23.2	.408	.613	30	30
30	23.1	.409	.613	30	30
45	91.8	.640	.762	30	30
60	96.9	.656	.775	31	31
65	97.0	.658	.780	31	31
70	97.0	.660	.778	31	32
75	97.0	.663	.786	32	32
80	97.1	.646	.802	32	32
85	97.0	.655	.822	32	33
90	97.0	.656	.823	33	33